



HAL
open science

A posteriori error estimates and adaptivity based on stopping criteria and adaptive mesh re finement for multiphase and thermal flows. Application to steam-assisted gravity drainage

Soleiman Yousef

► **To cite this version:**

Soleiman Yousef. A posteriori error estimates and adaptivity based on stopping criteria and adaptive mesh re finement for multiphase and thermal flows. Application to steam-assisted gravity drainage. Analysis of PDEs [math.AP]. Université Pierre et Marie Curie - Paris VI, 2013. English. NNT : . tel-00918782v2

HAL Id: tel-00918782

<https://theses.hal.science/tel-00918782v2>

Submitted on 26 Jun 2014

HAL is a multi-disciplinary open access archive for the deposit and dissemination of scientific research documents, whether they are published or not. The documents may come from teaching and research institutions in France or abroad, or from public or private research centers.

L'archive ouverte pluridisciplinaire **HAL**, est destinée au dépôt et à la diffusion de documents scientifiques de niveau recherche, publiés ou non, émanant des établissements d'enseignement et de recherche français ou étrangers, des laboratoires publics ou privés.



THÈSE

Pour l'obtention du grade de

DOCTEUR EN SCIENCES

DE L'UNIVERSITÉ PIERRE ET MARIE CURIE

Spécialité: Mathématiques Appliquées

Faculté de Mathématiques UFR 929

École Doctorale de Sciences Mathématiques de Paris Centre ED 386

par

Soleiman Yousef

Titre

**Étude d'estimations d'erreur a posteriori et d'adaptivité
basée sur des critères d'arrêt et raffinement de maillages
pour des problèmes d'écoulements multiphasiques et
thermiques**

Application aux procédés de récupération assistée d'huile

**Etude d'estimations d'erreur a posteriori et d'adaptivité basée sur des critères
d'arrêt et raffinement de maillages pour des problèmes d'écoulements
multiphasiques et thermiques**

Application aux procédés de récupération assistée d'huile

Résumé

L'objectif de cette thèse est l'analyse d'erreur a posteriori et la proposition de stratégies d'adaptivité basées sur des critères d'arrêt et de raffinement local de maillage. Nous traitons une classe d'équations paraboliques dégénérées multidimensionnelles modélisant des problèmes importants pour l'industrie.

Au chapitre 1 nous considérons le problème de Stefan instationnaire à deux phases qui modélise un processus de changement de phase régi par la loi de Fourier. Nous régularisons la relation entre l'enthalpie et la température et nous discrétisons le problème par la méthode d'Euler implicite en temps et un schéma numérique conforme en espace tel que les éléments finis conformes, ou les volumes finis centrés aux sommets du maillage. Nous démontrons une borne supérieure de la norme duale du résidu, de l'erreur sur l'enthalpie dans $L^2(0, T, H^{-1}(\Omega))$ et de l'erreur sur la température dans $L^2(0, T; L^2(\Omega))$, par des estimateurs d'erreur entièrement calculables. Ces estimateurs comprennent : un estimateur associé à l'erreur de régularisation, un estimateur associé à l'erreur d'une méthode de linéarisation (par exemple, la méthode de Newton), un estimateur associé à l'erreur en temps et un estimateur associé à l'erreur du schéma en espace. Par conséquent, ces estimateurs permettent de formuler un algorithme adaptatif de résolution où les erreurs associées peuvent être équilibrées. Nous proposons également une stratégie de raffinement local de maillages. Enfin, nous prouvons l'efficacité de nos estimations d'erreur a posteriori. Un test numérique illustre l'efficacité de nos estimateurs et la performance de l'algorithme adaptatif. En particulier, des indices d'efficacité proches de la valeur optimale de 1 sont obtenus.

Au chapitre 2 nous développons des estimations d'erreur a posteriori pour l'écoulement de Darcy polyphasique et isothermique, décrit par un système couplé d'équations aux dérivées partielles non linéaires et d'équations algébriques non linéaires. Ce système est discrétisé en espace par une méthode de volumes finis centrés par maille et la méthode d'Euler implicite en temps. Nous établissons une borne supérieure d'une norme duale du résidu augmentée d'un terme qui tient compte de la non-conformité des volumes finis par des estimateurs d'erreur a posteriori entièrement calculables. Dans ce chapitre, nous nous concentrons sur la formulation d'un critère d'arrêt de l'algorithme de linéarisation du problème discret (tel que la méthode de Newton) avec un critère d'arrêt du solveur algébrique de résolution du système linéarisé (par exemple la méthode GMRes), de sorte que les contributions des estimateurs d'erreur correspondant n'affectent plus la somme globale des estimateurs d'erreur de manière

significative. Nous appliquons notre analyse sur des exemples réalistes d'ingénierie de réservoir pour confirmer qu'en général notre ajustement des critères d'arrêt apporte une économie significative (jusqu'à un ordre de magnitude en termes du nombre total des itérations du solveur algébrique), déjà sur des maillages fixes, et ceci sans perte notable de précision.

Au chapitre 3 nous complétons le modèle décrit au chapitre 2 en considérant une condition non-isothermique pour l'écoulement afin de traiter le modèle général d'écoulement polyphasique thermique dans les milieux poreux. Pour ce problème, nous développons des estimateurs d'erreur analogues à ceux du chapitre 2 pour lesquels nous établissons une borne supérieure d'erreur entièrement calculable, pour une norme duale du résidu complétée par un terme d'évaluation de la non-conformité. Nous montrons ensuite comment estimer séparément chaque composante d'erreur, ce qui nous permet d'ajuster les critères d'arrêt et d'équilibrer les contributions des différents estimateurs d'erreur : erreur d'approximation en temps, erreur d'approximation en espace, erreur de linéarisation et erreur du solveur algébrique. Ce chapitre se termine par une application des estimateurs au modèle d'huile morte.

Finalement, au chapitre 4 nous considérons les procédés de récupération assistée d'huile. Plus précisément, nous étudions une technique de récupération thermique d'huile de type huile morte par injection de vapeur destinée à augmenter la mobilité des hydrocarbures. Dans ce chapitre, nous appliquons l'analyse a posteriori des chapitres 2 et 3, nous proposons une formule de quadrature pour simplifier l'évaluation des estimateurs, nous proposons un algorithme adaptatif de raffinement de maillages en espace et en temps basé sur les estimateurs et nous illustrons pas des essais numériques sur des exemples réalistes la performance de cette stratégie de raffinement. Notamment, des gains significatifs sont réalisés en terme du nombre de mailles nécessaires pour la simulation sur des exemples en dimension trois.

Mots-clefs : analyse d'erreur a posteriori, algorithme adaptatif, problème de Stefan à deux phases, écoulement compositionnel polyphasique de Darcy, écoulement thermique, méthode des volumes finis, erreur de discrétisation, erreur de régularisation, erreur de linéarisation, erreur du solveur algébrique, raffinement adaptatif de maillage, évaluation simplifiée des estimateurs, formule de quadrature.

A posteriori error estimates and adaptivity based on stopping criteria and adaptive mesh refinement for multiphase and thermal flows.

Application to steam-assisted gravity drainage

Abstract

The goal of this thesis is the a posteriori error analysis and the conception of adaptive strategies based on stopping criteria and local mesh refinement. We treat a class of multi-dimensional degenerate parabolic equations which represent typical examples of industrial interest.

In Chapter 1 we consider the time-dependent two-phase Stefan problem that models a phase change process governed by the Fourier law. We regularize the relation between the enthalpy and the temperature and we discretize the problem by the backward Euler temporal stepping method with a conforming spatial discretization, such as the finite element or the vertex-centered finite volume one. We prove an upper bound for the dual norm of the residual, the $L^2(0, T; H^{-1}(\Omega))$ error in the enthalpy, and $L^2(0, T; L^2(\Omega))$ error in the temperature, by fully computable error estimators. These estimators include: an estimator associated to the regularization error, an estimator associated to the linearization error, an estimator associated to the temporal error, and an estimator associated to the spatial error. Consequently, these estimators allow to formulate an adaptive resolution algorithm where the corresponding errors can be equilibrated. We also propose a strategy of local mesh refinement. Finally, we prove the efficiency of our a posteriori estimates. A numerical test illustrates the efficiency of our estimates and the performance of the adaptive algorithm. In particular, effectivity indices close to the optimal value of 1 are obtained.

In Chapter 2 we derive a posteriori error estimates for the isothermal compositional model of the multiphase Darcy flow in porous media, consisting of a system of strongly coupled nonlinear unsteady partial differential and nonlinear algebraic equations. This model is discretized by a cell-centered finite volume scheme in space with the backward Euler temporal stepping. We establish an upper bound for a dual norm of the residual augmented by a nonconformity evaluation term by fully computable estimators. We focus in this chapter on the formulation of criteria for the iterative linearization (such as the Newton method) and iterative algebraic solvers (such as the GMRes method) that stop the iterations when the corresponding error components no longer affect the overall estimate significantly. We apply our analysis to several real-life reservoir engineering examples to confirm that significant computational gains (up to an order of magnitude in terms of the total number of algebraic solver iterations) can be achieved thanks to our adaptive stopping criteria, already on fixed meshes, and this without any noticeable loss of precision.

In Chapter 3 we complete the model described in Chapter 2 by considering a nonisothermal condition for the flow in order to treat the general thermal multiphase compositional flow in

porous media. For this problem, we derive fully computable a posteriori error estimates analogous to Chapter 2 for a dual norm of the residual supplemented by a nonconformity evaluation term. We then show how to estimate separately the space, time, linearization, and algebraic errors, giving the possibility to formulate adaptive stopping and balancing criteria. Specification of the abstract theory to the so-called dead oil model closes the chapter.

Finally, in Chapter 4 we consider the Steam-Assisted Gravity Drainage (SAGD) process, more precisely a thermal oil-recovery technique of the deal oil type with steam injection designed to increase the oil mobility. The main subjects of this chapter are to apply the a posteriori error analysis of Chapters 2 and 3, propose a simplification and a quadrature formula for an easy evaluation of the estimators, propose a space-time adaptive mesh refinement algorithm, and illustrate by numerical results on real-life examples its performance. In particular, a significant gain in terms of the number of mesh cells is achieved on examples in 3 space dimensions.

Key words: a posteriori error analysis, adaptive algorithm, two-phase Stefan problem, multiphase compositional Darcy flow, thermal flow, finite volume method, discretization error, regularization error, linearization error, algebraic solver error, adaptive mesh refinement, simplified evaluation of estimators, quadrature formula.

Contents

Introduction	1
General context	2
General properties for an a posteriori error estimate	3
A posteriori error analysis based on equilibrated fluxes	3
Motivations	4
Moving boundary problems	5
Reservoir simulation	5
Outline	8
Chapter 1	8
Chapter 2	8
Chapter 3	10
Chapter 4	11
Bibliography	11
1 Adaptive regularization, linearization, and discretization and a posteriori error control for the two-phase Stefan problem	17
1.1 Introduction	19
1.2 Continuous and discrete settings	22
1.2.1 Continuous setting	22
1.2.2 Discrete setting	24
1.3 An a posteriori error estimate for the dual norm of the residual	25
1.3.1 Dual norm of the residual	25
1.3.2 General assumptions	25
1.3.3 A basic a posteriori error estimate	26
1.3.4 An a posteriori error estimate distinguishing the space, time, regularization, linearization, and quadrature errors	28
1.4 Balancing and stopping criteria, adaptive algorithm, and efficiency	30

1.4.1	Balancing and stopping criteria	30
1.4.2	Adaptive algorithm	31
1.4.3	Efficiency of the a posteriori error estimate	33
1.5	An a posteriori error estimate for the error in temperature and enthalpy . . .	34
1.5.1	Bounding the error of the temperature and enthalpy by the dual norm of the residual	34
1.5.2	The a posteriori error estimate	35
1.6	Application to a vertex-centered finite volume discretization	37
1.6.1	Dual and tertial space meshes	37
1.6.2	The vertex-centered finite volume scheme	37
1.6.3	Newton linearization	38
1.6.4	Flux reconstruction	39
1.7	Numerical experiments	40
1.7.1	Setting	40
1.7.2	Computing approximately the negative norms	41
1.7.3	Stopping criteria	42
1.7.4	Balancing criteria	43
1.7.5	Overall performance	44
1.A	Proofs	48
1.A.1	Proof of Theorem 1.4.4	49
1.A.2	Proof of Theorem 1.5.2	51
	Bibliography	54
2	A posteriori error estimates, stopping criteria, and adaptivity for multi- phase compositional flows in porous media	59
2.1	Introduction	61
2.2	Setting	64
2.2.1	The multiphase compositional model	64
2.2.2	An implicit finite volume scheme with phase-upwind and two-point dis- cretization of diffusive fluxes	68
2.3	A basic a posteriori error estimate	71
2.3.1	Weak solution	71
2.3.2	A generic approximate solution	72
2.3.3	Error measure	73
2.3.4	Flux and pressure reconstructions	74
2.3.5	A posteriori error estimate	74
2.4	Application to finite volume method and adaptivity based on distinguishing the different error components	76
2.4.1	Linearization and algebraic resolution	77

2.4.2	Approximate solution	78
2.4.3	Phase pressure reconstructions	80
2.4.4	Component flux reconstructions	80
2.4.5	Distinguishing the space, time, linearization, and algebraic errors . . .	81
2.4.6	A fully adaptive algorithm	84
2.5	Numerical results	85
2.5.1	Common setting	86
2.5.2	Compressible flow in a homogeneous porous medium	88
2.5.3	Compressible flow in a heterogeneous porous medium	91
2.5.4	Five-spots pattern	98
	Bibliography	105
3	A posteriori error estimates for thermal multiphase compositional flows in porous media	121
3.1	Introduction	123
3.2	Setting	124
3.3	Discretization of the energy equation	126
3.3.1	Two-point finite volume discretization	126
3.3.2	Linearization and algebraic resolution	127
3.4	Approximate solution and reconstructions	129
3.4.1	Postprocessing of the temperature	129
3.4.2	Saturations, molar fractions, and molar energy	129
3.4.3	H_0^1 -conforming temperature reconstruction	130
3.4.4	$\mathbf{H}(\text{div}; \Omega)$ -conforming energy flux reconstructions	130
3.5	A posteriori error estimate	131
3.5.1	Weak solution	131
3.5.2	Error measure	132
3.5.3	An a posteriori error estimate distinguishing the space, time, linearization, and algebraic errors	134
3.5.4	Balancing and stopping criteria	137
3.A	Application to the thermal dead oil model	137
3.A.1	Dead oil model	138
3.A.2	A posteriori error estimate for the thermal dead oil model	139
	Bibliography	143
4	Steam-assisted gravity drainage: a posteriori estimates with simplified evaluation and application of adaptive mesh refinement	151
4.1	Introduction	152
4.2	SAGD characterization and modeling	153

4.2.1	Common characteristics	153
4.2.2	Types of SAGD	154
4.2.3	SAGD modeling	154
4.2.4	Mathematical model of the thermal dead oil system	155
4.3	Evaluation of the estimators using a practical simplified formula	155
4.3.1	A general simplification formula	156
4.3.2	Evaluation of the estimators	157
4.4	SAGD test case	163
4.4.1	Model description	163
4.4.2	Initialization and production scheme	164
4.4.3	Model simulation	165
4.4.4	Approximate solution and a posteriori estimate	166
4.4.5	Adaptive mesh refinement	166
	Bibliography	168
	List of figures	176
	List of tables	179

Introduction

General context

Environmental and physical phenomena of technology and energy are related to many essential parts of our life. An important number of these phenomena is modeled by partial differential equations (PDEs). While a few PDEs can be solved analytically, this is not the case in general. Engineers and mathematicians have thus founded numerical methods in order to provide at least approximate solutions to these equations; the invention of numerical methods is considered as a milestone.

Computational mathematics brings the important issue of accuracy. First of all, do we have a good approximate solution? The answer to this question is given by the distance between the exact and approximate solutions. The *a priori error estimates* are used to estimate this error as a function of an unknown constant and the mesh size. Thus, an a priori estimate is a good theoretical tool for evaluating the asymptotic accuracy of a numerical method. However, as the bound in general depends on the exact solution, it can not be computed in practice, except when there exist test cases whose data can be adjusted to an exact solution, or when there exist significant benchmarks. In contrast to a priori error estimates, *a posteriori error estimates* rely on the knowledge of the discrete solution only. These estimates can be object-oriented in the sense that they assess a specific aspect of the computation, such as local mass conservation, or they evaluate physical quantities of interest, cf. Becker and Rannacher [11], Oden and Prudhomme [47], Giles and Süli [29], Loseille et al. [38], Ladevèze and Chamoin [34]. More often, they estimate some form of the error such as the distance of the approximate and exact solution in an energy norm, cf. Verfürth [53], Ainsworth and Oden [2], Babuška and Strouboulis [7], Neittaanmäki and Repin [43], Carstensen [17], or Repin [50].

In addition to the accuracy of the numerical method, we want to address two important issues:

- 1) The discretization of nonlinear PDEs by numerical methods ultimately leads to very large nonlinear systems. Solving these systems is a prevailing part of the total computational load. Therefore, we ask: Is it possible to save an important part of the computing time by reducing the number of linear systems to be solved or the number of iterations of linear algebraic solvers?
- 2) Most physical phenomena produce complex, discontinuous local behaviors, such as changes in phase, shocks, or boundary layers, caused by rough data and parameters, rough boundary conditions, or singular equations. It is important to approximate accurately these local behaviors. Although a priori estimates can be localized (see the work of Schatz and Wahlbin in [51, 52]), they still typically depend on the unknown exact solution. Thus, the question is: Can we design a tool that yields a good local estimation of the overall error distribution, as well as the distribution of its components?

General properties for an a posteriori error estimate

For model problems, the energy error between the unknown exact solution and the known approximate solution can be estimated by an a posteriori error estimate which does not feature any undetermined constant. In this case we say that we have a *fully computable upper bound*, which is especially important for practical applications. Distinguishing the *different error components* is another property of paramount importance. Typically, the approximation error of unsteady problems is composed of discretization errors in space and in time. These should be balanced by adjusting the size of the spatial mesh and of the time step, as suggested in, e.g., Bieterman and Babuška [13], Ladevèze and Moës [36], Ladevèze [33], Verfürth [54], Bergam et al. [12], Ern and Vohralík [24], and Carstensen et al. [18]. Likewise, we can separate errors coming from the different parts of the resolution of the problem as the linearization error and the linear algebraic solver error, cf. Becker et al. [10], Arioli et al. [4], Chaillou and Suri [20], Meidner et al. [40], or Ern and Vohralík [25]. Distinguishing these error components in the resolution allows to propose *stopping criteria* for the various iterative solvers whenever the corresponding error does not affect the overall error.

Ensuring a computable upper bound on the error and separating the different error components is an important tool in precision assessment and for economizing unnecessary iterations of resolution. However, error estimators are useful only if their computational load is negligible compared to the cost of obtaining the approximate solution. Therefore, good error estimators should also have a *small evaluation cost*, in order to be applicable to real-life problems and hopefully ensuring significant computational gains.

The *local efficiency* of the estimate is satisfied when the estimate on the error in each computational cell represents a lower bound for this error, up to a generic constant, in the given cell and possibly in its neighbourhood. The *robustness* of the a posteriori estimate is then ensured when the generic constant of the local efficiency does not depend on the parameters of the problem and on their variation. Lastly, the *asymptotic exactness* of the estimate is obtained when the effectivity index, given by the ratio of the estimated and the actual error, converges to the optimal value of one with increasing the resolution of the simulation.

An optimal a posteriori error estimate is an estimate providing a fully computable upper bound, distinguishing the different error components, ensuring a small evaluation cost, and satisfying the local efficiency, the robustness, and the asymptotic exactness.

A posteriori error analysis based on equilibrated fluxes

The a posteriori error analysis considered in this thesis belongs to a class of a posteriori error estimates called *equilibrated fluxes estimates*, cf. Prager and Synge [49], Destuynder and Métivet [23], Luce and Wohlmuth [39], Ainsworth [1], Braess and Schöberl [14], Hannukainen

et al. [30], and the references therein. There exist many other categories of energy norm a posteriori error estimates: *explicit residual estimates*, cf. Babuška and Rheinboldt [6], Verfürth [53], and Carstensen [16], the *equilibrated residual method*, cf. Ladevèze and Leguillon [35] and Ainsworth and Oden [2], *averaging estimates*, see Zienkiewicz and Zhu [55], *functional a posteriori error estimates*, cf. Neittaanmki and Repin [43] and Repin [50], *hierarchical estimates*, see Bank and Smith [8], or *geometric a posteriori error estimates*, see Castro Díaz et al. [19] or Frey and Alauzet [27]. The advantage of equilibrated fluxes estimates is that they allow for optimality in the above-discussed sense.

The spirit of our work is to control a dual norm of the residual of the different problems under consideration, augmented (if necessary) by a nonconformity evaluation term. This is achieved by introducing $\mathbf{H}(\text{div}; \Omega)$ -conforming and locally conservative (equilibrated) flux reconstructions, and potential reconstructions if necessary. Moreover, in a specific case (the Stefan problem), we bound the dual norm of the residual from below as closely as possible by some energy-like norm. Thus, we obtain a fully computable a posteriori estimate on this norm as well. The local efficiencies of the a posteriori error estimates can also be proved here as a theoretical foundation for the fully adaptive algorithms.

Many advantages follow from this approach:

- We get a fully computable upper bound for a dual norm of the residual that can be localized in each element of the domain and at each time step during the simulation.
- The estimate allows to distinguish different error components corresponding to the resolution of the problem such as: space, time, linearization, algebraic solver, and regularization.
- Distinguishing the different error components leads us to formulate a criterion for the choice of the regularization parameter (if regularization is considered) and criteria for stopping the iterative algebraic solver and the iterative linearization solver, when the corresponding error components do not affect significantly the overall error. Additionally, we can also propose a balancing criterion to equilibrate the spatial and temporal errors, and a local mesh refinement strategy by adjusting the sizes of the spatial mesh and time step and evenly distributing the space error throughout the domain.
- Adaptive algorithms based on the previous criteria can be proposed and applied, ensuring significant computational gains in terms of the total number of linearization iterations, algebraic solver iterations, time steps, and mesh cells.

Practical motivations

We deal in this thesis with a class of multidimensional degenerate parabolic equations with important industrial applications: the two-phase *Stefan problem* representing solidification with a free boundary, and the *multiphase compositional* and *thermal flow* models in a porous medium describing the movement of several fluids through a porous medium reservoir.

Free boundary problems

A free boundary problem describes a physical phenomenon in a domain with moving boundaries or moving interfaces separating subdomains, where the model of the phenomenon is governed by different equations. A frequent example occurs when the phenomenon involves a change in phase. Due to its industrial impact, this type of problems has been widely studied, cf. Jerome and Rose [31], Amiez and Gremaud [3], Nochetto et al. [45], Picasso [48], Nochetto et al. [46].

The two-phase Stefan problem models a phase change process which is governed by the Fourier law, cf. Kamenomostskaja [32], Friedman [28], Meyer [42] or Meirmanov [41]. The two phases, typically solid and liquid, are separated by a moving interface, whose motion is governed by the so-called Stefan condition. Herein, we consider it as a model problem that can be analyzed mathematically in full details.

Reservoir simulation

Reservoir modeling is an important branch of petroleum engineering which provides predictive tools to elaborate reservoir exploration and oil production strategies, cf. Aziz and Settari [5]. From a mathematical standpoint, the underlying models require the numerical solution of highly nontrivial problems resulting from nonlinear, strongly coupled systems of partial differential and algebraic equations cf. Bear [9], Chavent and Jaffré [21], and Chen et al. [22]. Our focus is on the simulation of problems representative of enhanced oil recovery techniques.

The EOR (*enhanced oil recovery*), see Lake [37], is a generic term describing methods that increase the volume of hydrocarbons extracted from a petroleum reservoir (recovery rate). The EOR is the implementation of techniques for oil recovery occurring after a *primary* initial recovery of hydrocarbons, very often followed by a step of water injection. Water injection method is then typically referred to as *secondary* recovery. The injection of gas can be also used as a method of secondary recovery, especially in geographical areas where it is difficult to have water of sufficient quality for injection. Some EOR processes are even considered at the onset of production from the reservoir (thus primary recovery), typically in the case of reservoirs of heavy or extra heavy hydrocarbons so viscous that they can only be produced by thermal processes.

All EOR methods are based on two principles invoked individually or in combination: An increase in the capillary number and / or decrease in the mobility ratio, compared to their respective values in the secondary phase of production. This simple characterization of the EOR frames the research efforts to improve the recovery rate, the main aim of any EOR operation. Despite this apparent simplicity, the aspects related to their implementation are complex.

EOR processes include *gas injection*, *chemical methods* where the injection of polymer

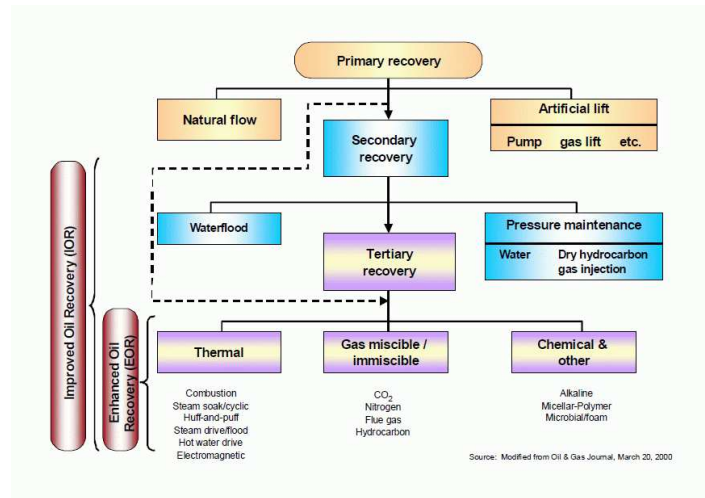


Figure 1: Classification of hydrocarbon recovery methods.

type, alkali, or surfactants change the ratio of mobility and / or the interfacial tensions of the phases moving in the reservoir, and the *thermal recovery* by heat injection changing the thermodynamic properties of fluids, see Figure 1. Our focus will be on methods of *gas injection*, and *thermal recovery*.

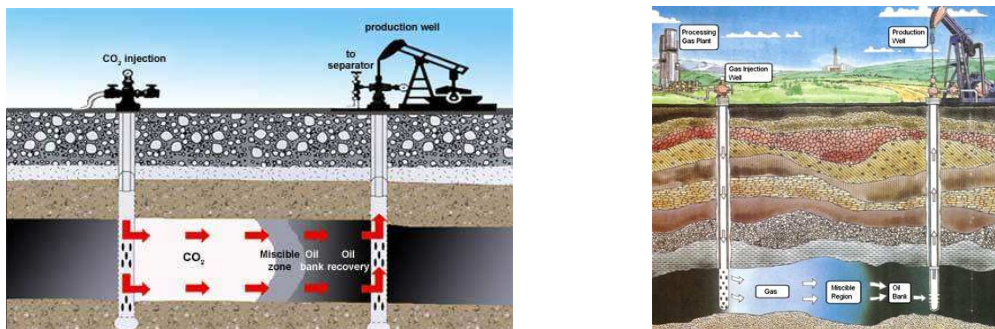


Figure 2: Gas injection.

Gas injection

Gas injection is the most commonly used EOR process to date, cf. Lake [37]. The obtained effect is an increase of the reservoir pressure in the injection zone and consequently a displacement of the fluids in place. We are then talking about the sweeping of the oil reservoir by the injected gas (solvent flooding, miscible gas-gas flooding, or flooding). However, in this EOR process, gas injection provides more than pressurization and movement because the compositions and properties of the fluids in place are changed. Thus, according to the miscibility of the injected gas, mass transfer between the fluid in place and the injection fluid (solvent) is more or less important. The capillary number increase (or the reduction of the

gas–oil interfacial tension) acts on the resulting sweep efficiency. The injected products are miscible / immiscible hydrocarbon gas, miscible / immiscible CO₂, nitrogen, or combustion gases (miscible and immiscible).

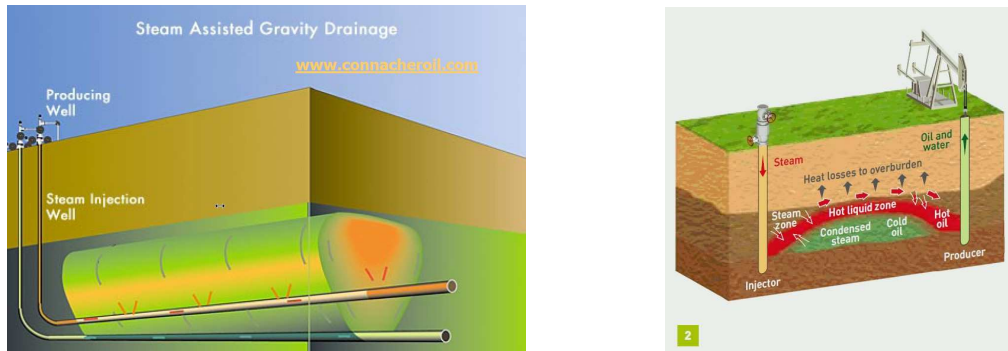


Figure 3: SAGD (left) and Steam Drive (right) process.

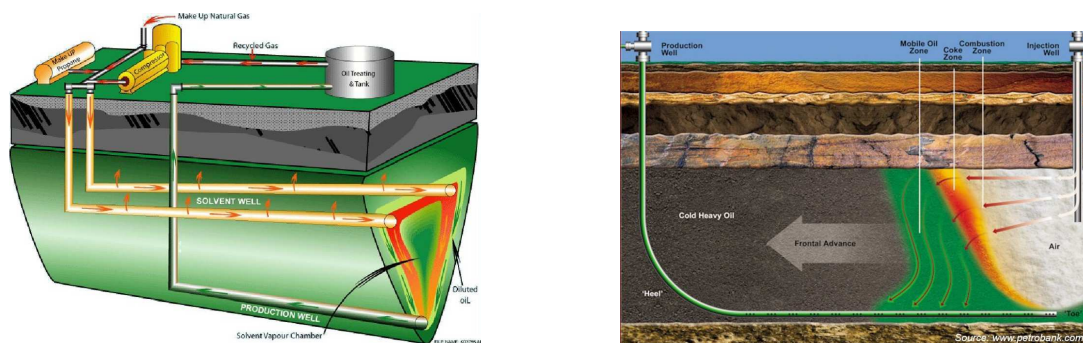


Figure 4: Vapex (left) and Thai (right) process.

Thermal methods

In this approach, see Butler [15], different methods are used to heat the crude oil in the formation to reduce its viscosity and / or to vaporize a portion of the oil. Research in recent years led to the development of management methods of steam (distribution of steam in the reservoir) to improve the efficiency of the injection / production. A notable example of this effort is the SAGD (Steam-Assisted Gravity Drainage), cf. Farouq [26]. Here, one drills two horizontal wells. The top well is used to inject steam, while the bottom one is the producer. As the temperature effect is particularly pronounced for viscous crudes, this system is increasingly used to recover heavy oils.

The thermal methods include cyclic injection of steam, sweeping steam for heavy oil (viscous but mobile), SAGD process, cf. Figure 3, VAPEX (vapor extraction), THAI (Toe-to-Heel-Air-Injection), cf. Figure 4, and the combustion for bitumens. All these methods improve the efficiency of sweeping by facilitating the movement of fluids.

Outline

This thesis is organized as follows:

Chapter 1

In this chapter we consider the time-dependent two-phase Stefan problem: Given an initial enthalpy u_0 and a source function f , find the *enthalpy* u such that

$$\begin{aligned} \partial_t u - \nabla \cdot (\nabla \beta(u)) &= f && \text{in } \Omega \times (0, t_F), \\ u(\cdot, 0) &= u_0 && \text{in } \Omega, \\ \beta(u) &= 0 && \text{on } \partial\Omega \times (0, t_F), \end{aligned}$$

where $\Omega \subset \mathbb{R}^d$, $d \in \{2, 3\}$, is an open bounded polygonal or polyhedral domain, not necessarily convex, and $t_F > 0$.

Considering that the *temperature* $\beta(u)$ cannot be more than Lipschitz continuous, it is often proposed to regularize the Stefan problem, see, e.g., [44, 48], by replacing the function β by a smooth, strictly increasing regularized function $\beta_\epsilon \in C^1(\mathbb{R})$, $\beta'_\epsilon \geq \epsilon$, for a parameter $\epsilon > 0$. This ensures that the regularized flux $-\nabla \beta_\epsilon(u)$ has no jump discontinuity across the interface.

We derive a posteriori error estimates for the two-phase Stefan problem and propose adaptive strategies for its conforming spatial and backward Euler temporal discretizations. As in Nochetto et al. [46], our approach is based on the dual norm of the residual. However, we proceed differently in order to have fully and easily computable estimates not featuring any undetermined constants. Our estimators yield also a guaranteed and fully computable upper bound on the $L^2(L^2)$ error of the temperature and the $L^2(H^{-1})$ error of the enthalpy. We split our estimate into estimators characterizing the space, time, regularization, linearization, and quadrature errors in order to provide a criterion for the choice of the regularization parameter and a stopping criterion for an iterative linearization such as the Newton method, giving rise to a fully adaptive algorithm. The efficiency of the estimate is also proved.

We present numerical results which show that our estimate can predict the location of the moving boundary, make the spatial mesh follow the front, adapt the time step, save many useless linearization iterations, and finally control the choice of the parameter of regularization ϵ . Importantly, we get an effectivity index close to the optimal value of one for the dual norm, as well as an excellent effectivity index for the energy norms.

Chapter 2

We focus in this chapter on the compositional model of multiphase Darcy flow in porous media under the assumption that the flow process is isothermal. The equations that govern this model are the *conservation of the amount of each component* supplemented by algebraic

equations expressing the *conservation of volume*, the *conservation of the quantity of matter*, and the *thermodynamic equilibrium*.

As an example used in the numerical experiments, we consider a model of a miscible two-phase flow: The phases in this model are gas and oil, corresponding to $\mathcal{P} = \{\text{g}, \text{o}\}$, composed of $N_{\mathcal{C}}$ hydrocarbon components forming the set of component \mathcal{C} . Mass interchange is allowed between the phases. The system of equations can be written as

$$\begin{aligned} \partial_t(\phi(\zeta_{\text{o}}S_{\text{o}}C_{\text{o},c} + \zeta_{\text{g}}S_{\text{g}}C_{\text{g},c})) + \nabla \cdot \left(\frac{\zeta_{\text{o}}k_{\text{r},\text{o}}}{\mu_{\text{o}}}C_{\text{o},c}\mathbf{v}_{\text{o}} + \frac{\zeta_{\text{g}}k_{\text{r},\text{g}}}{\mu_{\text{g}}}C_{\text{g},c}\mathbf{v}_{\text{g}} \right) &= q_c, & \forall c \in \mathcal{C}, \\ S_{\text{o}} + S_{\text{g}} &= 1, \\ \sum_{c \in \mathcal{C}_{\text{o}}} C_{\text{o},c} &= 1, \\ \sum_{c \in \mathcal{C}_{\text{g}}} C_{\text{g},c} &= 1, \\ K_c^{\text{o},\text{g}}(P, \mathbf{C}_{\text{o}}, \mathbf{C}_{\text{g}})C_{\text{o},c} &= C_{\text{g},c}, & \forall c \in \mathcal{C}, \end{aligned}$$

with P the *pressure*, ϕ the *porosity* of the medium, $\zeta_p, \mu_p, S_p, k_{\text{r},p}$ respectively the *molar density*, *viscosity*, *saturation*, and *relative permeability* for the phase $p \in \mathcal{P}$, $C_{p,c}$ the *molar fraction* of the component $c \in \mathcal{C}$ in the phase $p \in \mathcal{P}$, $K_c^{\text{o},\text{g}}$ the equilibrium constant between the oil and gas phases for the component $c \in \mathcal{C}$, q_c the source term, and finally, \mathbf{v}_p the *average phase velocity* given by Darcy's law

$$\mathbf{v}_p = -\mathbb{K}(\nabla P_p + \rho_p g \nabla z), \quad p \in \mathcal{P},$$

with \mathbb{K} the *absolute permeability* tensor, ρ_p the *mass density* of the phase p , and g the *gravity*.

We derive a posteriori error estimates for the general multiphase compositional system of strongly coupled nonlinear unsteady partial differential and algebraic equations. We show how to control a dual norm of the residual augmented by a nonconformity term by fully computable estimators. We then decompose the estimators into the space, time, linearization, and algebraic error components in order to formulate criteria for stopping the iterative algebraic solver and the iterative linearization solver when the corresponding error components do not affect significantly the overall error.

We present numerical results on the above two-phase example. We employ the cell-centered two-point finite volume method with fully implicit Euler time stepping, the Newton linearization, and the GMRes algebraic solver. We consider both homogeneous and heterogeneous porous media. Our results show that the a posteriori error estimates detect all the error components in the resolution, the moving front of the saturation, and warrant that the adaptive algorithm does not affect the rate of oil production in comparison with a classical simulation with very tight stopping criteria. They also confirm a speed-up factor of order 10 in terms of the total number of algebraic solver iterations in comparison with the classical resolution.

Chapter 3

In this chapter we complete the multiphase compositional model, introduced in Chapter 2, by a nonisothermal condition for treating the general case of thermal multiphase compositional flows in porous media. This condition is expressed by an additional equation representing the *conservation of energy*. We propose an analogous analysis for the additional PDE. Fully computable a posteriori estimators are derived to control a similar dual norm of the residual augmented by a nonconformity evaluation term. Distinguishing the different components of the error is also carried out to formulate criteria for stopping the iterative algebraic solver and the iterative linearization solver. An application to the discretization by an implicit cell-centered finite volume scheme with phase-upwind and two-point discretization of diffusive fluxes is presented.

In the appendix of this chapter we apply the a posteriori analysis to a special case of the thermal multiphase compositional model called the *dead oil* model, involving three phases, the *oil phase*, *water phase*, and *steam phase*, represented by lowercase letters w, o, s as indices, respectively. We use also the uppercase letters W, O as indices to represent the two *components* of the model: *water* and *oil*, respectively. The unknowns of the dead oil model are the *pressure* P , *temperature* T , and *phase saturations* $S_p, p \in \mathcal{P}$. The system of equations can be expressed as follows:

$$(\mathbf{P}) \left\{ \begin{array}{l}
 \partial_t(\phi(\zeta_w S_w + \zeta_s S_s)) + \nabla \cdot (\nu_w \mathbf{v}_w + \nu_s \mathbf{v}_s) = q_W, \\
 \partial_t(\phi \zeta_o S_o) + \nabla \cdot (\nu_o \mathbf{v}_o) = q_O, \\
 \mathbf{v}_p = -\mathbb{K}(\nabla P_p + \rho_p g \nabla z), \quad p \in \{w, o, s\}, \\
 \nu_p = \zeta_p \frac{k_{rp}}{\mu_p}, \quad p \in \{w, o, s\}, \\
 \\
 \partial_t e_H + \nabla \cdot (\mathbf{u} - \lambda \nabla T) = Q_H, \\
 e_H := \phi e + (1 - \phi) \zeta_r e_r, \\
 e := S_w \zeta_w e_w + S_o \zeta_o e_o + S_s \zeta_s e_s, \\
 \mathbf{u} := \zeta_w H_w \mathbf{v}_w + \zeta_o H_o \mathbf{v}_o + \zeta_s H_s \mathbf{v}_s, \\
 \\
 S_w + S_o + S_s = 1, \\
 \\
 C_w = C_o = C_s = 1, \\
 \\
 S_s S_w (T - T_{\text{sat}}(P)) = 0.
 \end{array} \right.$$

Here $Q_H, q_c, c \in \{W, O\}$, represent source terms, g the *gravity*, ϕ the *porosity* of the medium, $\zeta_p(P, T)$ the *molar density*, $\rho_p(P, T)$ the *mass density*, $\mathbf{v}_p(P, T, S_p)$ the *phase velocity*, \mathbb{K} the *absolute permeability* tensor, $\mu_p(P, T)$ the *viscosity*, $k_{rp}(S_p)$ the *relative permeability*, $\nu_p(P, T, \mathbf{S})$

the *mobility*, $e_r(P, T)$ the *rock internal energy*, ζ_r the *rock molar density*, λ the *thermal conductivity*, $H_p(P, T)$, the *phase enthalpy* (thermodynamic potential), and T_{sat} the temperature of saturation at which steam is in equilibrium with its liquid (water) phase.

Chapter 4

We consider in this chapter the Steam-Assisted Gravity Drainage (SAGD) model. An example is the thermal dead oil model presented above. Thus the a posteriori analysis of the isothermal model of Chapter 2 and of the nonisothermal condition of Chapter 3 applies directly. In order to insert these a posteriori estimators into industrial codes we simplify/approximate in this chapter their computation. This avoids the implementation, in the code, of discrete $\mathbf{H}(\text{div}; \Omega)$ spaces like the Raviart–Thomas–Nédélec ones, together with any physical construction of the reconstructed equilibrated fluxes. The evaluation of the estimators becomes straightforward via a simple local quadrature formula. We also focus here on an adaptive mesh refinement combined with a balancing criterion on the choice of the time step. Numerical results for a real-life reservoir engineering example of the dead oil model are discussed. We obtain an important reduction in the number of cells using the adaptive refinement strategy compared to a fine mesh resolution, without affecting the accuracy of the predicted oil production.

Bibliography

- [1] M. Ainsworth. A synthesis of a posteriori error estimation techniques for conforming, non-conforming and discontinuous Galerkin finite element methods. In *Recent advances in adaptive computation*, volume 383 of *Contemp. Math.*, pages 1–14, Providence, RI, 2005. Amer. Math. Soc.
- [2] M. Ainsworth and J. T. Oden. A posteriori error estimation in finite element analysis. *Pure and Applied Mathematics (New York)*, 2000.
- [3] G. Amiez and P.-A. Gremaud. On a numerical approach to Stefan-like problems. *Numer. Math.*, 59(1):71–89, 1991.
- [4] M. Arioli, D. Loghin, and A. J. Wathen. Stopping criteria for iterations in finite element methods. *Numer. Math.*, 99(3):381–410, 2005.
- [5] K. Aziz and A. Settari. *Petroleum Reservoir Simulation*. Applied Science Publisher, Ltd, London, 1979.
- [6] I. Babuška and W. C. Rheinboldt. Error estimates for adaptive finite element computations. *SIAM J. Numer. Anal.*, 15(4):736–754, 1978.
- [7] I. Babuška and T. Strouboulis. *The finite element method and its reliability*. Numerical Mathematics and Scientific Computation. The Clarendon Press Oxford University Press, New York, 2001.
- [8] R. E. Bank and R. K. Smith. A posteriori error estimates based on hierarchical bases. *SIAM J. Numer. Anal.*, 30(4):921–935, 1993.
- [9] J. Bear. *Dynamics of fluids in porous media*. American Elsevier, New York, 1972.
- [10] R. Becker, C. Johnson, and R. Rannacher. Adaptive error control for multigrid finite element methods. *Computing*, 55(4):271–288, 1995.
- [11] R. Becker and R. Rannacher. An optimal control approach to a posteriori error estimation in finite element methods. *Acta Numer.*, 10:1–102, 2001.
- [12] A. Bergam, C. Bernardi, and Z. Mghazli. A posteriori analysis of the finite element discretization of some parabolic equations. *Math. Comp.*, 74(251):1117–1138, 2005.

-
- [13] M. Bieterman and I. Babuška. The finite element method for parabolic equations. II. A posteriori error estimation and adaptive approach. *Numer. Math.*, 40(3):373–406, 1982.
- [14] D. Braess and J. Schöberl. Equilibrated residual error estimator for edge elements. *Math. Comp.*, 77(262):651–672, 2008.
- [15] R. Butler. *Thermal recovery of oil and bitumen*. Prentice Hall, Englewoods Cliffs, New Jersey, 1991.
- [16] C. Carstensen. A posteriori error estimate for the mixed finite element method. *Math. Comp.*, 66(218):465–476, 1997.
- [17] C. Carstensen. A unifying theory of a posteriori finite element error control. *Numer. Math.*, 100(4):617–637, 2005.
- [18] C. Carstensen, M. Eigel, R. H. W. Hoppe, and C. Löbhard. A review of unified a posteriori finite element error control. *Numer. Math. Theory Methods Appl.*, 5(4):509–558, 2012.
- [19] M. J. Castro-Díaz, F. Hecht, B. Mohammadi, and O. Pironneau. Anisotropic unstructured mesh adaptation for flow simulations. *Internat. J. Numer. Methods Fluids*, 25(4):475–491, 1997.
- [20] A. L. Chaillou and M. Suri. Computable error estimators for the approximation of nonlinear problems by linearized models. *Comput. Methods Appl. Mech. Engrg.*, 196(1-3):210–224, 2006.
- [21] G. Chavent and J. Jaffré. *Mathematical models and finite elements for reservoir simulation*. North-Holland, Amsterdam, 1986. Studies in Mathematics and Its Applications, Vol. 17.
- [22] Z. Chen, G. Huan, and Y. Ma. *Computational methods for multiphase flows in porous media*. Computational Science & Engineering. Society for Industrial and Applied Mathematics (SIAM), Philadelphia, PA, 2006.
- [23] P. Destuynder and B. Métivet. Explicit error bounds in a conforming finite element method. *Math. Comp.*, 68(228):1379–1396, 1999.
- [24] A. Ern and M. Vohralík. A posteriori error estimation based on potential and flux reconstruction for the heat equation. *SIAM J. Numer. Anal.*, 48(1):19–223, 2010.
- [25] A. Ern and M. Vohralík. Adaptive inexact Newton methods with a posteriori stopping criteria for nonlinear diffusion PDEs. *SIAM J. Sci. Comput.*, 35(4):A1761–A1791, 2013.
- [26] A. Farouq. *SAGD steam assisted gravity drainage*. University of Alberta, Edmonton, Canada, 1997.
- [27] P. J. Frey and F. Alauzet. Anisotropic mesh adaptation for CFD computations. *Comput. Methods Appl. Mech. Engrg.*, 194(48):5068–5082, 2005.
- [28] A. Friedman. The Stefan problem in several space variables. *Trans. Amer. Math. Soc.*, 133:51–87, 1968.

-
- [29] M. B. Giles and E. Süli. Adjoint methods for PDEs: a posteriori error analysis and postprocessing by duality. *Acta Numer.*, 11:145–236, 2002.
- [30] A. Hannukainen, R. Stenberg, and M. Vohralík. A unified framework for a posteriori error estimation for the Stokes problem. *Numer. Math.*, 122(4):725–769, 2012.
- [31] J. W. Jerome and M. E. Rose. Error estimates for the multidimensional two-phase Stefan problem. *Math. Comp.*, 39(160):377–414, 1982.
- [32] S. L. Kamenomostskaja. On Stefan’s problem. *Mat. Sb. (N.S.)*, 53 (95):489–514, 1961.
- [33] P. Ladevèze. Constitutive relation error estimators for time-dependent nonlinear FE analysis. *Comput. Methods Appl. Mech. Engrg.*, 4(188):775–788, 2000.
- [34] P. Ladevèze and L. Chamoin. Calculation of strict error bounds for finite element approximations of non-linear pointwise quantities of interest. *Internat. J. Numer. Methods Engrg.*, 84(13):1638–1664, 2010.
- [35] P. Ladevèze and D. Leguillon. Error estimate procedure in the finite element method and applications. *SIAM J. Numer. Anal.*, 20(3):485–509, 1983.
- [36] P. Ladevèze and N. Moës. A new a posteriori error estimation for nonlinear time-dependent finite element analysis. *Comput. Methods Appl. Mech. Engrg.*, 157(1-2):45–68, 1998.
- [37] Lake, L. W. *Enhanced Oil Recovery*. Old Tappan, NJ; Prentice Hall Inc., 1989.
- [38] A. Loseille, A. Dervieux, and F. Alauzet. Fully anisotropic goal-oriented mesh adaptation for 3D steady Euler equations. *J. Comput. Phys.*, 229(8):2866–2897, 2010.
- [39] R. Luce and B. I. Wohlmuth. A local a posteriori error estimator based on equilibrated fluxes. *SIAM J. Numer. Anal.*, 42(4):1394–1414, 2004.
- [40] D. Meidner, R. Rannacher, and J. Vihharev. Goal-oriented error control of the iterative solution of finite element equations. *J. Numer. Math.*, 17(2):143–172, 2009.
- [41] A. M. Meirmanov. *The Stefan problem*, volume 3 of *de Gruyter Expositions in Mathematics*. Walter de Gruyter & Co., Berlin, 1992. Translated from the Russian by Marek Niezgodka and Anna Crowley, With an appendix by the author and I. G. Götz.
- [42] G. H. Meyer. Multidimensional Stefan problems. *SIAM J. Numer. Anal.*, 10:522–538, 1973.
- [43] P. Neittaanmäki and S. Repin. *Reliable methods for computer simulation*, volume 33 of *Studies in Mathematics and its Applications*. Elsevier Science B.V., Amsterdam, 2004. Error control and a posteriori estimates.
- [44] R. H. Nochetto. Error estimates for multidimensional singular parabolic problems. *Japan J. Appl. Math.*, 4(1):111–138, 1987.
- [45] R. H. Nochetto, M. Paolini, and C. Verdi. An adaptive finite element method for two-phase Stefan problems in two space dimensions. I. Stability and error estimates. *Math. Comp.*, 57(195):73–108, 1991.

-
- [46] R. H. Nochetto, A. Schmidt, and C. Verdi. A posteriori error estimation and adaptivity for degenerate parabolic problems. *Math. Comp.*, 69(229):1–24, 2000.
- [47] J. T. Oden and S. Prudhomme. Goal-oriented error estimation and adaptivity for the finite element method. *Comput. Math. Appl.*, 41(5-6):735–756, 2001.
- [48] M. Picasso. An adaptive finite element algorithm for a two-dimensional stationary Stefan-like problem. *Comput. Methods Appl. Mech. Engrg.*, 124(3):213–230, 1995.
- [49] W. Prager and J. L. Synge. Approximations in elasticity based on the concept of function space. *Quart. Appl. Math.*, 5:241–269, 1947.
- [50] S. Repin. *A posteriori estimates for partial differential equations*, volume 4 of *Radon Series on Computational and Applied Mathematics*. Walter de Gruyter GmbH & Co. KG, Berlin, 2008.
- [51] A. H. Schatz and L. B. Wahlbin. Maximum norm estimates in the finite element method on plane polygonal domains. Part 1. *Math. Comp.*, 32:73–109, 1978.
- [52] A. H. Schatz and L. B. Wahlbin. Maximum norm estimates in the finite element method on plane polygonal domains. Part 2. Refinements. *Math. Comp.*, 33:465–492, 1979.
- [53] R. Verfürth. A review of a posteriori error estimation and adaptive mesh-refinement techniques. *Teubner-Wiley, Stuttgart*, 1996.
- [54] R. Verfürth. A posteriori error estimates for finite element discretizations of the heat equation. *Calcolo*, 40(3):195–212, 2003.
- [55] O. C. Zienkiewicz and J. Z. Zhu. A simple error estimator and adaptive procedure for practical engineering analysis. *Internat. J. Numer. Methods Engrg.*, 24(2):337–357, 1987.

Chapter 1

Adaptive regularization, linearization, and discretization and a posteriori error control for the two-phase Stefan problem

This chapter consists of an article accepted for publication in the journal Mathematics of Computation, written with Daniele Di Pietro and Martin Vohralik

Contents

1.1	Introduction	19
1.2	Continuous and discrete settings	22
1.2.1	Continuous setting	22
1.2.2	Discrete setting	24
1.3	An a posteriori error estimate for the dual norm of the residual	25
1.3.1	Dual norm of the residual	25
1.3.2	General assumptions	25
1.3.3	A basic a posteriori error estimate	26
1.3.4	An a posteriori error estimate distinguishing the space, time, regularization, linearization, and quadrature errors	28
1.4	Balancing and stopping criteria, adaptive algorithm, and efficiency	30
1.4.1	Balancing and stopping criteria	30
1.4.2	Adaptive algorithm	31
1.4.3	Efficiency of the a posteriori error estimate	33
1.5	An a posteriori error estimate for the error in temperature and enthalpy	34
1.5.1	Bounding the error of the temperature and enthalpy by the dual norm of the residual	34
1.5.2	The a posteriori error estimate	35

1.6	Application to a vertex-centered finite volume discretization . . .	37
1.6.1	Dual and tertial space meshes	37
1.6.2	The vertex-centered finite volume scheme	37
1.6.3	Newton linearization	38
1.6.4	Flux reconstruction	39
1.7	Numerical experiments	40
1.7.1	Setting	40
1.7.2	Computing approximately the negative norms	41
1.7.3	Stopping criteria	42
1.7.4	Balancing criteria	43
1.7.5	Overall performance	44
1.A	Proofs	48
1.A.1	Proof of Theorem 1.4.4	49
1.A.2	Proof of Theorem 1.5.2	51
	Bibliography	54

Abstract

We consider in this chapter the time-dependent two-phase Stefan problem and derive a posteriori error estimates and adaptive strategies for its conforming spatial and backward Euler temporal discretizations. Regularization of the enthalpy–temperature function and iterative linearization of the arising systems of nonlinear algebraic equations are considered. Our estimators yield a guaranteed and fully computable upper bound on the dual norm of the residual, as well as on the $L^2(L^2)$ error of the temperature and the $L^2(H^{-1})$ error of the enthalpy. Moreover, they allow to distinguish the space, time, regularization, and linearization error components. An adaptive algorithm is proposed, which ensures computational savings through the online choice of a sufficient regularization parameter, a stopping criterion for the linearization iterations, local space mesh refinement, time step adjustment, and equilibration of the spatial and temporal errors. We also prove the efficiency of our estimate. Our analysis is quite general and is not focused on a specific choice of the space discretization and of the linearization. As an example, we apply it to the vertex-centered finite volume (finite element with mass lumping and quadrature) and Newton methods. Numerical results illustrate the effectiveness of our estimates and the performance of the adaptive algorithm.

Key words: a posteriori error analysis, adaptive algorithms, two-phase Stefan problem, vertex-centered finite volume method, discretization error, regularization error, linearization error, adaptive mesh refinement.

1.1 Introduction

The two-phase Stefan problem models a phase change process which is governed by the Fourier law, Friedman [22]. The two phases, typically solid and liquid, are separated by a moving interface, whose motion is governed by the so-called Stefan condition. Let $\Omega \subset \mathbb{R}^d$, $d \in \{2, 3\}$, be an open bounded polygonal or polyhedral domain, not necessarily convex, and let $t_F > 0$. The mathematical statement of the problem is as follows: given an initial enthalpy u_0 and a source function f , find the enthalpy u such that

$$\partial_t u - \nabla \cdot (\nabla \beta(u)) = f \quad \text{in } \Omega \times (0, t_F), \quad (1.1.1a)$$

$$u(\cdot, 0) = u_0 \quad \text{in } \Omega, \quad (1.1.1b)$$

$$\beta(u) = 0 \quad \text{on } \partial\Omega \times (0, t_F). \quad (1.1.1c)$$

For the sake of simplicity, we assume that u is normalized so that the (specific) enthalpies of the two phases are 0 and 1, respectively, and only consider the homogeneous Dirichlet boundary condition (1.1.1c). The temperature $\beta(u)$ is expressed as a function of the enthalpy u . In what follows, we assume that $\beta(\cdot)$ is a nondecreasing Lipschitz continuous function which vanishes in the interval $(0, 1)$. The latter condition reflects the latent heat in the phase change.

The numerical analysis of the Stefan problem has been considered in several works. A finite difference method for the multi-dimensional Stefan problem is discussed in Meyer [32]. The author presents a convergent numerical scheme which is the implicit analogue of the method of Kamenomostskaja [27]. In Ciavaldini [12], the numerical approach is based on finite elements of first order. The author describes the different schemes used and the nature of their convergence. Elliott [16] presents a finite element approximation of an elliptic variational inequality deduced from a semi-discretization in time of the weak formulation of the two-phase Stefan problem. Discretization schemes for regularized versions of the Stefan problem based on piecewise linear Lagrange finite elements in space and backward differencing in time are presented by Jerome and Rose [25]. Jäger and Kačur [24] use the enthalpy formulation and a variational technique to analyze the convergence of linearized semi-discrete-in-time and fully discrete schemes for nonlinear degenerate parabolic systems of porous medium type. In Amiez and Gremaud [2], a numerical scheme based on the approximation of the enthalpy formulation by semi-implicit finite differences in time combined with continuous piecewise linear finite elements in space is presented. Nochetto [33] employs the regularization technique to derive a priori error estimates in $L^2(0, t_F; L^2(\Omega))$ for the enthalpy and temperature errors of respectively one half and first order for an implicit finite element scheme, under suitable conditions on the data and relation of the space and time steps.

More recently, attention has been paid to finite volume methods which can be used on a large variety of meshes. The framework of semigroup theory has been used by Baughman and Walkington [4] for the study of the co-volume method, which is a special instance of the finite volume method. The analysis predicts one half order rates of convergence for approximate solutions of the enthalpy in $L^\infty(0, t_F; H^{-1}(\Omega))$ and of the temperature in $L^2(0, t_F; L^2(\Omega))$. In Eymard et al. [21] the authors give a convergence proof in the case that a finite volume scheme on a general mesh is used for the space discretization. Weak-* convergence for u in L^∞ and strong convergence for $\beta(u)$ in L^2 is shown by means of a priori estimates in L^∞ and use of the Kolmogorov theorem on relative compactness of subsets of L^2 . Half order error estimates via regularization have also been obtained in Pop et al. [42], whereas extensions to degenerate hyperbolic–parabolic equations can be found in Andreianov et al. [3].

A technique often used in various numerical approaches, Nochetto [33], Nochetto and Verdi [37], Picasso [40], Beckett et al. [6], or Pop et al. [42], employs a regularization of the nonsmooth and nonstrictly increasing function β by a smooth and strictly increasing one. This allows, in particular, to use the Newton method for the solution of the arising system of nonlinear algebraic equations, albeit its use without regularization has been advocated in Wheeler [52] or in Baughman and Walkington [4] and studied in Kelley and Rulla [28]. Alternative approaches such as transformation of dependent variables of Čermák and Zlámal [10] have also been proposed.

An inevitable tool in practical simulations seems to be an a posteriori error estimate-driven adaptive mesh refinement. One of the first works on a posteriori error estimates for

the steady Stefan problem is that of Picasso [40]. Therein, the author derives estimates based on the residual equation for a two-dimensional regularized Stefan problem and proposes a space adaptive finite element algorithm. A posteriori indicators for unsteady phase change problems were derived by Nchetto et al. in [34, 35], together with an adaptive algorithm which equilibrates space and time discretization errors. Many other adaptive refinement algorithms such as that of Beckett et al. [6] have also been proposed. Rigorous a posteriori error estimates for nonlinear parabolic problems seem much less developed. In nondegenerate cases, Verfürth [46, 47] was able to obtain an estimator which is both reliable and efficient. A pioneering contribution for degenerate parabolic problems has been obtained by Nchetto et al. in [36]. Therein, $L^\infty(0, t_F; H^{-1}(\Omega))$ estimates for the error in the enthalpy and $L^2(0, t_F; L^2(\Omega))$ estimates for the error in the temperature are obtained. The approach is based on the relation of these errors to the residual of (1.1.1a) obtained through the corresponding dual partial differential equation and subsequent use of the Galerkin orthogonality of the finite element discretization. Recently, rigorous a posteriori error analysis in a space–time dual norm, including some degenerate cases, was given in [14].

The aim of this chapter is to derive fully computable a posteriori error estimates and adaptive strategies for the two-phase Stefan problem (1.1.1) for conforming spatial discretization schemes such as the finite element, co-volume, or vertex-centered finite volume ones with backward Euler time stepping. As in Nchetto et al. [36], our approach is based on the dual norm of the residual. However, we proceed differently in order to have a fully and easily computable estimates not featuring any undetermined constants. This is achieved by introducing $\mathbf{H}(\text{div}; \Omega)$ -conforming and locally conservative flux reconstructions following Prager–Synge [43], Ladevèze [29], Destuynder and Métivet [13], Luce and Wohlmuth [30], Braess and Schöberl [8], Repin [45], and [50, 18, 15, 14, 19], see also the references therein.

In Section 1.2 we give a weak formulation, introduce a regularized problem with a regularization parameter $\epsilon > 0$, and fix the notation for temporal and spatial meshes. In Section 1.3, we identify the residual and its dual norm and we derive an a posteriori error estimate on this problem-dependent error measure. We next split this estimate into estimators characterizing the space, time, regularization, linearization, and quadrature errors.

Section 1.4 subsequently presents a criterion for the choice of the regularization parameter ϵ and a stopping criterion for an iterative linearization such as the Newton method. The former is designed to facilitate the treatment of the degeneracy while not spoiling the accuracy, whereas the latter is designed to avoid performing an excessive number of nonlinear solver iterations. These criteria are inspired mainly from [26, 15, 19]. We then propose an adaptive algorithm which uses these criteria while simultaneously performing the usual local mesh refinement and equilibration of the spatial and temporal errors. This algorithm is inspired from [34, 35, 40, 36, 6] and from the work [18, 23, 14, 19]. We conclude Section 1.4 by proving that, under these criteria, our estimators are also efficient while representing a lower bound for the dual norm of the residual.

In Section 1.5, we show how to bound the $L^2(0, t_F; H^{-1}(\Omega))$ -type error in the enthalpy and $L^2(0, t_F; L^2(\Omega))$ -type error in the temperature by the above dual norm of the residual. We in particular focus on the use of the Gronwall lemma with as small overestimation as possible and no appearance of the exponential term e^{t_F} elsewhere than in the approximation of the initial condition. Guaranteed and fully computable a posteriori error estimates on these natural norms immediately follow.

Section 1.6 presents the application of all these developments to the vertex-centered finite volume (or, equivalently, finite element with mass lumping and numerical quadrature) discretization in space, backward Euler discretization in time, and Newton linearization. Illustrative numerical results fill up Section 1.7 and, finally, Appendix 1.A collects the more involved proofs of the various theorems of the chapter.

1.2 Continuous and discrete settings

This section fixes the basic continuous and discrete settings. More precisely, Section 1.2.1 presents the continuous problem and the regularization, whereas the basic assumptions on the discretization are introduced in Section 1.2.2.

1.2.1 Continuous setting

1.2.1.1 The continuous problem

The starting point for our a posteriori analysis is the weak form of problem (1.1.1). To give it, we need to introduce the assumptions on the data and set up some notation. We suppose that: (i) the enthalpy–temperature function $\beta : \mathbb{R} \rightarrow \mathbb{R}$ is a Lipschitz continuous function such that

$$\beta(s) = 0 \quad \text{in } (0, 1),$$

β is strictly increasing in \mathbb{R}^- and $\mathbb{R}^+ \setminus (0, 1)$, and there exist $c, C > 0$ such that, for all $s \in \mathbb{R} \setminus (0, 1)$, $\text{sign}(s)\beta(s) \geq c|s| - C$, see Figure 1.1; the Lipschitz constant of β is denoted by L_β ; (ii) the initial enthalpy u_0 is such that $u_0 \in L^2(\Omega)$; (iii) the source term is such that $f \in L^2(0, t_F; L^2(\Omega))$.

We will repeatedly use throughout the chapter the two following spaces:

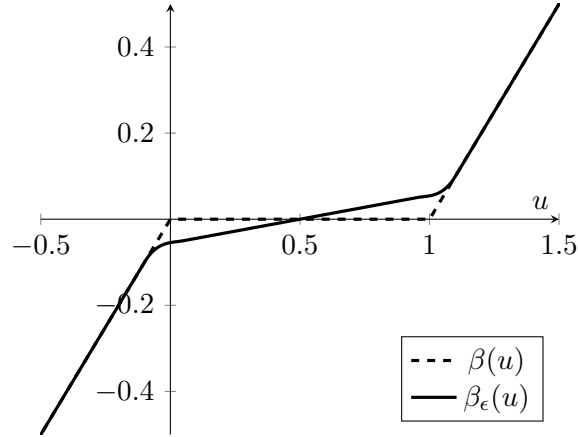
$$X := L^2(0, t_F; H_0^1(\Omega)), \quad Z := H^1(0, t_F; H^{-1}(\Omega)). \quad (1.2.1)$$

We will also need the dual space X' of X ,

$$X' = L^2(0, t_F; H^{-1}(\Omega)),$$

and equip the space X with the norm

$$\|\varphi\|_X := \left\{ \int_0^{t_F} \|\nabla\varphi(\cdot, t)\|_{L^2(\Omega)}^2 dt \right\}^{\frac{1}{2}}.$$

Figure 1.1: An example of a function β and a regularization β_ϵ

We denote by $\langle \cdot, \cdot \rangle$ the duality pairing between $H^{-1}(\Omega)$ and $H_0^1(\Omega)$, while $(\cdot, \cdot)_S$ is the usual scalar product in $L^2(S)$ or $[L^2(S)]^d$, with the subscript omitted when $S = \Omega$.

The weak formulation of problem (1.1.1) can now be stated. It reads: find

$$u \in Z \quad \text{with} \quad \beta(u) \in X \quad (1.2.2a)$$

such that

$$u(\cdot, 0) = u_0 \quad \text{in } \Omega \quad (1.2.2b)$$

and, for a.e. $s \in (0, t_F)$,

$$\langle \partial_t u(\cdot, s), \varphi \rangle + (\nabla \beta(u(\cdot, s)), \nabla \varphi) = (f(\cdot, s), \varphi) \quad \forall \varphi \in H_0^1(\Omega). \quad (1.2.2c)$$

Existence and uniqueness of the solution to this problem are known [22, 1, 38, 7].

1.2.1.2 A regularization

An important feature of the problem (1.2.2) is that, as a result of the assumptions on β , the normal component of the temperature flux $-\nabla \beta(u)$ may jump across the interface

$$I(t) := \{\mathbf{x} \in \Omega : \beta(u)(\mathbf{x}, t) = 0\}.$$

This fact may hinder both the design and the convergence analysis of a discretization method. Additionally, the lack of smoothness in the dependency of the solution on the problem data can severely affect the convergence of nonlinear iterations. A possible and often employed approach [33, 37, 40, 6] to overcome these difficulties consists in regularizing the problem (1.2.2) by replacing the function β by a smooth, strictly increasing regularized function $\beta_\epsilon \in C^1(\mathbb{R})$, $\beta'_\epsilon \geq \epsilon$, for a parameter $\epsilon > 0$; see Figure 1.1 for an example. The regularized problem reads as follows: find

$$u^\epsilon \in Z \quad \text{with} \quad \beta_\epsilon(u^\epsilon) \in X \quad (1.2.3a)$$

such that

$$u^\epsilon(\cdot, 0) = \beta_\epsilon^{-1}(\beta(u_0)) \quad \text{in } \Omega, \quad (1.2.3b)$$

and, for a.e. $s \in (0, t_F)$,

$$\langle \partial_t u^\epsilon(\cdot, s), \varphi \rangle + (\nabla \beta_\epsilon(u^\epsilon(\cdot, s)), \nabla \varphi) = (f(\cdot, s), \varphi) \quad \forall \varphi \in H_0^1(\Omega). \quad (1.2.3c)$$

1.2.2 Discrete setting

We describe here the basic discrete setting that will be sufficient for the developments of Sections 1.3–1.5. Further details are given in Section 1.6.

1.2.2.1 Time mesh

Our focus is on first-order time discretizations based on the backward Euler scheme. Let $\{\tau^n\}_{1 \leq n \leq N}$ denote a sequence of positive real numbers corresponding to the discrete time steps such that $t_F = \sum_{n=1}^N \tau^n$. We let $t^0 := 0$ and, for $1 \leq n \leq N$, we introduce the discrete times $t^n := \sum_{i=1}^n \tau^i$ and the time intervals $I_n := (t^{n-1}, t^n)$.

1.2.2.2 Space meshes

Let $\{\mathcal{K}^n\}_{0 \leq n \leq N}$ denote a family of matching simplicial meshes of the space domain Ω . The initial mesh \mathcal{K}^0 is used to approximate the initial condition u_0 , while \mathcal{K}^n is used to march in time from t^{n-1} to t^n . The meshes can be refined or coarsened as time evolves. For the developments of Section 1.4.3 below, we are led to suppose that \mathcal{K}^n , $1 \leq n \leq N$, is obtained from \mathcal{K}^{n-1} by refining (a limited number of times) some elements and coarsening (a limited number of times) some other ones. We denote by $\mathcal{K}^{n-1,n}$ the coarsest common submesh (overlay) of both \mathcal{K}^n and \mathcal{K}^{n-1} and, once again for the developments of Section 1.4.3, suppose that the meshes $\{\mathcal{K}^{n-1,n}\}_{1 \leq n \leq N}$ are shape-regular in the sense that there exists a constant $\kappa_{\mathcal{K}} > 0$ such that

$$\min_{K \in \mathcal{K}^{n-1,n}} \frac{\rho_K}{h_K} \geq \kappa_{\mathcal{K}}$$

for all $1 \leq n \leq N$, where ρ_K denotes the diameter of the largest ball inscribed in the element K and h_K the diameter of K . For $0 \leq n \leq N$, we denote by Π_0^n the L^2 -orthogonal projection onto the space of piecewise constant functions on \mathcal{K}^n .

For $0 \leq n \leq N$, let \mathcal{F}^n denote the set of mesh faces. Boundary faces are collected in the set $\mathcal{F}^{b,n} := \{F \in \mathcal{F}^n; F \subset \partial\Omega\}$ and we let $\mathcal{F}^{i,n} := \mathcal{F}^n \setminus \mathcal{F}^{b,n}$. For a given face $F \in \mathcal{F}^{i,n}$ we fix an arbitrary orientation and denote the corresponding unit normal vector by \mathbf{n}_F ; for $F \in \mathcal{F}^{b,n}$, \mathbf{n}_F coincides with the exterior unit normal \mathbf{n}_Ω of Ω . A similar notation for the faces $\mathcal{F}^{n-1,n}$ of the meshes $\mathcal{K}^{n-1,n}$ will also be used.

1.3 An a posteriori error estimate for the dual norm of the residual

In this section we derive an a posteriori estimate for the error measured by the dual norm of the residual that we first identify. We then give a basic estimate that we subsequently refine to distinguish the space, time, linearization, regularization, and quadrature errors.

1.3.1 Dual norm of the residual

As in Picasso [40] or Nochetto et al. [36], our key for deriving a posteriori error estimates for the Stefan problem (1.1.1) will be the residual and its dual norm. Recall that u denotes the weak solution of the Stefan problem given by (1.2.2) and the definition of the space X (1.2.1). Let $u_{h\tau} \in Z$ such that $\beta(u_{h\tau}) \in X$ be arbitrary. In practice, $u_{h\tau}$ will be the result of the numerical simulation. We define the residual $\mathcal{R}(u_{h\tau}) \in X'$ such that

$$\langle \mathcal{R}(u_{h\tau}), \varphi \rangle_{X', X} := \int_0^{t_F} \{ \langle \partial_t(u - u_{h\tau}), \varphi \rangle + (\nabla \beta(u) - \nabla \beta(u_{h\tau}), \nabla \varphi) \} (s) ds, \quad \varphi \in X. \quad (1.3.1)$$

Using (1.2.2c), we can infer the following alternative expression for (1.3.1):

$$\langle \mathcal{R}(u_{h\tau}), \varphi \rangle_{X', X} = \int_0^{t_F} \{ (f, \varphi) - \langle \partial_t u_{h\tau}, \varphi \rangle - (\nabla \beta(u_{h\tau}), \nabla \varphi) \} (s) ds, \quad \varphi \in X.$$

The norm of the residual in the dual space X' is then given by

$$\|\mathcal{R}(u_{h\tau})\|_{X'} := \sup_{\varphi \in X, \|\varphi\|_X=1} \langle \mathcal{R}(u_{h\tau}), \varphi \rangle_{X', X}. \quad (1.3.2)$$

The key problem-specific measure of the distance between $u_{h\tau}$ and u that we will use in this chapter is given by

$$\|\mathcal{R}(u_{h\tau})\|_{X'} + \|u_0 - u_{h\tau}(\cdot, 0)\|_{H^{-1}(\Omega)}. \quad (1.3.3)$$

It follows from (1.2.2) that the measure (1.3.3) is zero if and only if the function $u_{h\tau}$ coincides with the exact solution u . As we shall see below in Section 1.5, it in fact controls the energy error between u and $u_{h\tau}$ and $\beta(u)$ and $\beta(u_{h\tau})$. Moreover, this quantity can be easily bounded in terms of error estimators based on $\mathbf{H}(\text{div}; \Omega)$ -conforming flux reconstructions for piecewise affine-in-time $u_{h\tau}$ that we show next.

1.3.2 General assumptions

In order to proceed with the analysis further, without the necessity to specify at this point any details on how the approximate solution $u_{h\tau}$ was obtained, we are lead to make the following assumption. It requires Z - and X - conformity and $u_{h\tau}$ to be piecewise affine and continuous in time on the time mesh $\{I_n\}_{1 \leq n \leq N}$ of Section 1.2.2.1:

Assumption 1.3.1 (Approximate solution). *The function $u_{h\tau}$ is such that*

$$\begin{aligned} u_{h\tau} \in Z, \quad \partial_t u_{h\tau} \in L^2(0, t_F; L^2(\Omega)), \quad \beta(u_{h\tau}) \in X, \\ u_{h\tau}|_{I_n} \text{ is affine in time on } I_n \quad \forall 1 \leq n \leq N. \end{aligned}$$

Note that, consequently, the function $u_{h\tau}$ is uniquely determined by the $N + 1$ functions $u_h^n := u_{h\tau}(\cdot, t^n)$, $0 \leq n \leq N$, and $\partial_t u_{h\tau}^n := \partial_t u_{h\tau}|_{I_n} \equiv (u_h^n - u_h^{n-1})/\tau^n$, $1 \leq n \leq N$. We will also employ the abridged notation $u_{h\tau}^n$ for $u_{h\tau}|_{I_n}$.

The second assumption that we make is the existence of a piecewise constant-in-time $\mathbf{H}(\text{div}; \Omega)$ -conforming flux reconstruction \mathbf{t}_h , locally conservative on the meshes \mathcal{K}^n of Section 1.2.2.2. Let us first denote by \hat{f} the piecewise constant-in-time function given by the time-mean values of the source function f on the intervals I_n , $1 \leq n \leq N$.

Assumption 1.3.2 (Equilibrated flux reconstruction). *For all $1 \leq n \leq N$, there exists a vector field $\mathbf{t}_h^n \in \mathbf{H}(\text{div}; \Omega)$ such that*

$$(\nabla \cdot \mathbf{t}_h^n, 1)_K = (\hat{f}^n, 1)_K - (\partial_t u_{h\tau}^n, 1)_K \quad \forall K \in \mathcal{K}^n.$$

We denote by \mathbf{t}_h the space-time function such that $\mathbf{t}_h|_{I_n} := \mathbf{t}_h^n$ for all $1 \leq n \leq N$.

In Section 1.6 below, we show how to construct an equilibrated flux reconstruction \mathbf{t}_h in the context of vertex-centered finite volume (finite element with mass lumping and quadrature) spatial discretization.

1.3.3 A basic a posteriori error estimate

We now give an a posteriori error estimate in the general setting of Assumptions 1.3.1 and 1.3.2. Note that the regularization of Section 1.2.1.2 is not used at the present stage.

We will estimate the error measure (1.3.3) by the local residual expressed with the flux \mathbf{t}_h and by the difference of \mathbf{t}_h and the temperature flux, in the spirit of [43, 29, 13, 30, 8, 45] and [50, 18, 15, 14, 19]. More specifically, for $1 \leq n \leq N$, \mathbf{t}_h^n as in Assumption 1.3.2, and $K \in \mathcal{K}^n$, we define the *residual estimator* $\eta_{R,K}^n$ and the *flux estimator* $\eta_{F,K}^n$ as follows:

$$\eta_{R,K}^n := C_{P,K} h_K \left\| \hat{f}^n - \partial_t u_{h\tau}^n - \nabla \cdot \mathbf{t}_h^n \right\|_{L^2(K)}, \quad (1.3.4a)$$

$$\eta_{F,K}^n(t) := \left\| \mathbf{t}_h^n + \nabla \beta(u_{h\tau}(\cdot, t)) \right\|_{L^2(K)} \quad t \in I_n. \quad (1.3.4b)$$

Here, $C_{P,K}$ is the constant from the Poincaré inequality

$$\|\varphi - \Pi_0^n \varphi\|_{L^2(K)} \leq C_{P,K} h_K \|\nabla \varphi\|_{L^2(K)} \quad \forall \varphi \in H^1(K). \quad (1.3.5)$$

There holds $C_{P,K} = 1/\pi$ as the simplices K are convex, see [5, 39]. Finally, we define the *initial condition estimator* by

$$\eta_{IC} := \|u_0 - u_{h\tau}(\cdot, 0)\|_{H^{-1}(\Omega)}. \quad (1.3.6)$$

We then have:

Theorem 1.3.3 (A posteriori estimate for the error measure (1.3.3)). *Let u be the weak solution given by (1.2.2) and let $u_{h\tau}$ and \mathbf{t}_h fulfill Assumptions 1.3.1 and 1.3.2, respectively. Then, there holds*

$$\|\mathcal{R}(u_{h\tau})\|_{X'} + \|u_0 - u_{h\tau}(\cdot, 0)\|_{H^{-1}(\Omega)} \leq \eta + \eta_{\text{IC}}, \quad (1.3.7)$$

where

$$\eta := \left\{ \sum_{n=1}^N \int_{I_n} \sum_{K \in \mathcal{K}^n} (\eta_{\mathbb{R},K}^n + \eta_{\mathbb{F},K}^n(t))^2 dt \right\}^{\frac{1}{2}} + \|f - \hat{f}\|_{X'}. \quad (1.3.8)$$

Proof. Let $\varphi \in X$ with $\|\varphi\|_X = 1$ be given. Then there holds, adding and subtracting $(\mathbf{t}_h, \nabla\varphi)$ and using Green's theorem,

$$\begin{aligned} \langle \mathcal{R}(u_{h\tau}), \varphi \rangle_{X',X} &= \int_0^{t_{\text{F}}} \{ (f - \partial_t u_{h\tau} - \nabla \cdot \mathbf{t}_h, \varphi) - (\mathbf{t}_h + \nabla \beta(u_{h\tau}), \nabla \varphi) \} (s) ds \\ &= \int_0^{t_{\text{F}}} \{ (f - \hat{f}, \varphi) + (\hat{f} - \partial_t u_{h\tau} - \nabla \cdot \mathbf{t}_h, \varphi) - (\mathbf{t}_h + \nabla \beta(u_{h\tau}), \nabla \varphi) \} (s) ds \\ &=: \mathfrak{I}_1 + \mathfrak{I}_2 + \mathfrak{I}_3. \end{aligned}$$

For the first term we infer $\mathfrak{I}_1 \leq \|f - \hat{f}\|_{X'} \|\varphi\|_X = \|f - \hat{f}\|_{X'}$. The second term can be rewritten as follows:

$$\mathfrak{I}_2 = \sum_{n=1}^N \int_{I_n} (\hat{f}^n - \partial_t u_{h\tau}^n - \nabla \cdot \mathbf{t}_h^n, \varphi)(s) ds.$$

For all $1 \leq n \leq N$ and $t \in I_n$, there holds (the dependence of φ on the time variable is omitted for brevity),

$$\begin{aligned} (\hat{f}^n - \partial_t u_{h\tau}^n - \nabla \cdot \mathbf{t}_h^n, \varphi) &= \sum_{K \in \mathcal{K}^n} (\hat{f}^n - \partial_t u_{h\tau}^n - \nabla \cdot \mathbf{t}_h^n, \varphi)_K \\ &= \sum_{K \in \mathcal{K}^n} (\hat{f}^n - \partial_t u_{h\tau}^n - \nabla \cdot \mathbf{t}_h^n, \varphi - \Pi_0^n \varphi)_K \\ &\leq \sum_{K \in \mathcal{K}^n} \left\| \hat{f}^n - \partial_t u_{h\tau}^n - \nabla \cdot \mathbf{t}_h^n \right\|_{L^2(K)} \|\varphi - \Pi_0^n \varphi\|_{L^2(K)} \\ &\leq \sum_{K \in \mathcal{K}^n} C_{\text{P},K} h_K \left\| \hat{f}^n - \partial_t u_{h\tau}^n - \nabla \cdot \mathbf{t}_h^n \right\|_{L^2(K)} \|\nabla \varphi\|_{L^2(K)} \\ &= \sum_{K \in \mathcal{K}^n} \eta_{\mathbb{R},K}^n \|\nabla \varphi\|_{L^2(K)}, \end{aligned}$$

where we have used the regularity of the arguments, Assumption 1.3.2, the Cauchy–Schwarz inequality, and the Poincaré inequality (1.3.5). For the third term, an application of the Cauchy–Schwarz inequality yields

$$\mathfrak{I}_3 \leq \sum_{n=1}^N \int_{I_n} \sum_{K \in \mathcal{K}^n} \eta_{\mathbb{F},K}^n \|\nabla \varphi\|_{L^2(K)}(s) ds.$$

Collecting the above estimates, using the definition (1.3.2) of the dual norm of the residual, and using the Cauchy–Schwarz inequality yields (1.3.7). \square

1.3.4 An a posteriori error estimate distinguishing the space, time, regularization, linearization, and quadrature errors

Our next goal is to distinguish the different error components. This is an instrumental step to design an adaptive algorithm where the time step, the space mesh, the regularization parameter, and the stopping criterion for the linearization iterations are chosen optimally. We start by localizing in time the error measure introduced in Section 1.3.1. For $1 \leq n \leq N$, we let

$$X_n := L^2(I_n; H_0^1(\Omega)), \quad Z_n := H^1(I_n; H^{-1}(\Omega)).$$

We localize in time the dual norm of the residual (1.3.2) by setting

$$\|\mathcal{R}(u_{h\tau})\|_{X'_n} := \sup_{\varphi \in X_n, \|\varphi\|_{X_n}=1} \int_{I_n} \{(\partial_t(u - u_{h\tau}), \varphi) + (\nabla\beta(u) - \nabla\beta(u_{h\tau}), \nabla\varphi)\} (s) ds. \quad (1.3.9)$$

Note that, consequently,

$$\|\mathcal{R}(u_{h\tau})\|_{X'}^2 = \sum_{n=1}^N \|\mathcal{R}(u_{h\tau})\|_{X'_n}^2$$

for any $u_{h\tau} \in Z$ with $\beta(u_{h\tau}) \in X$.

Suppose now that we are marching in time from time t^{n-1} to time t^n with a given time step τ^n , starting from the approximation u_h^{n-1} . We also suppose that the regularization of Section 1.2.1.2 has been used for a given value of the parameter ϵ , and that we are on the k -th step of some iterative linearization algorithm. We denote by $u_h^{n,\epsilon,k}$ the approximation of the solution u at time t^n and prescribe the space–time function $u_{h\tau}^{n,\epsilon,k}$ by the value u_h^{n-1} at time t^{n-1} , by the value $u_h^{n,\epsilon,k}$ at time t^n , and by affine behavior in time on I_n , i.e.,

$$u_{h\tau}^{n,\epsilon,k}(\cdot, t) = (1 - \rho(t))u_h^{n-1} + \rho(t)u_h^{n,\epsilon,k}, \quad \rho(t) := \frac{t - t^{n-1}}{\tau^n}. \quad (1.3.10)$$

We summarize our general requirements in the following:

Assumption 1.3.4 (Adaptive setting). *For all $1 \leq n \leq N$, a regularization parameter $\epsilon \geq 0$, and a linearization step $k \geq 1$:*

(i) $u_{h\tau}^{n,\epsilon,k}$ is the approximate solution given by (1.3.10), $u_{h\tau}^{n,\epsilon,k} \in Z_n$ with $\partial_t u_{h\tau}^{n,\epsilon,k} \in L^2(I_n; L^2(\Omega))$ and $\beta(u_{h\tau}^{n,\epsilon,k}) \in X_n$;

(ii) there exists an equilibrated flux $\mathbf{t}_h^{n,\epsilon,k} \in \mathbf{H}(\text{div}; \Omega)$ such that

$$(\nabla \cdot \mathbf{t}_h^{n,\epsilon,k}, 1)_K = (\hat{f}^n, 1)_K - (\partial_t u_{h\tau}^{n,\epsilon,k}, 1)_K \quad \forall K \in \mathcal{K}^n; \quad (1.3.11)$$

(iii) $\mathbf{l}_h^{n,\epsilon,k} \in [L^2(\Omega)]^d$ is the available approximation of the flux $\nabla\beta_\epsilon(u(\cdot, t^n))$;

(iv) Π^n is an operator used for interpolatory numerical integration.

An example of the approximate solution $u_{h\tau}^{n,\epsilon,k}$, the linearized flux $\mathbf{l}_h^{n,\epsilon,k}$, and the operator Π^n in the context of the implicit vertex-centered finite volume discretization and Newton linearization is provided in Section 1.6.3 below.

Proceeding as in Theorem 1.3.3, it is immediately inferred

$$\left\| \mathcal{R}(u_{h\tau}^{n,\epsilon,k}) \right\|_{X'_n} \leq \left\{ \int_{I_n} \sum_{K \in \mathcal{K}^n} \left(\eta_{R,K}^{n,\epsilon,k} + \eta_{F,K}^{n,\epsilon,k}(t) \right)^2 dt \right\}^{\frac{1}{2}} + \|f - \hat{f}\|_{X'_n}, \quad (1.3.12)$$

where

$$\begin{aligned} \eta_{R,K}^{n,\epsilon,k} &:= C_{P,K} h_K \left\| \hat{f}^n - \partial_t u_{h\tau}^{n,\epsilon,k} - \nabla \cdot \mathbf{t}_h^{n,\epsilon,k} \right\|_{L^2(K)}, \\ \eta_{F,K}^{n,\epsilon,k}(t) &:= \left\| \mathbf{t}_h^{n,\epsilon,k} + \nabla \beta(u_{h\tau}^{n,\epsilon,k}(\cdot, t)) \right\|_{L^2(K)}, \quad t \in I_n. \end{aligned}$$

For all $K \in \mathcal{K}^n$, we next define the local *spatial*, *temporal*, *quadrature*, *regularization*, and *linearization estimators* as follows:

$$\eta_{\text{sp},K}^{n,\epsilon,k} := \eta_{R,K}^{n,\epsilon,k} + \left\| \mathbf{l}_h^{n,\epsilon,k} + \mathbf{t}_h^{n,\epsilon,k} \right\|_{L^2(K)}, \quad (1.3.13a)$$

$$\eta_{\text{tm},K}^{n,\epsilon,k}(t) := \left\| \nabla(\Pi^n \beta(u_{h\tau}^{n,\epsilon,k}(\cdot, t))) - \nabla(\Pi^n \beta(u_h^{n,\epsilon,k})) \right\|_{L^2(K)}, \quad t \in I_n, \quad (1.3.13b)$$

$$\eta_{\text{qd},K}^{n,\epsilon,k}(t) := \left\| \nabla(\beta(u_{h\tau}^{n,\epsilon,k}(\cdot, t))) - \nabla(\Pi^n \beta(u_{h\tau}^{n,\epsilon,k}(\cdot, t))) \right\|_{L^2(K)}, \quad t \in I_n, \quad (1.3.13c)$$

$$\eta_{\text{reg},K}^{n,\epsilon,k} := \left\| \nabla(\Pi^n \beta(u_h^{n,\epsilon,k})) - \nabla(\Pi^n \beta_\epsilon(u_h^{n,\epsilon,k})) \right\|_{L^2(K)}, \quad (1.3.13d)$$

$$\eta_{\text{lin},K}^{n,\epsilon,k} := \left\| \nabla(\Pi^n \beta_\epsilon(u_h^{n,\epsilon,k})) - \mathbf{l}_h^{n,\epsilon,k} \right\|_{L^2(K)}. \quad (1.3.13e)$$

Global versions of these estimators are given by,

$$(\eta_{\text{sp}}^{n,\epsilon,k})^2 := \tau^n \sum_{K \in \mathcal{K}^n} \left(\eta_{\text{sp},K}^{n,\epsilon,k} \right)^2, \quad (1.3.14a)$$

$$(\eta_{\text{tm}}^{n,\epsilon,k})^2 := \int_{I_n} \sum_{K \in \mathcal{K}^n} \left(\eta_{\text{tm},K}^{n,\epsilon,k}(t) \right)^2 dt, \quad (1.3.14b)$$

$$(\eta_{\text{qd}}^{n,\epsilon,k})^2 := \int_{I_n} \sum_{K \in \mathcal{K}^n} \left(\eta_{\text{qd},K}^{n,\epsilon,k}(t) \right)^2 dt, \quad (1.3.14c)$$

$$(\eta_{\text{reg}}^{n,\epsilon,k})^2 := \tau^n \sum_{K \in \mathcal{K}^n} \left(\eta_{\text{reg},K}^{n,\epsilon,k} \right)^2, \quad (1.3.14d)$$

$$(\eta_{\text{lin}}^{n,\epsilon,k})^2 := \tau^n \sum_{K \in \mathcal{K}^n} \left(\eta_{\text{lin},K}^{n,\epsilon,k} \right)^2. \quad (1.3.14e)$$

Using the inequality (1.3.12) followed by the triangle inequality we obtain the following estimate:

Corollary 1.3.5 (Distinguishing the space, time, quadrature, regularization, linearization, and data oscillation errors). *Let u be the weak solution given by (1.2.2), let $1 \leq n \leq N$, $\epsilon \geq 0$,*

and $k \geq 1$, and let $u_{h\tau}^{n,\epsilon,k}$, $\mathbf{t}_h^{n,\epsilon,k}$, $\mathbf{l}_h^{n,\epsilon,k}$, and Π^n be as described in Assumption 1.3.4. Then there holds

$$\left\| \mathcal{R}(u_{h\tau}^{n,\epsilon,k}) \right\|_{X'_n} \leq \eta_{\text{sp}}^{n,\epsilon,k} + \eta_{\text{tm}}^{n,\epsilon,k} + \eta_{\text{qd}}^{n,\epsilon,k} + \eta_{\text{reg}}^{n,\epsilon,k} + \eta_{\text{lin}}^{n,\epsilon,k} + \left\| f - \hat{f} \right\|_{X'_n}.$$

Remark 1.3.6 (Time oscillation of the source term). *The error due to the time oscillation of the source term $\left\| f - \hat{f} \right\|_{X'_n}$ is zero provided that the source function f is piecewise constant in time.*

1.4 Balancing and stopping criteria, adaptive algorithm, and efficiency

The individual error component estimators of Corollary 1.3.5 are used in this section to define adaptive criteria to stop the iterative linearizations, to select the value of the regularization parameter ϵ , to locally adapt the quadrature rule, to adjust the time step, and to select the mesh elements to refine/derefine. These criteria are incorporated in a fully adaptive algorithm detailed in Section 1.4.2. Finally, in Section 1.4.3 we show the efficiency of our estimators when the adaptive balancing and stopping criteria are used.

1.4.1 Balancing and stopping criteria

Following [26, 15, 19], this section introduces stopping criteria for the iterative algorithms based on the estimators of Corollary 1.3.5. The goal is to stop the iterations as soon as the corresponding error component no longer affects significantly the overall error. We assume in what follows that we are marching in time from time t^{n-1} to time t^n . Let three user-given parameters $\Gamma_{\text{lin}}, \Gamma_{\text{reg}}, \Gamma_{\text{qd}} \in (0, 1)$ be given. The criteria are:

- (i) *Linearization.* The linearization iteration is pursued until step k_n such that

$$\eta_{\text{lin}}^{n,\epsilon,k_n} \leq \Gamma_{\text{lin}} \left(\eta_{\text{sp}}^{n,\epsilon,k_n} + \eta_{\text{tm}}^{n,\epsilon,k_n} + \eta_{\text{qd}}^{n,\epsilon,k_n} + \eta_{\text{reg}}^{n,\epsilon,k_n} \right). \quad (1.4.1)$$

- (ii) *Regularization.* The regularization parameter ϵ is reduced until the value ϵ_n such that

$$\eta_{\text{reg}}^{n,\epsilon_n,k_n} \leq \Gamma_{\text{reg}} \left(\eta_{\text{sp}}^{n,\epsilon_n,k_n} + \eta_{\text{tm}}^{n,\epsilon_n,k_n} + \eta_{\text{qd}}^{n,\epsilon_n,k_n} \right). \quad (1.4.2)$$

- (iii) *Quadrature.* The quadrature rule is improved until

$$\eta_{\text{qd}}^{n,\epsilon_n,k_n} \leq \Gamma_{\text{qd}} \left(\eta_{\text{sp}}^{n,\epsilon_n,k_n} + \eta_{\text{tm}}^{n,\epsilon_n,k_n} \right). \quad (1.4.3)$$

Note that all the linearization, regularization, and quadrature errors may be classified as subsidiary as they can be made as small as desired by increasing the computational effort for fixed mesh and time step; it is thus reasonable to expect that the above criteria will be

attained. Local, element by element, versions of the criteria (1.4.1)–(1.4.3) can be formulated using the local estimators (1.3.13) (see [26, 15, 19]), and require that the inequalities hold for all $K \in \mathcal{K}^n$; (1.7.4) for an example.

In the spirit of [41, 36, 48] and [18, 23, 14], we also propose the usual space–time adaptivity:

- (iv) *Space–time error balancing.* The space and time error components should be equilibrated by selecting the time step τ^n and adjusting the spatial meshes \mathcal{K}^n in such a way that

$$\gamma_{\text{tm}} \eta_{\text{sp}}^{n,\epsilon_n,k_n} \leq \eta_{\text{tm}}^{n,\epsilon_n,k_n} \leq \Gamma_{\text{tm}} \eta_{\text{sp}}^{n,\epsilon_n,k_n}. \quad (1.4.4)$$

Above, $\Gamma_{\text{tm}} > \gamma_{\text{tm}} > 0$ are again user-given parameters, typically close to 1.

- (v) *Adaptive mesh refinement.* The error in space should be evenly distributed throughout the domain Ω by local adaptation (refinement, coarsening) of the space mesh \mathcal{K}^n in such a way that, for all $K_1, K_2 \in \mathcal{K}^n$,

$$\eta_{\text{sp},K_1}^{n,\epsilon_n,k_n} \approx \eta_{\text{sp},K_2}^{n,\epsilon_n,k_n}.$$

In contrast to (1.4.1)–(1.4.3), the goal is to make $\eta_{\text{sp}}^{n,\epsilon_n,k_n}$ and $\eta_{\text{tm}}^{n,\epsilon_n,k_n}$ of comparable size as these error components are substantial and cannot be made arbitrarily small for a given choice of the mesh and of the time step.

1.4.2 Adaptive algorithm

In this section we propose an adaptive algorithm that implements the balancing and stopping criteria of Section 1.4.1. Moreover, for a prescribed $\zeta > 0$, we aim at satisfying the relation

$$\frac{\sum_{n=1}^N \|\mathcal{R}(u_{h\tau})\|_{X_n'}^2}{\sum_{n=1}^N \left\| \mathbf{t}_h^{n,\epsilon,k} \right\|_{L^2(I_n; L^2(\Omega))}^2} \leq \zeta^2, \quad (1.4.5)$$

i.e., to bring the relative error under the user-given precision ζ . To account for limited computing resources, we fix refinement thresholds $\underline{h}, \underline{\tau} > 0$ for both the mesh size and the time step and require, for all $0 \leq n \leq N$,

$$\min_{K \in \mathcal{K}^n} h_K \geq \underline{h}, \quad \tau^n \geq \underline{\tau}. \quad (1.4.6)$$

Note that, in particular because of (1.4.6), the attainment of (1.4.5) is not guaranteed.

Recall that $u_h^{n,\epsilon,k}$ stands for the approximation of the solution u_h^n at discrete time t^n obtained after k linearization iterations using a regularization parameter ϵ . At each linearization iteration k , the new approximation $u_h^{n,\epsilon,k}$ is obtained solving the linear problem written schematically as $u_h^{n,\epsilon,k} = \Psi(u_h^{n,\epsilon,k-1}, \tau^n, \mathcal{K}^n)$. For the sake of simplicity, in what follows we neglect the quadrature and data oscillation estimators. Our adaptive algorithm is the following:

Algorithm 1.4.1 (Adaptive algorithm).

Fix the fractions of cells to refine, c_{ref} , and to derefine, c_{deref}

Choose an initial mesh \mathcal{K}^0 , regularization parameter ϵ_0 , and a tolerance $\zeta_{\text{IC}} > 0$

$u_h^0 \leftarrow \Pi^0(\beta_{\epsilon_0}^{-1}(\beta(u_0)))$

repeat {Initial mesh and regularization parameter adaptation}

 Compute η_{IC}

 Refine the cells $K \in \mathcal{K}^0$ such that $\eta_{\text{IC},K} \geq c_{\text{ref}} \max_{L \in \mathcal{K}^0} \{\eta_{\text{IC},L}\}$ in accordance with (1.4.6) and adjust the regularization parameter ϵ_0

$u_h^0 \leftarrow \Pi^0(\beta_{\epsilon_0}^{-1}(\beta(u_0)))$

until $\eta_{\text{IC}} \leq \zeta_{\text{IC}} \|\nabla(\beta_{\epsilon_0}(u_h^0))\|_{L^2(\Omega)}$

Choose an initial time step τ^0

$\epsilon \leftarrow \epsilon_0, t^0 \leftarrow 0, n \leftarrow 0$

while $t^n \leq t_{\text{F}}$ **do** {Time loop}

$n \leftarrow n + 1$

$\mathcal{K}^n \leftarrow \mathcal{K}^{n-1}$

$\tau^n \leftarrow \tau^{n-1}$

$u_h^{n,\epsilon,0} \leftarrow u_h^{n-1}$

repeat {Space refinement}

repeat {Space and time error balancing}

repeat {Regularization}

$k \leftarrow 0$

repeat {Nonlinear solver}

$k \leftarrow k + 1$

$u_h^{n,\epsilon,k} = \Psi(u_h^{n,\epsilon,k-1}, \tau^n, \mathcal{K}^n)$

 Compute $\eta_{\text{sp}}^{n,\epsilon,k}, \eta_{\text{tm}}^{n,\epsilon,k}, \eta_{\text{reg}}^{n,\epsilon,k}, \eta_{\text{lin}}^{n,\epsilon,k}$

until (1.4.1) is satisfied

$k_n \leftarrow k$

if (1.4.2) does not hold **then**

$\epsilon \leftarrow \epsilon/2$

end if

until (1.4.2) is satisfied

$\epsilon_n \leftarrow \epsilon$

if $\eta_{\text{tm}}^{n,\epsilon_n,k_n} < \gamma_{\text{tm}} \eta_{\text{sp}}^{n,\epsilon_n,k_n}$ **then**

$\tau^n \leftarrow 2\tau^n$

else if $\eta_{\text{tm}}^{n,\epsilon_n,k_n} > \Gamma_{\text{tm}} \eta_{\text{sp}}^{n,\epsilon_n,k_n}$ and $\tau^n \geq 2\tau$ **then**

$\tau^n \leftarrow \tau^n/2$

end if

until (1.4.4) is satisfied or $\tau^n = \tau$

 Refine the cells $K \in \mathcal{K}^n$ such that $\eta_{\text{sp},K}^{n,\epsilon_n,k_n} \geq c_{\text{ref}} \max_{L \in \mathcal{K}^n} \{\eta_{\text{sp},L}^{n,\epsilon_n,k_n}\}$ in accordance

with (1.4.6)

until $\eta_{\text{sp},n,\epsilon_n,k_n}^+ \eta_{\text{tm}}^{n,\epsilon_n,k_n} + \eta_{\text{reg}}^{n,\epsilon_n,k_n} + \eta_{\text{lin}}^{n,\epsilon_n,k_n} \leq \zeta \left\| \mathbf{l}_h^{n,\epsilon_n,k_n} \right\|_{L^2(I_n;L^2(\Omega))}$ or $(h_K = \underline{h}, \forall K \in \mathcal{K}^n)$

Derefine the cells $K \in \mathcal{K}^n$ such that $\eta_{\text{sp},K}^{n,\epsilon_n,k_n} \leq c_{\text{deref}} \max_{L \in \mathcal{K}^n} \{ \eta_{\text{sp},L}^{n,\epsilon_n,k_n} \}$

$u_h^n \leftarrow u_h^{n,\epsilon_n,k_n}$

$t^n \leftarrow t^{n-1} + \tau^n$

$\epsilon \leftarrow 2\epsilon$

end while

1.4.3 Efficiency of the a posteriori error estimate

In this section we investigate the global efficiency of the estimators of Corollary 1.3.5 under the stopping and balancing criteria of Section 1.4.1. Hence, the quantities at discrete time t^n are those obtained after performing k_n linearization iterations to meet the criterion (1.4.1), using a regularization parameter ϵ_n and a quadrature rule such that, respectively, (1.4.2) and (1.4.3) are satisfied, and a time step ensuring the time and space error balance (1.4.4). As usual, in order to use the argument of equivalence of norms on finite-dimensional spaces, we need to assume here:

Assumption 1.4.2 (Polynomial approximations). *For all $1 \leq n \leq N$, the function $u_{h\tau}^{n,\epsilon_n,k_n}$ is affine in time on the time interval I_n and piecewise polynomial of order m in space on the mesh $\mathcal{K}^{n-1,n}$; the functions $\mathbf{l}_h^{n,\epsilon_n,k_n}$ and $\mathbf{t}_h^{n,\epsilon_n,k_n}$ are piecewise polynomial of order m in space on $\mathcal{K}^{n-1,n}$.*

For $1 \leq n \leq N$, we introduce the standard residual-based a posteriori error estimators, [48]:

$$(\eta_{\text{res},1}^n)^2 := \tau^n \sum_{K \in \mathcal{K}^{n-1,n}} h_K^2 \left\| \hat{f}^n - \partial_t u_{h\tau}^{n,\epsilon_n,k_n} + \nabla \cdot \mathbf{l}_h^{n,\epsilon_n,k_n} \right\|_{L^2(K)}^2, \quad (1.4.7a)$$

$$(\eta_{\text{res},2}^n)^2 := \tau^n \sum_{F \in \mathcal{F}^{i,n-1,n}} h_F \left\| \llbracket \mathbf{l}_h^{n,\epsilon_n,k_n} \rrbracket \cdot \mathbf{n}_F \right\|_{L^2(F)}^2. \quad (1.4.7b)$$

Let C be a generic constant only depending on the shape regularity parameter $\kappa_{\mathcal{K}}$ of the meshes $\mathcal{K}^{n-1,n}$, $1 \leq n \leq N$, the space dimension d , and the polynomial degree m . In order to still proceed generally, without the specification of a particular spatial discretization scheme, we will suppose the following:

Assumption 1.4.3 (Approximation property). *For all $1 \leq n \leq N$, there holds*

$$\tau^n \sum_{K \in \mathcal{K}^{n-1,n}} \left\| \mathbf{l}_h^{n,\epsilon_n,k_n} + \mathbf{t}_h^{n,\epsilon_n,k_n} \right\|_{L^2(K)}^2 \leq C \left((\eta_{\text{res},1}^n)^2 + (\eta_{\text{res},2}^n)^2 \right). \quad (1.4.8)$$

This property will be verified in Section 1.6 below for the vertex-centered finite volume spatial discretization and specific constructions of the fluxes $\mathbf{t}_h^{n,\epsilon_n,k_n}$ and $\mathbf{l}_h^{n,\epsilon_n,k_n}$.

Under these assumptions, we have the following result, showing the equivalence of the error $\left\| \mathcal{R}(u_{h\tau}^{n,\epsilon_n,k_n}) \right\|_{X'_n}$ and the estimators of Corollary 1.3.5, up to data oscillation:

Theorem 1.4.4 (Global efficiency). *Let, for all $1 \leq n \leq N$, the stopping criteria (1.4.1)–(1.4.3) as well as the second inequality in the balancing criterion (1.4.4) be satisfied with the parameters Γ_{lin} , Γ_{reg} , Γ_{qd} , and Γ_{tm} small enough. Let Assumptions 1.4.2 and 1.4.3 hold true. Then*

$$\eta_{\text{sp}}^{n,\epsilon_n,k_n} + \eta_{\text{tm}}^{n,\epsilon_n,k_n} + \eta_{\text{qd}}^{n,\epsilon_n,k_n} + \eta_{\text{reg}}^{n,\epsilon_n,k_n} + \eta_{\text{lin}}^{n,\epsilon_n,k_n} \leq C \left(\left\| \mathcal{R}(u_{h\tau}^{n,\epsilon_n,k_n}) \right\|_{X'_n} + \left\| f - \hat{f} \right\|_{X'_n} \right).$$

The proof of this result follows the techniques of [49] and the approach of [15]. It is given in Appendix 1.A.1.

1.5 An a posteriori error estimate for the error in temperature and enthalpy

In the previous sections we have given a posteriori error estimators for the dual norm of the residual. In this section we prove that these same estimators also bound an error in temperature and enthalpy. We rely on a duality argument which reveals simpler than using the dual partial differential equation as in [36].

1.5.1 Bounding the error of the temperature and enthalpy by the dual norm of the residual

For brevity of notation we let for $t \in (0, t_{\text{F}}]$,

$$Q_t := L^2(0, t; L^2(\Omega)), \quad X_t := L^2(0, t; H_0^1(\Omega)), \quad X'_t := L^2(0, t; H^{-1}(\Omega)).$$

It is convenient to stress that the result of this section applies to all functions $u_{h\tau} \in Z$ such that $\beta(u_{h\tau}) \in X$. We first state the following bound:

Lemma 1.5.1 (Simple bounds for the temperature and enthalpy errors). *Let u be the solution of (1.2.2) and let $u_{h\tau} \in Z$ be such that $\beta(u_{h\tau}) \in X$. Then there holds*

$$\begin{aligned} \frac{L_\beta}{2} \|u - u_{h\tau}\|_{X'}^2 + \frac{L_\beta}{2} \|(u - u_{h\tau})(\cdot, t_{\text{F}})\|_{H^{-1}(\Omega)}^2 + \|\beta(u) - \beta(u_{h\tau})\|_{Q_{t_{\text{F}}}}^2 \\ \leq \frac{L_\beta}{2} (2e^{t_{\text{F}}} - 1) \left(\|\mathcal{R}(u_{h\tau})\|_{X'}^2 + \|u_0 - u_{h\tau}(\cdot, 0)\|_{H^{-1}(\Omega)}^2 \right), \end{aligned}$$

and

$$\frac{L_\beta}{2} \|(u - u_{h\tau})(\cdot, t_{\text{F}})\|_{H^{-1}(\Omega)}^2 + \|\beta(u) - \beta(u_{h\tau})\|_{Q_{t_{\text{F}}}}^2 \leq \frac{L_\beta}{2} e^{t_{\text{F}}} \left(\|\mathcal{R}(u_{h\tau})\|_{X'}^2 + \|u_0 - u_{h\tau}(\cdot, 0)\|_{H^{-1}(\Omega)}^2 \right).$$

The results of Lemma 1.5.1 are classical; we obtain them as a byproduct in the proof of Theorem 1.5.2 in Section 1.A.2 below. These results are, however, not sufficiently precise. In particular, the use of the Gronwall lemma in its proof implies the appearance of the term e^{t_F} on the right-hand sides, which grows exponentially with the final time t_F . The purpose of the following theorem is to improve considerably this point. Indeed, note that, in Theorem 1.5.2, the term e^{t_F} does not appear elsewhere than in the approximation of the initial condition $\|u_0 - u_{h\tau}(\cdot, 0)\|_{H^{-1}(\Omega)}^2$ which can be made sufficiently small. Theorem 1.5.2 takes a more complicated form than Lemma 1.5.1 but the numerical results based on its use, see Section 1.7, reveal excellent, which is not the case for the framework of Lemma 1.5.1:

Theorem 1.5.2 (An improved bound for the temperature and enthalpy errors). *Let u be the solution of (1.2.2) and let $u_{h\tau} \in Z$ be such that $\beta(u_{h\tau}) \in X$. Then there holds*

$$\begin{aligned} & \frac{L_\beta}{2} \|u - u_{h\tau}\|_{X'}^2 + \frac{L_\beta}{2} \|(u - u_{h\tau})(\cdot, t_F)\|_{H^{-1}(\Omega)}^2 + \|\beta(u) - \beta(u_{h\tau})\|_{Q_{t_F}}^2 \\ & + 2 \int_0^{t_F} \left(\|\beta(u) - \beta(u_{h\tau})\|_{Q_t}^2 + \int_0^t \|\beta(u) - \beta(u_{h\tau})\|_{Q_s}^2 e^{t-s} ds \right) dt \\ & \leq \frac{L_\beta}{2} \left\{ (2e^{t_F} - 1) \|u_0 - u_{h\tau}(\cdot, 0)\|_{H^{-1}(\Omega)}^2 + \|\mathcal{R}(u_{h\tau})\|_{X'}^2 \right. \\ & \left. + 2 \int_0^{t_F} \left(\|\mathcal{R}(u_{h\tau})\|_{X'_t}^2 + \int_0^t \|\mathcal{R}(u_{h\tau})\|_{X'_s}^2 e^{t-s} ds \right) dt \right\}. \end{aligned}$$

The proof of this result is given in Section 1.A.2.

1.5.2 The a posteriori error estimate

The upper bound in Theorem 1.5.2 can be combined with the results of Section 1.3.3 to obtain an a posteriori estimate for the temperature and enthalpy errors.

Theorem 1.5.3 (A posteriori estimate for the temperature and enthalpy errors). *Let u be the solution of (1.2.2) and let $u_{h\tau}$ and \mathbf{t}_h fulfill Assumptions 1.3.1 and 1.3.2, respectively. Then there holds*

$$\begin{aligned} & \frac{L_\beta}{2} \|u - u_{h\tau}\|_{X'}^2 + \frac{L_\beta}{2} \|(u - u_{h\tau})(\cdot, t_F)\|_{H^{-1}(\Omega)}^2 + \|\beta(u) - \beta(u_{h\tau})\|_{Q_{t_F}}^2 \\ & + 2 \int_0^{t_F} \left(\|\beta(u) - \beta(u_{h\tau})\|_{Q_t}^2 + \int_0^t \|\beta(u) - \beta(u_{h\tau})\|_{Q_s}^2 e^{t-s} ds \right) dt \\ & \leq \frac{L_\beta}{2} \left\{ (2e^{t_F} - 1) \eta_{\text{IC}}^2 + \eta^2 \right. \\ & \left. + 2 \left(\sum_{n=1}^N \tau^n \sum_{l=1}^n (\eta^l)^2 + \sum_{n=1}^N \sum_{l=1}^n J_{nl} \left\{ \sum_{i=1}^l (\eta^i)^2 \right\} \right) \right\}, \end{aligned} \tag{1.5.1}$$

with η_{IC} defined by (1.3.6), η defined by (1.3.8), η^n , $1 \leq n \leq N$, defined by

$$\eta^n := \left\{ \int_{I_n} \sum_{K \in \mathcal{K}^n} (\eta_{\text{R},K}^n + \eta_{\text{F},K}^n(t))^2 dt \right\}^{\frac{1}{2}} + \|f - \hat{f}\|_{X'_n}, \quad (1.5.2)$$

and setting, for $1 \leq n, l \leq N$,

$$J_{nl} := \int_{I_n} \int_{I_l} e^{t-s} ds dt.$$

Proof. To prove the result, we rely on Theorem 1.5.2. Applying Theorem 1.3.3, it follows that $\|\mathcal{R}(u_{h\tau})\|_{X'} \leq \eta$, so we are left to estimate the following right-hand side contributions in terms of the a posteriori error estimators:

$$\mathfrak{J}_1 := \int_0^{t_{\text{F}}} \|\mathcal{R}(u_{h\tau})\|_{X'_t}^2 dt, \quad \mathfrak{J}_2 := \int_0^{t_{\text{F}}} \left(\int_0^t \|\mathcal{R}(u_{h\tau})\|_{X'_s}^2 e^{t-s} ds \right) dt.$$

As in Theorem 1.3.3, it is readily inferred that $\|\mathcal{R}(u_{h\tau})\|_{X'_l} \leq \eta^l$ for all $1 \leq l \leq N$, so that

$$\|\mathcal{R}(u_{h\tau})\|_{X'_{t_n}}^2 = \sum_{l=1}^n \|\mathcal{R}(u_{h\tau})\|_{X'_l}^2 \leq \sum_{l=1}^n (\eta^l)^2.$$

Using the fact that $\|\mathcal{R}(u_{h\tau})\|_{X'_t}$ is a nondecreasing function of the time t together with the above inequality yields for the first term

$$\mathfrak{J}_1 \leq \sum_{n=1}^N \int_{I_n} \|\mathcal{R}(u_{h\tau})\|_{X'_{t_n}}^2 dt \leq \sum_{n=1}^N \int_{I_n} \sum_{l=1}^n (\eta^l)^2 dt = \sum_{n=1}^N \tau^n \sum_{l=1}^n (\eta^l)^2.$$

Proceeding in a similar way, for the second term \mathfrak{J}_2 we obtain

$$\begin{aligned} \mathfrak{J}_2 &\leq \sum_{n=1}^N \int_{I_n} \sum_{l=1}^n \int_{I_l} \|\mathcal{R}(u_{h\tau})\|_{X'_t}^2 e^{t-s} ds dt \\ &\leq \sum_{n=1}^N \int_{I_n} \sum_{l=1}^n \left\{ \int_{I_l} \sum_{i=1}^l (\eta^i)^2 e^{t-s} ds \right\} dt \\ &= \sum_{n=1}^N \sum_{l=1}^n \left\{ \int_{I_n} \int_{I_l} e^{t-s} ds dt \right\} \times \left\{ \sum_{i=1}^l (\eta^i)^2 \right\} = \sum_{n=1}^N \sum_{l=1}^n J_{nl} \left\{ \sum_{i=1}^l (\eta^i)^2 \right\}, \end{aligned}$$

whence the conclusion follows. \square

Remark 1.5.4 (Simplified versions of the a posteriori estimate). *In the spirit of Lemma 1.5.1, the following simplified versions of the a posteriori estimate of Theorem 1.5.3 hold:*

$$\begin{aligned} \frac{L_\beta}{2} \|u - u_{h\tau}\|_{X'}^2 + \frac{L_\beta}{2} \|(u - u_{h\tau})(\cdot, t_{\text{F}})\|_{H^{-1}(\Omega)}^2 + \|\beta(u) - \beta(u_{h\tau})\|_{Q_{t_{\text{F}}}}^2 &\leq \frac{L_\beta}{2} (2e^{t_{\text{F}}} - 1) (\eta^2 + \eta_{\text{IC}}^2), \\ \frac{L_\beta}{2} \|(u - u_{h\tau})(\cdot, t_{\text{F}})\|_{H^{-1}(\Omega)}^2 + \|\beta(u) - \beta(u_{h\tau})\|_{Q_{t_{\text{F}}}}^2 &\leq \frac{L_\beta}{2} e^{t_{\text{F}}} (\eta^2 + \eta_{\text{IC}}^2). \end{aligned}$$

Remark 1.5.5 (An a posteriori error estimate distinguishing the different error components). *While relying on Corollary 1.3.5 instead of Theorem 1.3.3, equivalents of Theorem 1.5.3 and of the bounds of Remark 1.5.4 distinguishing the different error components can immediately be obtained.*

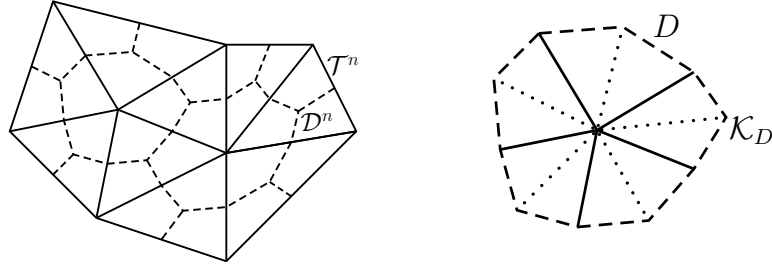


Figure 1.2: Simplicial mesh \mathcal{T}^n and the associated vertex-centered dual mesh \mathcal{D}^n (left) and the fine simplicial mesh \mathcal{K}_D of $D \in \mathcal{D}^n$ (right)

1.6 Application to a vertex-centered finite volume discretization

In this section, we consider the vertex-centered finite volume spatial and backward Euler temporal discretization of the Stefan problem (1.1.1). The regularization of Section 1.2.1.2 is considered and the Newton linearization is used. We show how to construct the equilibrated flux $\mathbf{t}_h^{n,\epsilon,k}$, the linearized flux $\mathbf{l}_h^{n,\epsilon,k}$, and the interpolation operator Π^n of Assumption 1.3.4 (in generalization of Assumptions 1.3.1 and 1.3.2) and verify Assumptions 1.4.2 and 1.4.3. Thus, all the results of Sections 1.3–1.5 will apply.

1.6.1 Dual and tertial space meshes

The vertex-centered finite volume method is defined using a sequence of dual meshes $\{\mathcal{D}^n\}_{0 \leq n \leq N}$ of the space domain Ω . For a given family of matching simplicial primal meshes $\{\mathcal{T}^n\}_{0 \leq n \leq N}$, we construct $\{\mathcal{D}^n\}_{0 \leq n \leq N}$ as follows: for any $1 \leq n \leq N$ and with every vertex \mathbf{a} of the mesh \mathcal{T}^n , we associate one dual volume D , constructed by connecting the barycenters of the simplices sharing \mathbf{a} through edge (and face for $d = 3$) barycenters, see Figure 1.2, left, for $d = 2$. We split every set \mathcal{D}^n into interior dual volumes $\mathcal{D}^{n,i}$ and boundary dual volumes $\mathcal{D}^{n,b}$. The simplicial mesh \mathcal{K}^n appearing in Sections 1.2–1.5 is constructed by dividing each $D \in \mathcal{D}^n$ into a mesh \mathcal{K}_D as indicated in Figure 1.2, right, if $d = 2$ and similarly for $d = 3$.

1.6.2 The vertex-centered finite volume scheme

Let, for $1 \leq n \leq N$,

$$V_h^n := \{\varphi_h \in C^0(\overline{\Omega}); \varphi_h|_K \in \mathbb{P}_1(K) \quad \forall K \in \mathcal{T}^n\}$$

and let

$$\Pi^n : C^0(\overline{\Omega}) \rightarrow V_h^n \quad \text{be the Lagrange interpolation operator,} \quad (1.6.1)$$

Ciarlet [11], which to a function $\varphi \in C^0(\overline{\Omega})$ associates a function $\varphi_h \in V_h^n$ by setting $\varphi_h(\mathbf{a}) := \varphi(\mathbf{a})$ for any vertex \mathbf{a} of the mesh \mathcal{T}^n .

Let $u_h^0 \in V_h^0$ be a suitable approximation of the regularized initial enthalpy $\beta_\epsilon^{-1}(\beta(u_0))$, see Algorithm 1.4.1. Let next $1 \leq n \leq N$, $u_h^{n-1} \in V_h^{n-1}$, and a mesh \mathcal{T}^n (and consequently \mathcal{D}^n) be given. The vertex-centered finite volume scheme for the regularized Stefan problem (1.2.3) reads: find $u_h^{n,\epsilon} \in V_h^n$ such that $\beta_\epsilon(u_h^{n,\epsilon})(\mathbf{a}) = 0$ for all vertices \mathbf{a} of \mathcal{T}^n on $\partial\Omega$ and such that

$$\frac{1}{\tau^n}(u_h^{n,\epsilon} - u_h^{n-1}, 1)_D - (\nabla \Pi^n(\beta_\epsilon(u_h^{n,\epsilon})) \cdot \mathbf{n}_D, 1)_{\partial D} = (\hat{f}^n, 1)_D \quad \forall D \in \mathcal{D}^{n,i}. \quad (1.6.2)$$

Then the continuous and piecewise affine-in-time function $u_{h\tau}$ appearing in the previous sections is given by $u_{h\tau}|_{I_n} := u_{h\tau}^{n,\epsilon}$,

$$u_{h\tau}^{n,\epsilon}(\cdot, t) = (1 - \rho(t))u_h^{n-1} + \rho(t)u_h^{n,\epsilon}, \quad \rho(t) := \frac{t - t^{n-1}}{\tau^n} \quad t \in I_n. \quad (1.6.3)$$

Remark 1.6.1 (Regularization). *It is also possible to consider the vertex-centered finite volume discretization without any regularization, i.e., use β in place of β_ϵ in (1.6.2), with $u_h^0 \in V_h^0$ an approximation of the initial enthalpy u_0 .*

Remark 1.6.2 (Links to the discretizations of [36, 4, 21]). *Let for simplicity the meshes \mathcal{T}^n (and consequently \mathcal{D}^n) do not move in time and let \hat{f}^n be piecewise constant on \mathcal{D}^n . Consider the case without regularization. Then the second and third terms of the scheme (1.6.2) coincide with that of [36, equation (4.4)], because of the links of the vertex-centered finite volumes and finite elements with mass lumping/quadrature for the source term. Similarly, in two space dimensions and when all the angles of \mathcal{T}^n are smaller than or equal to 90° , replacing the triangle barycenters by the triangle circumcenters in the construction of \mathcal{D}^n , the second and third terms of the scheme (1.6.2) coincide with that in the co-volume method of [4]. More generally, whenever \mathcal{T}^n is Delaunay and the mesh \mathcal{D}^n is its Voronoï dual, the same link holds true with the cell-centered finite volume scheme of [21], e.g., [36, 4, 21], [11, 20], or [51, Section 3]. Hence the only slight difference between (1.6.2) and these schemes is in the treatment of the time evolution term which is not mass-lumped herein.*

Remark 1.6.3 (Assumption 1.3.1). *By the definition of $u_{h\tau}$ by (1.6.2)–(1.6.3) and by the fact that $u_{h\tau}$ lies in a finite-dimensional space, $u_{h\tau} \in Z$ and $\beta(u_{h\tau}) \in X$, so that Assumption 1.3.1 is satisfied. A uniform bound could also be obtained by a priori stability analysis such as those in [36, 4, 21], but is not necessary in our setting.*

1.6.3 Newton linearization

Let $1 \leq n \leq N$ and the mesh \mathcal{T}^n (and \mathcal{D}^n) be fixed. Let the vector G^{n-1} be given by its components associated with the dual volumes $D \in \mathcal{D}^{n,i}$, $G_D^{n-1} := (u_h^{n-1}, 1)_D$, and similarly for the vector F^n , $F_D^n := (\hat{f}^n, 1)_D$. Let $u_h^{b,n,\epsilon} \in V_h^n$ take the values $\beta_\epsilon^{-1}(0)$ (0.5 for the example of Figure 1.1) at the boundary vertices of \mathcal{T}^n and the value zero at the other vertices of \mathcal{T}^n . The last vector that we need is $H^{n,\epsilon}$, $H_D^{n,\epsilon} := (u_h^{b,n,\epsilon}, 1)_D$. Let, for a given dual volume $E \in \mathcal{D}^{n,i}$, ϕ_E stand for the hat basis function of the space V_h^n associated with E : this is a

function that takes the value 1 in the vertex associated with E and the value 0 at all other vertices of \mathcal{T}^n . We also define two matrices, with the components on the line associated with the dual volume $D \in \mathcal{D}^{n,i}$ and on the column associated with the dual volume $E \in \mathcal{D}^{n,i}$ given by $\mathbf{M}_{D,E}^n := (\phi_E, 1)_D$, $\mathbf{K}_{D,E}^n := (\nabla \phi_E \cdot \mathbf{n}_D, 1)_{\partial D}$. All the vectors are of size $\mathbb{R}^{|\mathcal{D}^{n,i}|}$ and the matrices of size $\mathbb{R}^{|\mathcal{D}^{n,i}| \times |\mathcal{D}^{n,i}|}$, with $|\mathcal{D}^{n,i}|$ the number of dual volumes in $\mathcal{D}^{n,i}$ (equal to the number of interior vertices of \mathcal{T}^n). The equation (1.6.2) can be written in matrix form as follows: find the vector $U^{n,\epsilon}$ such that

$$\mathbf{M}^n U^{n,\epsilon} - \tau^n \mathbf{K}^n \beta_\epsilon(U^{n,\epsilon}) = \tau^n F^n + G^{n-1} - H^{n,\epsilon}, \quad (1.6.4)$$

where $(\beta_\epsilon(U^{n,\epsilon}))_D := \beta_\epsilon(U_D^{n,\epsilon})$. We have $u_h^{n,\epsilon} = \sum_{E \in \mathcal{D}^{n,i}} U_E^{n,\epsilon} \phi_E + u_h^{b,n,\epsilon}$.

The algebraic system (1.6.4) is nonlinear. Its solution is approximated using the Newton linearization. Let $U^{n,\epsilon,0}$ be fixed; typically, $U^{n,\epsilon,0} := U^{n-1}$. Then, for $k \geq 1$, we approximate

$$\beta_\epsilon(U^{n,\epsilon,k}) \approx \beta_\epsilon(U^{n,\epsilon,k-1}) + \beta'_\epsilon(U^{n,\epsilon,k-1})(U^{n,\epsilon,k} - U^{n,\epsilon,k-1}). \quad (1.6.5)$$

The Newton linearization (1.6.5) is well defined since the regularized enthalpy–temperature function β_ϵ is continuously differentiable. At every Newton iteration k , we are thus lead to solve the following system of linear algebraic equations: find the vector $U^{n,\epsilon,k}$ such that

$$\begin{aligned} \left(\mathbf{M}^n - \tau^n \mathbf{K}^n \beta'_\epsilon(U^{n,\epsilon,k-1}) \right) U^{n,\epsilon,k} &= \tau^n F^n + G^{n-1} - H^{n,\epsilon} \\ &\quad - \tau^n \mathbf{K}^n (\beta'_\epsilon(U^{n,\epsilon,k-1}) U^{n,\epsilon,k-1} - \beta_\epsilon(U^{n,\epsilon,k-1})). \end{aligned} \quad (1.6.6)$$

At each linearization step k , we set

$$u_h^{n,\epsilon,k} := \sum_{E \in \mathcal{D}^{n,i}} U_E^{n,\epsilon,k} \phi_E + u_h^{b,n,\epsilon}, \quad (1.6.7)$$

which is the function appearing in Section 1.3.4. The corresponding linearized flux of Assumption 1.3.4 is given by

$$\mathbf{t}_h^{n,\epsilon,k} := \nabla \left(\sum_{E \in \mathcal{D}^{n,i}} \left\{ \beta_\epsilon(U_E^{n,\epsilon,k-1}) + \beta'_\epsilon(U_E^{n,\epsilon,k-1})(U_E^{n,\epsilon,k} - U_E^{n,\epsilon,k-1}) \right\} \phi_E \right). \quad (1.6.8)$$

We perform the Newton iterations until we meet the convergence criterion discussed in Section 1.4.1.

1.6.4 Flux reconstruction

Let a time step $1 \leq n \leq N$, a regularization parameter $\epsilon > 0$, and a Newton linearization step k be fixed. We now show how to construct the flux $\mathbf{t}_h^{n,\epsilon,k}$ of Assumption 1.3.4. For this purpose, we will solve a local Neumann problem by mixed finite elements on every dual

volume, following [30, 17, 51]. For a given $D \in \mathcal{D}^n$, we introduce the spaces

$$\begin{aligned} \mathbf{RTN}(\mathcal{K}_D) &:= \{\mathbf{v}_h \in \mathbf{H}(\operatorname{div}; D); \mathbf{v}_h|_K \in [\mathbb{P}_0(K)]^d + \mathbf{x}\mathbb{P}_0(K) \quad \forall K \in \mathcal{K}_D\}, \\ \mathbf{RTN}_N(\mathcal{K}_D) &:= \{\mathbf{v}_h \in \mathbf{RTN}(\mathcal{K}_D); \mathbf{v}_h \cdot \mathbf{n}_F = -\mathbf{l}_h^{n,\epsilon,k} \cdot \mathbf{n}_F \quad \forall F \in \partial\mathcal{K}_D^i\}, \\ \mathbf{RTN}_{N,0}(\mathcal{K}_D) &:= \{\mathbf{v}_h \in \mathbf{RTN}(\mathcal{K}_D); \mathbf{v}_h \cdot \mathbf{n}_F = 0 \quad \forall F \in \partial\mathcal{K}_D^i\}, \end{aligned}$$

where $\partial\mathcal{K}_D^i$ stands for all the faces of the submesh \mathcal{K}_D which are on the boundary of the dual volume D but not on the boundary of Ω . We will also need the space $\mathcal{P}_0^*(\mathcal{K}_D)$ which consists of piecewise constants functions on \mathcal{K}_D ; when $D \in \mathcal{D}^{n,i}$, we additionally impose a zero mean value over D . The local problem consists in finding $\mathbf{t}_h^{n,\epsilon,k} \in \mathbf{RTN}_N(\mathcal{K}_D)$ and $q_h \in \mathcal{P}_0^*(\mathcal{K}_D)$, the mixed finite element approximations of local Neumann problems on $D \in \mathcal{D}^{n,i}$ and local Neumann/Dirichlet problems on $D \in \mathcal{D}^{n,b}$:

$$(\mathbf{t}_h^{n,\epsilon,k} + \mathbf{l}_h^{m,\epsilon,k}, \mathbf{v}_h)_D - (q_h, \nabla \cdot \mathbf{v}_h)_D = 0 \quad \forall \mathbf{v}_h \in \mathbf{RTN}_{N,0}(\mathcal{K}_D), \quad (1.6.9a)$$

$$(\nabla \cdot \mathbf{t}_h^{n,\epsilon,k}, \phi_h)_D - (\hat{f}^n - \partial_t u_{h\tau}^{n,\epsilon,k}, \phi_h)_D = 0 \quad \forall \phi_h \in \mathcal{P}_0^*(\mathcal{K}_D). \quad (1.6.9b)$$

Note that the problem (1.6.9) is well-posed and one can take all $\phi_h \in \mathcal{P}_0(\mathcal{K}_D)$ as the test functions in (1.6.9b). Indeed, it follows from (1.6.6) and (1.6.8) that (compare to (1.6.2)) that

$$\frac{1}{\tau^n} (u_h^{n,\epsilon,k} - u_h^{n-1}, 1)_D - (\mathbf{l}_h^{n,\epsilon,k} \cdot \mathbf{n}_D, 1)_{\partial D} = (\hat{f}^n, 1)_D \quad \forall D \in \mathcal{D}^{n,i}. \quad (1.6.10)$$

From (1.6.10), we see that the Neumann boundary condition encoded in $\mathbf{RTN}_N(\mathcal{K}_D)$ is in equilibrium with the boundary datum $\hat{f}^n - \partial_t u_{h\tau}^{n,\epsilon,k}$ of (1.6.9). We have the following key result:

Lemma 1.6.4 (Assumptions 1.3.4, 1.4.2, and 1.4.3). *Let $1 \leq n \leq N$, $\epsilon > 0$, and $k \geq 1$ be fixed. Let $u_h^{n,\epsilon,k}$ be given by (1.6.6)–(1.6.7), $\mathbf{l}_h^{n,\epsilon,k}$ by (1.6.8), $\mathbf{t}_h^{n,\epsilon,k}$ by (1.6.9), and Π^n by (1.6.1). Then Assumptions 1.3.4, 1.4.2, and 1.4.3 hold true.*

Proof. The equilibrium property (1.3.11) follows immediately from (1.6.9b), so that Assumption 1.3.4 is easily satisfied. Whereas Assumption 1.4.2 is trivial, Assumption 1.4.3 is obtained by proceeding exactly as in [51, proof of Theorem 5.5] or [15, proof of Lemma 5.3]. \square

1.7 Numerical experiments

We illustrate in this section our theoretical results on a series of numerical experiments for the vertex-centered finite volume discretization approach of Section 1.6.

1.7.1 Setting

We consider the two-dimensional test case proposed by Nochetto et al. [34, 35] on the space–time domain $\Omega \times (0, t_F)$ with $\Omega = (0, 5)^2$ and $t_F = \pi/1.25$. The function $\beta(\cdot)$ is given

by $\beta(u) = u^\ominus + (u - 1)^\oplus$. The exact temperature has the following expression:

$$(\beta(u))(x, y, t) = \begin{cases} 0.75(r^2 - 1), & \text{if } r < 1, \\ \left(1.5 - \rho'(t)\frac{y - \rho(t)}{r}\right)(r - 1), & \text{if } r \geq 1, \end{cases} \quad (1.7.1)$$

where $r^2 := x^2 + (y - \rho(t))^2$ and $\rho(t) := 0.5 + \sin(1.25t)$. The exact interface $I(t)$ is a circle with center $(0, \rho(t))$ and radius 1. The motion of the interface is governed by the Stefan law which prescribes that the normal velocity \mathbf{v} satisfies

$$(\nabla\beta(u)^+ - \nabla\beta(u)^-) \cdot \mathbf{n} = \mathbf{v} \quad \text{on } I(t),$$

where $\nabla\beta(u)^+$ and $\nabla\beta(u)^-$ denote the values of the temperature gradient on each side of the interface, while \mathbf{n} is the unit normal to the interface with suitable orientation. The enthalpy u on $\Omega \setminus I(t)$ can be obtained from the expression (1.7.1) of $\beta(u)$. The homogeneous Neumann condition $\nabla\beta(u) \cdot \mathbf{n} = 0$ is enforced at $x = 0$, whereas Dirichlet boundary conditions on the temperature are prescribed at $y = 0$, $y = 5$, and $x = 5$ using (1.7.1). The initial enthalpy u_0 and the source term f are likewise imposed using (1.7.1). The vertex-centered finite volume discretization of Section 1.6 is considered. No adaptation of the quadrature rule is performed; this is a reasonable simplification since the enthalpy–temperature function $\beta(\cdot)$ is piecewise affine.

1.7.2 Computing approximately the negative norms

In practice we cannot compute the negative norms as the initial data indicator η_{IC} , the data oscillation $\|f - \hat{f}\|_{X'}$, and the dual norm of the residual $\|\mathcal{R}(u_{h\tau})\|_{X'}$, even if the exact solution u is known. For numerical experiments below, the dual norms are approximated by solving auxiliary problems. More specifically, for a function $v \in X'$ to compute the negative norm $\|v\|_{X'}$, we consider for a.e. $t \in (0, t_F)$ the problem: find $\psi(\cdot, t) \in H_0^1(\Omega)$ such that

$$(\nabla\psi(\cdot, t), \nabla\varphi) = \langle v(\cdot, t), \varphi \rangle, \quad \forall \varphi \in H_0^1(\Omega). \quad (1.7.2)$$

Then

$$\begin{aligned} \|v\|_{X'}^2 &= \int_0^{t_F} \left\{ \sup_{\varphi \in H_0^1(\Omega), \|\nabla\varphi\|_{L^2(\Omega)}=1} \langle v(\cdot, t), \varphi \rangle \right\}^2 dt \\ &= \int_0^{t_F} \left\{ \sup_{\varphi \in H_0^1(\Omega), \|\nabla\varphi\|_{L^2(\Omega)}=1} (\nabla\psi(\cdot, t), \nabla\varphi) \right\}^2 dt \\ &= \int_0^{t_F} \|\nabla\psi\|_{L^2(\Omega)}^2(t) dt = \|\nabla\psi\|_{L^2(0, t_F; L^2(\Omega))}^2. \end{aligned}$$

We obtain an approximation of the function ψ by solving the problem (1.7.2) numerically by the vertex-centered finite volume scheme on a refined spatial mesh and on discrete times which refine the given temporal mesh. We suppose that the ensuing discretization error is small and can be ignored. The computation of η_{IC} is easier as it only involves the initial time $t = 0$.

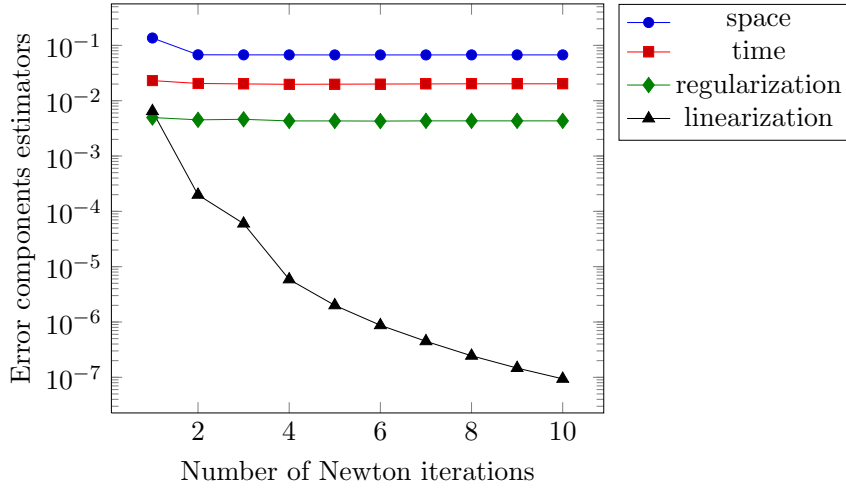


Figure 1.3: Evolution of the spatial, temporal, regularization, and linearization error estimators (1.3.14) as a function of Newton iterations for a fixed mesh, time step, and regularization parameter

1.7.3 Stopping criteria

We start by assessing the performance of the balancing and stopping criteria introduced in Section 1.4.1. Figure 1.3 depicts the evolution of the spatial (1.3.14a), temporal (1.3.14b), regularization (1.3.14d), and linearization (1.3.14e) error estimators as a function of the number of Newton iterations for a fixed mesh \mathcal{K} with $h_{\mathcal{K}} = 0.25$, time step $\tau = 0.1$, and regularization parameter $\epsilon = 0.05$. As expected, the linearization error steadily decreases, while the other components stagnate starting from the second iteration. The stopping criterion (1.4.1) with $\Gamma_{\text{lin}} = 10^{-2}$ allows to profit from this behavior by stopping the Newton algorithm after the second iteration, while a classical criterion based on a fixed threshold,

$$\eta_{\text{lin}}^{n,\epsilon,k} \leq \zeta_{\text{lin}}, \quad \zeta_{\text{lin}} = 10^{-7}, \quad (1.7.3)$$

would require 10 iterations to converge.

The overall gain for an entire simulation in terms of linearization iterations can be appreciated considering the results in Figure 1.4, left. We use the adaptive Algorithm 1.4.1 with different choices for the linearization stopping criterion: the classical criterion (1.7.3) then the stopping criterion (1.4.1) with $\Gamma_{\text{lin}} = 0.01$ and $\Gamma_{\text{lin}} = 0.1$. The others parameters used in the Algorithm are: $\Gamma_{\text{reg}} = 0.1$, $\zeta = 1$, $\zeta_{\text{IC}} = 1$, $h_{\mathcal{K}^0} = 0.1$, $\tau^0 = 0.1$, $\epsilon^0 = 0.25$, $\underline{h} = 10^{-2}$, $\underline{\tau} = 10^{-2}$, $c_{\text{ref}} = 0.7$, $c_{\text{deref}} = 0.2$, $\gamma_{\text{tm}} = 0.7$, and $\Gamma_{\text{tm}} = 1.3$. For the sake of completeness we also add a comparison with the local version of the stopping criterion (1.4.1), namely

$$\eta_{\text{lin},K}^{n,\epsilon,k_n} \leq \Gamma_{\text{lin},\text{loc}} \left(\eta_{\text{sp},K}^{n,\epsilon,k_n} + \eta_{\text{tm},K}^{n,\epsilon,k_n} + \eta_{\text{qd},K}^{n,\epsilon,k_n} + \eta_{\text{reg},K}^{n,\epsilon,k_n} \right) \quad \forall K \in \mathcal{K}^n. \quad (1.7.4)$$

Even with this more stringent criterion, Figure 1.4, right, shows that a considerable gain in

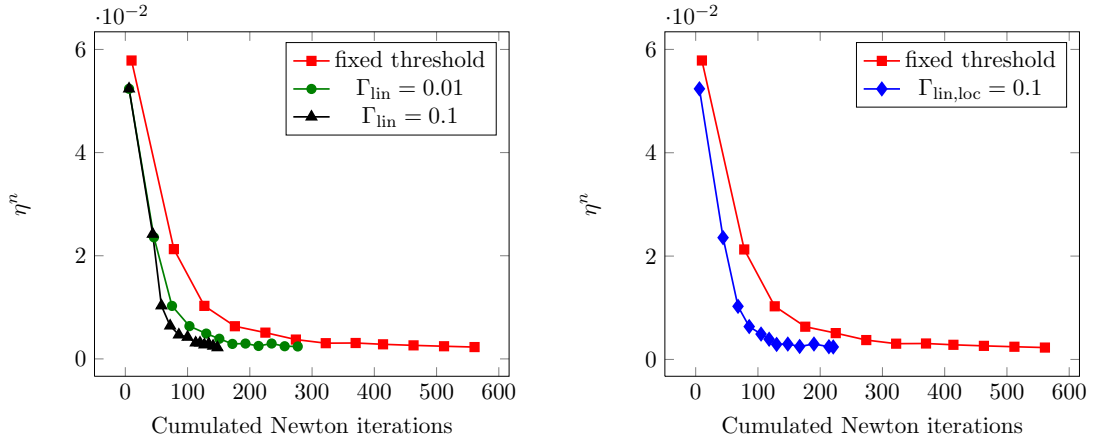


Figure 1.4: Error estimator η^n (1.5.2) as a function of the cumulated Newton iterations at each time step (time steps are identified by markers). Global stopping criterion (1.4.1) (*left*), local stopping criterion (1.7.4) (*right*)

terms of number of linearization iterations can be achieved, whereas the precision on each time step (expressed by our error estimator η^n (1.5.2)) is basically unchanged.

Figure 1.5 shows similar results concerning the criterion (1.4.2) for the choice of the regularization parameter ϵ for a fixed mesh \mathcal{K} with $h_{\mathcal{K}} = 0.25$ and time step $\tau = 0.1$. For each value of ϵ , the Newton iterations are stopped according to (1.4.1) with $\Gamma_{\text{lin}} = 0.1$. The regularization error estimator decreases as expected when ϵ decreases, while the space and time error estimators stagnate starting from the third iteration. The criterion (1.4.2) with $\Gamma_{\text{reg}} = 0.1$ leads to stopping the iterations after the fourth step.

1.7.4 Balancing criteria

The next series of numerical experiments aims at assessing the space–time balancing criterion (1.4.4) by showing its impact on the estimated error (1.3.8) as a function of the total number of space–time unknowns $\sum_{n=1}^N |\mathcal{D}^{n,i}|$. In Figure 1.6, bottom left, we started by an initial mesh \mathcal{K}^0 with $h_{\mathcal{K}^0} = 0.4$ and a time step $\tau^0 = 0.1$. Then the time step is adapted in order to satisfy (1.4.4), with $\gamma_{\text{tm}} = 0.7$, $\Gamma_{\text{tm}} = 1.3$. As a result, the spatial (1.3.14a) and temporal (1.3.14b) error estimators stay equilibrated during the whole simulation. Figure 1.6, top, on the other hand, shows two possible disequilibrated patterns corresponding to space and time over-refinement. In the top left we started by an initial mesh \mathcal{K}^0 with $h_{\mathcal{K}^0} = 0.2$ and a time step $\tau^0 = 0.2$, we fixed also $\gamma_{\text{tm}} = 2$ and $\Gamma_{\text{tm}} = 3$, while in the top right we started by an initial mesh \mathcal{K}^0 with $h_{\mathcal{K}^0} = 0.5$ and time step $\tau^0 = 0.05$ and we fixed $\gamma_{\text{tm}} = \frac{1}{3}$ and $\Gamma_{\text{tm}} = \frac{1}{2}$. Finally, Figure 1.6, bottom right shows the effect of this violating of the balancing criterion (1.4.4) on the total error. These results make it apparent that the performance of an adaptive code may be considerably reduced when time and space errors are not balanced,

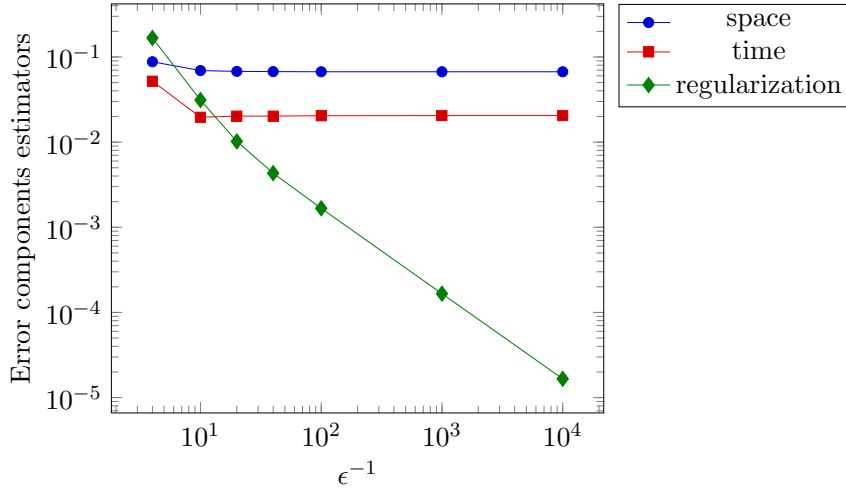


Figure 1.5: Evolution of the spatial, temporal, and regularization error estimators (1.3.14) as a function of ϵ^{-1} for a fixed mesh and time step

and advocate the use of (1.4.4).

Next, we compare in Figure 1.7 the actual and predicted error distribution using the adaptive Algorithm 1.4.1 with $\Gamma_{\text{lin}} = \Gamma_{\text{reg}} = 0.1$, $\zeta = 1$, $\zeta_{\text{IC}} = 1$, $h_{\mathcal{K}^0} = 0.25$, $\tau^0 = 0.05$, $\epsilon^0 = 0.25$, $\underline{h} = 10^{-2}$, $\underline{\tau} = 10^{-2}$, $c_{\text{ref}} = 0.7$, $c_{\text{deref}} = 0.2$, $\gamma_{\text{tm}} = 0.7$, and $\Gamma_{\text{tm}} = 1.3$. We present the results at time $t = 0.1$. We see that the actual and predicted error distributions match very nicely. The corresponding exact and discrete enthalpies are depicted in Figure 1.8.

1.7.5 Overall performance

In this section we assess the overall performance of the adaptive algorithm of Section 1.4.2 in terms of precision vs. the number of unknowns.

In Figure 1.9, left, we depict the error and estimates as a function of the total number of space–time unknowns in the fully adaptive case and in the uniform case. In the adaptive case, we use Algorithm 1.4.1 with the parameters detailed in Section 1.7.4. In the uniform case, the temporal and spatial meshes as well as the regularization parameter are fixed during the simulation, and linearization is stopped when (1.7.3) is satisfied. The error is measured in the dual norm (1.3.3) and estimated by Theorem 1.3.3 in the top part of Figure 1.9, whereas the energy-like norm (1.5.1) and the estimate of Theorem 1.5.3 are used in the bottom part of Figure 1.9. In both cases the adaptive strategy yields much better results than the uniform one, as expected. The right part of Figure 1.9 displays the corresponding effectivity indices, given by the ratio of the estimates over the error. These are remarkably close to the optimal value of one for the dual norm (1.3.3), even for the present time-dependent, degenerate problem with a moving free boundary. We regard the effectivity indices corresponding to Theorem 1.5.3 as likewise excellent; they are in particular several orders of magnitude smaller

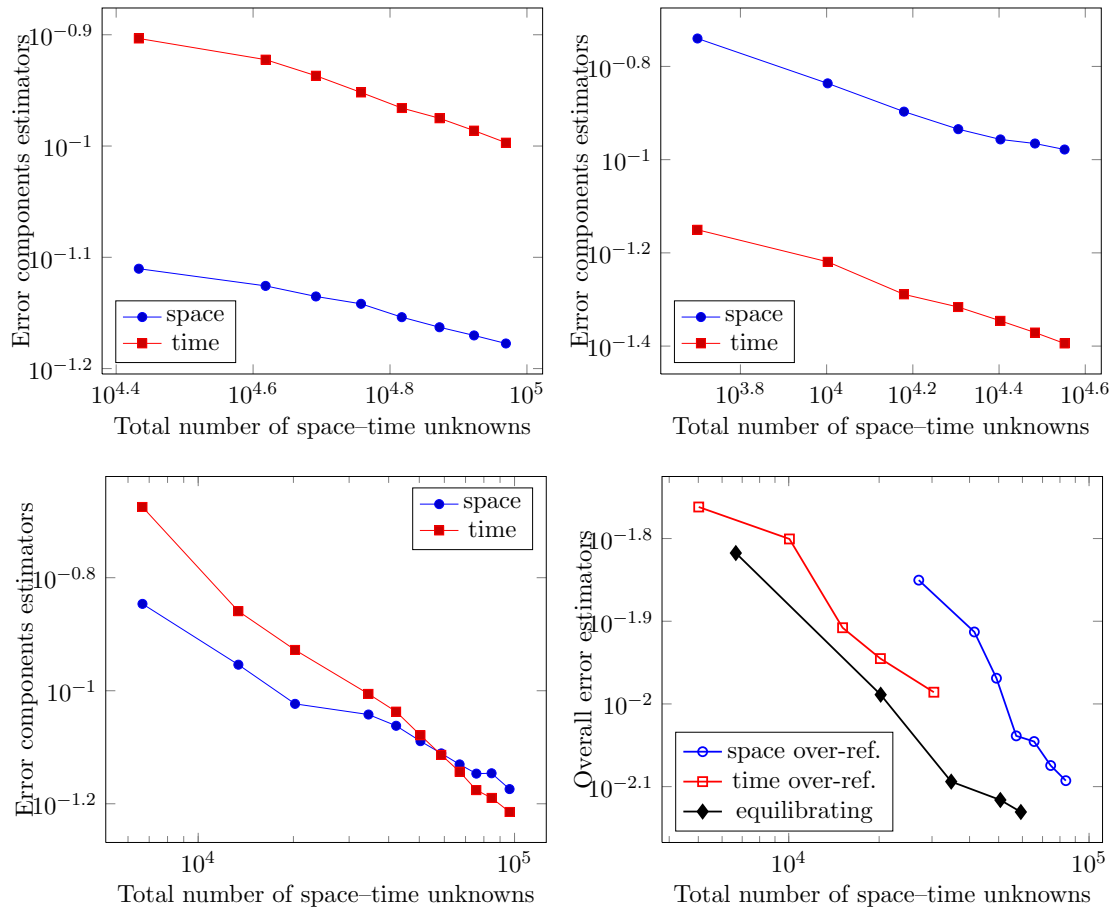


Figure 1.6: Effect of the time step adaptation strategy on the global error estimator (1.3.8). Violations of the balancing criterion (1.4.4) by space over-refinement (*top left*) and time over-refinement (*top right*). Time step refinement honoring (1.4.4) (*bottom left*). Overall comparison (*bottom right*)

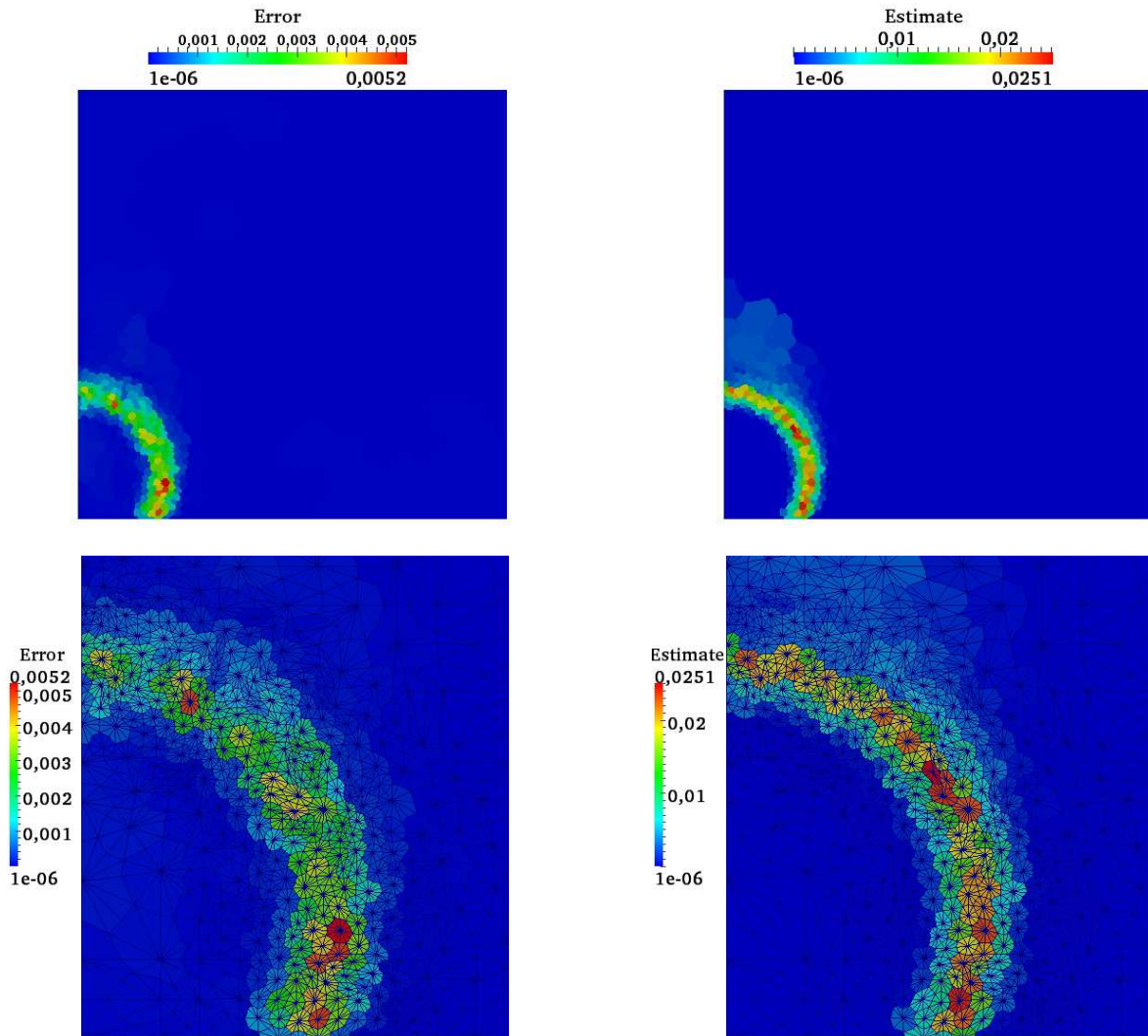


Figure 1.7: Actual (*left*) and estimated (*right*) error distribution for $\Gamma_{\text{lin}} = \Gamma_{\text{reg}} = 0.1$, adaptive Algorithm 1.4.1, entire domain (*top*), interface zoom (*bottom*)

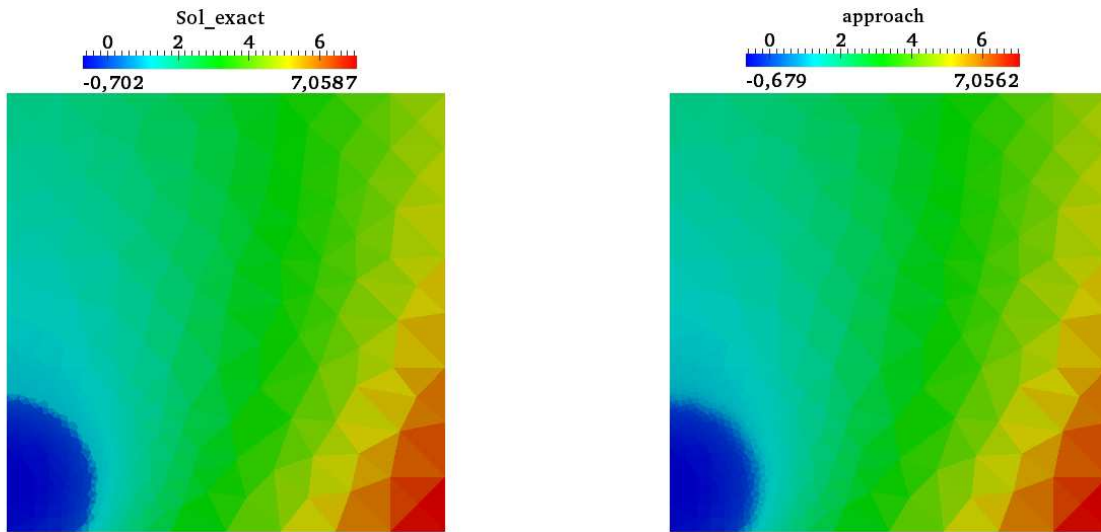


Figure 1.8: Exact (*left*) and approximate (*right*) enthalpy corresponding to the results of Figure 1.7

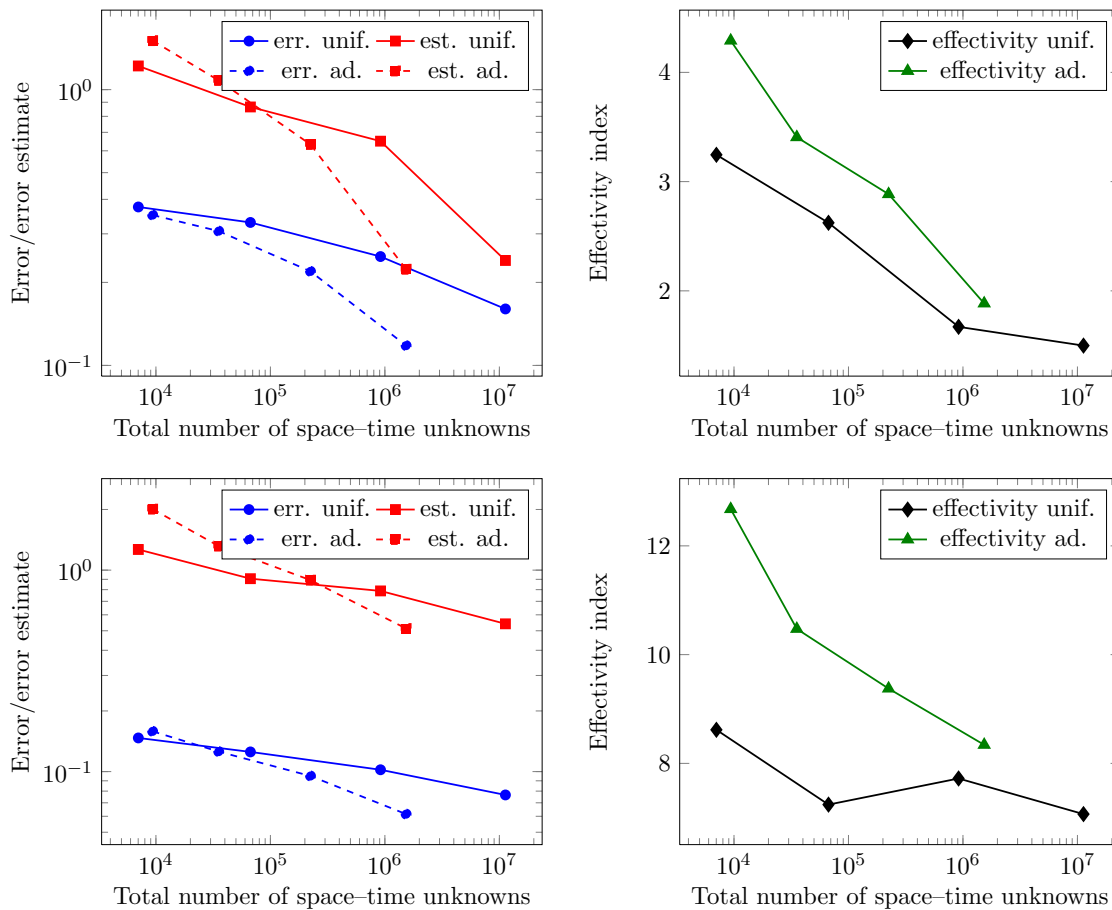


Figure 1.9: Comparison between adaptive and uniform refinement. Dual norm (1.3.3) (*top*), energy-like norm (1.5.1) (*bottom*). Error and estimators (*left*), effectivity indices (*right*)

Table 1.1: Comparison of the experimental orders of convergence (e.o.c.) in the uniform and fully adaptive cases. The total number of space–time unknowns is denoted by N_{st} . The actual error $\|\mathcal{R}(u_{h\tau})\|_{X'}$ and the estimated error η are defined by (1.3.2) and (1.3.8) respectively.

(a) Uniform case						
N_{st}	$\ \beta(u) - \beta(u_{h\tau})\ _{Q_{t_F}}$	e.o.c.	$\ \mathcal{R}(u_{h\tau})\ _{X'}$	e.o.c.	η	e.o.c.
7020	7.13e-02	–	3.75e-01	–	1.22e-00	–
66906	6.02e-02	0.224	3.30e-01	0.172	8.65e-01	0.455
915840	5.07e-02	0.197	2.48e-01	0.364	6.50e-01	0.392
1.12963e+07	2.19e-02	0.221	1.60e-01	0.115	2.40e-01	0.261
(b) Adaptive case						
N_{st}	$\ \beta(u) - \beta(u_{h\tau})\ _{Q_{t_F}}$	e.o.c.	$\ \mathcal{R}(u_{h\tau})\ _{X'}$	e.o.c.	η	e.o.c.
9360	6.55e-02	–	3.51e-01	–	1.51e-00	–
35370	5.28e-02	0.486	3.07e-01	0.303	1.08e-00	0.751
224082	4.06e-02	0.427	2.19e-01	0.546	6.32e-01	0.868
1.53329e+06	1.10e-02	0.392	1.18e-01	0.186	2.23e-01	0.312

than the effectivity indices corresponding to the setting of Remark 1.5.4 that we have also assessed (not presented).

A quantitative evaluation of the performance in terms of precision vs. the number of unknowns can be obtained by computing the *experimental order of convergence* (e.o.c.), defined as follows:

$$\text{e.o.c.} := \frac{\log(e_{N_{\text{st}}}) - \log(e_{M_{\text{st}}})}{-\frac{1}{3}(\log N_{\text{st}} - \log M_{\text{st}})},$$

where e denotes the chosen error measure while N_{st} and M_{st} are the total number of space–time unknowns corresponding to two subsequent levels of refinement. The results for the uniform and adaptive cases are collected in Tables 1.1a and 1.1b, respectively. We evaluate the dual norm of the residual (1.3.2), the $L^2(0, t_F; L^2(\Omega))$ error in the temperature, and the estimator η of (1.3.8). We observe roughly twice faster convergence in the adaptive case in comparison with the uniform one.

1.A Proofs

In this appendix, we collect the more involved proofs of some theorems of the chapter.

1.A.1 Proof of Theorem 1.4.4

In this section, we will use the notation $a \lesssim b$ for the inequality $a \leq Cb$ with a generic constant C only depending on the shape regularity parameter $\kappa_{\mathcal{K}}$ of the meshes $\mathcal{K}^{n-1,n}$, $1 \leq n \leq N$, the space dimension d , and the polynomial degree m . Fix $1 \leq n \leq N$. We start by observing that, owing to the stopping criteria (1.4.1)–(1.4.3) and to the second inequality in the balancing criterion (1.4.4),

$$\eta_{\text{sp}}^{n,\epsilon_n,k_n} + \eta_{\text{tm}}^{n,\epsilon_n,k_n} + \eta_{\text{qd}}^{n,\epsilon_n,k_n} + \eta_{\text{reg}}^{n,\epsilon_n,k_n} + \eta_{\text{lin}}^{n,\epsilon_n,k_n} \lesssim \eta_{\text{sp}}^{n,\epsilon_n,k_n}. \quad (1.A.1)$$

Recall that we have supposed in Section 1.2.2.2 that the mesh \mathcal{K}^n , $1 \leq n \leq N$, is obtained from \mathcal{K}^{n-1} by limited refinement/coarsening and that the common refinements $\mathcal{K}^{n-1,n}$ are uniformly shape regular. Thus, for $K \in \mathcal{K}^n$, using the triangle inequality, Assumption 1.4.2, and the inverse inequality, [44, Proposition 6.3.2], the first term of (1.3.13a) can be bounded by

$$\begin{aligned} \eta_{\text{R},K}^{n,\epsilon_n,k_n} &= C_{\text{P},K} h_K \left\| \hat{f}^n - \partial_t u_{h\tau}^{n,\epsilon_n,k_n} - \nabla \cdot \mathbf{t}_h^{n,\epsilon_n,k_n} \right\|_{L^2(K)} \\ &\leq C_{\text{P},K} h_K \left\| \hat{f}^n - \partial_t u_{h\tau}^{n,\epsilon_n,k_n} + \nabla \cdot \mathbf{l}_h^{n,\epsilon_n,k_n} \right\|_{L^2(K)} + C_{\text{P},K} h_K \left\| \nabla \cdot (\mathbf{l}_h^{n,\epsilon_n,k_n} + \mathbf{t}_h^{n,\epsilon_n,k_n}) \right\|_{L^2(K)} \\ &\lesssim \left\{ \sum_{K' \in \mathcal{K}^{n-1,n}, K' \subset K} h_{K'}^2 \left\| \hat{f}^n - \partial_t u_{h\tau}^{n,\epsilon_n,k_n} + \nabla \cdot \mathbf{l}_h^{n,\epsilon_n,k_n} \right\|_{L^2(K')}^2 \right\}^{\frac{1}{2}} \\ &\quad + \left\{ \sum_{K' \in \mathcal{K}^{n-1,n}, K' \subset K} \left\| \mathbf{l}_h^{n,\epsilon_n,k_n} + \mathbf{t}_h^{n,\epsilon_n,k_n} \right\|_{L^2(K')}^2 \right\}^{\frac{1}{2}}. \end{aligned}$$

Consequently, employing Assumption 1.4.3,

$$\eta_{\text{sp}}^{n,\epsilon_n,k_n} \lesssim \eta_{\text{res},1}^n + \eta_{\text{res},2}^n. \quad (1.A.2)$$

Proving the efficiency of the estimators introduced in Section 1.3.4 thus amounts to proving the efficiency of the residual estimators $\eta_{\text{res},1}^n$ and $\eta_{\text{res},2}^n$.

Henceforth, to simplify, we will use the shorthand notation

$$u_{h\tau}^n = u_{h\tau}^{n,\epsilon_n,k_n}, \quad \mathbf{l}_h^n = \mathbf{l}_h^{n,\epsilon_n,k_n}$$

and denote

$$(\eta_{\text{LRQT}}^n)^2 := \int_{I_n} \sum_{K \in \mathcal{K}^{n-1,n}} \left\| \nabla \beta(u_{h\tau}^n(\cdot, t)) - \mathbf{l}_h^n \right\|_{L^2(K)}^2 dt. \quad (1.A.3)$$

We have:

Lemma 1.A.1 (Estimate of $\eta_{\text{res},1}^n$). *Under the assumptions of Theorem 1.4.4, there holds*

$$\eta_{\text{res},1}^n \lesssim \|\mathcal{R}(u_{h\tau}^n)\|_{X'_n} + \eta_{\text{LRQT}}^n + \|f - \hat{f}\|_{X'_n}. \quad (1.A.4)$$

Proof. For all $K \in \mathcal{K}^{n-1,n}$, we let $v_K := (\hat{f}^n - \partial_t u_{h\tau}^n + \nabla \cdot \mathbf{l}_h^n)|_K$. By Assumption 1.4.2, v_K is polynomial in K . We denote by ψ_K the usual bubble function on K , i.e., the product of the $(d+1)$ hat basis functions (barycentric coordinates) $\psi_{\mathbf{a}}$ associated with the vertices \mathbf{a} of the element K , set $\lambda_K := h_K^2 \psi_K v_K$ for all $K \in \mathcal{K}^{n-1,n}$, and let $\lambda := \sum_{K \in \mathcal{K}^{n-1,n}} \lambda_K$. Clearly, $\lambda \in H_0^1(\Omega)$ and $\lambda|_K \in H_0^1(K)$ for all $K \in \mathcal{K}^{n-1,n}$. Using the equivalence of norms on finite-dimensional spaces, integrating by parts in space, the weak form (1.2.2c), and (1.3.9) together with the Cauchy–Schwarz inequality, we infer, [49],

$$\begin{aligned}
(\eta_{\text{res},1}^n)^2 &\lesssim \int_{I_n} \sum_{K \in \mathcal{K}^{n-1,n}} h_K^2 (v_K, \psi_K v_K)_K \, ds \\
&= \int_{I_n} \{ \langle \partial_t(u - u_{h\tau}^n), \lambda \rangle + (\nabla \beta(u) - \nabla \beta(u_{h\tau}^n), \nabla \lambda) \\
&\quad + (\nabla \beta(u_{h\tau}^n) - \mathbf{l}_h^n, \nabla \lambda) + (\hat{f}^n - f, \lambda) \} \, ds \\
&\leq \left(\|\mathcal{R}(u_{h\tau}^n)\|_{X'_n} + \eta_{\text{LRQT}}^n + \|f - \hat{f}\|_{X'_n} \right) \|\lambda\|_{X_n}.
\end{aligned} \tag{1.A.5}$$

By the shape regularity of the mesh $\mathcal{K}^{n-1,n}$ and the inverse inequality, [44, Proposition 6.3.2], we have, for any $K \in \mathcal{K}^{n-1,n}$,

$$\|\nabla \lambda\|_{L^2(K)} = h_K^2 \|\nabla(\psi_K v_K)\|_{L^2(K)} \lesssim h_K \|\psi_K v_K\|_{L^2(K)} \leq h_K \|v_K\|_{L^2(K)}.$$

An immediate consequence is that $\|\lambda\|_{X_n} \lesssim \eta_{\text{res},1}^n$ and (1.A.4) follows. \square

Lemma 1.A.2 (Estimate of $\eta_{\text{res},2}^n$). *Under the assumptions of Theorem 1.4.4, there holds*

$$\eta_{\text{res},2}^n \lesssim \|\mathcal{R}(u_{h\tau}^n)\|_{X'_n} + \eta_{\text{LRQT}}^n + \|f - \hat{f}\|_{X'_n}. \tag{1.A.6}$$

Proof. Let $F \in \mathcal{F}^{i,n-1,n}$. We denote by \mathcal{K}_F the simplices $K \in \mathcal{K}^{n-1,n}$ that share the face F . Let $v_F := \llbracket \mathbf{l}_h^n \rrbracket \cdot \mathbf{n}_F$ and keep the same notation for the constant extension of v_F into \mathcal{K}_F along the vectors face barycenter–opposite vertex. Owing to Assumption 1.4.2, v_F is a polynomial on \mathcal{K}_F . Let ψ_F be the usual face bubble function supported on \mathcal{K}_F , i.e., the product of the d hat basis functions (barycentric coordinates) $\psi_{\mathbf{a}}$ associated with the vertices \mathbf{a} of the face F . For all $F \in \mathcal{F}^{i,n-1,n}$, set $\lambda_F := h_F \psi_F v_F$ and let $\lambda := \sum_{F \in \mathcal{F}^{i,n-1,n}} \lambda_F$. Note that $\lambda \in H_0^1(\Omega)$ and $\lambda|_{\mathcal{K}_F} \in H_0^1(\mathcal{K}_F)$ for all $F \in \mathcal{F}^{i,n-1,n}$. Using the equivalence of norms in finite-dimensional spaces, integrating by parts in space, using the weak form (1.2.2c), and (1.3.9) together with

the Cauchy–Schwarz inequality, it is inferred, [49],

$$\begin{aligned}
(\eta_{\text{res},2}^n)^2 &\lesssim \int_{I_n} \sum_{F \in \mathcal{F}^{i,n-1,n}} h_F (v_F, \psi_F v_F)_F ds \\
&= \int_{I_n} \sum_{F \in \mathcal{F}^{i,n-1,n}} \sum_{K \in \mathcal{K}_F} \{(\nabla \cdot \mathbf{l}_h^n, \lambda_F)_K + (\mathbf{l}_h^n, \nabla \lambda_F)_K\} ds \\
&= \int_{I_n} \{(\nabla \cdot \mathbf{l}_h^n, \lambda) + (\mathbf{l}_h^n, \nabla \lambda)\} ds \\
&= \int_{I_n} \{ \langle \partial_t(u_{h\tau}^n - u), \lambda \rangle + (\nabla \beta(u_{h\tau}^n) - \nabla \beta(u), \nabla \lambda) + (\hat{f}^n - \partial_t u_{h\tau}^n + \nabla \cdot \mathbf{l}_h^n, \lambda) \\
&\quad + (\mathbf{l}_h^n - \nabla \beta(u_{h\tau}^n), \nabla \lambda) + (f - \hat{f}^n, \lambda) \} ds \\
&\lesssim \left(\|\mathcal{R}(u_{h\tau}^n)\|_{X'_n} + \eta_{\text{LRQT}}^n + \|f - \hat{f}\|_{X'_n} \right) \|\lambda\|_{X_n} \\
&\quad + \eta_{\text{res},1}^n \left\{ \tau^n \sum_{K \in \mathcal{K}^{n-1,n}} h_K^{-2} \|\lambda\|_{L^2(K)}^2 \right\}^{\frac{1}{2}}.
\end{aligned} \tag{1.A.7}$$

Using the fact that, for all $F \in \mathcal{F}^{i,n-1,n}$ and $K \in \mathcal{K}_F^{n-1,n}$, $\|\psi_F v_F\|_{L^2(K)} \lesssim h_F^{\frac{1}{2}} \|v_F\|_{L^2(F)}$, it is inferred that $\tau^n \sum_{K \in \mathcal{K}^{n-1,n}} h_K^{-2} \|\lambda\|_{L^2(K)}^2 \lesssim (\eta_{\text{res},2}^n)^2$, whence by the inverse inequality, $\|\lambda\|_{X_n} \lesssim \eta_{\text{res},2}^n$. Using this fact in (1.A.7) in conjunction with (1.A.4), (1.A.6) follows. \square

Proof of Theorem 1.4.4. It follows from Lemmas 1.A.1 and 1.A.2 and from (1.A.2) that

$$\eta_{\text{sp}}^{n,\epsilon_n,k_n} \lesssim \left\| \mathcal{R}(u_{h\tau}^{n,\epsilon_n,k_n}) \right\|_{X'_n} + \eta_{\text{LRQT}}^n + \|f - \hat{f}\|_{X'_n}. \tag{1.A.8}$$

In order to bound the term η_{LRQT}^n , we proceed as follows. The triangle inequality and the definitions (1.3.13) and (1.3.14) give

$$\eta_{\text{LRQT}}^n \leq \eta_{\text{lin}}^{n,\epsilon_n,k_n} + \eta_{\text{reg}}^{n,\epsilon_n,k_n} + \eta_{\text{qd}}^{n,\epsilon_n,k_n} + \eta_{\text{tm}}^{n,\epsilon_n,k_n}.$$

Thus, proceeding as for the bound (1.A.1),

$$\eta_{\text{LRQT}}^n \leq C \eta_{\text{sp}}^{n,\epsilon_n,k_n},$$

where the constant C only depends on the parameters Γ_{lin} , Γ_{reg} , and Γ_{qd} in the stopping criteria (1.4.1)–(1.4.3) and Γ_{tm} in the balancing criterion (1.4.4). Thus, choosing these parameters small enough, the term η_{LRQT}^n can be made small enough to be discarded from the right-hand side of (1.A.8), [15, Theorem 4.4] and the assertion of Theorem 1.4.4 follows from (1.A.1). \square

1.A.2 Proof of Theorem 1.5.2

We start by proving the following intermediate result.

Lemma 1.A.3 (Duality bound). *Let u be the solution to (1.2.2) and let $u_{h\tau} \in Z$ be such that $\beta(u_{h\tau}) \in X$. Then, there holds, for a.e. $t \in (0, t_F)$,*

$$\begin{aligned} & \frac{2}{L_\beta} \|\beta(u) - \beta(u_{h\tau})\|_{Q_t}^2 \\ & + \|(u - u_{h\tau})(\cdot, t)\|_{H^{-1}(\Omega)}^2 \leq \|u_0 - u_{h\tau}(\cdot, 0)\|_{H^{-1}(\Omega)}^2 + \|\mathcal{R}(u_{h\tau})\|_{X_t'}^2 + \|u - u_{h\tau}\|_{X_t'}^2. \end{aligned} \quad (1.A.9)$$

Proof. For a.e. $t \in (0, t_F)$, we denote by $W(\cdot, t) \in H_0^1(\Omega)$ the solution to

$$(\nabla W(\cdot, t), \nabla \psi) = ((u - u_{h\tau})(\cdot, t), \psi) \quad \forall \psi \in H_0^1(\Omega). \quad (1.A.10)$$

The existence and uniqueness of $W(\cdot, t)$ follow from the Lax–Milgram lemma. Moreover, since $u, u_{h\tau} \in Z$, there holds $W \in X$. Using (1.A.10), it is inferred that

$$\begin{aligned} \|\nabla W(\cdot, t)\|_{L^2(\Omega)} &= \sup_{\psi \in H_0^1(\Omega), \|\nabla \psi\|_{L^2(\Omega)}=1} (\nabla W(\cdot, t), \nabla \psi) \\ &= \sup_{\psi \in H_0^1(\Omega), \|\nabla \psi\|_{L^2(\Omega)}=1} ((u - u_{h\tau})(\cdot, t), \psi) = \|(u - u_{h\tau})(\cdot, t)\|_{H^{-1}(\Omega)}. \end{aligned} \quad (1.A.11)$$

This duality technique is rather standard; see [9] and the references therein. Its origins can be traced back at least to the elliptic projection of Wheeler [53]. In some aspects, it is close to the elliptic reconstruction of Makridakis and Nochetto [31]; however, in [31] it is used to restore optimal order of the a posteriori estimate in $L^\infty(0, t_F; L^2(\Omega))$, whereas here we employ it to obtain a bound on an energy-like norm.

Taking $\varphi = W1_{(0,t)}$ with $1_{(0,t)}$ the characteristic function of the interval $(0, t)$ in definition (1.3.1) and using (1.A.11) and the Young inequality, it is inferred

$$\langle \mathcal{R}(u_{h\tau}), W \rangle_{X_t', X_t} \leq \|\mathcal{R}(u_{h\tau})\|_{X_t'} \|u - u_{h\tau}\|_{X_t'} \leq \frac{1}{2} \|\mathcal{R}(u_{h\tau})\|_{X_t'}^2 + \frac{1}{2} \|u - u_{h\tau}\|_{X_t'}^2. \quad (1.A.12)$$

Moreover,

$$\langle \mathcal{R}(u_{h\tau}), W \rangle_{X_t', X_t} = \int_0^t \langle \partial_t(u - u_{h\tau}), W \rangle(s) ds + \int_0^t (\nabla \beta(u) - \nabla \beta(u_{h\tau}), \nabla W)(s) ds =: \mathfrak{R}_1 + \mathfrak{R}_2. \quad (1.A.13)$$

Recalling (1.A.10), and since $u - u_{h\tau} \in H^1(0, t_F; H^{-1}(\Omega))$, there holds $\partial_t W \in X$ and, for a.e. $s \in (0, t_F)$, $\partial_t W(\cdot, s)$ satisfies in a weak sense

$$\begin{aligned} -\nabla \cdot (\nabla \partial_t W(\cdot, s)) &= \partial_t(u - u_{h\tau})(\cdot, s) && \text{in } \Omega, \\ \partial_t W(\cdot, s) &= 0 && \text{on } \partial\Omega. \end{aligned}$$

Thus, it follows from the definition (1.A.10) of W and from the norm characterization (1.A.11) that

$$\begin{aligned} \mathfrak{R}_1 &= \int_0^t (\partial_t \nabla W, \nabla W)(s) ds = \frac{1}{2} \left(\|\nabla W(\cdot, t)\|_{L^2(\Omega)}^2 - \|\nabla W(\cdot, 0)\|_{L^2(\Omega)}^2 \right) \\ &= \frac{1}{2} \left(\|(u - u_{h\tau})(\cdot, t)\|_{H^{-1}(\Omega)}^2 - \|u_0 - u_{h\tau}(\cdot, 0)\|_{H^{-1}(\Omega)}^2 \right). \end{aligned} \quad (1.A.14)$$

Invoking again the definition (1.A.10) and using the fact that β is nondecreasing and L_β -Lipschitz continuous, there holds

$$\begin{aligned} \mathfrak{R}_2 &= \int_0^t (u - u_{h\tau}, \beta(u) - \beta(u_{h\tau}))(s) ds \geq \frac{1}{L_\beta} \int_0^t (\beta(u) - \beta(u_{h\tau}), \beta(u) - \beta(u_{h\tau}))(s) ds \\ &= \frac{1}{L_\beta} \|\beta(u) - \beta(u_{h\tau})\|_{Q_t}^2. \end{aligned} \tag{1.A.15}$$

The conclusion follows using inequalities (1.A.12), (1.A.14), and (1.A.15) in equation (1.A.13). \square

Corollary 1.A.4 (Application of the Gronwall lemma). *Under the assumptions of Lemma 1.A.3, there holds*

$$\begin{aligned} \|u - u_{h\tau}\|_{X'}^2 &\leq (e^{t_F} - 1) \|u_0 - u_{h\tau}(\cdot, 0)\|_{H^{-1}(\Omega)}^2 + \int_0^{t_F} \left(\|\mathcal{R}(u_{h\tau})\|_{X'_t}^2 + \int_0^t \|\mathcal{R}(u_{h\tau})\|_{X'_s}^2 e^{t-s} ds \right) dt \\ &\quad - \frac{2}{L_\beta} \int_0^{t_F} \left(\|\beta(u) - \beta(u_{h\tau})\|_{Q_t}^2 + \int_0^t \|\beta(u) - \beta(u_{h\tau})\|_{Q_s}^2 e^{t-s} ds \right) dt. \end{aligned}$$

Proof. Using (1.A.9) followed by the Gronwall lemma

$$\xi(t) \leq \alpha(t) + \int_0^t \xi(s) ds \implies \xi(t) \leq \alpha(t) + \int_0^t \alpha(s) e^{t-s} ds,$$

with $\xi(t) := \|(u - u_{h\tau})(\cdot, t)\|_{H^{-1}(\Omega)}^2$ and

$$\alpha(t) := \|u_0 - u_{h\tau}(\cdot, 0)\|_{H^{-1}(\Omega)}^2 + \|\mathcal{R}(u_{h\tau})\|_{X'_t}^2 - \frac{2}{L_\beta} \|\beta(u) - \beta(u_{h\tau})\|_{Q_t}^2,$$

it is inferred, for a.e. $t \in (0, t_F)$,

$$\begin{aligned} \|(u - u_{h\tau})(\cdot, t)\|_{H^{-1}(\Omega)}^2 &\leq e^t \|u_0 - u_{h\tau}(\cdot, 0)\|_{H^{-1}(\Omega)}^2 + \|\mathcal{R}(u_{h\tau})\|_{X'_t}^2 + \int_0^t \|\mathcal{R}(u_{h\tau})\|_{X'_s}^2 e^{t-s} ds \\ &\quad - \frac{2}{L_\beta} \left(\|\beta(u) - \beta(u_{h\tau})\|_{Q_t}^2 + \int_0^t \|\beta(u) - \beta(u_{h\tau})\|_{Q_s}^2 e^{t-s} ds \right). \end{aligned}$$

The assertion follows by integrating over the interval $(0, t_F)$. \square

We are now ready to prove Theorem 1.5.2:

Proof of Theorem 1.5.2. Using (1.A.9) with $t = t_F$ and adding $\|u - u_{h\tau}\|_{X'}^2$ to both sides we infer

$$\begin{aligned} \mathfrak{L} &:= \frac{2}{L_\beta} \|\beta(u) - \beta(u_{h\tau})\|_{Q_{t_F}}^2 + \|u - u_{h\tau}\|_{X'}^2 + \|(u - u_{h\tau})(\cdot, t_F)\|_{H^{-1}(\Omega)}^2 \\ &\leq \|u_0 - u_{h\tau}(\cdot, 0)\|_{H^{-1}(\Omega)}^2 + \|\mathcal{R}(u_{h\tau})\|_{X'}^2 + 2\|u - u_{h\tau}\|_{X'}^2. \end{aligned}$$

Using Corollary 1.A.4 to estimate the last term in the right-hand side we obtain

$$\begin{aligned} \mathfrak{L} \leq & (2e^{t_F} - 1) \|u_0 - u_{h\tau}(\cdot, 0)\|_{H^{-1}(\Omega)}^2 + \|\mathcal{R}(u_{h\tau})\|_{X'}^2 \\ & + 2 \int_0^{t_F} \left(\|\mathcal{R}(u_{h\tau})\|_{X'_t}^2 + \int_0^t \|\mathcal{R}(u_{h\tau})\|_{X'_s}^2 e^{t-s} ds \right) dt \\ & - \frac{4}{L_\beta} \int_0^{t_F} \left(\|\beta(u) - \beta(u_{h\tau})\|_{Q_t}^2 + \int_0^t \|\beta(u) - \beta(u_{h\tau})\|_{Q_s}^2 e^{t-s} ds \right) dt. \end{aligned}$$

The conclusion follows multiplying both sides by $L_\beta/2$ and rearranging the terms. \square

Bibliography

- [1] H. W. Alt and S. Luckhaus. Quasilinear elliptic-parabolic differential equations. *Math. Z.*, 183(3):311–341, 1983.
- [2] G. Amiez and P.-A. Gremaud. On a numerical approach to Stefan-like problems. *Numer. Math.*, 59(1):71–89, 1991.
- [3] B. Andreianov, M. Bendahmane, and K. H. Karlsen. Discrete duality finite volume schemes for doubly nonlinear degenerate hyperbolic-parabolic equations. *J. Hyperbolic Differ. Equ.*, 7(1):1–67, 2010.
- [4] L. A. Baughman and N. J. Walkington. Co-volume methods for degenerate parabolic problems. *Numer. Math.*, 64(1):45–67, 1993.
- [5] M. Bebendorf. A note on the Poincaré inequality for convex domains. *Z. Anal. Anwendungen*, 22(4):751–756, 2003.
- [6] G. Beckett, J. A. Mackenzie, and M. L. Robertson. A moving mesh finite element method for the solution of two-dimensional Stefan problems. *J. Comput. Phys.*, 168(2):500–518, 2001.
- [7] P. Benilan and P. Wittbold. On mild and weak solutions of elliptic-parabolic problems. *Adv. Differential Equations*, 1(6):1053–1073, 1996.
- [8] D. Braess and J. Schöberl. Equilibrated residual error estimator for edge elements. *Math. Comp.*, 77(262):651–672, 2008.
- [9] C. Cancès, I. S. Pop, and M. Vohralík. An a posteriori error estimate for vertex-centered finite volume discretizations of immiscible incompressible two-phase flow. *Math. Comp.*, 2013. Accepted for publication.
- [10] L. Čermák and M. Zlámal. Transformation of dependent variables and the finite element solution of nonlinear evolution equations. *Internat. J. Numer. Methods Engrg.*, 15(1):31–40, 1980.
- [11] P. G. Ciarlet. *The finite element method for elliptic problems*, volume 40 of *Classics in Applied Mathematics*. Society for Industrial and Applied Mathematics (SIAM), Philadelphia, PA, 2002. Reprint of the 1978 original [North-Holland, Amsterdam].

-
- [12] J. F. Ciavaldini. Analyse numérique d'un problème de Stefan à deux phases par une méthode d'éléments finis. *SIAM J. Numer. Anal.*, 12:464–487, 1975.
- [13] P. Destuynder and B. Métivet. Explicit error bounds in a conforming finite element method. *Math. Comp.*, 68(228):1379–1396, 1999.
- [14] V. Dolejší, A. Ern, and M. Vohralík. A framework for robust a posteriori error control in unsteady nonlinear advection-diffusion problems. *SIAM J. Numer. Anal.*, 51(2):773–793, 2013.
- [15] L. El Alaoui, A. Ern, and M. Vohralík. Guaranteed and robust a posteriori error estimates and balancing discretization and linearization errors for monotone nonlinear problems. *Comput. Methods Appl. Mech. Engrg.*, 200(37-40):2782–2795, 2011.
- [16] C. M. Elliott. On the finite element approximation of an elliptic variational inequality arising from an implicit time discretization of the Stefan problem. *IMA J. Numer. Anal.*, 1(1):115–125, 1981.
- [17] A. Ern and M. Vohralík. Flux reconstruction and a posteriori error estimation for discontinuous Galerkin methods on general nonmatching grids. *C. R. Math. Acad. Sci. Paris*, 347(7-8):441–444, 2009.
- [18] A. Ern and M. Vohralík. A posteriori error estimation based on potential and flux reconstruction for the heat equation. *SIAM J. Numer. Anal.*, 48(1):19–223, 2010.
- [19] A. Ern and M. Vohralík. Adaptive inexact Newton methods with a posteriori stopping criteria for nonlinear diffusion PDEs. *SIAM J. Sci. Comput.*, 2013. Accepted for publication.
- [20] R. Eymard, T. Gallouët, and R. Herbin. Finite volume methods. In *Handbook of Numerical Analysis, Vol. VII*, pages 713–1020. North-Holland, Amsterdam, 2000.
- [21] R. Eymard, T. Gallouët, D. Hilhorst, and Y. Naït Slimane. Finite volumes and nonlinear diffusion equations. *RAIRO Modél. Math. Anal. Numér.*, 32(6):747–761, 1998.
- [22] A. Friedman. The Stefan problem in several space variables. *Trans. Amer. Math. Soc.*, 133:51–87, 1968.
- [23] D. Hilhorst and M. Vohralík. A posteriori error estimates for combined finite volume–finite element discretizations of reactive transport equations on nonmatching grids. *Comput. Methods Appl. Mech. Engrg.*, 200(5–8):597–613, 2011.
- [24] W. Jäger and J. Kačur. Solution of porous medium type systems by linear approximation schemes. *Numer. Math.*, 60(3):407–427, 1991.
- [25] J. W. Jerome and M. E. Rose. Error estimates for the multidimensional two-phase Stefan problem. *Math. Comp.*, 39(160):377–414, 1982.
- [26] P. Jiránek, Z. Strakoš, and M. Vohralík. A posteriori error estimates including algebraic error and stopping criteria for iterative solvers. *SIAM J. Sci. Comput.*, 32(3):1567–1590, 2010.

-
- [27] S. L. Kamenomostskaja. On Stefan's problem. *Mat. Sb. (N.S.)*, 53 (95):489–514, 1961.
- [28] C. T. Kelley and J. Rulla. Solution of the time discretized Stefan problem by Newton's method. *Nonlinear Anal.*, 14(10):851–872, 1990.
- [29] P. Ladevèze. *Comparaison de modèles de milieux continus*. Ph.D. thesis, Université Pierre et Marie Curie (Paris 6), 1975.
- [30] R. Luce and B. I. Wohlmuth. A local a posteriori error estimator based on equilibrated fluxes. *SIAM J. Numer. Anal.*, 42(4):1394–1414, 2004.
- [31] C. Makridakis and R. H. Nochetto. Elliptic reconstruction and a posteriori error estimates for parabolic problems. *SIAM J. Numer. Anal.*, 41(4):1585–1594, 2003.
- [32] G. H. Meyer. Multidimensional Stefan problems. *SIAM J. Numer. Anal.*, 10:522–538, 1973.
- [33] R. H. Nochetto. Error estimates for multidimensional singular parabolic problems. *Japan J. Appl. Math.*, 4(1):111–138, 1987.
- [34] R. H. Nochetto, M. Paolini, and C. Verdi. An adaptive finite element method for two-phase Stefan problems in two space dimensions. I. Stability and error estimates. *Math. Comp.*, 57(195):73–108, 1991.
- [35] R. H. Nochetto, M. Paolini, and C. Verdi. An adaptive finite element method for two-phase Stefan problems in two space dimensions. II. Implementation and numerical experiments. *SIAM J. Sci. Statist. Comput.*, 12(5):1207–1244, 1991.
- [36] R. H. Nochetto, A. Schmidt, and C. Verdi. A posteriori error estimation and adaptivity for degenerate parabolic problems. *Math. Comp.*, 69(229):1–24, 2000.
- [37] R. H. Nochetto and C. Verdi. The combined use of a nonlinear Chernoff formula with a regularization procedure for two-phase Stefan problems. *Numer. Funct. Anal. Optim.*, 9(11-12):1177–1192, 1987/88.
- [38] F. Otto. L^1 -contraction and uniqueness for quasilinear elliptic-parabolic equations. *J. Differential Equations*, 131(1):20–38, 1996.
- [39] L. E. Payne and H. F. Weinberger. An optimal Poincaré inequality for convex domains. *Arch. Rational Mech. Anal.*, 5:286–292 (1960), 1960.
- [40] M. Picasso. An adaptive finite element algorithm for a two-dimensional stationary Stefan-like problem. *Comput. Methods Appl. Mech. Engrg.*, 124(3):213–230, 1995.
- [41] M. Picasso. Adaptive finite elements for a linear parabolic problem. *Comput. Methods Appl. Mech. Engrg.*, 167(3-4):223–237, 1998.
- [42] I. S. Pop, M. Sepúlveda, F. A. Radu, and O. P. Vera Villagrán. Error estimates for the finite volume discretization for the porous medium equation. *J. Comput. Appl. Math.*, 234(7):2135–2142, 2010.

-
- [43] W. Prager and J. L. Synge. Approximations in elasticity based on the concept of function space. *Quart. Appl. Math.*, 5:241–269, 1947.
- [44] A. Quarteroni and A. Valli. *Numerical approximation of partial differential equations*, volume 23 of *Springer Series in Computational Mathematics*. Springer-Verlag, Berlin, 1994.
- [45] S. I. Repin. *A posteriori estimates for partial differential equations*, volume 4 of *Radon Series on Computational and Applied Mathematics*. Walter de Gruyter GmbH & Co. KG, Berlin, 2008.
- [46] R. Verfürth. A posteriori error estimates for nonlinear problems. $L^r(0, T; L^p(\Omega))$ -error estimates for finite element discretizations of parabolic equations. *Math. Comp.*, 67(224):1335–1360, 1998.
- [47] R. Verfürth. A posteriori error estimates for nonlinear problems: $L^r(0, T; W^{1,p}(\Omega))$ -error estimates for finite element discretizations of parabolic equations. *Numer. Methods Partial Differential Equations*, 14(4):487–518, 1998.
- [48] R. Verfürth. A posteriori error estimates for finite element discretizations of the heat equation. *Calcolo*, 40(3):195–212, 2003.
- [49] R. Verfürth. Robust a posteriori error estimates for stationary convection-diffusion equations. *SIAM J. Numer. Anal.*, 43(4):1766–1782, 2005.
- [50] M. Vohralík. A posteriori error estimation in the conforming finite element method based on its local conservativity and using local minimization. *C. R. Math. Acad. Sci. Paris*, 346(11–12):687–690, 2008.
- [51] M. Vohralík. Guaranteed and fully robust a posteriori error estimates for conforming discretizations of diffusion problems with discontinuous coefficients. *J. Sci. Comput.*, 46(3):397–438, 2011.
- [52] J. A. Wheeler. Permafrost design for the trans-Alaska. In P. T. Boggs, editor, *Moving boundary problems*. Academic Press, New York, 1978.
- [53] M. F. Wheeler. A priori L_2 error estimates for Galerkin approximations to parabolic partial differential equations. *SIAM J. Numer. Anal.*, 10:723–759, 1973.

Chapter 2

A posteriori error estimates, stopping criteria, and adaptivity for multiphase compositional flows in porous media

This chapter consists of an article submitted for publication, written with Daniele Di Pietro, Eric Flauraud, and Martin Vohralík, completed by some additional numerical experiments

Contents

2.1	Introduction	61
2.2	Setting	64
2.2.1	The multiphase compositional model	64
2.2.2	An implicit finite volume scheme with phase-upwind and two-point discretization of diffusive fluxes	68
2.3	A basic a posteriori error estimate	71
2.3.1	Weak solution	71
2.3.2	A generic approximate solution	72
2.3.3	Error measure	73
2.3.4	Flux and pressure reconstructions	74
2.3.5	A posteriori error estimate	74
2.4	Application to finite volume method and adaptivity based on distinguishing the different error components	76
2.4.1	Linearization and algebraic resolution	77
2.4.2	Approximate solution	78
2.4.3	Phase pressure reconstructions	80
2.4.4	Component flux reconstructions	80
2.4.5	Distinguishing the space, time, linearization, and algebraic errors	81

2.4.6	A fully adaptive algorithm	84
2.5	Numerical results	85
2.5.1	Common setting	86
2.5.2	Compressible flow in a homogeneous porous medium	88
2.5.3	Compressible flow in a heterogeneous porous medium	91
2.5.4	Five-spots pattern	98
	Bibliography	105

Abstract

In this chapter we derive a posteriori error estimates for the compositional model of multiphase Darcy flow in porous media, consisting of a system of strongly coupled nonlinear unsteady partial differential and algebraic equations. We show how to control the dual norm of the residual augmented by a nonconformity evaluation term by fully computable estimators. We then decompose the estimators into the space, time, linearization, and algebraic error components. This allows to formulate criteria for stopping the iterative algebraic solver and the iterative linearization solver when the corresponding error components do not affect significantly the overall error. Moreover, the spatial and temporal error components can be balanced by time step and space mesh adaptation. Our analysis applies to a broad class of standard numerical methods, and is independent of the linearization and of the iterative algebraic solvers employed. We exemplify it for the two-point finite volume method with fully implicit Euler time stepping, the Newton linearization, and the GMRes algebraic solver. Numerical results on real-life reservoir engineering examples confirm that significant computational gains can be achieved thanks to our adaptive stopping criteria, already on fixed meshes, without any noticeable loss of precision.

Key words: a posteriori error analysis, adaptive algorithms, compositional Darcy flow, finite volume methods, discretization error, linearization error, algebraic solver error.

2.1 Introduction

Reservoir modeling is an important branch of petroleum engineering which provides predictive tools to elaborate reservoir exploration and oil production strategies. From a mathematical standpoint, the underlying models require the numerical solution of highly nontrivial problems resulting from nonlinear, strongly coupled systems of partial differential and algebraic equations. Our goal is to show that also in such complex cases, one can devise efficient solution algorithms based on a posteriori error estimates that ensure error control and allow significant computational savings in numerical simulations. Improving the performance of reservoir simulators is a key point, since the simulation of complex Darcian flows in three space dimensions accounts for the largest part of the computational effort in optimization models for petroleum fields exploitation.

We focus on the Darcy flow of several fluids through a subsurface porous medium. We suppose that the fluids are composed of a finite number of components that constitute the phases in the reservoir. Under the assumption that the flow process is isothermal, the equations that govern the compositional model are the conservation of the amount of each component supplemented by algebraic equations expressing the conservation of volume, the conservation of the quantity of matter, and the thermodynamic equilibrium.

Several numerical methods have been proposed for the discretization of the compositional model. Finite difference and finite element methods can be used under some assumptions on

the physical data, see [4, 10, 26, 65] and references therein, but do not respect directly the local mass conservation. Mixed finite element methods do not suffer from such a drawback and have been extensively used and analyzed, see, e.g. [30, 24, 25] and references therein. They can moreover easily handle complicated geometries.

Recently, finite volume methods have become popular in reservoir engineering in view of their numerous advantages: they meet the industrial constraints of robustness and low computational cost, they satisfy local conservation, are simple to code, and can be used on a large variety of meshes. Several node-centered finite volume discretizations are presented and compared by Huber and Helming [43]. Cell-centered finite volume methods have been considered in [50, 62, 39, 40]. A symmetric and coercive cell-centered finite volume scheme for discretizing Darcy fluxes has been proposed in [6]. A particularly popular family of cell-centered finite volume schemes in the oil industry is that of multi-point methods, which can be easily plugged into traditional simulators thereby allowing to handle very complicated geometries. They have been studied in the multiphase compositional context by Aavatsmark et al. [1, 2], see also the references therein. More recently, a variation with compact stencil and increased stability has been proposed and analyzed in [5]. For an up-to-date review of discretization methods for diffusive fluxes in the context of geoscience models we refer to [28]; see also Droniou [31] for a wider-scope introduction to finite volume methods for diffusive problems on general meshes.

To the best of our knowledge, almost no work has been done to this day on a posteriori error estimates and stopping criteria for the general version of the multiphase compositional model allowing an arbitrary number of phases and components. The goal of the present work is to fill this gap.

A posteriori error estimates enable to monitor the computational error. For model unsteady nonlinear problems, some of the first rigorous results were obtained by Eriksson and Johnson [34] and by Verfürth [60, 61]. Degenerate problems have subsequently been studied by Nocketto et al. [52], Ohlberger [53], and lastly in [29]. An adaptation of the estimators for finite volume discretizations of hyperbolic conservation laws of Kröner and Ohlberger [48] to a steam-assisted gravity drainage two-component, three-phase flow has been presented by Marmaghani et al. [51]. For multiphase reservoir simulation, adaptive mesh refinement algorithms based on dynamic local grid refinement approaches were first considered by Heinemann [41] and Ewing et al. [37]. Then, in [57], Sammon discussed the development of adaptive techniques in the context of unstructured grids for compositional simulation. Local refinement based on structured grid adaptive mesh refinement was probably first applied by Hornung and Trangenstein in [42] and Trangenstein and Bi [59]. In Pau et al. [54, 55], another development of a structured grid adaptive mesh refinement algorithm for incompressible/compressible two-phase flow in porous media is discussed. Recently, the first rigorous results for immiscible incompressible two-phase flow have appeared. Reference [64] develops a general abstract framework for a posteriori estimates of the dual norm of the residual augmented by a noncon-

formity evaluation term, and proposes an adaptive algorithm with stopping criteria for the iterative solution of the arising linear systems and iterative linearization/iterative coupling, wherein the spatial and temporal errors are equilibrated. This leads to both error control and important computational savings. Rigorous energy-spaces-type bounds have then been obtained for vertex-centered finite volume discretizations in [20].

In this chapter we derive fully computable a posteriori error estimates for a general version of the multiphase compositional model. Following [64], the results are derived for the error measured as the dual norm of the residual augmented by a nonconformity evaluation term. This error measure has the advantage of simplifying the analysis because it stems directly from the given model. It has recently been proved, for conforming discretizations of model nonlinear problems such as the immiscible incompressible two-phase flow in [20] and of the two-phase Stefan problem in [29], that this error measure is an upper bound for an energy-spaces-type norm of the difference between the exact and approximate solutions.

Our a posteriori error estimate can be separated into parts identifying the various sources of the error in the numerical solution. More specifically, we construct: a spatial estimator incorporating the errors related to the space discretization and to the nonconformity of the scheme; a temporal estimator accounting for the time discretization error; a linearization estimator due to the approximate linearization; and, finally, an algebraic estimator due to the inexact solution of the arising linear algebraic systems. Distinguishing the different error components allows to formulate stopping criteria for the iterative linearization and iterative algebraic solvers that stop the iterations when the corresponding error components no longer affect significantly the overall error. We also propose to equilibrate the space and time errors by adapting the choice of the time step and adjusting adaptively the computational mesh. These criteria are collected to design an adaptive algorithm for the resolution of the multiphase compositional model ensuring a user-given precision and significant computational savings compared to the classical resolution of the model, and this already on fixed meshes. Additionally, our estimators prove capable of identifying relevant features of the solution such as well singularities and moving fronts. This anticipates them to be a good tool for the local adaptation of the spatial mesh. This topic will be treated in detail in a future work.

The chapter is organized as follows. In Section 2.2 we describe the system of equations for the multiphase compositional model and identify the unknowns and relevant physical properties along with their dependencies. We also discuss therein a fully implicit cell-centered finite volume discretization with phase upwind and two-point discretization of the diffusive fluxes. In Section 2.3 we introduce the corresponding weak formulation, define the error measure, and state our a posteriori error estimate. In Section 2.4 we distinguish the different arising error components and propose a fully adaptive algorithm. Finally, in Section 2.5 we illustrate our theoretical analysis by numerical results; already on fixed meshes, we obtain the same precision and a speed-up factor of order 10 in terms of the total number of algebraic solver iterations in comparison with the classical resolution.

2.2 Setting

We introduce in this section the multiphase compositional model and its finite volume discretization.

2.2.1 The multiphase compositional model

The compositional Darcy model describes the flow of several fluids through a porous medium reservoir occupying the space region $\Omega \subset \mathbb{R}^d$, $d \in \{2, 3\}$, over the time interval $(0, t_F)$, $t_F > 0$. It is assumed in what follows that Ω is a bounded connected polygon if $d = 2$ or polyhedron if $d = 3$.

2.2.1.1 Model unknowns

We consider a system where matter is present in different *phases* collected in the set $\mathcal{P} = \{p\}$, each containing one or more *components* from the set $\mathcal{C} = \{c\}$. For a given phase $p \in \mathcal{P}$, let $\mathcal{C}_p \subset \mathcal{C}$ be the set of its components, and, for a given component $c \in \mathcal{C}$, denote by \mathcal{P}_c the set of the phases which contain c . For a given phase $p \in \mathcal{P}$, S_p denotes the *saturation*, i.e., the fraction of the pore volume occupied by p , and, for each component $c \in \mathcal{C}_p$, $C_{p,c}$ is the corresponding *molar fraction* in p . Saturations are collected in the vector $\mathbf{S} = (S_p)_{p \in \mathcal{P}}$ while, for all $p \in \mathcal{P}$, molar fractions are collected in the vectors $\mathbf{C}_p := (C_{p,c})_{c \in \mathcal{C}_p}$. We tackle here the isothermal case where no energy source or sink is present and the temperature of both the fluids and the porous medium are fixed to a given value. The dependence on the temperature is hence not taken into account in what follows. We denote by P the *reference pressure* such that the *phase pressures* P_p , $p \in \mathcal{P}$, are expressed as

$$P_p = P_p(P, \mathbf{S}) := P + P_{c_p}(\mathbf{S}), \quad (2.2.1)$$

where $P_{c_p}(\mathbf{S})$ is a *generalized capillary pressure*. In a two-phase system, the standard capillary pressure is defined as the difference between the non-wetting and wetting phase pressures. In multiphase systems, capillary pressures are usually obtained by combining the expressions of capillary pressures for each couple of non-wetting and wetting phases. Formula (2.2.1) allows to deal with this aspect in a more abstract and mathematically convenient way by introducing a symmetry in the treatment of the phases. In practice, the reference pressure is chosen as the pressure of a suitable phase $p \in \mathcal{P}$, whose generalized capillary pressure is hence identically zero. The unknowns of the model are collected in the vector

$$\mathcal{X} := \begin{pmatrix} P \\ (S_p)_{p \in \mathcal{P}} \\ (C_{p,c})_{p \in \mathcal{P}, c \in \mathcal{C}_p} \end{pmatrix}.$$

This gives a total of $1 + N_{\mathcal{P}} + \sum_{p \in \mathcal{P}} N_{\mathcal{C}_p}$ unknowns, (here and in what follows, $N_{\mathcal{S}}$ stands for the cardinality of the set \mathcal{S}).

2.2.1.2 Physical properties

The porous medium is characterized by its *porosity* ϕ and its *absolute permeability* \mathbb{K} , both of which are assumed constant in time for the sake of simplicity. For each fluid phase $p \in \mathcal{P}$, the following properties are relevant to the model (the usual dependence is provided in brackets): (i) the *molar density* $\zeta_p(P_p, \mathbf{C}_p)$; (ii) the *mass density* $\rho_p(P_p, \mathbf{C}_p)$; (iii) the *viscosity* $\mu_p(P_p, \mathbf{C}_p)$; (iv) the *relative permeability* $k_{r,p}(\mathbf{S})$; (v) for all $c \in \mathcal{C}_p$, the *fugacity* $f_{c,p}(P_p, \mathbf{C}_p)$. It is also convenient to define for each phase $p \in \mathcal{P}$ the *mobility* given by $\nu_p(P_p, \mathbf{S}, \mathbf{C}_p) := \zeta_p(P_p, \mathbf{C}_p) \frac{k_{r,p}(\mathbf{S})}{\mu_p(P_p, \mathbf{C}_p)}$.

2.2.1.3 Governing partial differential equations

The governing partial differential equations (PDEs) are obtained by enforcing the conservation of the amounts of each component, using a constitutive law to relate the average phase velocities to the unknowns of the model. The conservation of the amount of each component is expressed by the following system of $N_{\mathcal{C}}$ PDEs:

$$\partial_t l_c + \nabla \cdot \Phi_c = q_c, \quad \forall c \in \mathcal{C}, \quad (2.2.2)$$

where, for each $c \in \mathcal{C}$, the *component flux* Φ_c has the following expression:

$$\Phi_c := \sum_{p \in \mathcal{P}_c} \Phi_{p,c}, \quad \Phi_{p,c} = \Phi_{p,c}(P_p, \mathbf{S}, \mathbf{C}_p) := \nu_p(P_p, \mathbf{S}, \mathbf{C}_p) C_{p,c} \mathbf{v}_p(P_p, \mathbf{C}_p), \quad (2.2.3)$$

and for all $p \in \mathcal{P}$, \mathbf{v}_p represents the *average phase velocity* given by Darcy's law,

$$\mathbf{v}_p = \mathbf{v}_p(P_p, \mathbf{C}_p) = -\mathbb{K} (\nabla P_p - \rho_p(P_p, \mathbf{C}_p) \mathbf{g}) = -\mathbb{K} (\nabla P_p + \rho_p(P_p, \mathbf{C}_p) g \nabla z), \quad (2.2.4)$$

where \mathbf{g} denotes the *gravity vector* acting in the negative z direction and g its Euclidian norm. Additionally, in (2.2.2), $q_c \in L^2((0, t_F); L^2(\Omega))$ denotes a *source or sink* and l_c is the *amount* (in moles) of component c per unit volume,

$$l_c = l_c(\mathcal{X}) = \phi \sum_{p \in \mathcal{P}_c} \zeta_p(P_p, \mathbf{C}_p) S_p C_{p,c}. \quad (2.2.5)$$

For the sake of simplicity, we assume that no-flow boundary conditions are prescribed for all the component fluxes,

$$\Phi_c \cdot \mathbf{n}_\Omega = 0 \quad \text{on } \partial\Omega \times (0, t_F) \quad \forall c \in \mathcal{C}, \quad (2.2.6)$$

where $\partial\Omega$ denotes the boundary of Ω and \mathbf{n}_Ω its unit outward normal. At $t = 0$ we prescribe the *initial amount* of each component,

$$l_c(\cdot, 0) = l_c^0 \quad \forall c \in \mathcal{C}. \quad (2.2.7)$$

2.2.1.4 Closure algebraic equations

The governing PDEs of the previous section need to be supplemented by a system of algebraic equations imposing the volume conservation, the conservation of the quantity of matter, and local thermodynamic equilibria. First, it is assumed that the pore volume is saturated by the phases, i.e.,

$$\sum_{p \in \mathcal{P}} S_p = 1. \quad (2.2.8)$$

Next, by definition, the molar fractions satisfy

$$\sum_{c \in \mathcal{C}_p} C_{p,c} = 1 \quad \forall p \in \mathcal{P}, \quad (2.2.9)$$

which corresponds to a total of $N_{\mathcal{P}}$ algebraic equations. Finally, we assume the thermodynamic equilibrium expressed by

$$\sum_{c \in \mathcal{C}} (N_{\mathcal{P}_c} - 1) = \sum_{p \in \mathcal{P}} N_{\mathcal{C}_p} - N_{\mathcal{C}} \quad (2.2.10)$$

equalities of fugacities. Formulating the thermodynamic equilibrium (2.2.10) for an arbitrary number of phases and components lies out of the scope of the present work, and we limit ourselves in the next section to two examples. For further details we refer to Bear [14] or Chen et al. [25].

2.2.1.5 Examples

To fix the ideas, we now present two common examples of multiphase compositional flows in the context of reservoir simulation.

Example 1 (Three-phase flow). *We consider three phases, typically water, gas, and oil, $\mathcal{P} = \{w, g, o\}$, containing $N_{\mathcal{C}}$ components decomposed into $N_{\mathcal{H}} := N_{\mathcal{C}} - 1$ hydrocarbon components from the set \mathcal{H} , and one water component e . Usually, under isothermal conditions, mass interchange occurs only between the gas phase and the oil phase. Thus, the water phase contains only the water component e with molar fraction $C_{w,e} = 1$. The equations from (2.2.10) expressing the thermodynamic equilibrium between the oil and gas phases take here the form*

$$f_{c,o}(P, \mathbf{C}_o) = f_{c,g}(P, \mathbf{C}_g), \quad \forall c \in \mathcal{H}, \quad (2.2.11)$$

which corresponds to $N_{\mathcal{H}}$ algebraic equations. Condition (2.2.11) is often reformulated as

$$K_c^o(P, \mathbf{C}_o) C_{o,c} = K_c^g(P, \mathbf{C}_g) C_{g,c}, \quad \forall c \in \mathcal{H}, \quad (2.2.12)$$

where K_c^o, K_c^g are the so-called equilibrium constants for the component $c \in \mathcal{H}$ in the oil and gas phases, respectively. Letting $K_c^{o,g} := \frac{K_c^o}{K_c^g}$, we can write (2.2.11) as

$$C_{g,c} = K_c^{o,g}(P, \mathbf{C}_o, \mathbf{C}_g) C_{o,c}, \quad \forall c \in \mathcal{H}, \quad (2.2.13)$$

with $K_c^{\text{o,g}}$ the equilibrium constant between the oil and gas phases for the component $c \in \mathcal{H}$. Using the equations of mass conservation (2.2.2), volume conservation (2.2.8), conservation of the quantity of matter (2.2.9), and the thermodynamic equilibrium (2.2.13), the three-phase compositional model reads

$$\begin{aligned}
\partial_t(\phi\zeta_w S_w C_{w,e}) + \nabla \cdot \left(\frac{\zeta_w k_{r,w}}{\mu_w} C_{w,e} \mathbf{v}_w \right) &= q_e, \\
\partial_t(\phi(\zeta_o S_o C_{o,c} + \zeta_g S_g C_{g,c})) + \nabla \cdot \left(\frac{\zeta_o k_{r,o}}{\mu_o} C_{o,c} \mathbf{v}_o + \frac{\zeta_g k_{r,g}}{\mu_g} C_{g,c} \mathbf{v}_g \right) &= q_c \quad \forall c \in \mathcal{H}, \\
S_w + S_o + S_g &= 1, \\
C_{w,e} &= 1, \\
\sum_{c \in \mathcal{C}_o} C_{o,c} &= 1, \\
\sum_{c \in \mathcal{C}_g} C_{g,c} &= 1, \\
K_c^{\text{o,g}}(P, \mathbf{C}_o, \mathbf{C}_g) C_{o,c} &= C_{g,c}, \quad \forall c \in \mathcal{H},
\end{aligned} \tag{2.2.14}$$

where the phase pressures are given by (2.2.1) and the Darcy velocities by (2.2.4), while the boundary and initial conditions are respectively specified by (2.2.6) and (2.2.7). The total number of equations is $2N_{\mathcal{C}} + 3$. Recall that the unknowns are one reference pressure, $N_{\mathcal{P}}$ saturations, and $\sum_{p \in \mathcal{P}} N_{\mathcal{C}_p}$ molar fractions, totaling

$$1 + N_{\mathcal{P}} + \sum_{p \in \mathcal{P}} N_{\mathcal{C}_p} = 1 + 3 + (1 + 2 \times (N_{\mathcal{C}} - 1)) = 2N_{\mathcal{C}} + 3,$$

which gives us the same number of equations as unknowns.

Example 2 (Miscible two-phase flow). *We next examine how the model of Example 1 simplifies when water is not present. This is precisely the case considered in the numerical examples of Section 2.5 below. The phases are now gas and oil, corresponding to $\mathcal{P} = \{\text{g}, \text{o}\}$, composed of $N_{\mathcal{C}}$ hydrocarbon components with, using the notation of Example 1, $\mathcal{C} = \mathcal{H}$. Mass interchange is allowed between these two phases, and the thermodynamic equilibrium relations are given by (2.2.11) or (2.2.12) as in the previous example. The system of equations (2.2.14)*

simplifies to

$$\begin{aligned}
\partial_t(\phi(\zeta_o S_o C_{o,c} + \zeta_g S_g C_{g,c})) + \nabla \cdot \left(\frac{\zeta_o k_{r,o}}{\mu_o} C_{o,c} \mathbf{v}_o + \frac{\zeta_g k_{r,g}}{\mu_g} C_{g,c} \mathbf{v}_g \right) &= q_c, & \forall c \in \mathcal{C}, \\
S_o + S_g &= 1, \\
\sum_{c \in \mathcal{C}_o} C_{o,c} &= 1, \\
\sum_{c \in \mathcal{C}_g} C_{g,c} &= 1, \\
K_c^{o,g}(P, \mathbf{C}_o, \mathbf{C}_g) C_{o,c} &= C_{g,c}, & \forall c \in \mathcal{C},
\end{aligned} \tag{2.2.15}$$

amounting to $2N_{\mathcal{C}} + 3$ equations. Also in this case we have the same number of equations as unknowns, the latter equaling to

$$1 + N_{\mathcal{P}} + \sum_{p \in \mathcal{P}} N_{\mathcal{C}_p} = 1 + 2 + (2 \times (N_{\mathcal{C}})) = 2N_{\mathcal{C}} + 3.$$

2.2.2 An implicit finite volume scheme with phase-upwind and two-point discretization of diffusive fluxes

In this section we briefly discuss a fully implicit numerical scheme for the multiphase compositional model of Section 2.2.1 based on phase-upwind and two-point finite volume discretization of diffusive fluxes. The use of phase-upwind for the finite volume discretization of the Darcy problem is considered, e.g., in Brenier and Jaffré [16] and Eymard et al. [40]. This scheme is of primary importance due to its stability and consequent popularity in the oil industry.

2.2.2.1 Space-time meshes

Let $(\tau_n)_{1 \leq n \leq N}$ denote a sequence of positive real numbers corresponding to the discrete time steps such that $t_F = \sum_{n=1}^N \tau_n$. We consider the discrete times $(t^n)_{0 \leq n \leq N}$ such that $t^0 := 0$ and, for $1 \leq n \leq N$, $t^n := \sum_{i=1}^n \tau_i$; then we define the time intervals $I_n := (t^{n-1}, t^n)$. For a function of time v with sufficient regularity we denote $v^n := v(t^n)$, $0 \leq n \leq N$, and, for $1 \leq n \leq N$, we define the backward differencing operator

$$\partial_t^n v := \frac{1}{\tau^n} (v^n - v^{n-1}) \tag{2.2.16}$$

that we shall use for both scalar and vector functions.

Let $(\mathcal{M}^n)_{0 \leq n \leq N}$ denote a family of meshes of the space domain Ω superadmissible in the sense of Eymard et al. [38, Definition 3.1]. Common instances of superadmissible meshes are Cartesian orthogonal grids or matching simplicial meshes that satisfy the (strict) Delaunay condition. Superadmissibility requires, in particular, that for all $M \in \mathcal{M}^n$ there exists a point $\mathbf{x}_M \in M$ (the cell center), and for all mesh faces σ , there exists a point $\bar{\mathbf{x}}_\sigma \in \sigma$ (the face

center) such that, for all faces σ lying on the boundary of an element M , the line segment joining \mathbf{x}_M with $\bar{\mathbf{x}}_\sigma$ is \mathbb{K}^{-1} -orthogonal to σ . In what follows we let, for all $M \in \mathcal{M}^n$ and all $\sigma \in \mathcal{E}_M^{i,n}$, $d_{M,\sigma} := \text{dist}(\mathbf{x}_M, \bar{\mathbf{x}}_\sigma)$, where $\mathcal{E}_M^{i,n}$ denotes the faces of an element $M \in \mathcal{M}^n$ not lying on $\partial\Omega$. For every element $M \in \mathcal{M}^n$, we denote by $|M|$ its d -dimensional Lebesgue measure and by h_M its diameter. For $0 \leq n \leq N$, we denote by \mathcal{E}^n the set of mesh faces. Boundary faces are collected in the set $\mathcal{E}^{b,n} := \{\sigma \in \mathcal{E}^n; \sigma \subset \partial\Omega\}$ and we let $\mathcal{E}^{i,n} := \mathcal{E}^n \setminus \mathcal{E}^{b,n}$. For an internal face $\sigma \in \mathcal{E}^{i,n}$ we fix an arbitrary orientation and denote the corresponding unit normal vector by \mathbf{n}_σ . For a boundary face $\sigma \in \mathcal{E}^{b,n}$, \mathbf{n}_σ coincides with the exterior unit normal \mathbf{n}_Ω of Ω .

2.2.2.2 Finite volume discretization

In the context of cell-centered finite volume methods, the unknowns of the model are discretized using one value per cell: For all $0 \leq n \leq N$ we let

$$\mathcal{X}_M^n := (\mathcal{X}_M^n)_{M \in \mathcal{M}^n}, \quad \mathcal{X}_M^n := \begin{pmatrix} P_M^n \\ (S_{p,M}^n)_{p \in \mathcal{P}} \\ (C_{p,c,M}^n)_{p \in \mathcal{P}, c \in \mathcal{C}_p} \end{pmatrix} \quad \forall M \in \mathcal{M}^n. \quad (2.2.17)$$

In particular, in practice, the initial condition (2.2.7) needs to be augmented to

$$\mathcal{X}_M(\cdot, 0) = \mathcal{X}_M^0, \quad (2.2.18)$$

where \mathcal{X}_M^0 typically results from a steady-state equilibrium computation. For simplicity, we suppose that l_c^0 in (2.2.7) is piecewise constant on \mathcal{M}^0 and exactly satisfied by the corresponding components of \mathcal{X}_M^0 . For all time steps $0 \leq n \leq N$ and all $M \in \mathcal{M}^n$, the discrete phase saturations are collected in the vector $\mathbf{S}_M^n := (S_{p,M}^n)_{p \in \mathcal{P}}$ while, for all $p \in \mathcal{P}$, the discrete molar fractions are collected in the vector $\mathbf{C}_{p,M}^n := (C_{p,c,M}^n)_{c \in \mathcal{C}_p}$. We consider in what follows an isotropic, possibly heterogeneous medium such that the local (cell) permeability tensor satisfies $\mathbb{K}|_M = K_M \mathbf{Id}$ for all $M \in \mathcal{M}^n$ and a scalar $K_M > 0$. Since we consider superadmissible meshes, this assumption ensures the consistency of the two-point finite volume discretization of diffusive fluxes. We emphasize, in passing, that the consistency of the discretization scheme is not required in the a posteriori error analysis. As a matter of fact, the proof of Theorem 2.3.3 below does not require to specify the origin of the discrete approximation.

For each phase $p \in \mathcal{P}$, the corresponding phase pressure inside each cell $M \in \mathcal{M}^n$ at time step $0 \leq n \leq N$ is given by

$$P_{p,M}^n = P_{p,M}^n(P_M^n, \mathbf{S}_M^n) := P_M^n + P_{c_p}(\mathbf{S}_M^n). \quad (2.2.19)$$

The PDEs (2.2.2) expressing the conservation of the amount of each component are discretized as follows: For all $1 \leq n \leq N$, we require

$$|M| \partial_t^n l_{c,M} + \sum_{\sigma \in \mathcal{E}_M^{i,n}} F_{c,M,\sigma}(\mathcal{X}_M^n) = |M| q_{c,M}^n, \quad \forall c \in \mathcal{C}, \forall M \in \mathcal{M}^n, \quad (2.2.20)$$

where $q_{c,M}^n := \int_{I_n} \int_M q_c / (|M| \tau_n)$ (more details about the source term will be given in the numerical tests), and the accumulation term is given, for all $0 \leq n \leq N$, by the following discrete version of (2.2.5):

$$l_{c,M}^n = l_{c,M}(\mathcal{X}_M^n) := \phi \sum_{p \in \mathcal{P}_c} \zeta_p(P_{p,M}^n, \mathbf{C}_{p,M}^n) S_{p,M}^n C_{p,c,M}^n \quad \forall c \in \mathcal{C}, \forall M \in \mathcal{M}^n. \quad (2.2.21)$$

For each component $c \in \mathcal{C}$, its total flux across σ results from the sum of the corresponding fluxes for each phase $p \in \mathcal{P}_c$, i.e.,

$$F_{c,M,\sigma}(\mathcal{X}_M^n) := \sum_{p \in \mathcal{P}_c} F_{p,c,M,\sigma}(\mathcal{X}_M^n), \quad (2.2.22)$$

where, for all $p \in \mathcal{P}_c$, all $M \in \mathcal{M}^n$, and all $\sigma \in \mathcal{E}_M^{i,n}$ with $\sigma = \partial M \cap \partial L$,

$$F_{p,c,M,\sigma}(\mathcal{X}_M^n) = \nu_p^\uparrow(\mathcal{X}_M^n) C_{p,c,M_p^\uparrow}^n F_{p,M,\sigma}(\mathcal{X}_M^n), \quad M_p^\uparrow = \begin{cases} M & \text{if } P_{p,M}^n - P_{p,L}^n \geq 0, \\ L & \text{otherwise,} \end{cases} \quad (2.2.23)$$

and with $C_{p,c,M_p^\uparrow}^n$ and $\nu_p^\uparrow(\mathcal{X}_M^n) := \nu_p(P_{p,M_p^\uparrow}^n, \mathbf{S}_{M_p^\uparrow}^n, \mathbf{C}_{p,M_p^\uparrow}^n)$ denoting, respectively, the upstream molar fraction and upstream mobility. In (2.2.23), we have introduced the two-point finite volume approximation of the normal component of the average phase velocity on σ given by

$$F_{p,M,\sigma}(\mathcal{X}_M^n) := |\sigma| \frac{\alpha_M \alpha_L}{\alpha_M + \alpha_L} [P_{p,M}^n - P_{p,L}^n + \rho_{p,\sigma}^n g(z_M - z_L)], \quad \alpha_K := \frac{K_K}{d_{K\sigma}} \quad \forall K \in \{M, L\}, \quad (2.2.24)$$

where $\rho_{p,\sigma}^n$ is an approximation of the mass density of the phase p on the face σ given by (other choices are possible),

$$\rho_{p,\sigma}^n := \frac{(\chi_{p,M}^n \rho_p(P_{p,M}^n, \mathbf{C}_{p,M}^n) + \chi_{p,L}^n \rho_p(P_{p,L}^n, \mathbf{C}_{p,L}^n))}{\chi_{p,M}^n + \chi_{p,L}^n}, \quad \chi_{p,K}^n = \begin{cases} 1 & \text{if } S_{p,K}^n > 0, \\ 0 & \text{otherwise,} \end{cases} \quad K \in \{M, L\}.$$

Boundary fluxes are set to zero for all components to account for the homogeneous natural boundary condition (2.2.6).

Remark 2.2.1 (General meshes and full permeability tensors). *A straightforward variation of this scheme that is consistent on more general meshes and for full permeability tensors consists in using a multi-point expression for $F_{p,M,\sigma}$ (cf. (2.2.24)) in the spirit of [2, 32]; see also [5].*

At the discrete level, volume conservation is expressed by the following relation: For all $1 \leq n \leq N$,

$$\sum_{p \in \mathcal{P}} S_{p,M}^n = 1 \quad \forall M \in \mathcal{M}^n. \quad (2.2.25)$$

Similarly, the discrete conservation of matter in each phase reads, for all $1 \leq n \leq N$,

$$\sum_{c \in \mathcal{C}_p} C_{p,c,M}^n = 1 \quad \forall p \in \mathcal{P}, \forall M \in \mathcal{M}^n. \quad (2.2.26)$$

Finally, the thermodynamic equilibrium is enforced by requiring the equality of fugacities for all time steps inside each cell, leading to

$$\sum_{p \in \mathcal{P}} N_{C_p} - N_C \quad \text{equations} \quad \forall 1 \leq n \leq N, \forall M \in \mathcal{M}^n. \quad (2.2.27)$$

An important remark which can be exploited in the implementation is that (2.2.25), (2.2.26), and the thermodynamic equilibrium (2.2.27) express *local* algebraic relations between the unknowns in *each cell*. This allows to reduce the size of the global linear system to $N_{\mathcal{M}^n} \times N_C$ equations stemming from (2.2.20). A detailed treatment of local elimination strategies is out of the scope of the present work. We emphasize, however, that a local elimination procedure is indeed used in the numerical examples of Section 2.5.

2.3 A basic a posteriori error estimate

We derive here an a posteriori estimate for the error measured by the dual norm of the residual augmented by a nonconformity evaluation term. This choice of the error measure is naturally inspired by the problem, and allows to obtain a fully computable error upper bound. The results of this section are generic for an arbitrary approximation; we show how to apply them to the finite volume setting of Section 2.2.2 in Section 2.4 below.

2.3.1 Weak solution

At this stage, we need to characterize a weak solution for the multiphase compositional model (2.2.1)–(2.2.10). Let $(\cdot, \cdot)_D$ stand for the L^2 -scalar product on $D \subset \Omega$ and $\|\cdot\|_D$ for the associated norm; the same notation is used for both scalar and vector arguments, and the subscript is dropped whenever $D = \Omega$. We define

$$X := L^2((0, t_F); H^1(\Omega)), \quad (2.3.1a)$$

$$Y := H^1((0, t_F); L^2(\Omega)). \quad (2.3.1b)$$

Let $\varepsilon > 0$ be a (small) parameter which only needs to satisfy $\varepsilon \leq 1$. We equip the space X with the norm

$$\|\varphi\|_X := \left\{ \sum_{n=1}^N \int_{I_n} \sum_{M \in \mathcal{M}^n} \|\varphi\|_{X,M}^2 dt \right\}^{\frac{1}{2}}, \quad \|\varphi\|_{X,M}^2 := \varepsilon h_M^{-2} \|\varphi\|_M^2 + \|\nabla \varphi\|_M^2, \quad \varphi \in X. \quad (2.3.2)$$

This choice is motivated by the homogeneous Neumann boundary condition (2.2.6); taking $\varepsilon = 0$ is possible and classical when Dirichlet (pressure) boundary conditions prescribed at least on a part of the boundary, cf. [35, 64, 20]. We suppose sufficient regularity to satisfy:

Assumption 2.3.1 (Weak solution). *There exists a weak solution \mathcal{X} of (2.2.1)–(2.2.10) which can be characterized as follows:*

$$l_c \in Y \quad \forall c \in \mathcal{C}, \quad (2.3.3a)$$

$$P_p(P, \mathbf{S}) \in X \quad \forall p \in \mathcal{P}, \quad (2.3.3b)$$

$$\Phi_c \in [L^2((0, t_F); L^2(\Omega))]^d \quad \forall c \in \mathcal{C}, \quad (2.3.3c)$$

$$\int_0^{t_F} \{(\partial_t l_c, \varphi)(t) - (\Phi_c, \nabla \varphi)(t)\} dt = \int_0^{t_F} (q_c, \varphi)(t) dt \quad \forall \varphi \in X, \forall c \in \mathcal{C}, \quad (2.3.3d)$$

$$\text{the initial condition (2.2.7) holds,} \quad (2.3.3e)$$

$$\text{the algebraic closure equations (2.2.8)–(2.2.10) hold,} \quad (2.3.3f)$$

where P_p , l_c , and Φ_c are defined, respectively, by (2.2.1), (2.2.5), and (2.2.3).

Existence and uniqueness of a weak solution has to our knowledge not been established for the multiphase compositional model. In simplified settings, with typically only two phases present and each phase composed of a single component, such results can be found in [47, 22, 8, 9, 23, 19, 46, 7] and the references therein.

Remark 2.3.2 (Component fluxes). *It follows from (2.3.3a), the assumption $q_c \in L^2((0, t_F); L^2(\Omega))$, (2.3.3c), and (2.3.3d) that actually*

$$\Phi_c \in L^2((0, t_F); \mathbf{H}(\text{div}, \Omega)) \quad \forall c \in \mathcal{C}, \quad (2.3.4a)$$

$$\nabla \cdot \Phi_c = q_c - \partial_t l_c \quad \forall c \in \mathcal{C}, \quad (2.3.4b)$$

$$\Phi_c \cdot \mathbf{n}_\Omega = 0 \quad \text{on } \partial\Omega \times (0, t_F) \quad \forall c \in \mathcal{C}, \quad (2.3.4c)$$

so that the component fluxes Φ_c have the normal trace continuous in a proper sense, the governing equation (2.2.2) is satisfied with a weak divergence, and the boundary conditions (2.2.6) hold in the normal trace sense.

2.3.2 A generic approximate solution

In order to present the results of this section abstractly, not linked to any specific numerical discretization, we suppose here that for each $0 \leq n \leq N$ and $p \in \mathcal{P}$, we are given a piecewise H^1 in space (typically piecewise polynomial of degree ≥ 1 , possibly discontinuous) phase pressure $P_{p,h}^n$. Therefrom, the space–time functions $P_{p,h\tau}$ are created by prescribing $P_{p,h\tau}(t^n) := P_{p,h}^n$, $0 \leq n \leq N$, $P_{p,h\tau}$ thus being piecewise affine and continuous in time. By such an assumption, $P_{p,h\tau}$ are not necessarily included in the energy space X ; we henceforth understand by ∇ the broken gradient operator on the meshes \mathcal{M}^n . Similarly, the amounts of components $l_{c,h}^n$, $0 \leq n \leq N$, $c \in \mathcal{C}$, are supposed L^2 in space (typically piecewise polynomial of degree ≥ 0 , possibly discontinuous) and form the piecewise affine and continuous-in-time functions $l_{c,h\tau}$, $c \in \mathcal{C}$, by $l_{c,h\tau}(t^n) = l_{c,h}^n$. Thus $l_{c,h\tau} \in Y$, in a discrete equivalent of (2.3.3a).

We suppose that the space–time reference pressure, saturation, and molar fraction approximations $P_{h\tau}$, $S_{p,h\tau}$, and $C_{p,c,h\tau}$, $p \in \mathcal{P}$, $c \in \mathcal{C}_p$ are linked to $P_{p,h\tau}$ and $l_{c,h\tau}$ via (2.2.1) and (2.2.5), respectively. Similarly, we suppose that the algebraic closure equations (2.2.8)–(2.2.10) are satisfied exactly, and, for simplicity, that $l_{c,h}^0$ satisfies exactly the initial condition (2.2.7), i.e., $l_{c,h}^0 = l_c^0$. Below, the concise notation for the vector-valued space–time functions $\mathbf{P}_{h\tau} := (P_{p,h\tau})_{p \in \mathcal{P}}$, $\mathbf{S}_{h\tau} := (S_{p,h\tau})_{p \in \mathcal{P}}$ and, for all $p \in \mathcal{P}$, $\mathbf{C}_{p,h\tau} := (C_{p,c,h\tau})_{c \in \mathcal{C}_p}$, will be employed. We show how we obtain the above quantities in the finite volume setting of Section 2.2.2, or more precisely during the calculation including also an iterative linearization and iterative solution of the arising linear systems, in Section 2.4.2 below.

2.3.3 Error measure

Following [64], we consider an error measure for the above approximate solution inspired from the weak formulation (2.3.3), which consists of the dual norm of the residual supplemented by a nonconformity evaluation term. For nonlinear problems, it has been argued in, e.g., [21, 33, 36, 29] that the dual norm of the residual is a more natural choice than the energy norm. Moreover, in the two-phase flow setting with conforming approximations and Dirichlet boundary conditions, it has been shown in [20, Theorem 5.7] that the dual norm of the residual is an upper bound for an energy-type difference between the exact pressures and saturations. Concretely, our error measure is defined as

$$\mathcal{N} = \mathcal{N}(\mathbf{P}_{h\tau}, \mathbf{S}_{h\tau}, (\mathbf{C}_{p,h\tau})_{p \in \mathcal{P}}) := \left\{ \sum_{c \in \mathcal{C}} \mathcal{N}_c^2 \right\}^{\frac{1}{2}} + \left\{ \sum_{p \in \mathcal{P}} \mathcal{N}_p^2 \right\}^{\frac{1}{2}}, \quad (2.3.5)$$

where the quantities \mathcal{N}_c , $c \in \mathcal{C}$, and \mathcal{N}_p , $p \in \mathcal{P}$, have the same dependence as \mathcal{N} . They are defined, respectively, as

$$\mathcal{N}_c := \sup_{\varphi \in X, \|\varphi\|_X=1} \int_0^{t_F} \{(\partial_t l_c - \partial_t l_{c,h\tau}, \varphi)(t) - (\Phi_c - \Phi_{c,h\tau}, \nabla \varphi)(t)\} dt, \quad (2.3.6)$$

with the exact component fluxes Φ_c defined by (2.2.3) and $\Phi_{c,h\tau}$ given by

$$\Phi_{c,h\tau} := \sum_{p \in \mathcal{P}_c} \Phi_{p,c,h\tau}, \quad \Phi_{p,c,h\tau} := \nu_p(P_{p,h\tau}, \mathbf{S}_{h\tau}, \mathbf{C}_{p,h\tau}) C_{p,c,h\tau} \mathbf{v}_p(P_{p,h\tau}, \mathbf{C}_{p,h\tau}), \quad (2.3.7)$$

and

$$\mathcal{N}_p := \inf_{\delta_p \in X} \left\{ \sum_{c \in \mathcal{C}_p} \int_0^{t_F} \|\Psi_{p,c}(P_{p,h\tau})(t) - \Psi_{p,c}(\delta_p)(t)\|^2 dt \right\}^{\frac{1}{2}}, \quad (2.3.8)$$

where, for a space–time function $\varphi \in L^2((0, t_F); H^1(\mathcal{M}))$ (piecewise regular with respect to the partitions \mathcal{M}^n), we have let

$$\Psi_{p,c}(\varphi) := \nu_p(P_{p,h\tau}, \mathbf{S}_{h\tau}, \mathbf{C}_{p,h\tau}) C_{p,c,h\tau} \mathbb{K} \nabla \varphi. \quad (2.3.9)$$

The first term \mathcal{N}_c evaluates the non-satisfaction of (2.3.3d) at the discrete level, as $\Phi_{c,h\tau}$ given by (2.3.7) do not necessarily satisfy the conditions (2.3.4), while the second term \mathcal{N}_p quantifies the possible departure of the discrete phase pressures $P_{p,h\tau}$ from the energy space X .

2.3.4 Flux and pressure reconstructions

To estimate the terms \mathcal{N}_c in the error measure (2.3.5) we, for all $1 \leq n \leq N$, introduce N_C *component flux reconstructions* $(\Theta_{c,h}^n)_{c \in \mathcal{C}}$ such that, for all $c \in \mathcal{C}$, $\Theta_{c,h}^n \in \mathbf{H}(\text{div}; \Omega)$ and the following local conservation property holds:

$$(q_{c,h}^n - \partial_t^n l_{c,h\tau} - \nabla \cdot \Theta_{c,h}^n, 1)_M = 0 \quad \forall c \in \mathcal{C}, \forall M \in \mathcal{M}^n, \quad (2.3.10a)$$

where we have introduced the piecewise constant space functions $q_{c,h}^n$, $c \in \mathcal{C}$, such that $(q_{c,h}^n)|_M = \int_{I_n} \int_M q_c / (|M| \tau_n)$. For further use we also define the space–time functions $q_{c,h\tau}$, $c \in \mathcal{C}$, such that $q_{c,h\tau}|_{I_n} = q_{c,h}^n$ for all $1 \leq n \leq N$. It is also assumed that the boundary condition (2.2.6) is satisfied exactly, i.e.,

$$\Theta_{c,h}^n \cdot \mathbf{n}_\Omega = 0 \quad \text{on } \partial\Omega. \quad (2.3.10b)$$

We denote by $\Theta_{c,h\tau}$ the space–time function such that $\Theta_{c,h\tau}|_{I_n} = \Theta_{c,h}^n$ for all $1 \leq n \leq N$. Note that $\Theta_{c,h\tau}$ mimic the properties of the weak component fluxes Φ_c as expressed in Remark 2.3.2. In practice, $\Theta_{c,h}^n$ are constructed in the Raviart–Thomas–Nédélec finite-dimensional subspaces of $\mathbf{H}(\text{div}; \Omega)$; details in the finite volume context are given in Section 2.4.4 below.

To estimate the terms \mathcal{N}_p in (2.3.5), we need $N_{\mathcal{P}}$ *phase pressure reconstructions* $\mathfrak{P}_{p,h\tau}$, $p \in \mathcal{P}$, such that $\mathfrak{P}_{p,h\tau} \in X$ for all $p \in \mathcal{P}$. These reconstructions are typically piecewise polynomial continuous in space and piecewise affine continuous in time. Details in the finite volume context are given in Section 2.4.3 below.

2.3.5 A posteriori error estimate

We now derive a fully computable upper bound for the approximate solution as specified in Section 2.3.2, the error measure introduced in Section 2.3.3, and based on the pressure and flux reconstructions of Section 2.3.4. A key ingredient is the following Poincaré inequality:

$$\|\varphi - \varphi_M\|_M \leq C_{P,M} h_M \|\nabla \varphi\|_M \quad \forall \varphi \in H^1(M), \forall M \in \mathcal{M}^n, 1 \leq n \leq N, \quad (2.3.11)$$

where $\varphi_M := \int_M \varphi / |M|$ denotes the mean value of the function φ on M . We recall that $C_{P,M} = 1/\pi$ for convex cells M (see [56, 15]).

For all $1 \leq n \leq N$, $M \in \mathcal{M}^n$, and $c \in \mathcal{C}$, we define the *residual estimators* $\eta_{R,M,c}^n$, the *flux estimators* $\eta_{F,M,c}^n(t)$, $t \in I_n$, and the *nonconformity estimators* $\eta_{NC,M,p,c}^n(t)$, $t \in I_n$, $p \in \mathcal{P}_c$, as

follows:

$$\eta_{\mathbb{R},M,c}^n := \min\{C_{P,M}, \varepsilon^{-\frac{1}{2}}\} h_M \|q_{c,h}^n - \partial_t^n l_{c,h\tau} - \nabla \cdot \Theta_{c,h}^n\|_M, \quad (2.3.12a)$$

$$\eta_{\mathbb{F},M,c}^n(t) := \|\Theta_{c,h}^n - \Phi_{c,h\tau}(t)\|_M, \quad (2.3.12b)$$

$$\eta_{\mathbb{NC},M,p,c}^n(t) := \|\Psi_{p,c}(P_{p,h\tau})(t) - \Psi_{p,c}(\mathfrak{P}_{p,h\tau})(t)\|_M. \quad (2.3.12c)$$

Theorem 2.3.3 (A posteriori estimate for the error measure (2.3.5)). *Under Assumption 2.3.1, for the flux and pressure reconstructions of Section 2.3.4, and with the estimators given by (2.3.12), there holds*

$$\mathcal{N}_c \leq \left\{ \sum_{n=1}^N \int_{I_n} \sum_{M \in \mathcal{M}^n} (\eta_{\mathbb{R},M,c}^n + \eta_{\mathbb{F},M,c}^n(t))^2 dt \right\}^{\frac{1}{2}} + \|q_c - q_{c,h\tau}\|_{X'}, \quad c \in \mathcal{C}, \quad (2.3.13a)$$

$$\mathcal{N}_p \leq \left\{ \sum_{c \in \mathcal{C}_p} \sum_{n=1}^N \int_{I_n} \sum_{M \in \mathcal{M}^n} (\eta_{\mathbb{NC},M,p,c}^n(t))^2 dt \right\}^{\frac{1}{2}} \quad p \in \mathcal{P}. \quad (2.3.13b)$$

Remark 2.3.4 (Source term). *In reservoir simulation, the source terms q_c , $c \in \mathcal{C}$, are typically piecewise constant on the space–time mesh. Then, the last term in the estimate (2.3.13a), called data oscillation in numerical analysis literature, vanishes.*

Proof. The proof is simple using the equilibrated flux reconstructions $\Theta_{c,h}^n$. To bound \mathcal{N}_c , let $\varphi \in X$ be such that $\|\varphi\|_X = 1$. There holds

$$\begin{aligned} \Gamma(\varphi) &:= \int_0^{t_F} \{(\partial_t l_c - \partial_t l_{c,h\tau}, \varphi)(t) - (\Phi_c - \Phi_{c,h\tau}, \nabla \varphi)(t)\} dt \\ &= \int_0^{t_F} \{(q_c - \partial_t l_{c,h\tau}, \varphi)(t) + (\Phi_{c,h\tau}, \nabla \varphi)(t)\} dt \\ &= \int_0^{t_F} \{(q_{c,h\tau} - \partial_t l_{c,h\tau} - \nabla \cdot \Theta_{c,h\tau}, \varphi)(t) - (\Theta_{c,h\tau} - \Phi_{c,h\tau}, \nabla \varphi)(t)\} dt \\ &\quad + \int_0^{t_F} (q_c - q_{c,h\tau}, \varphi)(t) dt \\ &= \sum_{n=1}^N \int_{I_n} \{(q_{c,h}^n - \partial_t^n l_{c,h\tau} - \nabla \cdot \Theta_{c,h}^n, \varphi)(t) - (\Theta_{c,h}^n - \Phi_{c,h\tau}, \nabla \varphi)(t)\} dt \\ &\quad + \int_0^{t_F} (q_c - q_{c,h\tau}, \varphi)(t) dt, \end{aligned}$$

where we have used (2.3.3d) in the second line and we have added and subtracted $(\Theta_{c,h\tau}, \nabla \varphi)(t)$ and used Green's theorem along with (2.3.10b) to infer $(\nabla \cdot \Theta_{c,h\tau}, \varphi)(t) + (\Theta_{c,h\tau}, \nabla \varphi)(t) = 0$ in the third line. For all $1 \leq n \leq N$ and $t \in I_n$, using the local conservation property (2.3.10a) followed by the Cauchy–Schwarz and Poincaré's (2.3.11) inequalities,

and recalling (2.3.12a), it is inferred,

$$\begin{aligned}
(q_{c,h}^n - \partial_t^n l_{c,h\tau} - \nabla \cdot \Theta_{c,h}^n, \varphi)(t) &= \sum_{M \in \mathcal{M}^n} (q_{c,h}^n - \partial_t^n l_{c,h\tau} - \nabla \cdot \Theta_{c,h}^n, \varphi)_M(t) \\
&= \sum_{M \in \mathcal{M}^n} (q_{c,h}^n - \partial_t^n l_{c,h\tau} - \nabla \cdot \Theta_{c,h}^n, \varphi - \varphi_M)_M(t) \\
&\leq \sum_{M \in \mathcal{M}^n} \|q_{c,h}^n - \partial_t^n l_{c,h\tau} - \nabla \cdot \Theta_{c,h}^n\|_M \|\varphi - \varphi_M\|_M(t) \\
&\leq \sum_{M \in \mathcal{M}^n} \min\{C_{P,M}, \varepsilon^{-\frac{1}{2}}\} h_M \|q_{c,h}^n - \partial_t^n l_{c,h\tau} - \nabla \cdot \Theta_{c,h}^n\|_M \|\varphi\|_{X,M}(t) \\
&= \sum_{M \in \mathcal{M}^n} \eta_{R,M,c}^n \|\varphi\|_{X,M}(t).
\end{aligned}$$

Using again the Cauchy–Schwarz inequality yields for all $1 \leq n \leq N$ and $t \in I_n$,

$$-(\Theta_{c,h}^n - \Phi_{c,h\tau}, \nabla \varphi)(t) = \sum_{M \in \mathcal{M}^n} -(\Theta_{c,h}^n - \Phi_{c,h\tau}, \nabla \varphi)_M(t) \leq \sum_{M \in \mathcal{M}^n} \eta_{F,M,c}^n(t) \|\nabla \varphi\|_M(t).$$

Thus,

$$\Gamma(\varphi) \leq \sum_{n=1}^N \int_{I_n} \sum_{M \in \mathcal{M}^n} \{(\eta_{R,M,c}^n + \eta_{F,M,c}^n(t)) \|\varphi\|_{X,M}(t)\} dt + \|q_c - q_{c,h\tau}\|_{X'} \|\varphi\|_X. \quad (2.3.14)$$

Finally, using the Cauchy–Schwarz inequality together with the definition (2.3.2) of the norm on X and $\|\varphi\|_X = 1$ to bound the first term in equation (2.3.14) yields the estimate (2.3.13a).

The estimate (2.3.13b) is obtained using the X –regularity of the phase pressure reconstructions $\mathfrak{P}_{p,h\tau}$ defined in Section 2.3.4 to bound the infimum in (2.3.8). \square

2.4 Application to finite volume method and adaptivity based on distinguishing the different error components

We apply here the abstract result of the previous section to the finite volume discretization introduced in Section 2.2.2. Moreover, we consider a practical implementation of (2.2.18)–(2.2.27), requiring the solution of the arising system of nonlinear algebraic equations at each time step. Distinguishing the different error components in the basic a posteriori error estimate of Theorem 2.3.3, we propose stopping criteria for the employed iterative algebraic and linearization solvers. An entirely adaptive algorithm, also balancing the time and space error components via adaptive time step choice and adaptive mesh refinement, is proposed. For the sake of simplicity, we assume henceforth that the source terms q_c , $c \in \mathcal{C}$, are piecewise constant on the space–time mesh, so that the last term in the estimate (2.3.13a) vanishes, cf. Remark 2.3.4.

2.4.1 Linearization and algebraic resolution

The finite volume method discussed in Section 2.2.2 requires to solve a *system of nonlinear algebraic equations* at each time step. Recalling (2.2.16), for all $1 \leq n \leq N$, the discrete conservation of components (2.2.20) can be rewritten as

$$R_{c,M}^n(\mathcal{X}_M^n) := \frac{|M|}{\tau^n} (l_{c,M}(\mathcal{X}_M^n) - l_{c,M}^{n-1}) + \sum_{\sigma \in \mathcal{E}_M^{i,n}} F_{c,M,\sigma}(\mathcal{X}_M^n) - |M| q_{c,M}^n = 0 \quad \forall c \in \mathcal{C}, \forall M \in \mathcal{M}^n. \quad (2.4.1)$$

System (2.4.1) can be solved by any suitable linearization. In what follows, we focus on the *Newton linearization algorithm*, although the a posteriori error analysis developed in this work can be easily adapted to accommodate other linearization algorithms in the spirit of [36].

For $1 \leq n \leq N$ and $\mathcal{X}_M^{n,0}$ fixed (typically, $\mathcal{X}_M^{n,0} = \mathcal{X}_M^{n-1}$), the Newton algorithm generates a sequence $(\mathcal{X}_M^{n,k})_{k \geq 1}$ with $\mathcal{X}_M^{n,k}$ solution to the following *system of linear algebraic equations*: For all $c \in \mathcal{C}$ and all $M \in \mathcal{M}^n$,

$$\sum_{M' \in \mathcal{M}^n} \frac{\partial R_{c,M}^n}{\partial \mathcal{X}_{M'}^n}(\mathcal{X}_M^{n,k-1}) \cdot (\mathcal{X}_{M'}^{n,k} - \mathcal{X}_{M'}^{n,k-1}) + R_{c,M}^n(\mathcal{X}_M^{n,k-1}) = 0. \quad (2.4.2)$$

The (approximate) solution to (2.4.2) is typically obtained using an *iterative algebraic solver*. For $1 \leq n \leq N$, a given Newton iteration $k \geq 1$, and $\mathcal{X}_M^{n,k,0}$ fixed (typically, $\mathcal{X}_M^{n,k,0} = \mathcal{X}_M^{n,k-1}$), the iterative solver generates a sequence $(\mathcal{X}_M^{n,k,i})_{i \geq 1}$ solving (2.4.2) up to the residuals, given for all $c \in \mathcal{C}$ and all $M \in \mathcal{M}^n$ by

$$R_{c,M}^{n,k,i} := \sum_{M' \in \mathcal{M}^n} \frac{\partial R_{c,M}^n}{\partial \mathcal{X}_{M'}^n}(\mathcal{X}_M^{n,k-1}) \cdot (\mathcal{X}_{M'}^{n,k,i} - \mathcal{X}_{M'}^{n,k-1}) + R_{c,M}^n(\mathcal{X}_M^{n,k-1}). \quad (2.4.3)$$

Plugging (2.4.1) into (2.4.3), it is inferred

$$\begin{aligned} R_{c,M}^{n,k,i} &= \sum_{M' \in \mathcal{M}^n} \frac{|M|}{\tau^n} \frac{\partial l_{c,M}}{\partial \mathcal{X}_{M'}^n}(\mathcal{X}_M^{n,k-1}) \cdot (\mathcal{X}_{M'}^{n,k,i} - \mathcal{X}_{M'}^{n,k-1}) \\ &\quad + \sum_{M' \in \mathcal{M}^n} \sum_{\sigma \in \mathcal{E}_M^{i,n}} \frac{\partial F_{c,M,\sigma}}{\partial \mathcal{X}_{M'}^n}(\mathcal{X}_M^{n,k-1}) \cdot (\mathcal{X}_{M'}^{n,k,i} - \mathcal{X}_{M'}^{n,k-1}) + R_{c,M}^n(\mathcal{X}_M^{n,k-1}). \end{aligned} \quad (2.4.4)$$

The first and the second terms in the right-hand side of (2.4.4) are linear perturbations of the corresponding terms in (2.4.1). The linear perturbation in the accumulation is

$$\mathcal{L}_{c,M}^{n,k,i} := \sum_{M' \in \mathcal{M}^n} \frac{\partial l_{c,M}}{\partial \mathcal{X}_{M'}^n}(\mathcal{X}_M^{n,k-1}) \cdot (\mathcal{X}_{M'}^{n,k,i} - \mathcal{X}_{M'}^{n,k-1}), \quad (2.4.5)$$

whereas the linearized component flux reads

$$F_{c,M,\sigma}^{n,k,i} := \sum_{p \in \mathcal{P}_c} F_{p,c,M,\sigma}^{n,k,i}, \quad (2.4.6)$$

with linearized phase component fluxes

$$F_{p,c,M,\sigma}^{n,k,i} := F_{p,c,M,\sigma}(\mathcal{X}_{\mathcal{M}}^{n,k-1}) + \sum_{M' \in \mathcal{M}^n} \frac{\partial F_{p,c,M,\sigma}}{\partial \mathcal{X}_{M'}^n}(\mathcal{X}_{\mathcal{M}}^{n,k-1}) \cdot (\mathcal{X}_{M'}^{n,k,i} - \mathcal{X}_{M'}^{n,k-1}). \quad (2.4.7)$$

In conclusion, at time step n , Newton iteration $k \geq 1$, and linear solver iteration $i \geq 1$, the residual vector $R_{c,M}^{n,k,i}$ is given by

$$R_{c,M}^{n,k,i} = \frac{|M|}{\tau^n} \left(l_{c,M}(\mathcal{X}_{\mathcal{M}}^{n,k-1}) + \mathcal{L}_{c,M}^{n,k,i} - l_{c,M}^{n-1} \right) + \sum_{\sigma \in \mathcal{E}_M^{i,n}} F_{c,M,\sigma}^{n,k,i} - |M|q_{c,M}^n \quad \forall c \in \mathcal{C}, \forall M \in \mathcal{M}^n. \quad (2.4.8)$$

2.4.2 Approximate solution

In this section we identify the approximate solutions, as discussed in Section 2.3.2, for the finite volume setting of Sections 2.2.2 and 2.4.1. We will need some finite-dimensional subspaces of $\mathbf{H}(\text{div}, \Omega)$. When the meshes \mathcal{M}^n consist of rectangular parallelepipeds, as it is the case in the numerical experiments of Section 2.5 below, we use

$$\begin{aligned} \mathbf{RTN}(\mathcal{M}^n) := \{ & \mathbf{v}_h \in \mathbf{H}(\text{div}; \Omega); \mathbf{v}_h|_M \in \mathbb{Q}_{0,1}(M) \times \mathbb{Q}_{1,0}(M) \text{ if } d = 2, \\ & \mathbb{Q}_{0,1,1}(M) \times \mathbb{Q}_{1,0,1}(M) \times \mathbb{Q}_{1,1,0}(M) \text{ if } d = 3, \forall M \in \mathcal{M}^n \}. \end{aligned} \quad (2.4.9)$$

For general meshes, one typically introduces matching simplicial submeshes of \mathcal{M}^n , here still denoted \mathcal{M}^n , and uses

$$\mathbf{RTN}(\mathcal{M}^n) := \left\{ \mathbf{v}_h \in \mathbf{H}(\text{div}; \Omega); \mathbf{v}_h|_M \in [\mathbb{P}_0(M)]^d + \mathbf{x}\mathbb{P}_0(M), \forall M \in \mathcal{M}^n \right\}. \quad (2.4.10)$$

For more details on the lowest-order Raviart–Thomas–Nédélec spaces (2.4.9) and (2.4.10), we refer to Brezzi and Fortin [17].

Remark 2.4.1 (General meshes and full permeability tensors). *For more general polygonal or polyhedral meshes and full permeability tensors, one possibility is to replace the Raviart–Thomas–Nédélec spaces (2.4.9) and (2.4.10) by the generalization proposed in [27, Appendix A], which has the remarkable property that it guarantees $\mathbf{H}(\text{div}; \Omega)$ -conformity without the need for a subdivision of the elements into tetrahedra in three space dimensions.*

2.4.2.1 Phase pressure postprocessings

As explained in Sections 2.3.2 and 2.3.3, we need to evaluate the broken gradient of the discrete phase pressures $P_{p,h}^n$, $p \in \mathcal{P}$, $0 \leq n \leq N$. The original finite volume pressure approximations $F_{p,M}^n$ of (2.2.19), or, more precisely, $F_{p,M}^{n,k,i}$ obtained from $\mathcal{X}_{\mathcal{M}}^{n,k,i}$ in Section 2.4.1, are only piecewise constant. We thus, following [63], define piecewise quadratic, possibly discontinuous phase pressures as follows. Let $1 \leq n \leq N$, a Newton linearization iteration $k \geq 1$,

and an algebraic solver iteration $i \geq 1$ be fixed. For all $p \in \mathcal{P}$ we define $\mathbf{\Gamma}_{p,h}^{n,k,i} \in \mathbf{RTN}(\mathcal{M}^n)$ such that, for all $M \in \mathcal{M}^n$ and all $\sigma \in \mathcal{E}_M^{i,n}$,

$$(\mathbf{\Gamma}_{p,h}^{n,k,i} \cdot \mathbf{n}_M, 1)_\sigma = F_{p,M,\sigma}(\mathcal{X}_{\mathcal{M}}^{n,k,i}),$$

with $F_{p,M,\sigma}$ defined by (2.2.24) and $\mathbf{\Gamma}_{p,h}^{n,k,i} \cdot \mathbf{n}_\Omega = 0$ on $\partial\Omega$. The fluxes $\mathbf{\Gamma}_{p,h}^{n,k,i}$ are thus discrete versions of the Darcy velocities \mathbf{v}_p from (2.2.4). Motivated by (2.2.4), we then, for each $p \in \mathcal{P}$, introduce the piecewise quadratic phase pressure $P_{p,h}^{n,k,i}$ such that, for all $M \in \mathcal{M}^n$,

$$(-\mathbb{K}\nabla P_{p,h}^{n,k,i})|_M = (\mathbf{\Gamma}_{p,h}^{n,k,i})|_M - (\mathbb{K}\rho_p(P_{p,M}^{n,k,i}, \mathbf{C}_{p,M}^{n,k,i})\mathbf{g})|_M \quad \text{and} \quad \frac{(P_{p,h}^{n,k,i}, 1)_M}{|M|} = P_{p,M}^{n,k,i}. \quad (2.4.11)$$

The space–time function $P_{p,h\tau}^{n,k,i}$ is then as usual continuous and piecewise affine in time, given by $P_{p,h}^{n,k,i}$ at the discrete times t^n ; for $n = 0$, the initial datum from (2.2.18) is used.

Remark 2.4.2 (General meshes and full permeability tensors). *On more general polygonal or polyhedral meshes and for full permeability tensors, one can alternatively define for all $p \in \mathcal{P}$ a piecewise affine, possibly discontinuous pressures $P_{p,h}^{n,k,i}$ replacing $(\mathbf{\Gamma}_{p,h}^{n,k,i})|_M$ in (2.4.11) by*

$$\sum_{\sigma \in \mathcal{E}_M^{i,n}} \frac{|\sigma|}{|M|} F_{p,M,\sigma}(\mathcal{X}_{\mathcal{M}}^{n,k,i})(\mathbf{x}_\sigma - \mathbf{x}_M).$$

The use of the above formula to lift fluxes is justified in [5, Section 2.3].

2.4.2.2 Reference pressure, saturations, molar fractions, and amounts of components

The approximations of all saturations, molar fractions, and amounts of components by the finite volume approach of Sections 2.2.2 and 2.4.1 is piecewise constant on the meshes \mathcal{M}^n . We keep them as such and use the notations (recall the definition of the function $l_{c,M}$ of (2.2.21))

$$(S_{p,h}^{n,k,i})|_M = S_{p,M}^{n,k,i}, \quad (2.4.12a)$$

$$(C_{p,c,h}^{n,k,i})|_M = C_{p,c,M}^{n,k,i}, \quad (2.4.12b)$$

$$(l_{c,h}^{n,k,i})|_M = l_{c,M}^{n,k,i} := l_{c,M}(\mathcal{X}_{\mathcal{M}}^{n,k,i}), \quad (2.4.12c)$$

for $0 \leq n \leq N$, $k \geq 1$, $i \geq 1$, $M \in \mathcal{M}^n$, $p \in \mathcal{P}$, and $c \in \mathcal{C}_p$. The space–time functions $S_{p,h\tau}^{n,k,i}$, $C_{p,c,h\tau}^{n,k,i}$, and $l_{c,h\tau}^{n,k,i}$ are then defined therefrom while being continuous and piecewise affine in time. In what concerns the reference pressure $P_{h\tau}^{n,k,i}$, it does not appear explicitly in what follows.

In Section 2.3.2, we have made the assumption that the links (2.2.1) and (2.2.5), as well as the algebraic closure equations (2.2.8)–(2.2.10), are satisfied exactly for the discrete

approximations $P_{h\tau}^{n,k,i}$, $S_{p,h\tau}^{n,k,i}$, $C_{p,c,h\tau}^{n,k,i}$, $P_{p,h\tau}^{n,k,i}$, and $l_{c,h\tau}^{n,k,i}$. This may not hold precisely for all of the required links for the above construction but we suppose the error from this non-satisfaction is negligible. Typically (2.2.8) and (2.2.9) holds precisely, but (2.2.1) and (2.2.5) may be violated (the capillary pressure function applied to a piecewise polynomial is typically no more a piecewise polynomial and a product of two piecewise affine-in-time functions is a piecewise quadratic-in-time function) and (2.2.10) will be violated if the local fugacity equations are not resolved exactly.

2.4.3 Phase pressure reconstructions

We define the phase pressure reconstructions discussed in Section (2.3.4) from $P_{p,h}^{n,k,i}$ of (2.4.11) by

$$\mathfrak{P}_{p,h}^{n,k,i} = \mathcal{I}(P_{p,h}^{n,k,i}) \quad p \in \mathcal{P}, \quad (2.4.13)$$

$0 \leq n \leq N$, $k \geq 1$, $i \geq 1$, where \mathcal{I} denotes the vertex-averaging interpolator. This operator has been introduced in the context of a posteriori error estimates for finite volume discretizations of Darcy's equations by Achdou et al. [3] and in the discontinuous Galerkin setting by Karakashian and Pascal [45]. As usual, $\mathfrak{P}_{p,h\tau}$ is then continuous and piecewise affine in time, given by $\mathfrak{P}_{p,h}^{n,k,i}$ at the discrete times t^n . Most importantly, it satisfies $\mathfrak{P}_{p,h\tau} \in X$.

2.4.4 Component flux reconstructions

We provide here details on how to build the component flux reconstructions in the spirit of Section 2.3.4 for the finite volume setting of Sections 2.2.2 and 2.4.1. Several different flux reconstructions will be introduced to accommodate the presence of different error components.

Let a time step $1 \leq n \leq N$, a Newton linearization iteration $k \geq 1$, and an algebraic solver iteration $i \geq 1$ be fixed. For all $c \in \mathcal{C}$, the *discretization flux reconstruction* $\Theta_{\text{dis},c,h}^{n,k,i} \in \mathbf{RTN}(\mathcal{M}^n)$ is such that, for all $M \in \mathcal{M}^n$ and all $\sigma \in \mathcal{E}_M^{i,n}$,

$$(\Theta_{\text{dis},c,h}^{n,k,i} \cdot \mathbf{n}_M, 1)_\sigma := F_{c,M,\sigma}(\mathcal{X}_M^{n,k,i}), \quad (2.4.14a)$$

with $F_{c,M,\sigma}$ defined by (2.2.22), while $\Theta_{\text{dis},c,h}^{n,k,i} \cdot \mathbf{n}_\Omega = 0$ on $\partial\Omega$ coherently with (2.2.6). For all $c \in \mathcal{C}$ we also define a *linearization error flux reconstruction* $\Theta_{\text{lin},c,h}^{n,k,i} \in \mathbf{RTN}(\mathcal{M}^n)$ such that, for all $M \in \mathcal{M}^n$ and for all $\sigma \in \mathcal{E}_M^{i,n}$,

$$(\Theta_{\text{lin},c,h}^{n,k,i} \cdot \mathbf{n}_M, 1)_\sigma = F_{c,M,\sigma}^{n,k,i} - F_{c,M,\sigma}(\mathcal{X}_M^{n,k,i}), \quad (2.4.14b)$$

with $F_{c,M,\sigma}^{n,k,i}$ defined by (2.4.6), and, similarly, an *algebraic error flux reconstruction* $\Theta_{\text{alg},c,h}^{n,k,i} \in \mathbf{RTN}(\mathcal{M}^n)$ such that, for all $M \in \mathcal{M}^n$ and for all $\sigma \in \mathcal{E}_M^{i,n}$,

$$(\Theta_{\text{alg},c,h}^{n,k,i} \cdot \mathbf{n}_M, 1)_{\partial M} := -R_{c,M}^{n,k,i}, \quad (2.4.14c)$$

with $R_{c,M}^{n,k,i}$ defined by (2.4.8). To complete both (2.4.14b) and (2.4.14c), we set respectively $\Theta_{\text{lin},c,h}^{n,k,i} \cdot \mathbf{n}_\Omega = 0$ and $\Theta_{\text{alg},c,h}^{n,k,i} \cdot \mathbf{n}_\Omega = 0$ on $\partial\Omega$. For all $c \in \mathcal{C}$, the equivalent of the component flux reconstruction $\Theta_{c,h}^n$ from Section 2.3.4 is then given by

$$\Theta_{c,h}^{n,k,i} := \Theta_{\text{dis},c,h}^{n,k,i} + \Theta_{\text{lin},c,h}^{n,k,i} + \Theta_{\text{alg},c,h}^{n,k,i}. \quad (2.4.14d)$$

Remark 2.4.3 (Algebraic error). *In practice it is rather difficult to satisfy (2.4.14c) exactly, though it is possible following, e.g., [44, Section 7.3]. Following [36, Section 4] we prefer to compute our algebraic error flux reconstruction by: (i) performing j additional iterations of the algebraic solver from the stage (2.4.3), with j a user-defined fixed number; (ii) computing $\Theta_{\text{dis},c,h}^{n,k,i+j}$ and $\Theta_{\text{lin},c,h}^{n,k,i+j}$ as in (2.4.14a) and (2.4.14b), respectively, with i replaced by $i+j$; (iii) defining the algebraic error flux reconstruction as $\Theta_{\text{alg},c,h}^{n,k,i} := \Theta_{\text{dis},c,h}^{n,k,i+j} + \Theta_{\text{lin},c,h}^{n,k,i+j} - (\Theta_{\text{dis},c,h}^{n,k,i} + \Theta_{\text{lin},c,h}^{n,k,i})$. Then, (2.4.14c) only holds approximately (the better the bigger j is), but turns out to work perfectly in practice.*

2.4.5 Distinguishing the space, time, linearization, and algebraic errors

In this section, we first give a time-localized version of Theorem 2.3.3. Subsequently, we derive an a posteriori error estimate distinguishing the space, time, linearization, and algebraic error components.

2.4.5.1 A time-localized a posteriori error estimate

Let $1 \leq n \leq N$, a Newton linearization iteration $k \geq 1$, and an algebraic solver iteration $i \geq 1$ be fixed. It follows from (2.4.8), the definition (2.4.14d) of the flux reconstruction $\Theta_{c,h}^{n,k,i}$, and Green's theorem that there holds, for all $c \in \mathcal{C}$,

$$\left(q_{c,h}^n - \frac{l_{c,M}(\mathcal{X}_M^{n,k-1}) + \mathcal{L}_{c,M}^{n,k,i} - l_{c,M}^{n-1}}{\tau^n} - \nabla \cdot \Theta_{c,h}^{n,k,i}, 1 \right)_M = 0 \quad \forall M \in \mathcal{M}^n. \quad (2.4.15)$$

Unfortunately, owing to the nonlinear accumulation term, compare the definition (2.4.12c) of $l_{c,h\tau}^{n,k,i}$ with (2.4.8), (2.4.15) is not a full equivalent of (2.3.10a). However, we can still elaborate Theorem 2.3.3 as follows. For all $c \in \mathcal{C}$, define the following refined version of the estimators of (2.3.12), with the additional *nonlinear accumulation estimator* $\eta_{\text{NA},M,c}^{n,k,i}$:

$$\eta_{\text{R},M,c}^{n,k,i} := \min\{C_{\text{P},M}, \varepsilon^{-\frac{1}{2}}\} h_M \left\| q_{c,h}^n - (\tau^n)^{-1} (l_{c,M}(\mathcal{X}_M^{n,k-1}) + \mathcal{L}_{c,M}^{n,k,i} - l_{c,M}^{n-1}) - \nabla \cdot \Theta_{c,h}^{n,k,i} \right\|_M, \quad (2.4.16a)$$

$$\eta_{\text{F},M,c}^{n,k,i}(t) := \left\| \Theta_{c,h}^{n,k,i} - \Phi_{c,h\tau}^{n,k,i}(t) \right\|_M \quad t \in I_n, \quad (2.4.16b)$$

$$\eta_{\text{NC},M,p,c}^{n,k,i}(t) := \left\| \Psi_{p,c}(P_{p,h\tau}^{n,k,i})(t) - \Psi_{p,c}(\mathfrak{P}_{p,h\tau}^{n,k,i})(t) \right\|_M \quad t \in I_n, p \in \mathcal{P}_c, \quad (2.4.16c)$$

$$\eta_{\text{NA},M,c}^{n,k,i} := \varepsilon^{-\frac{1}{2}} h_M (\tau^n)^{-1} \left\| l_{c,M}(\mathcal{X}_M^{n,k,i}) - l_{c,M}(\mathcal{X}_M^{n,k-1}) - \mathcal{L}_{c,M}^{n,k,i} \right\|_M, \quad (2.4.16d)$$

where the functions $\Psi_{p,c}$, $p \in \mathcal{P}$, $c \in \mathcal{C}_p$, are defined by (2.3.9), while

$$\Phi_{c,h\tau}^{n,k,i} := \sum_{p \in \mathcal{P}_c} \Phi_{p,c,h\tau}^{n,k,i}, \quad \Phi_{p,c,h\tau}^{n,k,i} := \nu_p(P_{p,h\tau}^{n,k,i}, \mathbf{S}_{h\tau}^{n,k,i}, \mathbf{C}_{p,h\tau}^{n,k,i}) C_{p,c,h\tau}^{n,k,i} \mathbf{v}_p(P_{p,h\tau}^{n,k,i}, \mathbf{C}_{p,h\tau}^{n,k,i}).$$

In the spirit of Section 2.3.3, we define the time-localized error measure,

$$\mathcal{N}^n := \left\{ \sum_{c \in \mathcal{C}} (\mathcal{N}_c^n)^2 \right\}^{\frac{1}{2}} + \left\{ \sum_{p \in \mathcal{P}} (\mathcal{N}_p^n)^2 \right\}^{\frac{1}{2}}, \quad (2.4.17)$$

where \mathcal{N}_c^n , $c \in \mathcal{C}$, and \mathcal{N}_p^n , $p \in \mathcal{P}$, are defined as (2.3.6) and (2.3.8), respectively, with the current approximations indexed n, k, i and the time integration performed on the time intervals I_n instead of $(0, t_F)$. Note that

$$\mathcal{N}_c = \sum_{n=1}^N (\mathcal{N}_c^n)^2, \quad \mathcal{N}_p = \sum_{n=1}^N (\mathcal{N}_p^n)^2.$$

We then have:

Corollary 2.4.4 (Time-localized a posteriori error estimate). *Consider a time step $1 \leq n \leq N$, a Newton linearization iteration $k \geq 1$, and an algebraic solver iteration $i \geq 1$. Under Assumption 2.3.1, for the approximate solution of Section 2.4.2, the phase pressure reconstructions of Section 2.4.3, the component flux reconstructions of Section 2.4.4, and with the estimators given by (2.4.16), there holds*

$$\mathcal{N}_c^n \leq \left\{ \int_{I_n} \sum_{M \in \mathcal{M}^n} (\eta_{R,M,c}^{n,k,i} + \eta_{F,M,c}^{n,k,i}(t) + \eta_{NA,M,c}^{n,k,i})^2 dt \right\}^{\frac{1}{2}} \quad c \in \mathcal{C}, \quad (2.4.18a)$$

$$\mathcal{N}_p^n \leq \left\{ \sum_{c \in \mathcal{C}_p} \int_{I_n} \sum_{M \in \mathcal{M}^n} (\eta_{NC,M,p,c}^{n,k,i}(t))^2 dt \right\}^{\frac{1}{2}} \quad p \in \mathcal{P}. \quad (2.4.18b)$$

Proof. The proof is a slight modification of that of Theorem 2.3.3. We only need to estimate

$$\begin{aligned} & \sum_{n=1}^N \int_{I_n} \sum_{M \in \mathcal{M}^n} (\partial_t l_{c,h\tau}^{n,k,i} - (\tau^n)^{-1} (l_{c,M}(\mathcal{X}_M^{n,k-1}) + \mathcal{L}_{c,M}^{n,k,i} - l_{c,M}^{n-1}), \varphi)_M(t) dt \\ &= \sum_{n=1}^N \int_{I_n} \sum_{M \in \mathcal{M}^n} ((\tau^n)^{-1} (l_{c,M}(\mathcal{X}_M^{n,k,i}) - l_{c,M}(\mathcal{X}_M^{n,k-1}) - \mathcal{L}_{c,M}^{n,k,i}), \varphi)_M(t) dt \\ &\leq \sum_{n=1}^N \int_{I_n} \sum_{M \in \mathcal{M}^n} \eta_{NA,M,c}^{n,k,i} \varepsilon^{\frac{1}{2}} h_M^{-1} \|\varphi\|_M(t) dt \leq \sum_{n=1}^N \int_{I_n} \sum_{M \in \mathcal{M}^n} \eta_{NA,M,c}^{n,k,i} \|\varphi\|_{X,M}(t) dt, \end{aligned}$$

to combine this bound with (2.3.14) and the definition (2.3.2) of the norm on the space X , and restrict the result to the given time interval. \square

2.4.5.2 Distinguishing the different error components

For all $1 \leq n \leq N$, $k \geq 1$, $i \geq 1$, $M \in \mathcal{M}^n$, and $c \in \mathcal{C}$, we define the *spatial estimators* evaluating the error related to the spatial mesh resolution,

$$\eta_{\text{sp},M,c}^{n,k,i}(t) := \eta_{\text{R},M,c}^{n,k,i} + \left\| \Theta_{\text{dis},c,h}^{n,k,i} - \Phi_{c,h\tau}^{n,k,i}(t^n) \right\|_M + \left\{ \sum_{p \in \mathcal{P}_c} (\eta_{\text{NC},M,p,c}^{n,k,i}(t))^2 \right\}^{\frac{1}{2}} \quad t \in I_n, \quad (2.4.19a)$$

the *temporal estimators* evaluating the error related to the size of the time step,

$$\eta_{\text{tm},M,c}^{n,k,i}(t) := \left\| \Phi_{c,h\tau}^{n,k,i}(t^n) - \Phi_{c,h\tau}^{n,k,i}(t) \right\|_M \quad t \in I_n, \quad (2.4.19b)$$

the *linearization estimators* measuring the error in the linearization of the nonlinear system (2.4.1),

$$\eta_{\text{lin},M,c}^{n,k,i} := \left\| \Theta_{\text{lin},c,h}^{n,k,i} \right\|_M + \eta_{\text{NA},M,c}^{n,k,i}, \quad (2.4.19c)$$

and the *algebraic estimators* that quantify the error in the algebraic iterative resolution of the linear system (2.4.2),

$$\eta_{\text{alg},M,c}^{n,k,i} := \left\| \Theta_{\text{alg},c,h}^{n,k,i} \right\|_M. \quad (2.4.19d)$$

For all $c \in \mathcal{C}$, global versions of these estimators are given by

$$\eta_{\text{sp},c}^{n,k,i} := \left\{ 4 \int_{I_n} \sum_{M \in \mathcal{M}^n} (\eta_{\text{sp},M,c}^{n,k,i}(t))^2 dt \right\}^{\frac{1}{2}}, \quad (2.4.20a)$$

$$\eta_{\text{tm},c}^{n,k,i} := \left\{ 2 \int_{I_n} \sum_{M \in \mathcal{M}^n} (\eta_{\text{tm},M,c}^{n,k,i}(t))^2 dt \right\}^{\frac{1}{2}}, \quad (2.4.20b)$$

$$\eta_{\text{lin},c}^{n,k,i} := \left\{ 2\tau^n \sum_{M \in \mathcal{M}^n} (\eta_{\text{lin},M,c}^{n,k,i})^2 \right\}^{\frac{1}{2}}, \quad (2.4.20c)$$

$$\eta_{\text{alg},c}^{n,k,i} := \left\{ 2\tau^n \sum_{M \in \mathcal{M}^n} (\eta_{\text{alg},M,c}^{n,k,i})^2 \right\}^{\frac{1}{2}}. \quad (2.4.20d)$$

Using the triangle inequality and Corollary 2.4.4, we can estimate the time-localized norm \mathcal{N}^n of (2.4.17) as follows:

Corollary 2.4.5 (Distinguishing the space, time, linearization, and algebraic errors). *Under the assumptions of Corollary 2.4.4, there holds, with the estimators given by (2.4.20),*

$$\mathcal{N}^n \leq \left\{ \sum_{c \in \mathcal{C}} (\eta_{\text{sp},c}^{n,k,i} + \eta_{\text{tm},c}^{n,k,i} + \eta_{\text{lin},c}^{n,k,i} + \eta_{\text{alg},c}^{n,k,i})^2 \right\}^{\frac{1}{2}}. \quad (2.4.21)$$

2.4.6 A fully adaptive algorithm

In this section we propose an adaptive algorithm based on the estimators (2.4.20). Let $\gamma_{\text{lin}}, \gamma_{\text{alg}} \in (0, 1)$ be user-given parameters; these express respectively the fraction allowed for the linearization and algebraic error components. Similarly, let the parameters for balancing the spatial and temporal errors $\Gamma_{\text{tm}} > \gamma_{\text{tm}} > 0$ be fixed. Finally, let crit_c^n stand for the maximal error allowed in the component c on the time interval I_n . Our algorithm is as follows:

1. Initialization

- (a) Choose an initial mesh \mathcal{M}^0 , an initial time step τ^0 , and set $t^0 := 0$ and $n := 0$.
- (b) Set up the initial approximation $\mathcal{X}_{\mathcal{M}}^0$.

2. Loop in time

- (a) Set $n := n + 1$, $\mathcal{M}^n := \mathcal{M}^{n-1}$, $\tau^n := \tau^{n-1}$, and $k := 0$.
- (b) Define $\mathcal{X}_{\mathcal{M}}^{n,0} := \mathcal{X}_{\mathcal{M}}^{n-1}$.
- (c) **Spatial and temporal errors balancing loop**

i. Newton linearization loop

A. Newton initialization

- Set $k := k + 1$ and $i := 0$.
- Define $\mathcal{X}_{\mathcal{M}}^{n,k,0} := \mathcal{X}_{\mathcal{M}}^{n,k-1}$.

B. Set up the linear system.

- Compute the linearized component fluxes $F_{c,M,\sigma}^{n,k,i}$, $c \in \mathcal{C}$, following (2.4.6).
- Compute the perturbation of the accumulation term $\mathcal{L}_{c,M}^{n,k,i}$, $c \in \mathcal{C}$, following (2.4.5).
- Assemble the linear system following (2.4.8).

C. Algebraic solver loop

- Set $i := i + 1$.
- Perform a step of the iterative algebraic solver for the solution of (2.4.8).
- **A posteriori estimators**
 - Build the postprocessed phase pressures following (2.4.11).
 - Construct the approximations of the saturations, molar fractions, and amounts of components following (2.4.12).
 - Prescribe the continuous phase pressure reconstructions following (2.4.13).
 - Construct the component flux reconstructions $\Theta_{\text{dis},c,h}^{n,k,i}$, $\Theta_{\text{lin},c,h}^{n,k,i}$, $\Theta_{\text{alg},c,h}^{n,k,i}$ and $\Theta_{c,h}^{n,k,i}$ following (2.4.14).
 - Evaluate the different estimators defined by (2.4.20).
- **Terminate the algebraic solver loop if**

$$\eta_{\text{alg},c}^{n,k,i} \leq \gamma_{\text{alg}} (\eta_{\text{sp},c}^{n,k,i} + \eta_{\text{tm},c}^{n,k,i} + \eta_{\text{lin},c}^{n,k,i}), \quad \forall c \in \mathcal{C}. \quad (2.4.22)$$

D. Update

- Update the unknowns; set $\mathcal{X}_{\mathcal{M}}^{n,k} := \mathcal{X}_{\mathcal{M}}^{n,k,i}$.

E. Terminate the Newton linearization loop if

$$\eta_{\text{lin},c}^{n,k,i} \leq \gamma_{\text{lin}}(\eta_{\text{sp},c}^{n,k,i} + \eta_{\text{tm},c}^{n,k,i}), \quad \forall c \in \mathcal{C}. \quad (2.4.23)$$

- ii. Adapt the time step if necessary.
- iii. If spatial mesh adaptation is considered, refine or coarsen the mesh \mathcal{M}^n in function of the distribution of the local spatial error estimators $\eta_{\text{sp},M,c}^{n,k,i}(t)$ of (2.4.19a).
- iv. **Terminate the spatial and temporal errors balancing loop if**

$$\gamma_{\text{tm}}\eta_{\text{sp},c}^{n,k,i} \leq \eta_{\text{tm},c}^{n,k,i} \leq \Gamma_{\text{tm}}\eta_{\text{sp},c}^{n,k,i} \quad \text{and} \quad \eta_{\text{sp},c}^{n,k,i} + \eta_{\text{tm},c}^{n,k,i} \leq \text{crit}_c^n \quad \forall c \in \mathcal{C}. \quad (2.4.24)$$

(d) Data update

- i. Set $\mathcal{X}_{\mathcal{M}}^n := \mathcal{X}_{\mathcal{M}}^{n,k,i}$ and $t^n := t^{n-1} + \tau^n$.

(e) End: Loop in time if ($t^n > t^F$).

Note that in (2.4.22) we propose to stop the iterative algebraic solver when the algebraic error components do not affect significantly the overall error. A variation in the spirit of Remark 2.4.3 can be considered where a user-defined number j of linear iterations are performed before recomputing the estimators, and the algebraic estimator is replaced by its approximate version. Similarly, the criterion (2.4.23) expresses the fact that there is no need to continue with the linearization iterations if the overall error is dominated by the space and time errors. Finally, by (2.4.24) we give a way to select the time step τ^n in order to equilibrate the space and time error components; congruently, the spatial mesh should be refined/derefinned. If local adaptive mesh refinement is considered, \mathcal{M}^n should be such that, for all $M_1, M_2 \in \mathcal{M}^n$ with $M_1 \neq M_2$,

$$\eta_{\text{sp},c,M_1}^{n,k,i} \approx \eta_{\text{sp},c,M_2}^{n,k,i}, \quad \forall c \in \mathcal{C}.$$

Local (elementwise) versions of the criteria (2.4.22) and (2.4.23) can be formulated using the local estimators (2.4.19); see [44, 33, 36].

2.5 Numerical results

In this section we illustrate our theoretical results on different test cases representative of enhanced oil recovery techniques of Figure 2.1b. More specifically, we focus on the case when oil recovery is improved by injecting components that are not originally present in the reservoir to increase the mobility, cf., e.g., [49, 58]. Both homogeneous and heterogeneous (but isotropic) porous media are considered.

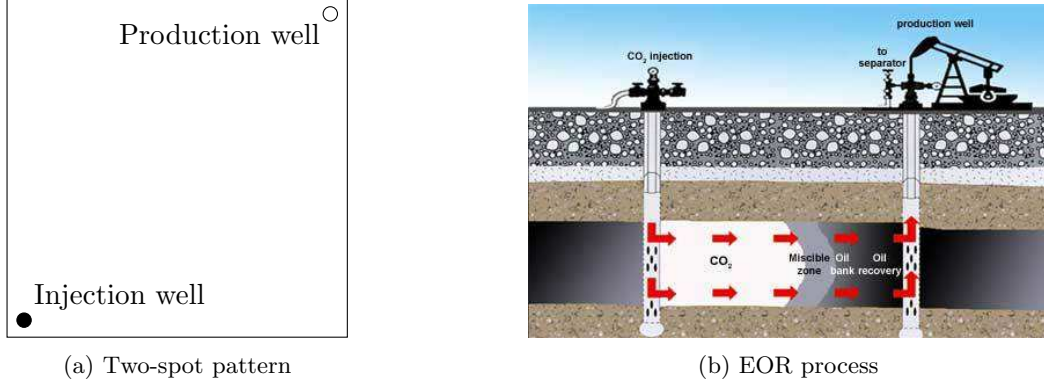


Figure 2.1: Configuration for the numerical test cases

2.5.1 Common setting

We consider the injection of gas composed of carbon dioxide CO_2 (component g_1) and nitrogen N_2 (component g_2) into a reservoir initially saturated with heptanol C_7H_{16} (component o). The three components, collected in the set $\mathcal{C} := \{o, g_1, g_2\}$, can be present in a liquid or gaseous phase corresponding to $\mathcal{P} := \{l, g\}$. This is therefore a special case of the more general problem considered in Example 2. For the test cases we consider two different configurations :

- A spatial domain $\Omega = (0, 1000)\text{m} \times (0, 1000)\text{m}$ with a two-spot pattern, see Figure 2.1a.
- A spatial domain $\Omega = (0, 1500)\text{m} \times (0, 1500)\text{m}$ with a five-spot pattern, see Figure 2.23a.

We have injection wells with pressure fixed to $P_{\text{inj}} = 1.1 \times 10^{10}\text{Pa}$ and one production well with pressure fixed to $P_{\text{pro}} = 9 \times 10^6\text{Pa}$. Wells are modeled as nonlinear source terms as detailed in the following. Denoting by M_{inj} and M_{prod} the cells containing the injection and production wells, respectively, the rates of injection and production of the component $c \in \mathcal{C}$, denoted by $q_{c, M_{\text{inj}}}$ and $q_{c, M_{\text{prod}}}$, are given by the following expressions:

$$|M_{\text{inj}}|q_{c, M_{\text{inj}}} = -\nu_{g, M_{\text{inj}}}(P_{\text{inj}}, S_{g, \text{inj}}, \mathbf{C}_{g, \text{inj}})C_{g, c, \text{inj}}\text{IP}_{M_{\text{inj}}}(P_{g, M_{\text{inj}}} - P_{\text{inj}}),$$

and,

$$|M_{\text{prod}}|q_{c, M_{\text{prod}}} = - \sum_{p \in \mathcal{C}_p} \{ \nu_{p, M_{\text{prod}}}(P_{p, M_{\text{prod}}}, S_{p, M_{\text{prod}}}, \mathbf{C}_{p, M_{\text{prod}}})C_{p, c, M_{\text{prod}}}\text{IP}_{M_{\text{prod}}}(P_{p, M_{\text{prod}}} - P_{\text{pro}}) \},$$

where $S_{g, \text{inj}} = 1$ is the injected gas saturation, $\mathbf{C}_{g, \text{inj}}$ is the vector of injected components molar fractions in gas

$$\mathbf{C}_{g, \text{inj}} = \{C_{g, o, \text{inj}} = 0, C_{g, g_1, \text{inj}} = 0.8, C_{g, g_2, \text{inj}} = 0.2\},$$

and IP_M is the well's production index given, for isotropic medium, by Peaceman's formula:

$$\text{IP}_M := \frac{2\pi k_M \Delta Z_M}{\log(0.14 \frac{r_d}{r_w})}, \quad r_d := \sqrt{\Delta x_M^2 + \Delta y_M^2},$$

with r_w the well radius set to 0.5m, ΔZ_M the perforated mesh height, and $\Delta x_M, \Delta y_M$ the dimensions of the perforated cell M along the x and y axis, respectively.

The required physical properties are chosen as follows: (i) porosity $\phi = 0.1$; (ii) phase molar density $\zeta_p = \sum_{c \in \mathcal{C}} \zeta_c(P) C_{c,p}$, $p \in \{1, g\}$, where ζ_c , $c \in \mathcal{C}$, takes the form

$$\zeta_c(P) = \alpha_c \frac{P - P_{\text{inj}}}{P_{\text{pro}} - P_{\text{inj}}} + \beta_c \frac{P - P_{\text{pro}}}{P_{\text{inj}} - P_{\text{pro}}},$$

with $(\alpha_o, \beta_o) = (6640.88, 6669.32)$, $(\alpha_{g_1}, \beta_{g_2}) = (4703.4, 5567.0)$, and $(\alpha_{g_2}, \beta_{g_2}) = (3062.5, 3676.4)$; (iii) the liquid phase viscosity $\mu_l = 3.2 \times 10^{-4} \text{Pa} \cdot \text{s}$ and the gas phase viscosity $\mu_g = 3.5 \times 10^{-5} \text{Pa} \cdot \text{s}$; (iv) the relative permeability

$$k_{r,p}(S_p) = \begin{cases} 1 & \text{if } S_p \geq 1, \\ \frac{S_p - S_p^{\text{res}}}{1 - S_p^{\text{res}}} & \text{if } S_p^{\text{res}} < S_p < 1, \\ 0 & \text{if } S_p \leq S_p^{\text{res}}, \end{cases}$$

where the residual saturations are respectively given by $S_1^{\text{res}} = 0.2$ and $S_g^{\text{res}} = 0.1$. Concerning the thermodynamic equilibrium between the oil and gas phases

$$C_{g,c} = K_c^{\text{o,g}}(P, C_o, C_g) C_{o,c}, \quad \forall c \in \mathcal{C},$$

we consider here a simple formula, depending just on the pressure, for the equilibrium constant $K_c^{\text{o,g}} = K_c^{\text{o,g}}(P)$ between the oil and gas phases for the component $c \in \mathcal{C}$ given by

$$K_c^{\text{o,g}}(P) = \gamma_c \frac{P - P_{\text{inj}}}{P_{\text{pro}} - P_{\text{inj}}} + \delta_c \frac{P - P_{\text{pro}}}{P_{\text{inj}} - P_{\text{pro}}},$$

with $(\gamma_o, \delta_o) = (1.2 \times 10^{-2}, 1 \times 10^{-2})$, $(\gamma_{g_1}, \delta_{g_1}) = (1.3 \times 10^1, 1.64 \times 10^1)$, and $(\gamma_{g_2}, \delta_{g_2}) = (64, 76)$. Note that, as we consider a horizontal 2D case, gravitational effects are not taken into account in the numerical tests, and the phase mass densities ρ_p , $p \in \mathcal{P}$, need not be specified. We shall test different cases, with a homogeneous porous medium and a heterogeneous one. The capillary pressure curves and the absolute permeability \mathbb{K} are problem-specific and will be described below.

We consider a uniform spatial mesh (mesh adaptation will be considered in the next chapters) and choose the initial time step as $\tau^0 = 5.184 \times 10^5 \text{s}$, which equals to 6 days. We consider the finite volume discretization of Section 2.2.2.2 with the Newton linearization detailed in Section 2.4.1; we obtain (2.4.8) with the GMRes iterative solver and ILU preconditioner with zero level fill-in. Our implementation uses PETSc [12, 11, 13] with the function `KSPSetConvergenceTest` allowing to enter a user-defined convergence criterion.

In order to compare the adaptive resolution with a classical one, let us introduce the relative residuals related to the linearization and algebraic resolutions. Consider, at every time step n , a resolution of a system of nonlinear algebraic equations $F^n(X) = 0$ by the Newton method. Starting from $X^{n,0}$, the relative linearization residual at step k is defined as

$$\text{err}_{\text{lin}}^{n,k} := \frac{\|F^n(X^{n,k})\|}{\|F^n(X^{n,0})\|}.$$

Similarly, consider the linear system resulting from the Newton method and written in the following form: $A^{n,k-1}X^{n,k} = b^{n,k-1}$. An iterative algebraic solver for this linear system: looks on step i for a vector $X^{n,k,i}$ whose relative algebraic residual is expressed by

$$\text{err}_{\text{lin}}^{n,k,i} := \frac{\|A^{n,k-1}X^{n,k,i} - b^{n,k-1}\|}{\|b^{n,k-1}\|}.$$

The comparison in numerical tests below will be done between the adaptive resolution where the stopping criteria for the GMRes and Newton iterations are given by, respectively, (2.4.22) and (2.4.23) with $\gamma_{\text{alg}} = \gamma_{\text{lin}} = 10^{-3}$, and a classical algorithm where iterations are stopped using a fixed threshold, i.e.,

$$\text{err}_{\text{alg}}^{n,k,i} \leq 10^{-8}, \quad (2.5.1)$$

for the GMRes iterations and

$$\text{err}_{\text{lin}}^{n,k} \leq 10^{-8}, \quad (2.5.2)$$

for the Newton linearization.

The algebraic error flux reconstruction $\Theta_{\text{alg},c,h}^{n,k,i}$ is obtained in the spirit of Remark 2.4.3 with $j = 2$. We thus perform two additional GMRes iterations before checking the criterion (2.4.22) (these additional steps are not wasted as we continue the iteration from the last obtained solution in the next GMRes step).

2.5.2 Compressible flow in a homogeneous porous medium

We first consider a simplified test case with a homogeneous permeability

$$\mathbb{K} = (9.869\,233 \times 10^{-14} \text{m}^2)\mathbf{I},$$

where \mathbf{I} is the identity tensor, and no capillary effects, setting $P_{c_p}(\mathcal{S}) \equiv 0$ for all $p \in \mathcal{P}$. We consider a simulation of $t_F = 7$ years. For a fixed time step and the first Newton iteration, we first show in the left part of Figure 2.2 the evolution of the different estimators as a function of the GMRes iterations at the classical resolution stopped following (2.5.1). We remark that the algebraic error steadily decreases, while the other components stagnate starting from the first iteration. For the same time step, in the right part of Figure 2.2 we depict the evolution of the spatial, temporal, and linearization error estimators as a function of the number of Newton iterations. The spatial and temporal errors stagnate starting from the third step while the linearization error $\eta_{\text{lin},M}^{n,k,i}$ decreases until 10^{-6} , which is equivalent to the value 10^{-8} for the relative linearization residual at which we satisfy the classical stopping criterion (2.5.2). These results justify our stopping criteria which economize many useless iterations.

Figure 2.3 shows the rate (in its left part) and the cumulated rate (in its right part) of oil production during the simulation for the classical and adaptive resolutions. We remark that using the adaptive algorithm does not affect the accuracy of the predicted oil production rate, which is the crucial engineering output of the simulation. We next in Figure 2.4 show

the evolution of the saturation in the liquid phase for both classical and adaptive resolutions at two times during the simulation. Values without any visible difference are found in these cases. Similarly, Figure 2.5 compares the resulting reference pressures using the adaptive algorithm and the classical one; again no loss of the precision is observed.

Figure 2.6 illustrates the evolution of the spatial estimators (2.4.19a) of the oil component. We see that this estimator detects the error caused by the two wells, as well as the error following the saturation front. This result pleads for a space mesh refinement/coarsening strategy using our estimators which will be considered in the last chapter in three dimension.

We next focus on computational savings resulting from our adaptive stopping criteria. In the left part of Figure 2.7, we show the number of Newton iterations at each time step for the entire simulation. The cumulated number of Newton iterations as a function of time is then

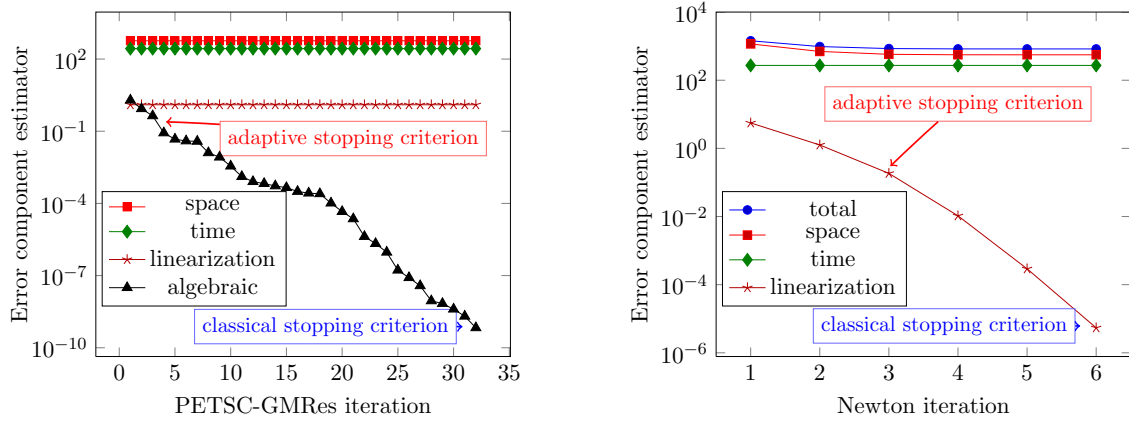


Figure 2.2: Evolution of the spatial, temporal, linearization, and algebraic error estimators (2.4.20) for all components for a fixed mesh at time $1.04 \cdot 10^6$ s, as a function of GMRes iterations on the first Newton iteration (left) and of Newton iterations (right)

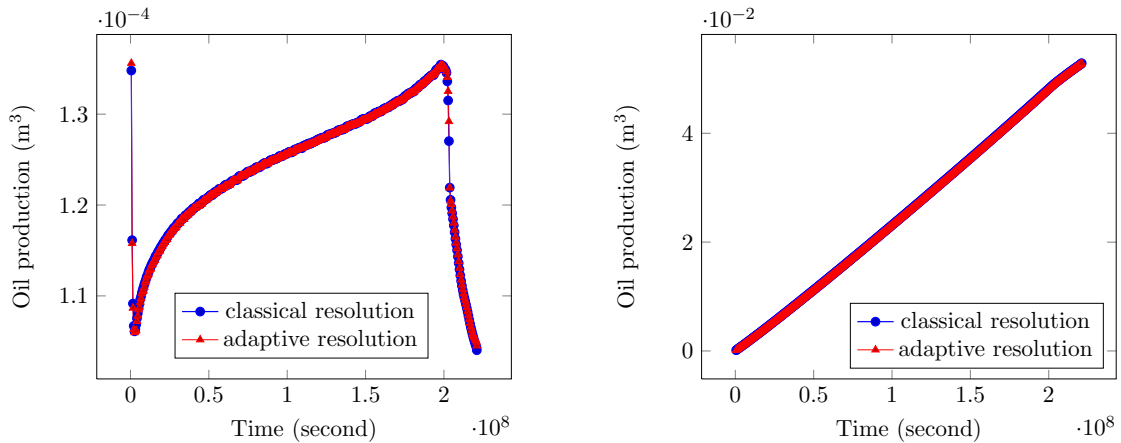


Figure 2.3: Rate (left) and cumulated rate (right) of oil production during the simulation, classical resolution vs. adaptive resolution for the test case of Section 2.5.2

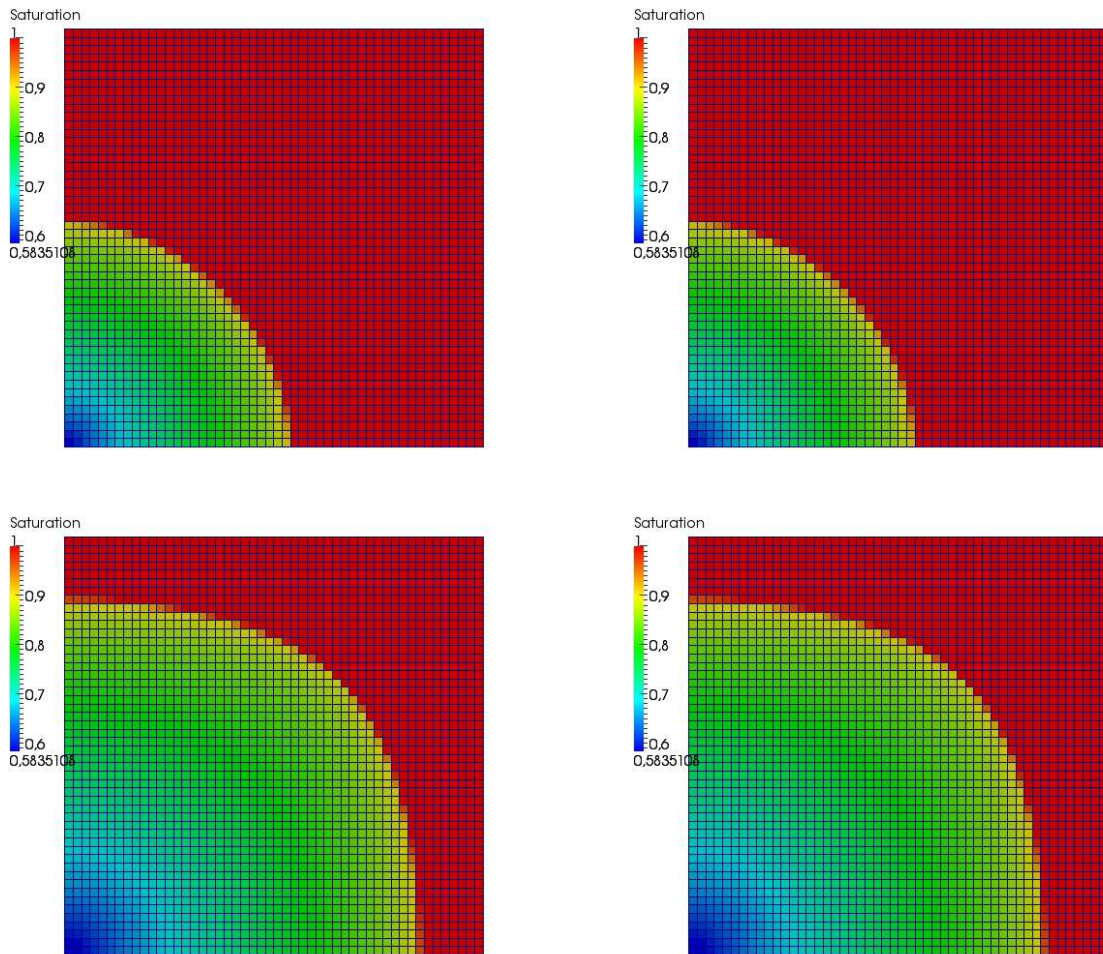


Figure 2.4: Liquid saturation, classical (left) vs. adaptive (right) resolution at times 30 months and 80 months for the test case of Section 2.5.2

presented in the right part of Figure 2.7. The overall gain in terms of linearization iterations obtained using our stopping criteria is quite significant.

Finally, similar results are obtained using the stopping criterion for the algebraic solver. We represent in the left part of Figure 2.8 the number of GMRes iterations at each time and Newton step. In the right part of Figure 2.8, we then depict the cumulated number of GMRes iterations as a function of time steps, where still more interesting results can be found. We see that during the simulation the gain in GMRes iterations reaches a factor of roughly 10 for the adaptive resolution compared with the classical one.

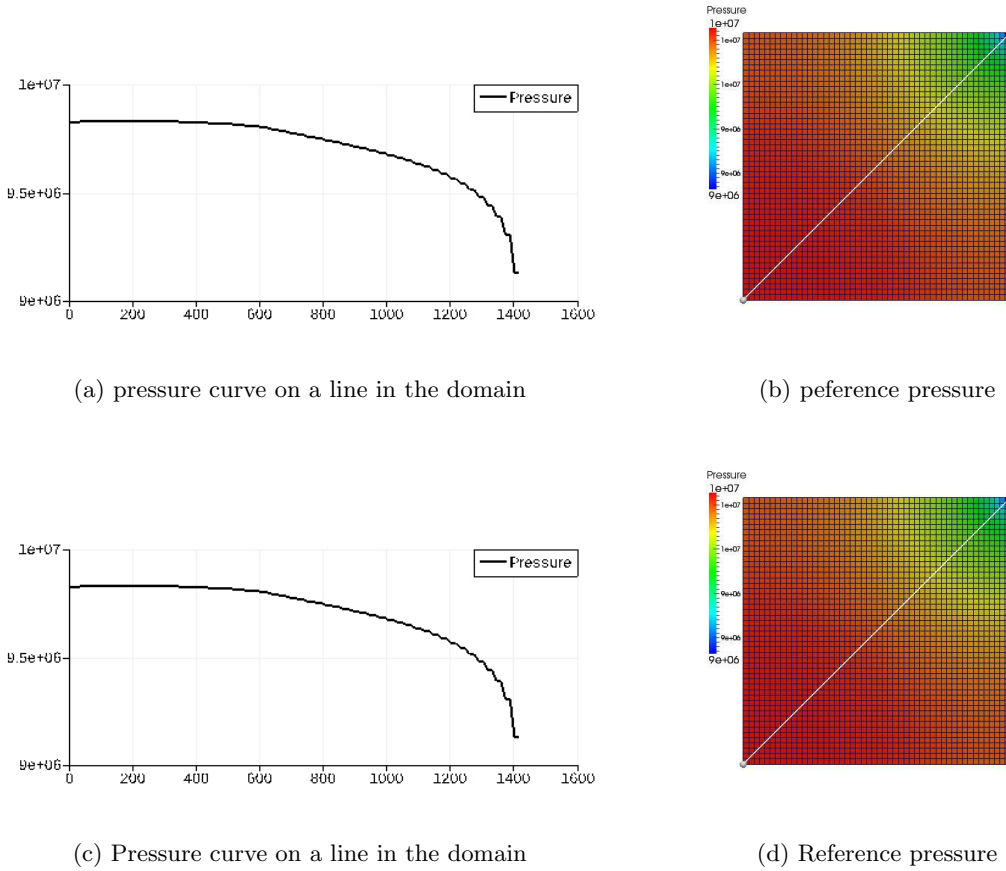


Figure 2.5: Reference pressure, classical (top) vs. adaptive (bottom) resolution at time 50 months for the test case of Section 2.5.2

2.5.3 Compressible flow in a heterogeneous porous medium

In what follows, for the phase pressures, we choose P_1 as the reference pressure P , i.e. $P_{c_1} \equiv 0$, and follow the Brooks–Corey model [18] for the gas phase capillary pressure law, i.e.,

$$P_g = P + P_{c_g}(S_g), \quad P_{c_g}(S_g) = P_e \cdot (S_e)^m, \quad S_e = 1 - \frac{S_g - S_g^{\text{res}}}{1 - S_1^{\text{res}} - S_g^{\text{res}}},$$

with $P_e = 8.73 \times 10^5 \text{ Pa}$, $m = -\frac{1}{2.89}$, and $S_1^{\text{res}}, S_g^{\text{res}}$ are the residual saturations defined previously.

2.5.3.1 Fingering permeability

In this case we consider the heterogeneous permeability shown in Figure 2.9b with a final time for simulation: $t_F = 7$ years. We compare in Figure 2.10 the rate of oil production resulting from both the classical and adaptive resolution and verify that our adaptive algorithm does not have any significant effect on the accuracy of production.

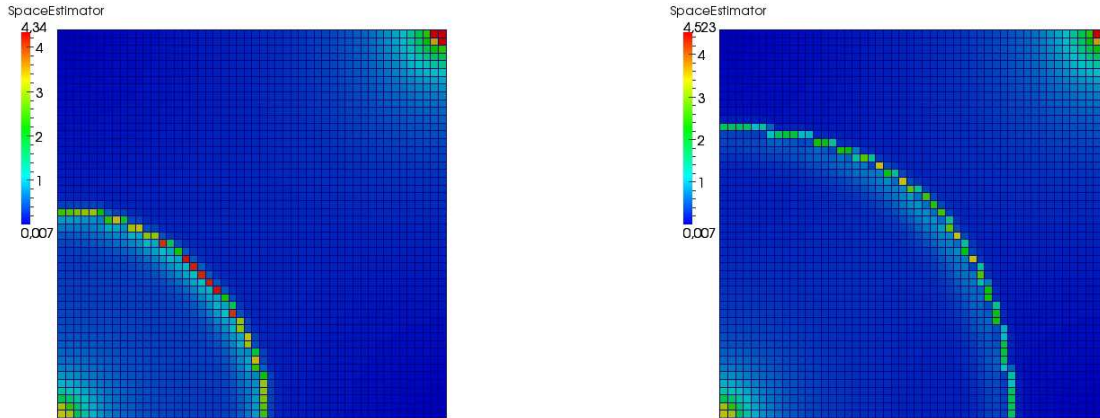


Figure 2.6: Spatial error distribution at times 30 months and 40 months for the test case of Section 2.5.2

In Figure 2.11 we show the evolution of the oil saturation at several time steps during the simulation. The results are given for classical resolution and the adaptive resolution based on our stopping criteria; we see also here that the precision of resolution is the same. Figure 2.12 presents the same result for the reference pressure.

Next, we illustrate in Figure 2.13 the spatial estimator evolution of the oil component at different time steps. The spatial estimator follows the saturation front through the heterogeneous medium with the time evolution, it detects also an error around the injection and production wells. Thus the heterogeneity of the medium does not prevent our estimator from localizing the error during the simulation.

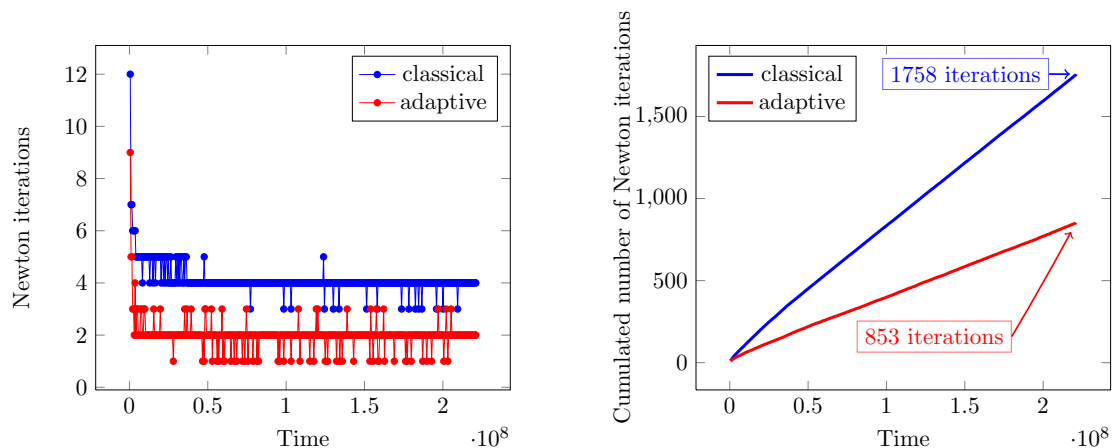


Figure 2.7: Newton iterations at each time step (left) and cumulated number of Newton iterations as a function of time (right) for the test case of Section 2.5.2. Average number of Newton iterations per time step: 4 iterations (classical), 2 iterations (adaptive)

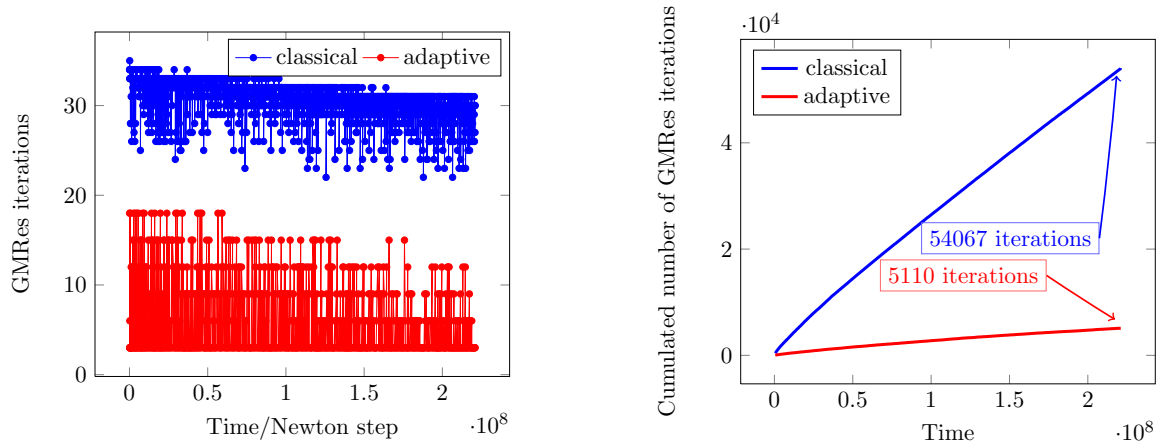


Figure 2.8: GMRes iterations for each time and Newton iteration step (left) and cumulated number of GMRes iterations as a function of time (right) for the test case of Section 2.5.2. Average number of GMRes iterations per time and Newton iteration step: 31 iterations (classical), 6 iterations (adaptive). Average number of GMRes iterations per time step: 126 iterations (classical), 12 iterations (adaptive)

As for the previous test cases, using our adaptive algorithm based on the stopping criteria (2.4.22) and (2.4.23), gives computational savings in terms of the number of iterations of both Newton and GMRes methods. A comparison between the number of iterations for the linearization method is shown in Figure 2.14. The saving in the cumulated number of Newton iterations can be deduced from the right part of this figure. The over-all gain in terms of GMRes iterations can be observed in the right part of Figure 2.15, with a speed-up factor reaching the value 9. In the left part of this figure we show the economy of GMRes iterations at every time and Newton iteration step.

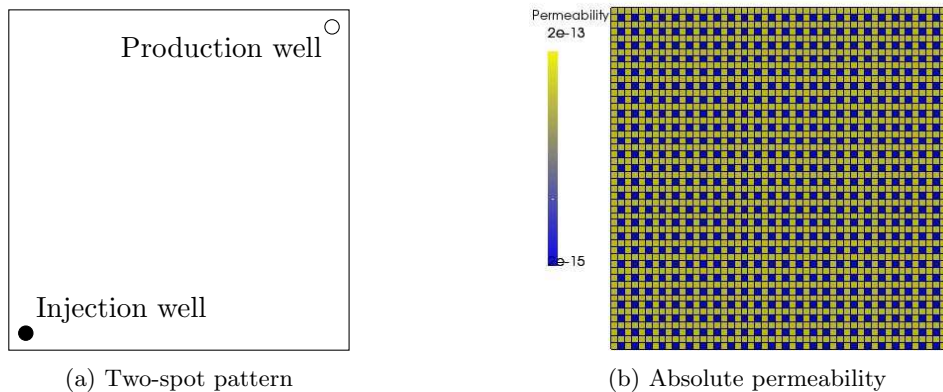


Figure 2.9: Configuration for the numerical test case of Section 2.5.3.1

2.5.3.2 Random permeability

We consider here the heterogeneous permeability field shown in Figure 2.16b corresponding to a log-normal distribution. The process is simulated for $t_F = 7$ years.

As for the homogeneous case, we verify in Figure 2.17 that the adaptive resolution does not affect the accuracy of the predicted oil production rate by comparing it with the results obtained using the classical resolution procedure based on the stopping criteria (2.5.1) and (2.5.2) for the GMRes and Newton iterations, respectively. Also, Figure 2.18 compares the liquid saturation obtained using the adaptive and classical resolutions. Again, applying the adaptive algorithm does not influence the precision. A similar comparison for the reference pressure is shown in Figure 2.19.

The evolution of the spatial estimator (2.4.19a) of the oil component at different time steps is shown in Figure 2.20. It again detects the error around the injection and production wells, while, advancing in time, the error follows the saturation front. As in the homogeneous case, we thus deem our estimators to be a good tool for adaptive mesh refinement.

The saved iterations from the linearization method at each time step can be found in the left part of Figure 2.21. In the right part of this figure we show the cumulated number of Newton iterations during the simulation as a function of time steps; again a considerable gain in terms of the number of Newton iterations is achieved.

Finally, in Figure 2.22 we compare our algebraic stopping criterion with the classical one. At every time and Newton iteration step, the economy of the GMRes iterations using the stopping criterion (2.4.22) can be appreciated in the left part of Figure 2.22. In its right part, the overall gain is presented. Here a little better than for the homogeneous case, the speed-up factor is roughly 10.

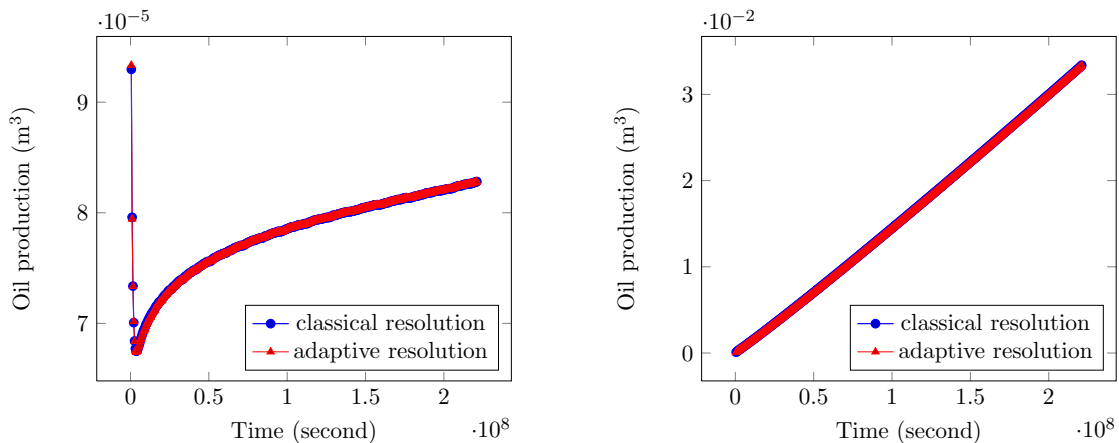


Figure 2.10: Rate (left) and cumulated rate (right) of oil production during the simulation, classical resolution vs. adaptive resolution for the test case of Section 2.5.3.1

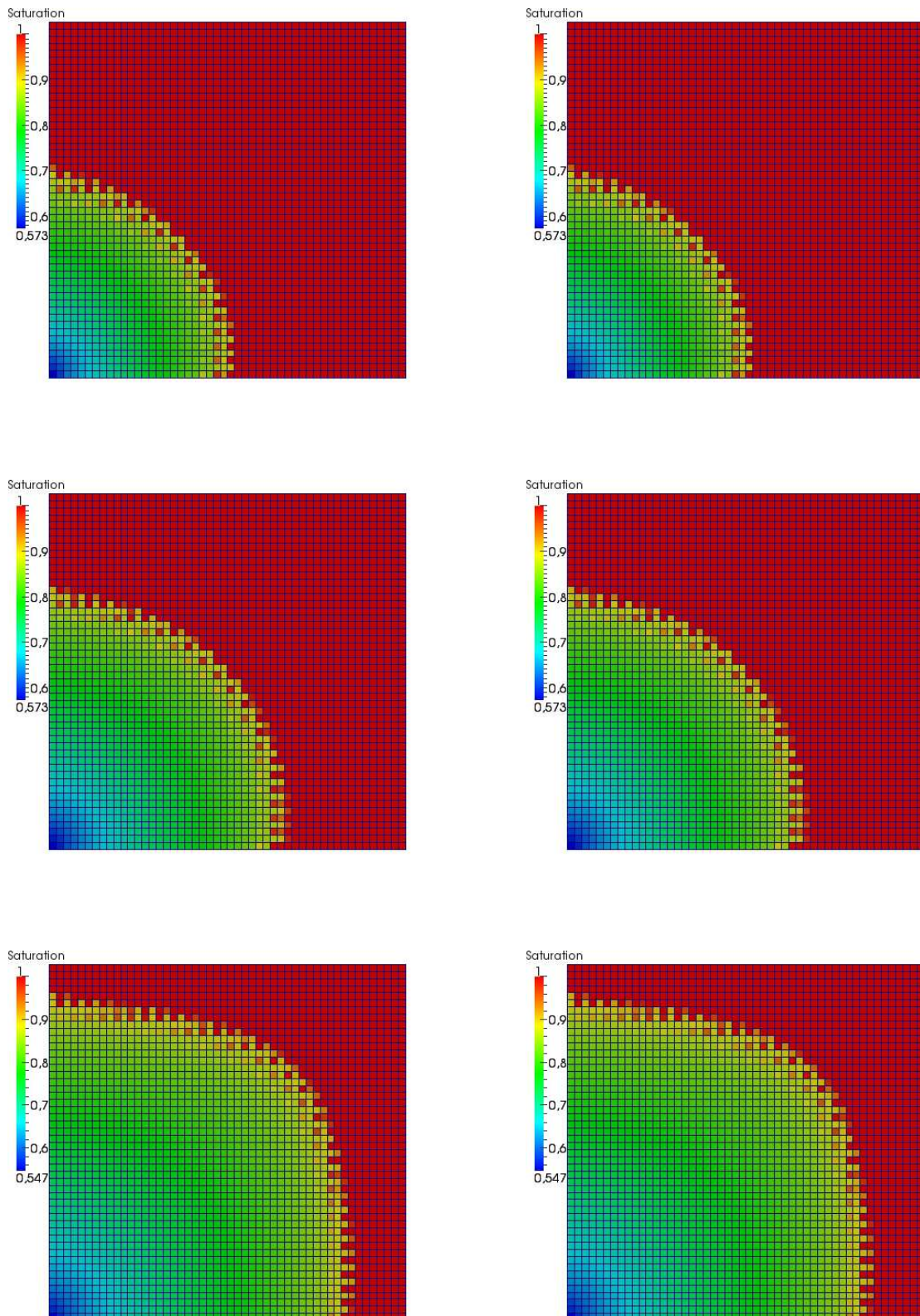
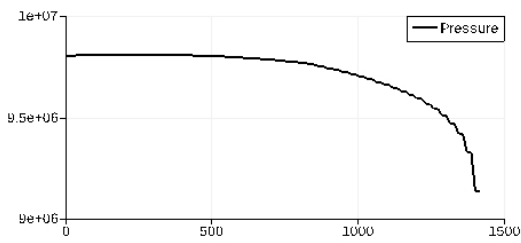
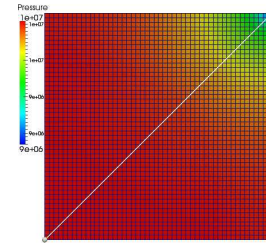


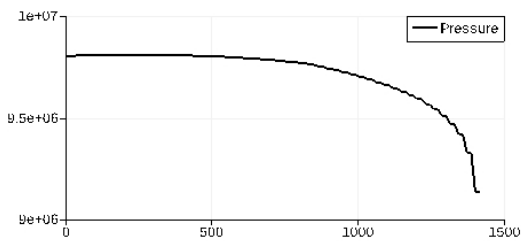
Figure 2.11: Liquid saturation, classical (left) and adaptive (right) resolutions at times 30 months, 50 months, and 84 months for the test case of Section 2.5.3.1



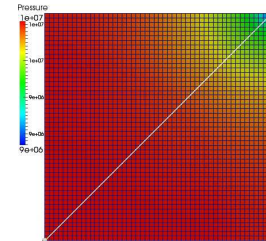
(a) pressure curve on a line in the domain



(b) Reference pressure



(c) pressure curve on a line in the domain



(d) Reference pressure

Figure 2.12: Reference Pressure, classical (top) and adaptive (bottom) resolution at time 70 months for the test case of Section 2.5.3.1

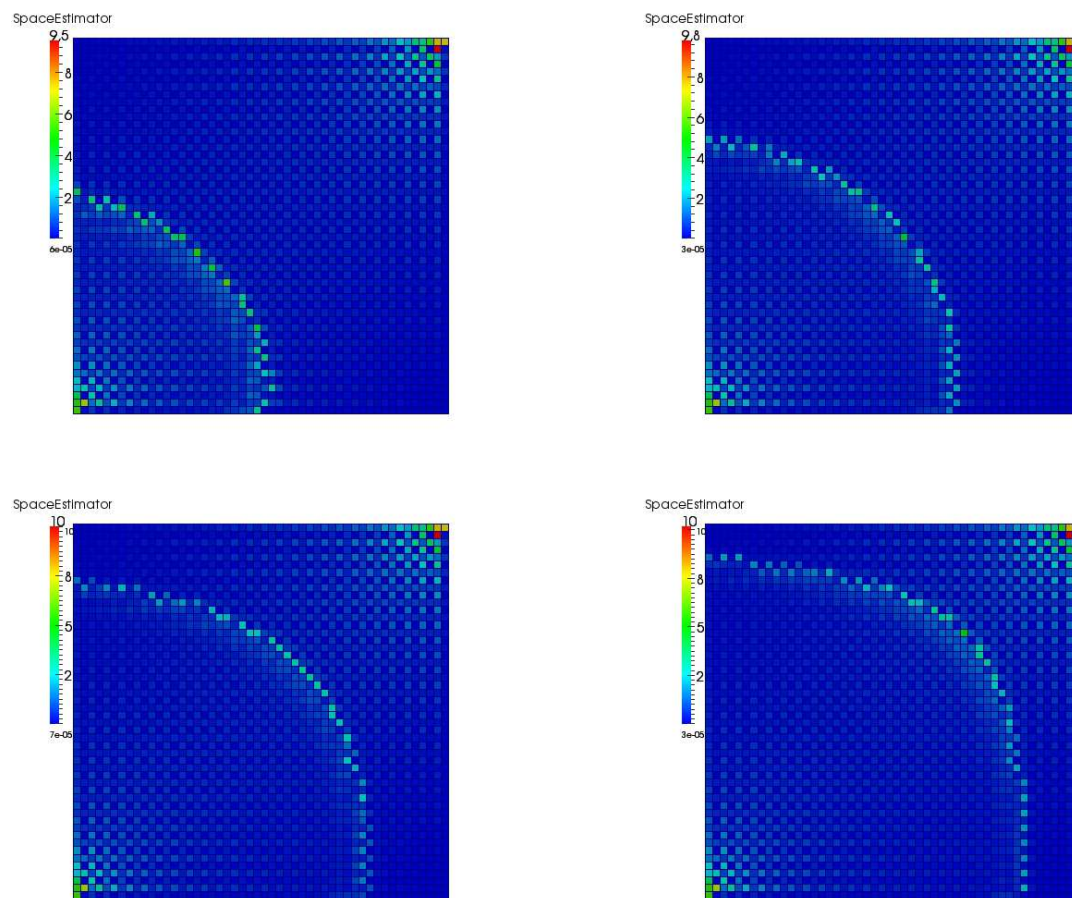


Figure 2.13: Spatial error distribution at times 30 months, 50 months, 70 months, and 84 months for the test case of Section 2.5.3.1

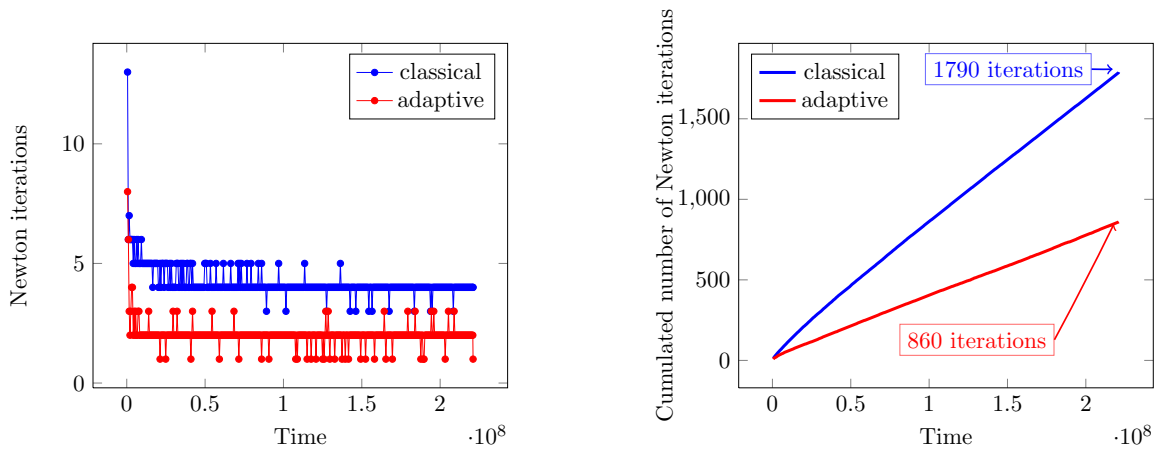


Figure 2.14: Newton iterations at each time step (left) and cumulated number of Newton iterations as a function of time (right) for the test case of Section 2.5.3.1. Average number of Newton iterations per time step: 4 iterations (classical), 2 iterations (adaptive)

2.5.4 Five-spots pattern

We consider here a five-spot pattern, see Figure 2.23a, with two different distributions of a heterogeneous permeability on the spatial domain $\Omega = (0, 1500)\text{m} \times (0, 1500)\text{m}$.

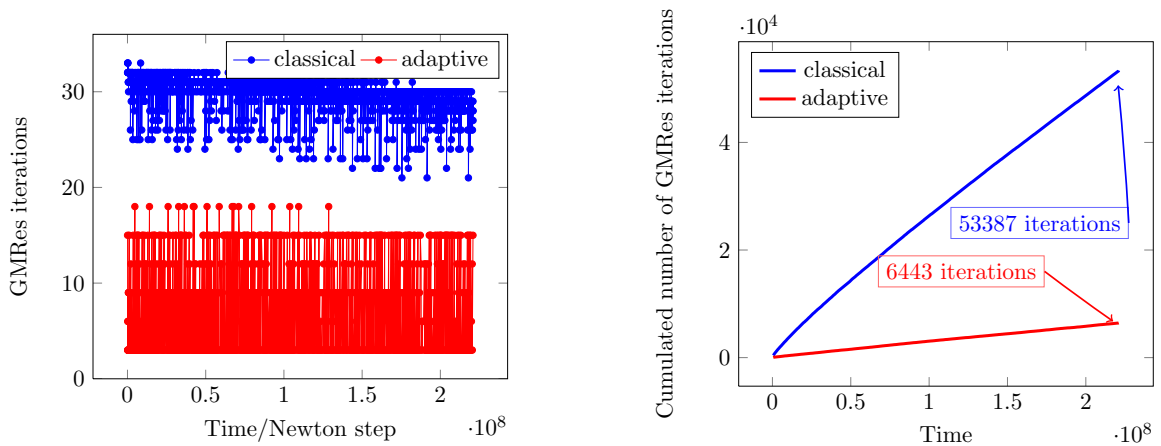


Figure 2.15: GMRes iterations at each time and Newton step (left) and cumulated number of GMRes iterations as a function of time (right) for the test case of Section 2.5.3.1. Average number of GMRes iterations per time and Newton iteration step: 31 iterations (classical), 7 iterations (adaptive). Average number of GMRes iterations per time step: 125 iterations (classical), 15 iterations (adaptive)

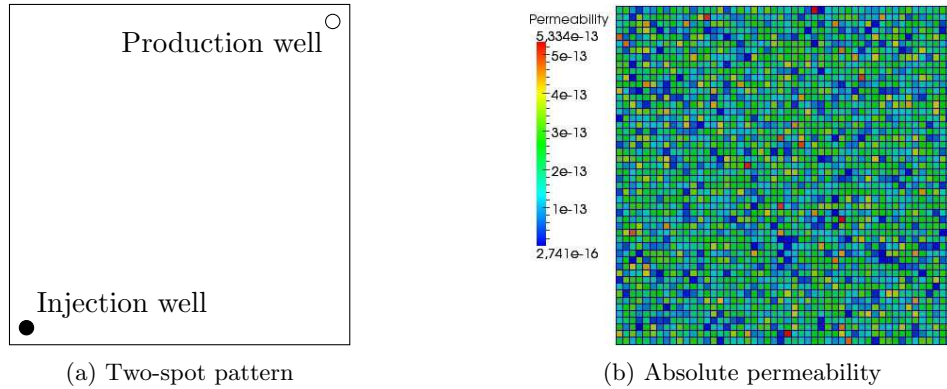


Figure 2.16: Configuration for the numerical test case of Section 2.5.3.2

2.5.4.1 Random permeability by zones

For this test case the process is simulated for $t_F = 15$ years and the heterogeneous permeability field is shown in Figure 2.23b. For every zone in this figure we consider a random permeability corresponding to a different log-normal distribution. We see that we have high permeability in the first and second zones which makes the fluid pass through the medium easily compared with the third and fourth zones where the permeability is lower.

Figure 2.24 presents the results for the rate and the cumulated rate of oil production during the simulation for adaptive and classical resolution. We see clearly that the production of the oil is the same for both resolutions, thus the adaptive resolution does not affect the accuracy of the oil production rate.

We then show in Figure 2.25 the evolution of the saturation at different time steps during the simulation also for both adaptive and classical resolution and verify by this resulting figure

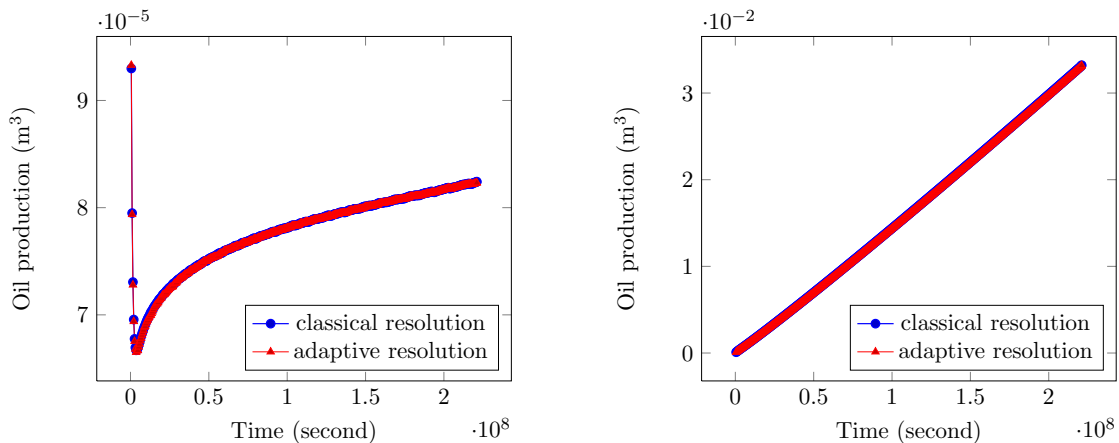


Figure 2.17: Rate (left) and cumulated rate (right) of oil production during the simulation, classical resolution vs. adaptive resolution for the test case of Section 2.5.3.2

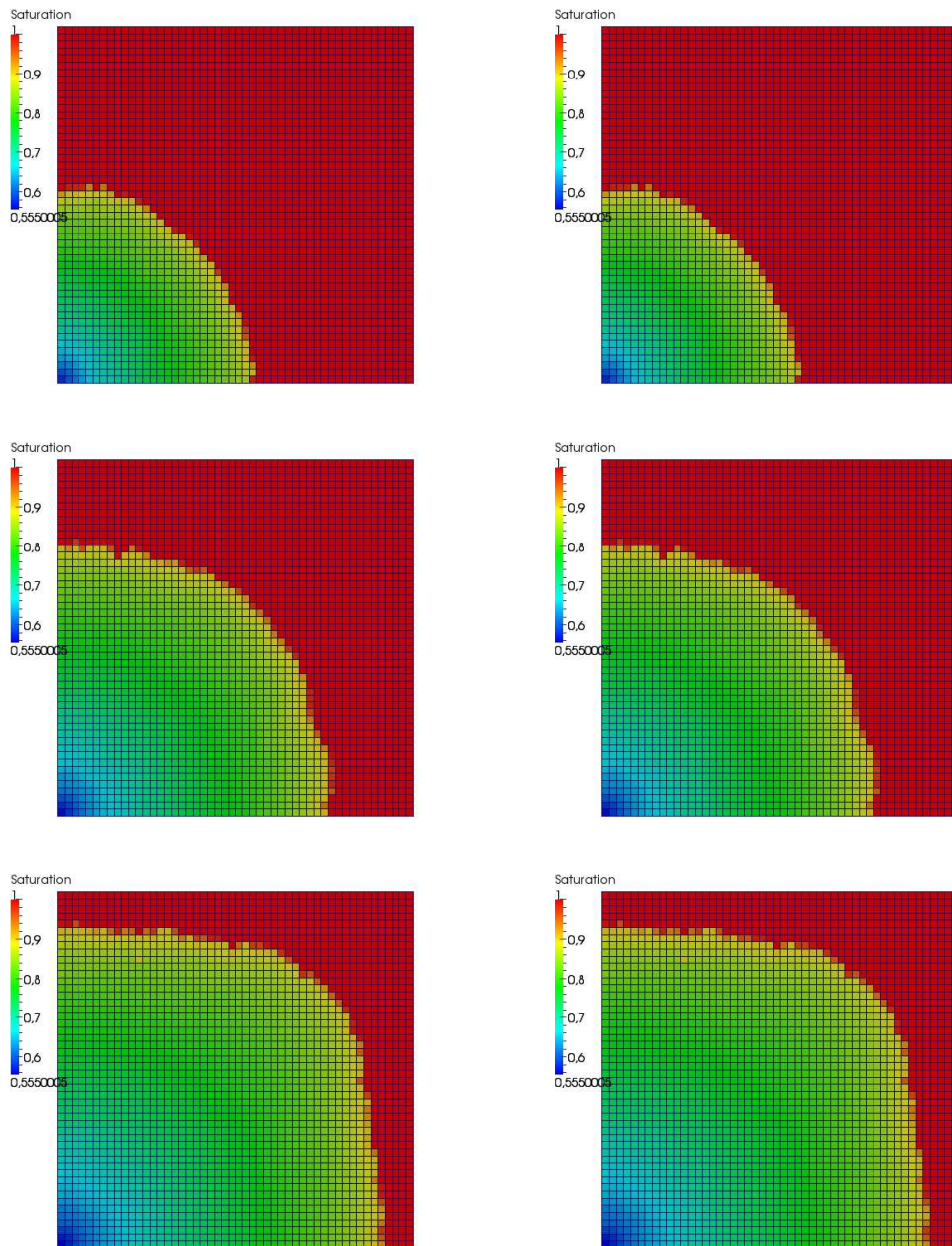


Figure 2.18: Liquid saturation, classical (left) and adaptive (right) resolutions at times 20 months, 40 months, and 60 months for the test case of Section 2.5.3.2

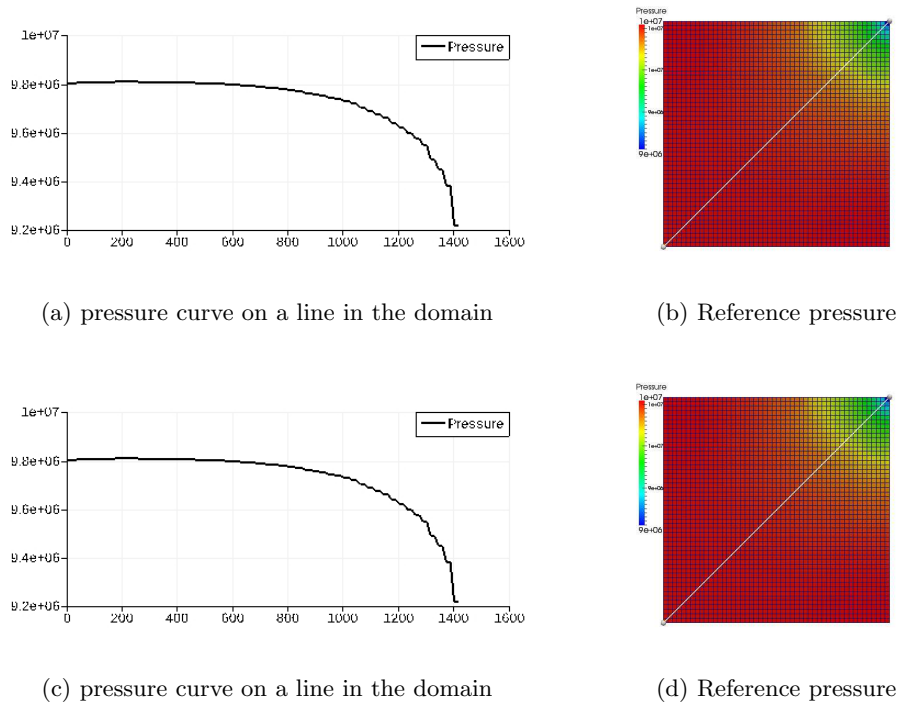


Figure 2.19: Reference pressure, classical (top) and adaptive (bottom) resolution at time 60 months for the test case of Section 2.5.3.2

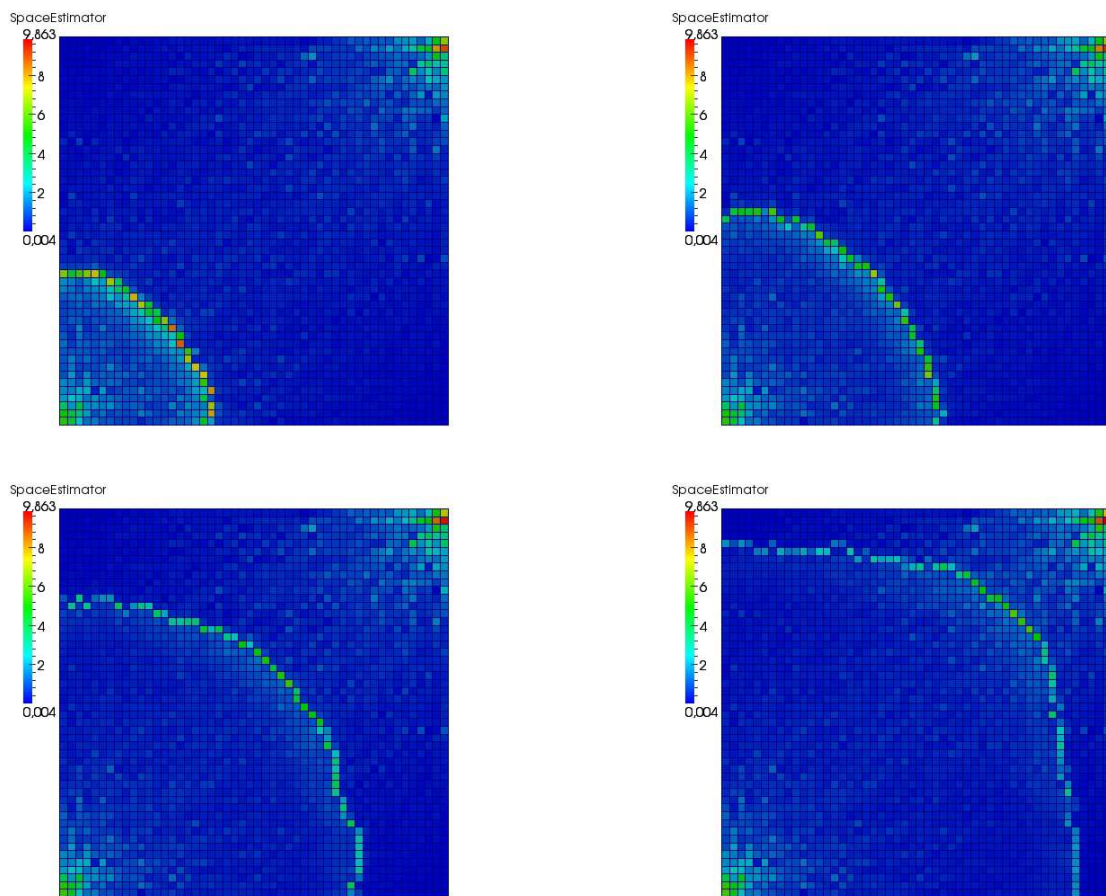


Figure 2.20: Spatial error distribution at times 10 months, 20 months, 40 months, and 60 months for the test case of Section 2.5.3.2

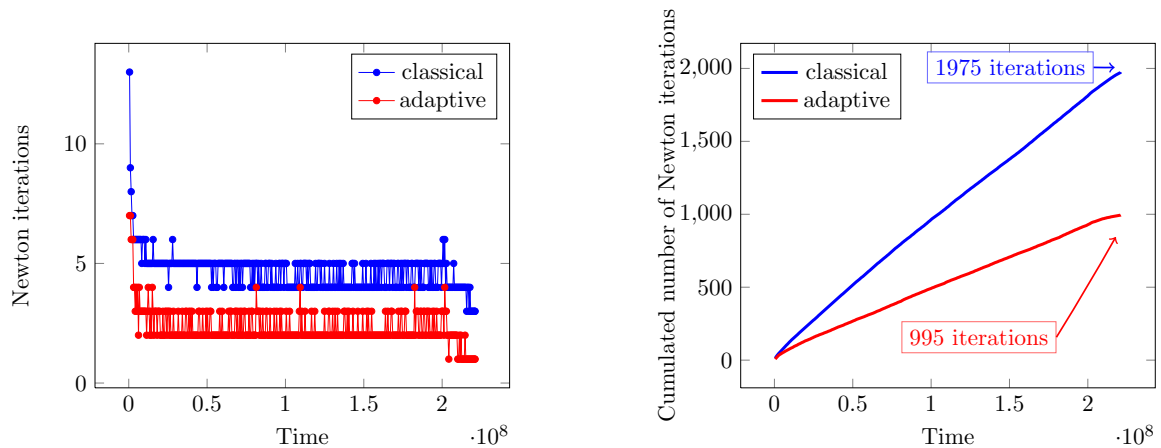


Figure 2.21: Newton iterations at each time step (left) and cumulated number of Newton iterations as a function of time (right) for the test case of Section 2.5.3.2. Average number of Newton iterations per time step: 5 iterations (classical), 2 iterations (adaptive)

that the adaptive resolution gives the same precision in the resolution. We see also in Figure 2.25 that the oil flows easily in the first and second zone of the domain (see Figure 2.23b) while the low permeability in the other zones obscures the flow of the oil.

Similar verification is shown for the reference pressure in Figures 2.26 and 2.27 where we show in the left part of these figures a curve of the pressure a cross diagonal lines on the domain to clearly compare the adaptive resolution with the classical one, and check that the

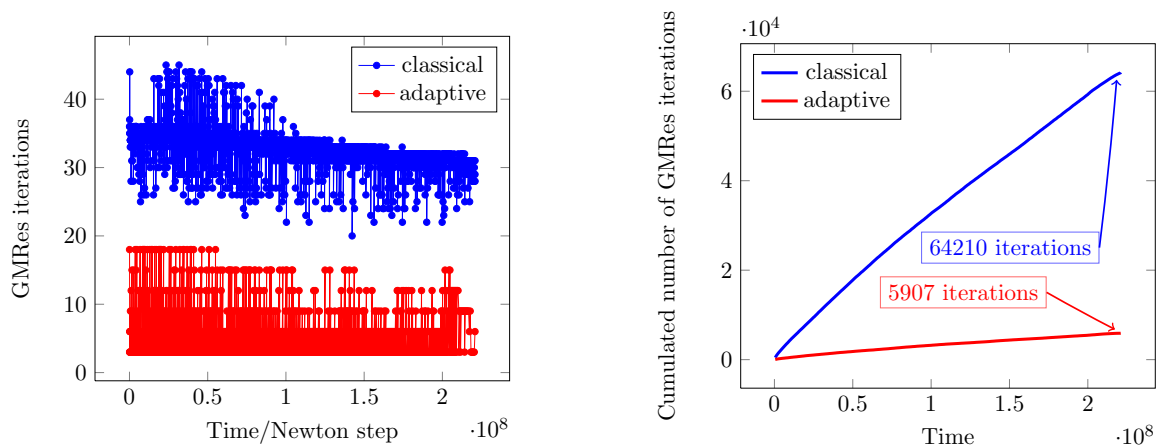


Figure 2.22: GMRes iterations at each time and Newton step (left) and cumulated number of GMRes iterations as a function of time (right) for the test case of Section 2.5.3.2. Average number of GMRes iterations per time and Newton iteration step: 33 iterations (classical), 6 iterations (adaptive). Average number of GMRes iterations per time step: 150 iterations (classical), 14 iterations (adaptive)

precision is not influenced by the savings of the adaptive algorithm.

Figure 2.28 illustrates the evolution of the spatial estimator of the oil component at different time steps where the estimator indicates errors around the injection wells, the production well, and moving error that detects the front of oil saturation at every time step. This result ensures the also for this configuration of a five-spot pattern with a heterogeneous permeability, the estimator is able to locate the important error in resolution and then it can be a good tool to an adaptive mesh refinement technique.

We still to show the economy in terms of iterations of the linearization method and algebraic resolution. Figure 2.29 illustrates in its left part the number of Newton iterations at every time step where we see locally that we need for the adaptive resolution half of the iterations of the classical resolution. In the right part of Figure 2.29 we see the total saving in Newton iterations for the whole simulation.

A similar comparison between the classical resolution and the adaptive resolution for the GMRes iterations is given in Figure 2.30. The saved iterations from the GMRes method at every time and Newton iteration can be observed in the left part this figure while in its right part we found the overall gain in GMRes iteration during the whole simulation. We remark a speed-up factor reaches to 10.

2.5.4.2 Random permeability

The simulation for this test case is done for $t_F = 10$ years and the heterogeneous permeability of the medium corresponds to a log-normal distribution over the domain (see Figure 2.31).

As for all previous test cases, we start with the rate and cumulated rate of oil production to confirm that the adaptive algorithm does not affect the precision of resolution. This result is shown in Figure 2.32 with a comparison between the classical and adaptive resolution.

Figure 2.33 shows the oil saturation for both adaptive and classical resolution at different time steps. Also for this test case we see by comparing between these two resolutions that

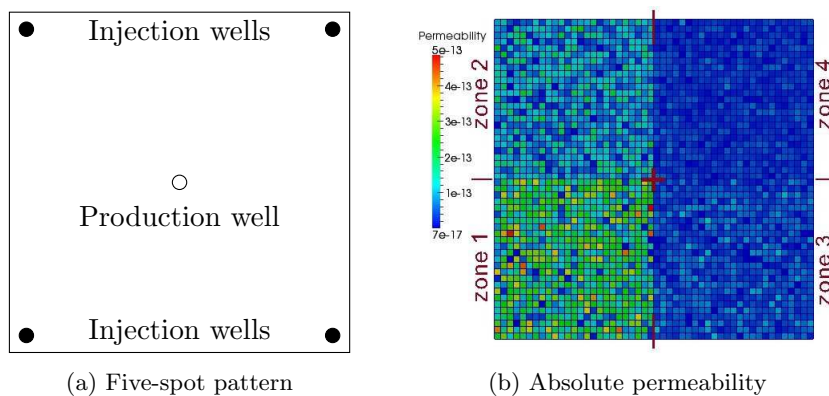


Figure 2.23: Configuration for the numerical test case of Section 2.5.4.1

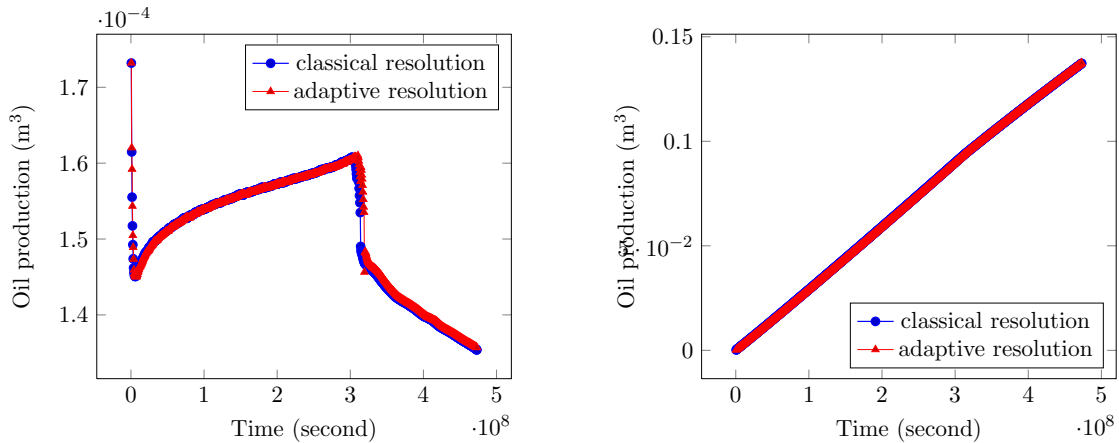


Figure 2.24: Rate (left) and cumulated rate (right) of oil production during the simulation, classical resolution vs. adaptive resolution for the test case of Section 2.5.4.1

the precision is the same. Similar verification is shown for the reference pressure at a chosen time step over the domain and for a pressure curve over a diagonal in the domain (see Figure 2.34).

The evolution of the spatial estimator of the oil component illustrated in Figure 2.35 indicates an error around the wells and an error that follows the front of oil saturation with time evolution. As for the previous test cases we observe in Figure 2.35 that the spatial estimator seems to be an efficient tool to adapt the computational mesh.

The final results witness the computational savings obtained by the adaptive algorithm and are given in terms of the iterations of the Newton and GMRes methods. In the left part of Figure 2.36 we show the number of Newton linearization iterations at every time step. We already observe an important local gain in terms of the Newton iterations. The overall gain in terms of Newton iterations can be found in the right part of Figure 2.36. The gain in terms of GMRes iterations is finally given in Figure 2.37. In the left part of this figure we observe at each time step and Newton iteration the savings in GMRes iterations by comparing adaptive and classical resolution. In the right part of this figure we illustrate the overall gain for adaptive resolution with a speed-up factor of 10.

We conclude from all previous numerical results that the issuing adaptive algorithm of Section 2.4.6 based on the stopping criteria (2.4.22) and (2.4.23) for the GMRes and Newton iterations, respectively, allows to achieve important computational savings, which typically reach a factor of around 10 in terms of the total number of algebraic solver iterations. It is to be noted that this happens already on fixed meshes without any observable loss in the precision of the resolution or of the accuracy of oil production. The estimator also appears to be a good tool to predicting the distribution of the error over the domain and consequently to perform an adaptive mesh refinement (AMR) technique. Such an approach is presented in the last chapter of this thesis in three space dimensions.

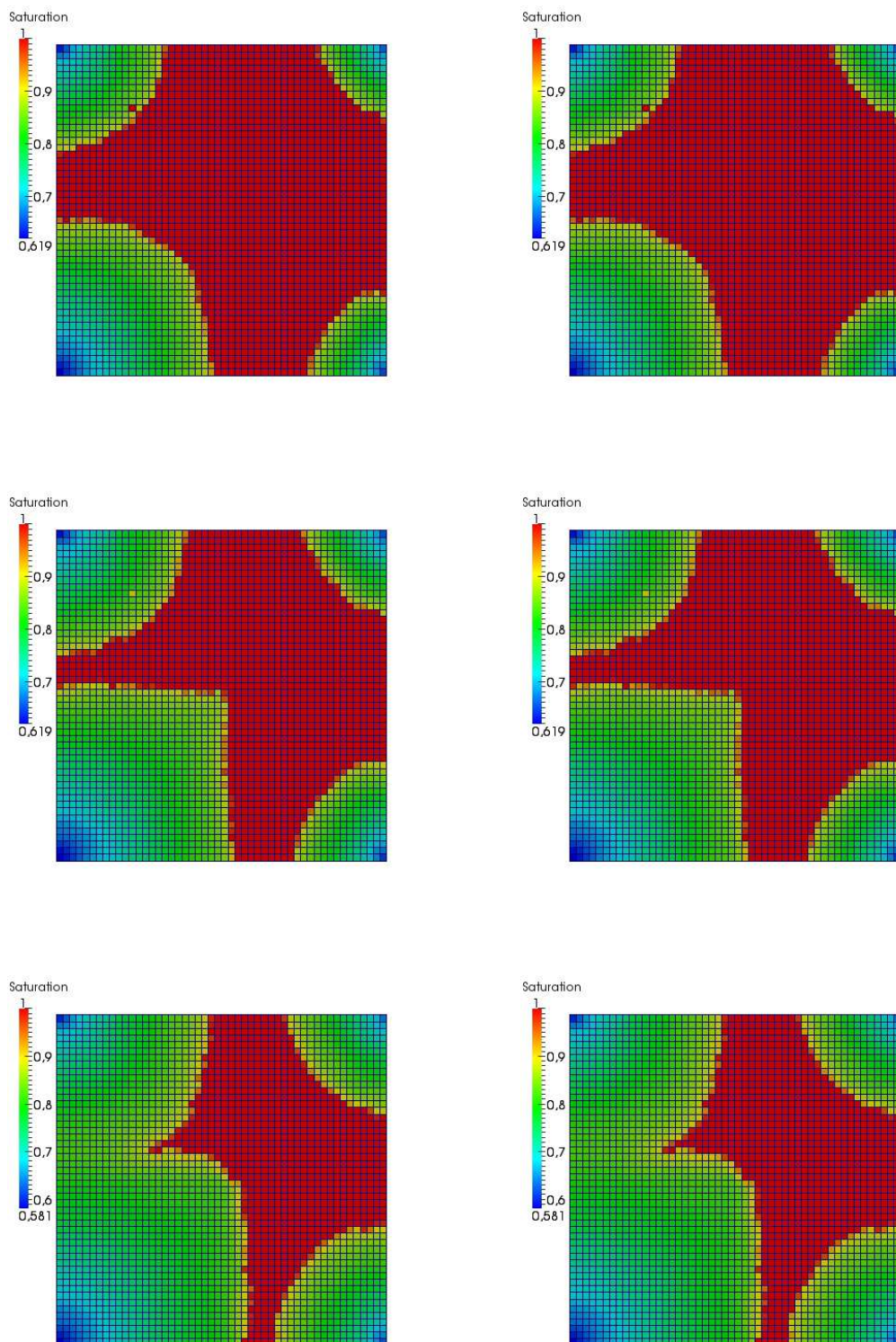
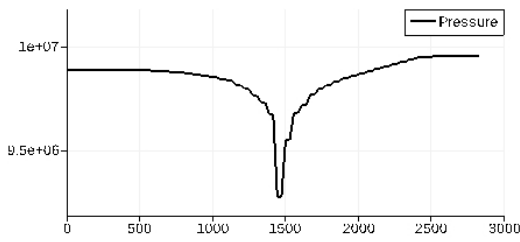
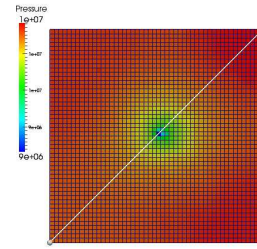


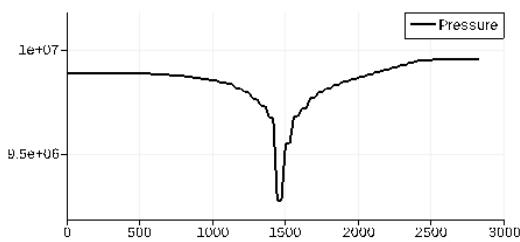
Figure 2.25: Liquid saturation, classical (left) and adaptive (right) resolutions at times 7 years, 10 years, and 15 years for the test case of Section 2.5.4.1



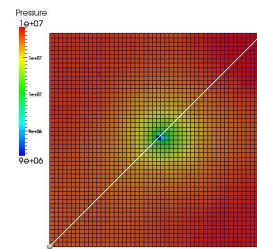
(a) pressure curve on a line in the domain



(b) Reference pressure

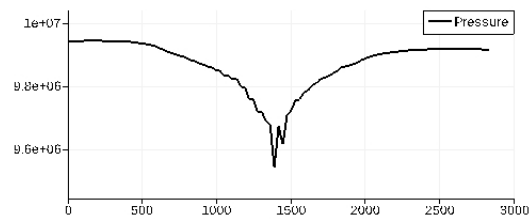


(c) pressure curve on a line in the domain

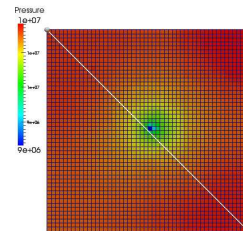


(d) Reference pressure

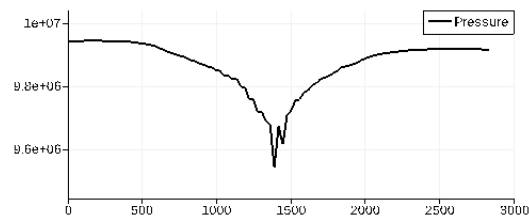
Figure 2.26: Reference pressure, classical (left) and adaptive (right) resolution at time 5.2×10^7 s for the test case of Section 2.5.4.1



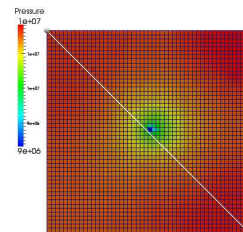
(a) pressure curve on a line in the domain



(b) Reference pressure



(c) pressure curve on a line in the domain



(d) Reference pressure

Figure 2.27: Reference pressure, classical (left) and adaptive (right) resolution at time 5.2×10^7 s for the test case of Section 2.5.4.1

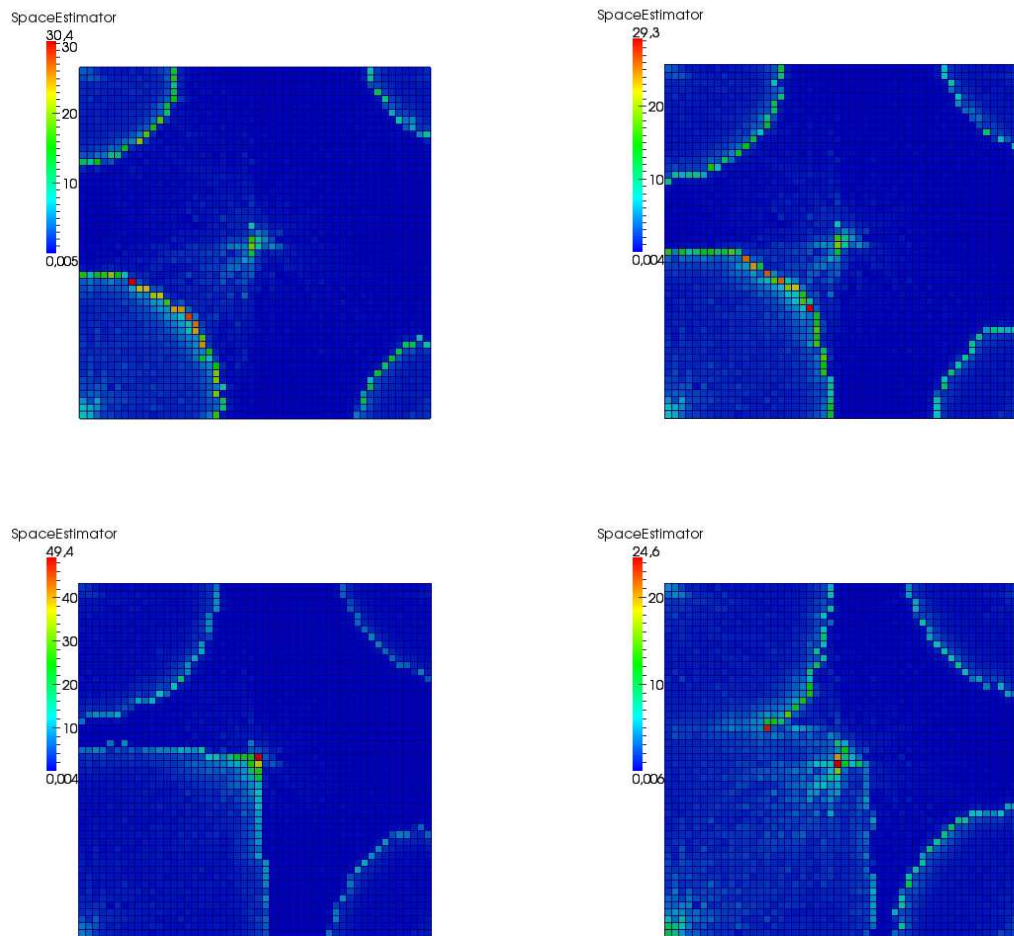


Figure 2.28: Spatial error distribution at times 5 years, 7 years, 10 years, and 15 years for the test case of Section 2.5.4.1

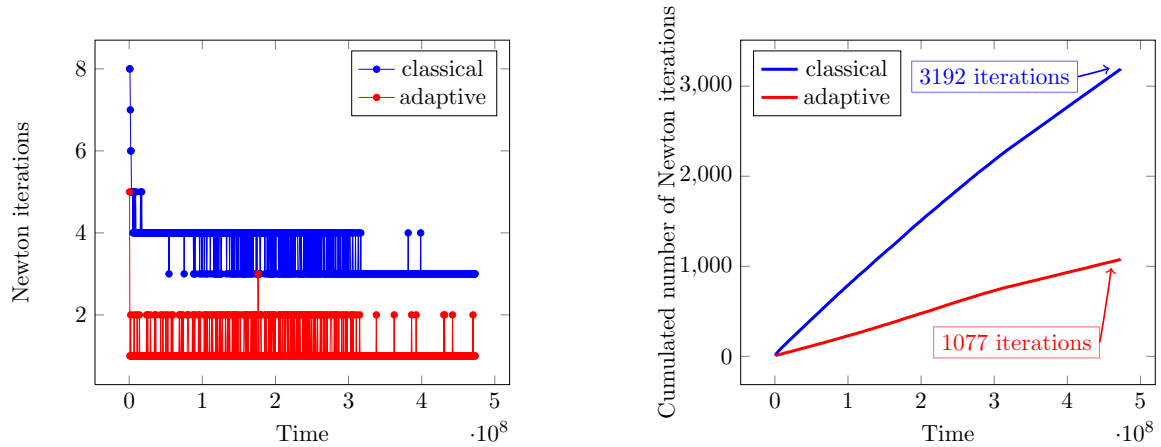


Figure 2.29: Newton iterations at each time step (left) and cumulated number of Newton iterations as a function of time (right) for the test case of Section 2.5.4.1. Average number of Newton iterations per time step: 4 iterations (classical), 1 iterations (adaptive)

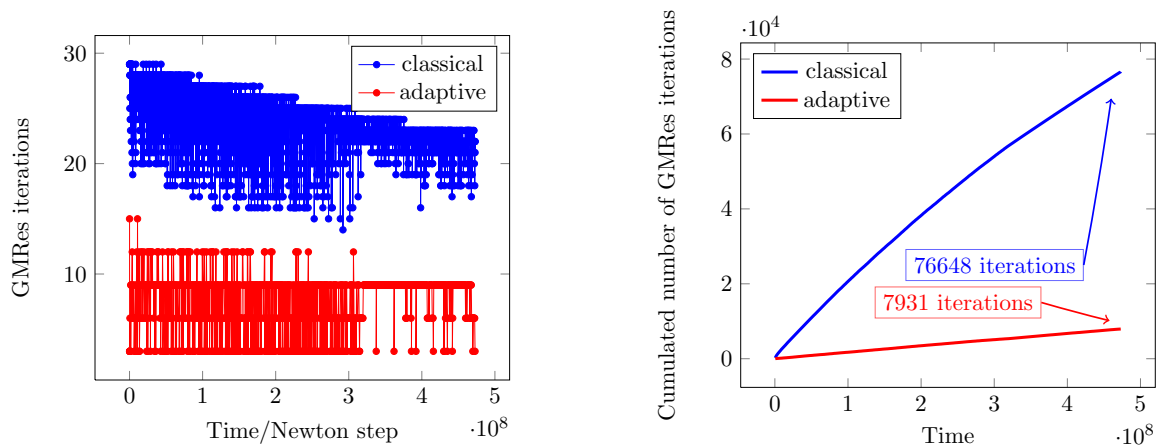


Figure 2.30: GMRes iterations at each time and Newton step (left) and cumulated number of GMRes iterations as a function of time (right) for the test case of Section 2.5.4.1. Average number of GMRes iterations per time and Newton iteration step: 27 iterations (classical), 6 iterations (adaptive). Average number of GMRes iterations per time step: 104 iterations (classical), 9 iterations (adaptive)

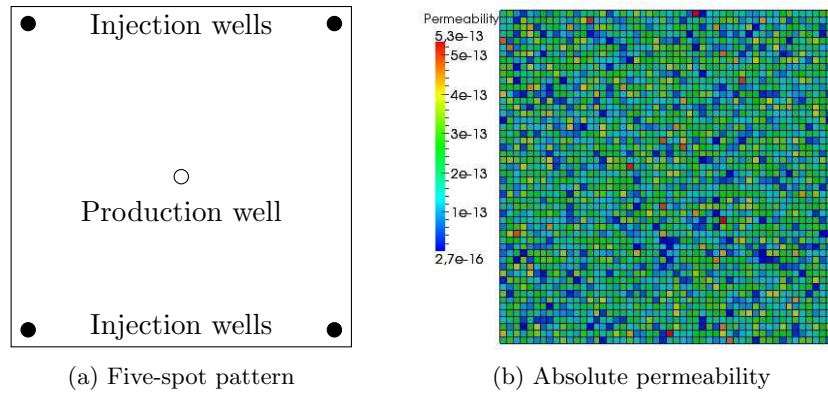


Figure 2.31: Configuration for the numerical test cases of Section 2.5.4.2

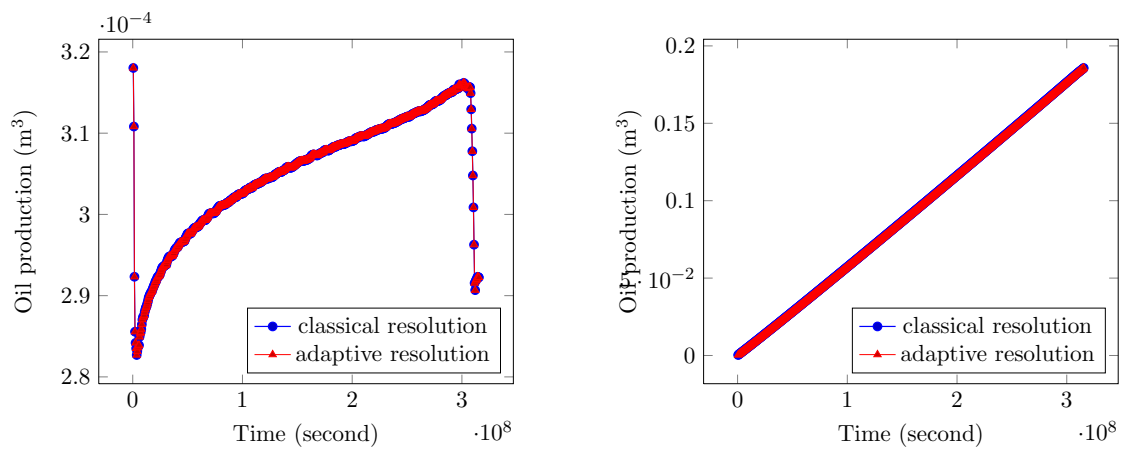


Figure 2.32: Rate (left) and cumulated rate (right) of oil production during the simulation, classical resolution vs. adaptive resolution for the test case of Section 2.5.4.2

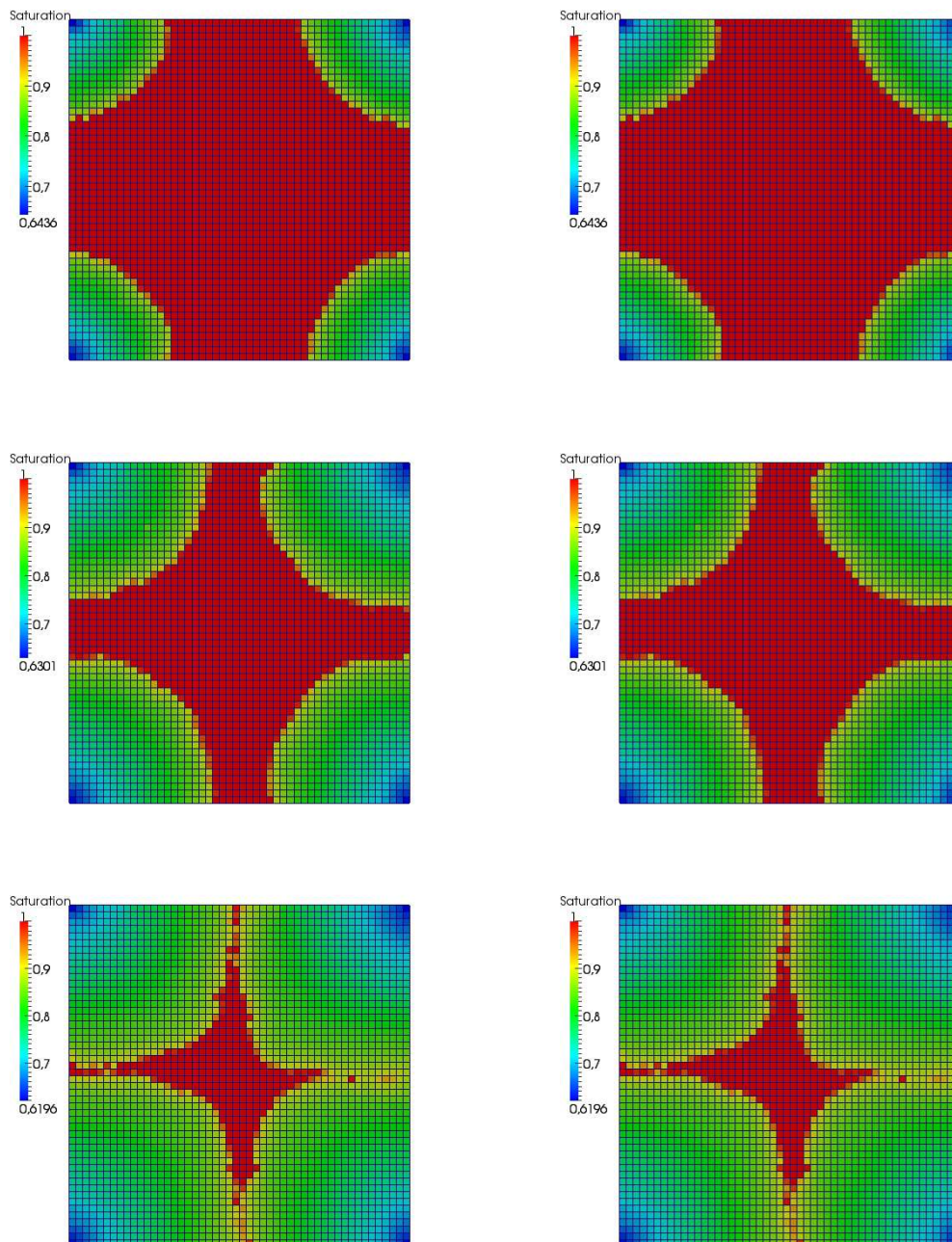
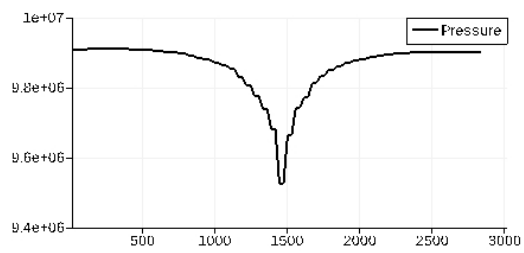
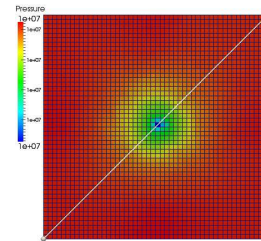


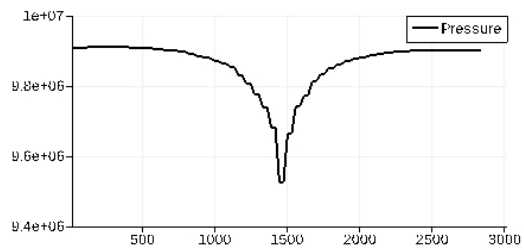
Figure 2.33: Liquid saturation, classical (left) and adaptive (right) resolutions at times 3 years, 6 years, and 9 years for the test case of Section 2.5.4.2



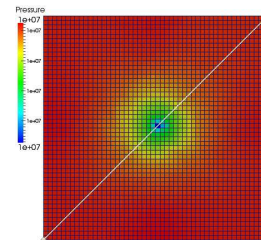
(a) pressure curve on a line in the domain



(b) Reference pressure



(c) pressure curve on a line in the domain



(d) Reference pressure

Figure 2.34: Reference pressure, classical (top) and adaptive (bottom) resolution at time 8 years for the test case of Section 2.5.4.2

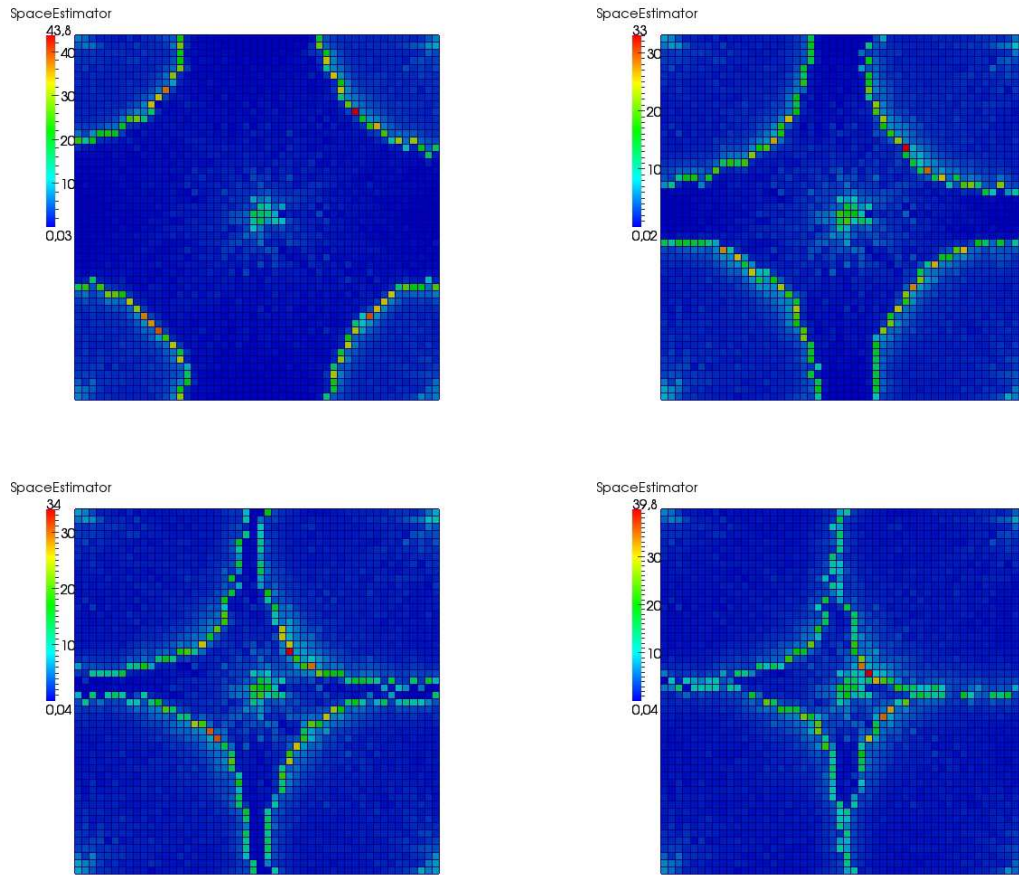


Figure 2.35: Spatial error distribution at times 3 years, 6 years, 8 years, and 9 years for the test case of Section 2.5.4.2

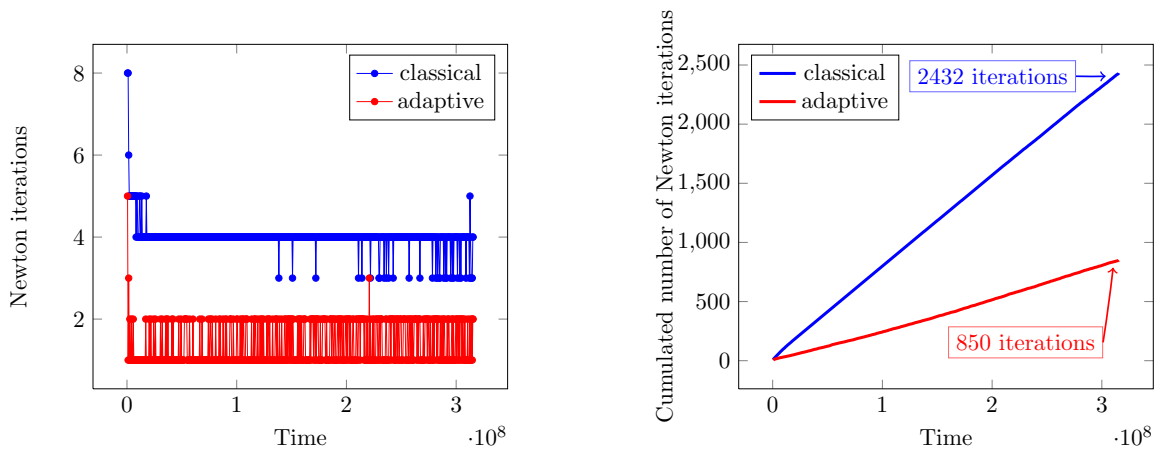


Figure 2.36: Newton iterations at each time step (left) and cumulated number of Newton iterations as a function of time (right) for the test case of Section 2.5.4.2. Average number of Newton iterations per time step: 4 iterations (classical), 1 iterations (adaptive)

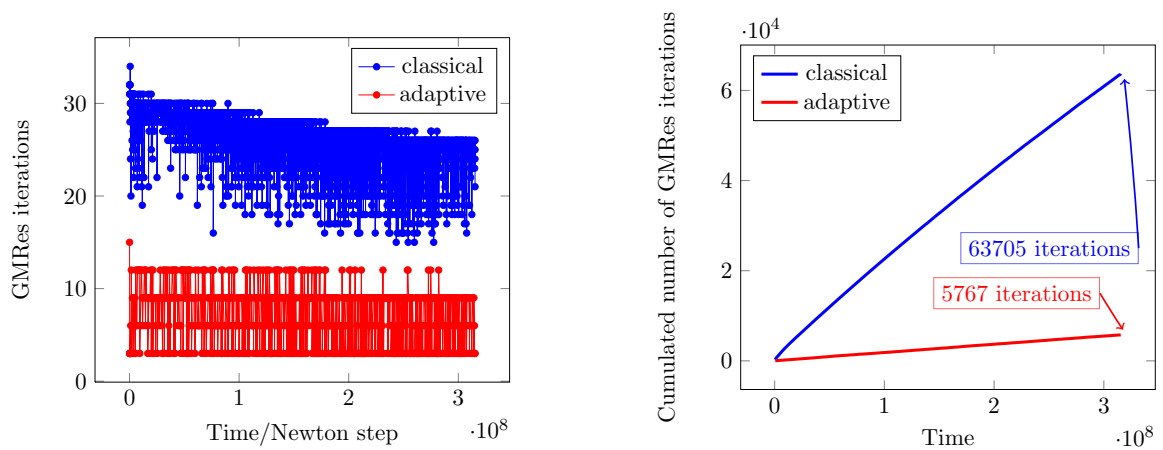


Figure 2.37: GMRes iterations at each time and Newton step (left) and cumulated number of GMRes iterations as a function of time (right) for the test case of Section 2.5.4.2. Average number of GMRes iterations per time and Newton iteration step: 27 iterations (classical), 6 iterations (adaptive). Average number of GMRes iterations per time step: 104 iterations (classical), 9 iterations (adaptive)

Bibliography

- [1] I. Aavatsmark, T. Barkve, O. Bøe, and T. Mannseth. Discretization on non-orthogonal, curvilinear grids for multi-phase flow. In *Proc. of the 4th European Conf. on the Mathematics of Oil Recovery*, volume D, Røros, Norway, 1994.
- [2] I. Aavatsmark, T. Barkve, Ø. Bøe, and T. Mannseth. Discretization on unstructured grids for inhomogeneous, anisotropic media. I. Derivation of the methods. *SIAM J. Sci. Comput.*, 19(5):1700–1716, 1998.
- [3] Y. Achdou, C. Bernardi, and F. Coquel. A priori and a posteriori analysis of finite volume discretizations of Darcy’s equations. *Numer. Math.*, 96(1):17–42, 2003.
- [4] G. Acs and E. Farkas. General purpose compositional model. *Society of Petroleum Engineers*, 25(4):543–553, 1985.
- [5] L. Agélas, D. A. Di Pietro, and J. Droniou. The G method for heterogeneous anisotropic diffusion on general meshes. *M2AN Math. Model. Numer. Anal.*, 44(4):597–625, 2010.
- [6] L. Agélas, D. A. Di Pietro, and R. Masson. A symmetric and coercive finite volume scheme for multiphase porous media flow problems with applications in the oil industry. In *Finite volumes for complex applications V*, pages 35–51. ISTE, London, 2008.
- [7] B. Amaziane, M. Jurak, and A. Žgaljić Keko. An existence result for a coupled system modeling a fully equivalent global pressure formulation for immiscible compressible two-phase flow in porous media. *J. Differential Equations*, 250(3):1685–1718, 2011.
- [8] S. N. Antontsev, A. V. Kazhikhov, and V. N. Monakhov. *Boundary value problems in mechanics of nonhomogeneous fluids*. North-Holland, Amsterdam, 1990. Studies in Mathematics and Its Applications, Vol. 22.
- [9] T. Arbogast. The existence of weak solutions to single porosity and simple dual-porosity models of two-phase incompressible flow. *Nonlinear Anal.*, 19(11):1009–1031, 1992.
- [10] K. Aziz and A. Settari. *Petroleum Reservoir Simulation*. Applied Science Publisher, Ltd, London, 1979.

-
- [11] S. Balay, J. Brown, K. Buschelman, V. Eijkhout, W. D. Gropp, D. Kaushik, M. G. Knepley, L. C. McInnes, B. F. Smith, and Z. H. PETSc users manual. Technical Report ANL-95/11 - Revision 3.3, Argonne National Laboratory, 2012.
- [12] S. Balay, J. Brown, K. Buschelman, W. D. Gropp, D. Kaushik, M. G. Knepley, L. C. McInnes, B. F. Smith, and H. Zhang. PETSc Web page, 2012. <http://www.mcs.anl.gov/petsc>.
- [13] S. Balay, W. D. Gropp, L. C. McInnes, and B. F. Smith. Efficient management of parallelism in object oriented numerical software libraries. In E. Arge, A. M. Bruaset, and H. P. Langtangen, editors, *Modern Software Tools in Scientific Computing*, pages 163–202. Birkhäuser Press, 1997.
- [14] J. Bear. *Dynamics of fluids in porous media*. American Elsevier, New York, 1972.
- [15] M. Bebendorf. A note on the Poincaré inequality for convex domains. *Z. Anal. Anwendungen*, 22(4):751–756, 2003.
- [16] Y. Brenier and J. Jaffré. Upstream differencing for multiphase flow in reservoir simulation. *SIAM J. Numer. Anal.*, 28:685–696, 1991.
- [17] F. Brezzi and M. Fortin. *Mixed and hybrid finite element methods*, volume 15 of *Springer Series in Computational Mathematics*. Springer-Verlag, New York, 1991.
- [18] R. J. Brooks and A. T. Corey. Hydraulic properties of porous media. *Hydrology Paper 3, Colorado State University, Fort Collins*, 1964.
- [19] C. Cancès, T. Gallouët, and A. Porretta. Two-phase flows involving capillary barriers in heterogeneous porous media. *Interfaces Free Bound.*, 11(2):239–258, 2009.
- [20] C. Cancès, I. S. Pop, and M. Vohralík. An a posteriori error estimate for vertex-centered finite volume discretizations of immiscible incompressible two-phase flow. *Math. Comp.*, 2013. Accepted for publication.
- [21] A. L. Chaillou and M. Suri. Computable error estimators for the approximation of nonlinear problems by linearized models. *Comput. Methods Appl. Mech. Engrg.*, 196(1-3):210–224, 2006.
- [22] G. Chavent and J. Jaffré. *Mathematical models and finite elements for reservoir simulation*. North-Holland, Amsterdam, 1986. Studies in Mathematics and Its Applications, Vol. 17.
- [23] Z. Chen. Degenerate two-phase incompressible flow. I. Existence, uniqueness and regularity of a weak solution. *J. Differential Equations*, 171(2):203–232, 2001.
- [24] Z. Chen and R. Ewing. From single-phase to compositional flow: Applicability of mixed finite elements. *Transport in Porous Media*, 27:225–242, 1997.
- [25] Z. Chen, G. Qin, and R. E. Ewing. Analysis of a compositional model for fluid flow in porous media. *SIAM J. Appl. Math.*, 60(3):747–777, 2000.

-
- [26] K. H. Coats. An equation of state compositional model. *Society of Petroleum Engineers*, 20(5):363–376, 1980.
- [27] D. A. Di Pietro and S. Lemaire. An extension of the Crouzeix–Raviart space to general meshes with application to quasi-incompressible linear elasticity and Stokes flow. Submitted. Preprint hal-00753660, 2012.
- [28] D. A. Di Pietro and M. Vohralík. A review of recent advances in discretization methods, a posteriori error analysis, and adaptive algorithms for numerical methods in geosciences. *OGST Oil & Gas Science and Technology*, 2013. Accepted for publication.
- [29] D. A. Di Pietro, M. Vohralík, and S. Yousef. Adaptive regularization, linearization, and discretization and a posteriori error control for the two-phase Stefan problem. HAL Preprint 00690862, submitted for publication, Apr. 2012.
- [30] J. Douglas, Jr., R. E. Ewing, and M. F. Wheeler. The approximation of the pressure by a mixed method in the simulation of miscible displacement. *RAIRO Anal. Numér.*, 17(1):17–33, 1983.
- [31] J. Droniou. Finite volume methods for diffusion equations: introduction to and review of recent methods. *M3AS Math. Models Meth. Appl. Sci.*, 2013. Submitted.
- [32] M. G. Edwards and C. F. Rogers. Finite volume discretization with imposed flux continuity for the general tensor pressure equation. *Comput. Geosci.*, 2:259–290, 1998.
- [33] L. El Alaoui, A. Ern, and M. Vohralík. Guaranteed and robust a posteriori error estimates and balancing discretization and linearization errors for monotone nonlinear problems. *Comput. Methods Appl. Mech. Engrg.*, 200(37-40):2782–2795, 2011.
- [34] K. Eriksson and C. Johnson. Adaptive finite element methods for parabolic problems. IV. Nonlinear problems. *SIAM J. Numer. Anal.*, 32(6):1729–1749, 1995.
- [35] A. Ern and M. Vohralík. A posteriori error estimation based on potential and flux reconstruction for the heat equation. *SIAM J. Numer. Anal.*, 48(1):198–223, 2010.
- [36] A. Ern and M. Vohralík. Adaptive inexact Newton methods with a posteriori stopping criteria for nonlinear diffusion PDEs. *SIAM J. Sci. Comput.*, 2013. DOI 10.1137/120896918.
- [37] R. E. Ewing, B. A. Boyett, D. K. Babu, and R. F. Heinemann. Efficient use of locally refined grids for multiphase reservoir simulation. *Society of Petroleum Engineers*, 1989.
- [38] R. Eymard, T. Gallouët, and R. Herbin. *The finite volume method*, volume 7 of *Handbook of Numerical Analysis*. P. G. Ciarlet and J.-L. Lions eds., North Holland, 2000.
- [39] R. Eymard, T. Gallouët, and R. Herbin. *Finite volume methods*, volume VII. In *Handbook of numerical analysis*, North-Holland, Amsterdam, 2000.
- [40] R. Eymard, R. Herbin, and A. Michel. Mathematical study of a petroleum-engineering scheme. *M2AN Math. Model. Numer. Anal.*, 37(6):937–972, 2003.
- [41] Z. E. Heinemann. Using local grid refinement in a multiple-application reservoir simulator. *Society of Petroleum Engineers*, 1983.

-
- [42] R. D. Hornung and J. A. Trangenstein. Adaptive mesh refinement and multilevel iteration for flow in porous media. *J. Comput. Phys.*, 136(2):522–545, 1997.
- [43] R. Huber and R. Helmig. Node-centered finite volume discretizations for the numerical simulation of multiphase flow in heterogeneous porous media. *Comput. Geosci.*, 4(2):141–164, 2000.
- [44] P. Jiránek, Z. Strakoš, and M. Vohralík. A posteriori error estimates including algebraic error and stopping criteria for iterative solvers. *SIAM J. Sci. Comput.*, 32(3):1567–1590, 2010.
- [45] O. A. Karakashian and F. Pascal. A posteriori error estimates for a discontinuous Galerkin approximation of second-order elliptic problems. *SIAM J. Numer. Anal.*, 41(6):2374–2399, 2003.
- [46] Z. Khalil and M. Saad. Degenerate two-phase compressible immiscible flow in porous media: the case where the density of each phase depends on its own pressure. *Math. Comput. Simulation*, 81(10):2225–2233, 2011.
- [47] D. Kröner and S. Luckhaus. Flow of oil and water in a porous medium. *J. Differential Equations*, 55(2):276–288, 1984.
- [48] D. Kröner and M. Ohlberger. A posteriori error estimates for upwind finite volume schemes for nonlinear conservation laws in multidimensions. *Math. Comp.*, 69(229):25–39, 2000.
- [49] Lake, L. W. *Enhanced Oil Recovery*. Old Tappan, NJ; Prentice Hall Inc., 1989.
- [50] M. R. Laydi and M. Ghilani. A general finite volume scheme for an elliptic-hyperbolic system using a variational approach. *Zeitschrift für angewandte Mathematik und Physik ZAMP*, 49(4):630–643, 1998.
- [51] M. Mamaghani, G. Enchéry, and C. Chainais-Hillairet. Development of a refinement criterion for adaptive mesh refinement in steam-assisted gravity drainage simulation. *Comput. Geosci.*, 15(1):17–34, 2011.
- [52] R. H. Nochetto, A. Schmidt, and C. Verdi. A posteriori error estimation and adaptivity for degenerate parabolic problems. *Math. Comp.*, 69(229):1–24, 2000.
- [53] M. Ohlberger. A posteriori error estimate for finite volume approximations to singularly perturbed nonlinear convection–diffusion equations. *Numer. Math.*, 87(4):737–761, 2001.
- [54] G. S. H. Pau, A. S. Almgren, J. B. Bell, and M. J. Lijewski. A parallel second-order adaptive mesh algorithm for incompressible flow in porous media. *Philos. Trans. R. Soc. Lond. Ser. A Math. Phys. Eng. Sci.*, 367(1907):4633–4654, 2009.
- [55] G. S. H. Pau, J. B. Bell, A. S. Almgren, K. M. Fagnan, and M. J. Lijewski. An adaptive mesh refinement algorithm for compressible two-phase flow in porous media. *Comput. Geosci.*, 16(3):577–592, 2012.

-
- [56] L. E. Payne and H. F. Weinberger. An optimal Poincaré inequality for convex domains. *Arch. Rational Mech. Anal.*, 5:286–292 (1960), 1960.
- [57] P. H. Sammon. Dynamic grid refinement and amalgamation for compositional simulation. *Society of Petroleum Engineers*, 2003.
- [58] S. Thomas. Récupération assistée du pétrole : panorama. *Oil & Gas Science and Technology - Rev. IFP*, 63(1):9–19, 2008.
- [59] J. A. Trangenstein and Z. Bi. Multi-scale iterative techniques and adaptive mesh refinement for flow in porous media. *Adv. Water Resour.*, pages 1175–1213, 2001.
- [60] R. Verfürth. A posteriori error estimates for nonlinear problems. $L^r(0, T; L^p(\Omega))$ -error estimates for finite element discretizations of parabolic equations. *Math. Comp.*, 67(224):1335–1360, 1998.
- [61] R. Verfürth. A posteriori error estimates for nonlinear problems: $L^r(0, T; W^{1,p}(\Omega))$ -error estimates for finite element discretizations of parabolic equations. *Numer. Methods Partial Differential Equations*, 14(4):487–518, 1998.
- [62] M. H. Vignal. Convergence of a finite volume scheme for an elliptic-hyperbolic system. *M2AN Math. Model. Numer. Anal.*, 30(7):841–872, 1996.
- [63] M. Vohralík. Residual flux-based a posteriori error estimates for finite volume and related locally conservative methods. *Numer. Math.*, 111(1):121–158, 2008.
- [64] M. Vohralík and M. F. Wheeler. A posteriori error estimates, stopping criteria, and adaptivity for two-phase flows. *Comput. Geosci.*, 2013. DOI 10.1007/s10596-013-9356-0.
- [65] L. C. Young and R. E. Stephenson. A generalized compositional approach for reservoir simulation. *Society of Petroleum Engineers*, 23(5):727–742, 1983.

A posteriori error estimates for thermal multiphase compositional flows in porous media

This chapter consists mainly of a theoretical part of an article submitted for publication, written with Daniele Di Pietro and Martin Vohralík

Contents

3.1	Introduction	123
3.2	Setting	124
3.3	Discretization of the energy equation	126
3.3.1	Two-point finite volume discretization	126
3.3.2	Linearization and algebraic resolution	127
3.4	Approximate solution and reconstructions	129
3.4.1	Postprocessing of the temperature	129
3.4.2	Saturations, molar fractions, and molar energy	129
3.4.3	H_0^1 -conforming temperature reconstruction	130
3.4.4	$\mathbf{H}(\text{div}; \Omega)$ -conforming energy flux reconstructions	130
3.5	A posteriori error estimate	131
3.5.1	Weak solution	131
3.5.2	Error measure	132
3.5.3	An a posteriori error estimate distinguishing the space, time, linearization, and algebraic errors	134
3.5.4	Balancing and stopping criteria	137
3.A	Application to the thermal dead oil model	137
3.A.1	Dead oil model	138
3.A.2	A posteriori error estimate for the thermal dead oil model	139

Bibliography	143
-------------------------------	------------

Abstract

We consider in this chapter thermal multiphase multicomponent flows in porous media. We derive fully computable a posteriori error estimates for the dual norm of the residual supplemented by a nonconformity evaluation term. We also show how to estimate separately the space, time, linearization, and algebraic errors giving the possibility to formulate adaptive stopping and balancing criteria. We consider the application of the theory to an implicit cell-centered finite volume scheme with phase-upwind and two-point discretization of diffusive fluxes. Specification of the abstract theory to the so-called dead oil model closes the chapter.

Key words: a posteriori error analysis, stopping criteria, balancing criteria, compositional Darcy flow, thermal flow, finite volume method, dead oil model.

3.1 Introduction

The model considered in the previous chapter has been developed under the condition that the flow is isothermal. In this chapter we consider the thermal multiphase compositional model in porous medium that describes the flow of several fluids through a subsurface under a nonisothermal condition. This model is governed by the same equations as the isothermal model, supplemented by a conservation of energy equation that adds a new dependent variable, the temperature, to the system, see [21, 22, 17].

Thermal models are especially important for the simulation of the enhanced oil recovery (see the discussion in the Introduction), where the increase of the temperature reduces the oil viscosity which in turn improves mobility and makes the production easier and leading to better recovery indices. Several methods of thermal simulation have been considered. We can cite, e.g., the recent works [40, 20, 46, 44, 37, 43, 23, 41]. Thermal processes play also an important role in the modeling of geothermal reservoirs, see, e.g., [45] and the references therein.

A mathematical structure of multiphase thermal models of flow in porous media is proposed in [51]. The authors give a formulation and numerical solution of equations for modeling multicomponent, two-phase, thermal fluid flow in porous media. For this purpose they develop an algorithm that achieves a better balance between stability and accuracy. This approach was used previously for reservoir simulation of black-oil model [11] and also for compositional models [10]. Recently, it has been proposed in [12, 41] to formulate the phase transitions as a set of local inequality constraints and to use the complementarity approach.

Many numerical methods have been proposed for the discretization of the multiphase compositional model: finite differences and finite element methods in, e.g., [3, 8, 21, 55], mixed finite element methods in, e.g., [28, 16, 18, 19], finite volume methods in, e.g., [38, 42, 35, 5, 1, 4], and recently vertex-centered methods on general 3D meshes in [34]. Many adaptive mesh refinement algorithms have also already been considered, cf. [36, 32, 20] for dynamic gridding to thermal and isothermal models, and other recent works, cf. [50, 49, 44, 46, 37, 43, 47, 48].

The discretization of the thermal multiphase multicomponent model leads to nonlinear, strongly coupled systems of differential and algebraic equations. The resolution of these systems requires an important computational effort. Therefore, proposing an adaptive algorithm to optimize this resolution holds a special interest in reservoir modeling. To the best of our knowledge, this work is the first to develop a posteriori error estimates to control the error and stopping criteria for the iterative algebraic and nonlinear solvers for the general version of the thermal multiphase compositional model. We follow [54, 14] where a rigorous a posteriori error analysis for the immiscible incompressible two-phase flow was given under the assumption that the flow process is isothermal, and Chapter 2 of this thesis (work corresponds to [25]), where a generalization to arbitrary number of phases and components, still in the isothermal case, was done. The goal of this chapter is to analyse the additional equation of conservation of energy and to undertake the a posteriori analysis for the thermal multiphase compositional model by developing a guaranteed upper bound for a well chosen residual error norm, to distinguish the different error components, and to devise a fully adaptive algorithm.

3.2 Setting

We consider a nonisothermal condition for the multiphase compositional flow of the previous chapter which will be completed by an additional equation representing the *conservation of energy*. This leads to an extra unknown to the system (2.2.1)–(2.2.10): the *temperature* of the fluids and of the porous medium, which is now not stable during the simulation. Recalling the characterization of the isothermal multiphase compositional model of Chapter 2, Section 2.2, we will have here some additional properties representing the nonisothermal condition and we will also consider the dependence of the temperature on other properties.

The vector of unknowns is now:

$$\mathcal{X} := \begin{pmatrix} P \\ T \\ (S_p)_{p \in \mathcal{P}} \\ (C_{p,c})_{p \in \mathcal{P}, c \in \mathcal{C}_p} \end{pmatrix}$$

and for each fluid phase $p \in \mathcal{P}$, we consider three additional properties:

- (a) the *thermal conductivity* λ ;
- (b) the *rock internal energy* $e_r(P_p, T)$;
- (c) the *rock molar density* ζ_r .

They are all assumed constant in time for the sake of simplicity. Before proceeding to the description of the thermal model we list in Table 3.1 the dependence of all the model parameters on the unknowns.

The additional conservation of energy PDE is given by

$$\partial_t e_H + \nabla \cdot \Phi_H = Q_H, \quad (3.2.1)$$

	$\forall p \in \mathcal{P}$		varying in space	$\forall p \in \mathcal{P}$			
	parameter			P_p	T	\mathbf{S}	\mathbf{C}_p
Medium properties	porosity	ϕ	\times				
	permeability	\mathbb{K}	\times				
	conductivity	λ	\times				
	rock molar density	ζ_r		\times	\times		\times
	rock internal energy	e_r		\times	\times		\times
Thermodynamic properties	relative permeability	k_{r_p}	\times		\times	\times	
	enthalpy	H_p		\times	\times		\times
	molar density	ζ_p		\times	\times		\times
	mass density	ρ_p		\times	\times		\times
	viscosity	μ_p		\times	\times		\times
	mobility	ν_p		\times	\times	\times	\times
	internal energy	e_p		\times	\times		\times

Table 3.1: Dependence of the model's parameters

where $Q_H \in L^2((0, t_F); L^2(\Omega))$ denotes an *thermal source or sink*. The *molar energy per unit volume* $e_H := e_H(\mathcal{X})$ has the following expression:

$$e_H = \phi \sum_{p \in \mathcal{P}} \zeta_p(P_p, T, \mathbf{C}_p) e_p(P_p, T, \mathbf{C}_p) S_p + (1 - \phi) \zeta_r e_r(P_p, T, \mathbf{C}_p), \quad (3.2.2)$$

and the flux Φ_H is given by

$$\Phi_H := \mathbf{J} + \sum_{p \in \mathcal{P}} \Phi_{p,H}, \quad (3.2.3)$$

with the *Fourier flux* $\mathbf{J} = \mathbf{J}(T)$,

$$\mathbf{J}(T) := -\lambda \nabla T$$

and the *phase enthalpy fluxes* are given for all $p \in \mathcal{P}$ by

$$\begin{aligned} \Phi_{p,H} = \Phi_{p,H}(P_p, T, \mathbf{S}, \mathbf{C}_p) &:= \frac{\zeta_p(P_p, T, \mathbf{C}_p) k_{r_p}(\mathbf{S})}{\mu_p(P_p, T, \mathbf{C}_p)} H_p(P_p, T, \mathbf{C}_p) \mathbf{v}_p(P_p, T, \mathbf{C}_p) \\ &= \nu_p(P_p, T, \mathbf{S}, \mathbf{C}_p) H_p(P_p, T, \mathbf{C}_p) \mathbf{v}_p(P_p, T, \mathbf{C}_p). \end{aligned}$$

Here, for all $p \in \mathcal{P}$, the *average phase velocity* \mathbf{v}_p is given by Darcy's law,

$$\mathbf{v}_p = \mathbf{v}_p(P_p, T, \mathbf{C}_p) = -\mathbb{K} (\nabla P_p - \rho_p(P_p, T, \mathbf{C}_p) \mathbf{g}) = -\mathbb{K} (\nabla P_p + \rho_p g \nabla z), \quad (3.2.4)$$

where \mathbf{g} denotes the gravity vector acting along $-z$ and g its Euclidian norm.

For the sake of simplicity, we assume that *no-flow boundary conditions* are prescribed,

$$\Phi_H \cdot \mathbf{n}_\Omega = 0 \quad \text{on } \partial\Omega \times (0, t_F), \quad (3.2.5)$$

where $\partial\Omega$ denotes the boundary of Ω and \mathbf{n}_Ω its outward normal. Finally, at $t = 0$ we enforce the *initial molar energy* by setting

$$e_H(\cdot, 0) = e_H^0, \quad (3.2.6)$$

where e_H^0 is supposed piecewise constant on the mesh introduced below.

3.3 Discretization of the energy equation

We have proposed in Section 2.2.2 a discretization of the isothermal multiphase compositional model based on an implicit cell-centered finite volume scheme with phase-upwind and two-point discretization of the diffusive fluxes. To complete the discretization of the thermal model, we discuss here how to discretize the additional equation of conservation of energy (3.2.1). We use the same notations and assumptions for the space-time mesh described in Section 2.2.2 of Chapter 2.

3.3.1 Two-point finite volume discretization

Recall the discretization of the isothermal multiphase compositional model's unknowns (2.2.17) in the context of finite volume method. Here we enrich the discrete vector with an additional discretization variable, the temperature. For all $0 \leq n \leq N$ we let

$$\mathcal{X}_M^n := (\mathcal{X}_M^n)_{M \in \mathcal{M}^n}, \quad \mathcal{X}_M^n := \begin{pmatrix} P_M^n \\ T_M^n \\ (S_{p,M}^n)_{p \in \mathcal{P}} \\ (C_{p,c,M}^n)_{p \in \mathcal{P}, c \in \mathcal{C}_p} \end{pmatrix} \quad \forall M \in \mathcal{M}^n,$$

where T_M^n denotes the temperature in the cell M at the n th time step. Note that, in practice, we complement the initial conditions (2.2.7) and (3.2.6) by the artificial condition to initialize the computation

$$\mathcal{X}_M(\cdot, 0) = \mathcal{X}_M^0, \quad (3.3.1)$$

where \mathcal{X}_M^0 typically results from a steady-state equilibrium computation. We also suppose that e_H^0 in (3.2.6) is piecewise constant on \mathcal{M}^0 and that the relation (3.2.2) between e_H^0 and the corresponding contributions of \mathcal{X}_M^0 is satisfied.

The PDE (3.2.1) is discretized by requiring, for all $0 \leq n \leq N$,

$$|M| \partial_t^n e_{H,M} + \sum_{\sigma \in \mathcal{E}_M^{i,n}} \left(F_{H,M,\sigma}(\mathcal{X}_M^n) + G_{M,\sigma}(\mathcal{X}_M^n) \right) = |M| Q_{H,M}^n, \quad \forall M \in \mathcal{M}^n, \quad (3.3.2)$$

where $Q_{H,M}^n := \int_{I_n} \int_M Q_H^n / (|M| \tau_n)$ and the accumulation term is given, for all $0 \leq n \leq N$, by the following discrete version of the molar energy (3.2.2):

$$\begin{aligned} e_{H,M}^n = e_{H,M}(\mathcal{X}_M^n) &:= \phi \sum_{p \in \mathcal{P}} \zeta_p(P_{p,M}^n, T_M^n, \mathbf{C}_{p,M}^n) e_p(P_{p,M}^n, T_M^n, \mathbf{C}_{p,M}^n) S_{p,M}^n \\ &\quad + (1 - \phi) \zeta_r e_r(P_{p,M}^n, T_M^n, \mathbf{C}_{p,M}^n) \quad \forall M \in \mathcal{M}^n. \end{aligned} \quad (3.3.3)$$

The flux $F_{H,M,\sigma}$ is given by the sum of the fluxes for each phase $p \in \mathcal{P}$, i.e.,

$$F_{H,M,\sigma}(\mathcal{X}_M^n) := \sum_{p \in \mathcal{P}} F_{p,H,M,\sigma}(\mathcal{X}_M^n), \quad (3.3.4)$$

where, for a given phase p , any $M \in \mathcal{M}^n$, and any $\sigma \in \mathcal{E}_M^{i,n}$ with $\sigma = \partial M \cap \partial L$,

$$F_{p,H,M,\sigma}(\mathcal{X}_M^n) = \nu_p^\uparrow H_{p,M_p^\uparrow}^\uparrow F_{p,M,\sigma}(\mathcal{X}_M^n), \quad M_p^\uparrow = \begin{cases} M & \text{if } P_{p,M}^n - P_{p,L}^n \geq 0, \\ L & \text{otherwise,} \end{cases} \quad (3.3.5)$$

with $H_{p,M_p^\uparrow}^\uparrow$ and $\nu_p^\uparrow(\mathcal{X}_M^n) := \nu_p(P_{p,M_p^\uparrow}^n, T_{M_p^\uparrow}^n, \mathbf{S}_{M_p^\uparrow}^n, \mathbf{C}_{p,M_p^\uparrow}^n)$ denoting, respectively, the upstream enthalpy and upstream mobility. In (3.3.5), we have introduced the two-point finite volume approximation of the normal component of the average phase velocity over the face σ given as in Section 2.2.2 by

$$F_{p,M,\sigma}(\mathcal{X}_M^n) := |\sigma| \frac{\alpha_M \alpha_L}{\alpha_M + \alpha_L} [P_{p,M}^n - P_{p,L}^n + \rho_{p,\sigma}^n g(z_M - z_L)], \quad \alpha_K := \frac{K_K}{d_{K\sigma}} \quad \forall K \in \{M, L\}, \quad (3.3.6)$$

where $\rho_{p,\sigma}^n$ is an interface mass density of the phase p obtained by averaging the cell values in M and L , defined by (other expressions are possible for $\rho_{p,\sigma}^n$),

$$\rho_{p,\sigma}^n := \frac{(\chi_{p,M}^n \rho_p(P_{p,M}^n, T_M^n, \mathbf{C}_{p,M}^n) + \chi_{p,L}^n \rho_p(P_{p,L}^n, T_L^n, \mathbf{C}_{p,L}^n))}{\chi_{p,M}^n + \chi_{p,L}^n}$$

with

$$\chi_{p,K}^n = \begin{cases} 1 & \text{if } S_{p,K}^n > 0, \\ 0 & \text{otherwise,} \end{cases} \quad K \in \{M, L\}.$$

Finally, for all $M \in \mathcal{M}^n$ and all $\sigma \in \mathcal{E}_M^{i,n}$ with $\sigma = \partial M \cap \partial L$, the discrete Fourier flux $G_{M,\sigma}$ is given by,

$$G_{M,\sigma}(\mathcal{X}_M^n) := |\sigma| \frac{\beta_M \beta_L}{\beta_M + \beta_L} (T_M^n - T_L^n), \quad \beta_K := \frac{\lambda_K}{d_{K\sigma}} \quad \forall K \in \{M, L\}. \quad (3.3.7)$$

All boundary fluxes are set to zero to account for the homogeneous boundary condition (3.2.5).

3.3.2 Linearization and algebraic resolution

The discretization method of Section 3.3.1 requires to solve a system of nonlinear algebraic equations at each time step, which we undertake using the Newton algorithm.

Recall the discrete conservation of energy (3.3.2). We define for all $1 \leq n \leq N$ and all $M \in \mathcal{M}^n$ the residual $R_{H,M}^n$ by

$$R_{H,M}^n(\mathcal{X}_M^n) := \frac{|M|}{\tau^n} (e_{H,M}(\mathcal{X}_M^n) - e_{H,M}^{n-1}) + \sum_{\sigma \in \mathcal{E}_M^{i,n}} (F_{H,M,\sigma}(\mathcal{X}_M^n) + G_{M,\sigma}(\mathcal{X}_M^n)) - |M| Q_{H,M}^n = 0. \quad (3.3.8)$$

For $1 \leq n \leq N$ and $\mathcal{X}_{\mathcal{M}}^{n,0}$ fixed (typically, $\mathcal{X}_{\mathcal{M}}^{n,0} = \mathcal{X}_{\mathcal{M}}^{n-1}$), the Newton algorithm generates a sequence $(\mathcal{X}_{\mathcal{M}}^{n,k})_{k \geq 1}$ with $\mathcal{X}_{\mathcal{M}}^{n,k}$ solution to the following linear system: For all $M \in \mathcal{M}^n$,

$$\sum_{M' \in \mathcal{M}^n} \frac{\partial R_{H,M}^n}{\partial \mathcal{X}_{M'}^n}(\mathcal{X}_{\mathcal{M}}^{n,k-1}) (\mathcal{X}_{M'}^{n,k} - \mathcal{X}_{M'}^{n,k-1}) + R_{H,M}^n(\mathcal{X}_{\mathcal{M}}^{n,k-1}) = 0. \quad (3.3.9)$$

The (approximate) solution to (2.4.2), (3.3.9) is typically obtained using an iterative algebraic solver. For $1 \leq n \leq N$, a given Newton iteration $k \geq 1$, and $\mathcal{X}_{\mathcal{M}}^{n,k,0}$ fixed (typically, $\mathcal{X}_{\mathcal{M}}^{n,k,0} = \mathcal{X}_{\mathcal{M}}^{n,k-1}$), the iterative solver generates a sequence $(\mathcal{X}_{\mathcal{M}}^{n,k,i})_{i \geq 1}$ solving the linear system up to the residuals given, for all $M \in \mathcal{M}^n$, by (2.4.3) and

$$\begin{aligned} R_{H,M}^{n,k,i} &= \frac{|M|}{\tau^n} \frac{\partial e_{H,M}}{\partial \mathcal{X}_M^n}(\mathcal{X}_M^{n,k-1}) (\mathcal{X}_M^{n,k,i} - \mathcal{X}_M^{n,k-1}) \\ &+ \sum_{M' \in \mathcal{M}^n} \sum_{\sigma \in \mathcal{E}_M^{i,n}} \frac{\partial F_{H,M,\sigma}}{\partial \mathcal{X}_{M'}^n}(\mathcal{X}_{\mathcal{M}}^{n,k-1}) (\mathcal{X}_{M'}^{n,k,i} - \mathcal{X}_{M'}^{n,k-1}) \\ &+ \sum_{M' \in \mathcal{M}^n} \sum_{\sigma \in \mathcal{E}_M^{i,n}} \frac{\partial G_{M,\sigma}}{\partial \mathcal{X}_{M'}^n}(\mathcal{X}_{\mathcal{M}}^{n,k-1}) (\mathcal{X}_{M'}^{n,k,i} - \mathcal{X}_{M'}^{n,k-1}) + R_{H,M}^n(\mathcal{X}_{\mathcal{M}}^{n,k-1}). \end{aligned} \quad (3.3.10)$$

Thus, at time step $1 \leq n \leq N$, Newton iteration $k \geq 1$, and linear solver iteration $i \geq 1$, the residual vector $R_{H,M}^{n,k,i}$ is given for all $M \in \mathcal{M}^n$ by

$$R_{H,M}^{n,k,i} = \frac{|M|}{\tau^n} \left(e_{H,M}(\mathcal{X}_{\mathcal{M}}^{n,k-1}) + \mathfrak{E}_M^{n,k,i} - e_{H,M}^{n-1} \right) + \sum_{\sigma \in \mathcal{E}_M^{i,n}} \left(F_{H,M,\sigma}^{n,k,i} + G_{M,\sigma}^{n,k,i} \right) - |M| Q_{H,M}^n, \quad (3.3.11)$$

where $\mathfrak{E}_M^{n,k,i}$ is the linear perturbations of the energy accumulation terms defined as,

$$\mathfrak{E}_M^{n,k,i} := \frac{\partial e_{H,M}}{\partial \mathcal{X}_M^n}(\mathcal{X}_M^{n,k-1}) (\mathcal{X}_M^{n,k,i} - \mathcal{X}_M^{n,k-1}),$$

whereas the linearized fluxes $F_{H,M,\sigma}^{n,k,i}$ read

$$F_{H,M,\sigma}^{n,k,i} := \sum_{p \in \mathcal{P}} F_{p,H,M,\sigma}^{n,k,i}, \quad (3.3.12)$$

with linearized phase fluxes

$$F_{p,H,M,\sigma}^{n,k,i} := F_{p,H,M,\sigma}(\mathcal{X}_{\mathcal{M}}^{n,k-1}) + \sum_{M' \in \mathcal{M}^n} \frac{\partial F_{p,H,M,\sigma}}{\partial \mathcal{X}_{M'}^n}(\mathcal{X}_{\mathcal{M}}^{n,k-1}) (\mathcal{X}_{M'}^{n,k,i} - \mathcal{X}_{M'}^{n,k-1}). \quad (3.3.13)$$

Finally, the linearized Fourier flux reads

$$G_{M,\sigma}^{n,k,i} := G_{M,\sigma}(\mathcal{X}_{\mathcal{M}}^{n,k-1}) + \sum_{M' \in \mathcal{M}^n} \frac{\partial G_{M,\sigma}}{\partial \mathcal{X}_{M'}^n}(\mathcal{X}_{\mathcal{M}}^{n,k-1}) (\mathcal{X}_{M'}^{n,k,i} - \mathcal{X}_{M'}^{n,k-1}), \quad (3.3.14)$$

and completes the linearized component fluxes (2.4.6).

3.4 Approximate solution and reconstructions

In this section, we first postprocess the original piecewise constant finite volume temperature approximations as we did in Section 2.4.2.1 for the phase pressures. We then detail how to obtain the energy flux reconstructions and smoothed temperature that enter the definitions of the a posteriori estimators proposed in Section 3.5 below.

We will employ, at each time step n , $\mathbf{H}(\text{div}; \Omega)$ -conforming discrete fluxes belonging to the lowest-order Raviart–Thomas–Nédélec space $\mathbf{RTN}(\mathcal{M}^n)$ (see Brezzi and Fortin [13]):

$$\begin{aligned} \mathbf{RTN}(\mathcal{M}^n) := \{ & \mathbf{v}_h \in \mathbf{H}(\text{div}; \Omega); \mathbf{v}_h|_M \in \mathbb{Q}_{0,1}(M) \times \mathbb{Q}_{1,0}(M) \text{ if } d = 2, \\ & \mathbf{v}_h|_M \in \mathbb{Q}_{0,1,1}(M) \times \mathbb{Q}_{1,0,1}(M) \times \mathbb{Q}_{1,1,0}(M) \text{ if } d = 3, \quad \forall M \in \mathcal{M}^n \}. \end{aligned}$$

For more general meshes one can either introduce a matching simplicial submesh of \mathcal{M}^n and use the simplicial version of $\mathbf{RTN}(\mathcal{M}^n)$, or use the construction proposed in [26, Appendix A].

3.4.1 Postprocessing of the temperature

The original finite volume approximation of the temperature is piecewise constant. To evaluate its gradient inside each cell, we define piecewise quadratic, possibly discontinuous temperature as described in the following. Let a time step $1 \leq n \leq N$, a Newton linearization iteration $k \geq 1$, and an algebraic solver iteration $i \geq 1$ be fixed. Following [33], we define the fluxes $\mathbf{\Gamma}_{T,h}^{n,k,i} \in \mathbf{RTN}(\mathcal{M}^n)$ such that, for all $M \in \mathcal{M}^n$ and all $\sigma \in \mathcal{E}_M^{i,n}$,

$$(\mathbf{\Gamma}_{T,h}^{n,k,i} \cdot \mathbf{n}_M, 1)_\sigma = G_{M,\sigma}(\mathcal{X}_M^{n,k,i}), \quad (3.4.1)$$

with $G_{M,\sigma}$ defined by (3.3.7), and $\mathbf{\Gamma}_{T,h}^{n,k,i} \cdot \mathbf{n}_\Omega = 0$ on $\partial\Omega$, thereby accounting for the no-flow boundary conditions (3.2.5). Following [53], we introduce the piecewise quadratic temperature reconstruction $T_h^{n,k,i}$ such that, for all $M \in \mathcal{M}^n$,

$$-\lambda \nabla T_h^{n,k,i}|_M = \mathbf{\Gamma}_{T,h}^{n,k,i}|_M \quad \text{and} \quad \frac{1}{|M|} (T_h^{n,k,i}, 1)_M = T_M^{n,k,i}. \quad (3.4.2)$$

From this reconstruction we finally define the space-time function $T_{h\tau}^{n,k,i}$ assuming an affine-in-time behavior from the converged values at time t^{n-1} and the (possibly not converged) values $T_h^{n,k,i}$ at t^n . Henceforth, ∇ is to be understood as the broken gradient operator on \mathcal{M}^n when used for $T_{h\tau}^{n,k,i}$.

3.4.2 Saturations, molar fractions, and molar energy

The approximations of saturations, molar fractions, and molar energy obtained using the finite volume discretization detailed in Sections 2.2.2 and 3.3 are piecewise constant in space.

We define for all $0 \leq n \leq N$, $k \geq 1$, and $i \geq 1$, the corresponding functions of space such that

$$\begin{aligned} (S_{p,h}^{n,k,i})|_M &= S_{p,M}^{n,k,i} & \forall p \in \mathcal{P}, \\ (C_{p,c,h}^{n,k,i})|_M &= C_{p,c,M}^{n,k,i} & \forall p \in \mathcal{P}, \forall c \in \mathcal{C}_p, \\ (l_{c,h}^{n,k,i})|_M &= l_{c,M}^{n,k,i} := l_{c,M}(\mathcal{X}_{\mathcal{M}}^{n,k,i}) & \forall c \in \mathcal{C}, \\ (e_{H,h}^{n,k,i})|_M &= e_{H,M}^{n,k,i} := e_{H,M}(\mathcal{X}_{\mathcal{M}}^{n,k,i}), \end{aligned}$$

with $l_{c,M}$ and $e_{H,M}$ defined by (2.2.21) and (3.3.3), respectively. The space–time functions $S_{p,h\tau}^{n,k,i}$, $p \in \mathcal{P}$, $C_{p,c,h\tau}^{n,k,i}$, $p \in \mathcal{P}$, $c \in \mathcal{C}_p$, $l_{c,h\tau}^{n,k,i}$, $c \in \mathcal{C}$, and $e_{H,h\tau}^{n,k,i}$ are then defined therefrom while being continuous and piecewise affine in time.

3.4.3 H_0^1 -conforming temperature reconstruction

The temperature approximation defined in Section 3.4.1 has sufficient regularity for the application of the piecewise gradient operator, but is nonconforming. In order to define our a posteriori estimators below, following [24, 6] in the model cases, we introduce space-continuous temperature reconstruction defined by $\mathfrak{T}_{h\tau}^{n,k,i} = \mathcal{I}_{\text{av}}(T_{h\tau}^{n,k,i})$, where \mathcal{I}_{av} denotes the vertex-averaging interpolator, cf., e.g., [2].

3.4.4 $\mathbf{H}(\text{div}; \Omega)$ -conforming energy flux reconstructions

Let a time step $1 \leq n \leq N$, a Newton linearization iteration $k \geq 1$, and an algebraic solver iteration $i \geq 1$ be fixed. We define the following energy flux reconstructions for use in the a posteriori estimates of Section 3.5:

- The *discretization flux* $\Theta_{\text{dis},H,h}^{n,k,i} \in \mathbf{RTN}(\mathcal{M}^n)$ such that, for all $M \in \mathcal{M}^n$ and all $\sigma \in \mathcal{E}_M^{i,n}$,

$$(\Theta_{\text{dis},H,h}^{n,k,i} \cdot \mathbf{n}_M, 1)_\sigma := F_{H,M,\sigma}(\mathcal{X}_{\mathcal{M}}^{n,k,i}) + G_{M,\sigma}(\mathcal{X}_{\mathcal{M}}^{n,k,i}), \quad (3.4.3a)$$

with $F_{H,M,\sigma}$, and $G_{M,\sigma}$ defined by (3.3.4), and (3.3.7), respectively, while $\Theta_{\text{dis},H,h}^{n,k,i} \cdot \mathbf{n}_\Omega = 0$ on $\partial\Omega$ coherently with (3.2.5).

- The *linearization error flux* $\Theta_{\text{lin},H,h}^{n,k,i} \in \mathbf{RTN}(\mathcal{M}^n)$ such that, for all $M \in \mathcal{M}^n$ and all $\sigma \in \mathcal{E}_M^{i,n}$,

$$(\Theta_{\text{lin},H,h}^{n,k,i} \cdot \mathbf{n}_M, 1)_\sigma = F_{H,M,\sigma}^{n,k,i} - F_{H,M,\sigma}(\mathcal{X}_{\mathcal{M}}^{n,k,i}) + G_{M,\sigma}^{n,k,i} - G_{M,\sigma}(\mathcal{X}_{\mathcal{M}}^{n,k,i}), \quad (3.4.3b)$$

with $F_{H,M,\sigma}^{n,k,i}$, and $G_{M,\sigma}^{n,k,i}$ defined by (3.3.12)–(3.3.14), while $\Theta_{\text{lin},H,h}^{n,k,i} \cdot \mathbf{n}_\Omega = 0$ on $\partial\Omega$.

- The *algebraic error flux* $\Theta_{\text{alg},H,h}^{n,k,i} \in \mathbf{RTN}(\mathcal{M}^n)$ such that, for all $M \in \mathcal{M}^n$ and for all $\sigma \in \mathcal{E}_M^{i,n}$,

$$(\Theta_{\text{alg},H,h}^{n,k,i} \cdot \mathbf{n}_M, 1)_{\partial M} := -R_{H,M}^{n,k,i}, \quad (3.4.3c)$$

with $R_{H,M}^{n,k,i}$ defined by (3.3.11), and setting $\Theta_{\text{alg},H,h}^{n,k,i} \cdot \mathbf{n}_\Omega = 0$ on $\partial\Omega$.

- The *total flux* $\Theta_{H,h}^{n,k,i} \in \mathbf{RTN}(\mathcal{M}^n)$ is then obtained from the above quantities letting

$$\Theta_{H,h}^{n,k,i} := \Theta_{\text{dis},H,h}^{n,k,i} + \Theta_{\text{lin},H,h}^{n,k,i} + \Theta_{\text{alg},H,h}^{n,k,i}. \quad (3.4.3d)$$

3.5 A posteriori error estimate

In this section we describe the weak solution for the thermal multiphase compositional model expressed by (2.2.1)–(2.2.7) and (3.2.1)–(3.2.6), we define an error measure composed of the dual norm of the residual augmented by a nonconformity evaluation term, and derive an a posteriori estimate allowing to distinguish the different components of the error.

3.5.1 Weak solution

We proceed in the same spirit as for the isothermal case considered in Chapter 2 (work corresponding to [25]). In the following, $(\cdot, \cdot)_D$ stands for the L^2 -scalar product on $D \subset \Omega$ and $\|\cdot\|_D$ for the associated norm; the same notation is used for both scalar and vector arguments, and the subscript is dropped whenever $D = \Omega$. We define

$$X := L^2((0, t_F); H^1(\Omega)), \quad Y := H^1((0, t_F); L^2(\Omega)). \quad (3.5.1)$$

Let $\varepsilon > 0$ be a (small) parameter which only needs to satisfy $\varepsilon \leq 1$. We equip the space X with the following norm:

$$\|\varphi\|_X := \left\{ \sum_{n=1}^N \int_{I_n} \sum_{M \in \mathcal{M}^n} \|\varphi\|_{X,M}^2 dt \right\}^{\frac{1}{2}}, \quad \|\varphi\|_{X,M}^2 := \varepsilon h_M^{-2} \|\varphi\|_M^2 + \|\nabla \varphi\|_M^2. \quad (3.5.2)$$

This choice is motivated by the homogeneous Neumann boundary condition (3.2.5). Taking $\varepsilon = 0$ is possible and classical when Dirichlet (pressure and temperature) boundary conditions are prescribed at least on a part of the boundary, cf. [30, 54, 14].

We suppose sufficient regularity to satisfy:

Assumption 3.5.1 (Regularity of the exact solution). *The weak solution of the multiphase compositional thermal problem can be characterized as follows:*

$$l_c \in Y \quad \forall c \in \mathcal{C}, \quad (3.5.3a)$$

$$e_H \in Y, \quad (3.5.3b)$$

$$P_p(P, \mathbf{S}) \in X \quad \forall p \in \mathcal{P}, \quad (3.5.3c)$$

$$T \in X, \quad (3.5.3d)$$

$$\Phi_c \in [L^2((0, t_F); L^2(\Omega))]^d \quad \forall c \in \mathcal{C}, \quad (3.5.3e)$$

$$\Phi_H \in [L^2((0, t_F); L^2(\Omega))]^d, \quad (3.5.3f)$$

$$\int_0^{t_F} \{(\partial_t l_c, \varphi)(t) - (\Phi_c, \nabla \varphi)(t)\} dt = \int_0^{t_F} (q_c, \varphi)(t) dt \quad \forall \varphi \in X, \forall c \in \mathcal{C}, \quad (3.5.3g)$$

$$\int_0^{t_F} \{(\partial_t e_H, \varphi)(t) - (\Phi_H, \nabla \varphi)(t)\} dt = \int_0^{t_F} (Q_H, \varphi)(t) dt \quad \forall \varphi \in X, \quad (3.5.3h)$$

the initial conditions (2.2.7) and (3.2.6) hold,

the algebraic closure equations (2.2.8)–(2.2.9) and the (in)equalities of fugacities (2.2.10) hold,

where P_p , l_c , e_H , Φ_c , and Φ_H are defined, respectively, by (2.2.1), (2.2.5), (3.2.2), (2.2.3), and (3.2.3).

We mention that existence and uniqueness of a weak solution has to our knowledge not been established for the general thermal multiphase compositional model.

Remark 3.5.2 (PDEs fluxes). *It follows from (3.5.3a)–(3.5.3b), the assumptions $q_c \in L^2((0, t_F); L^2(\Omega))$, $Q_H \in L^2((0, t_F); L^2(\Omega))$, (3.5.3e)–(3.5.3f), and (3.5.3g)–(3.5.3h) that actually*

$$\Phi_c, \Phi_H \in L^2((0, t_F); \mathbf{H}(\operatorname{div}; \Omega)), \quad (3.5.4a)$$

$$\nabla \cdot \Phi_c = q_c - \partial_t l_c \quad \forall c \in \mathcal{C}, \quad (3.5.4b)$$

$$\nabla \cdot \Phi_H = Q_H - \partial_t e_H, \quad (3.5.4c)$$

$$\Phi_c \cdot \mathbf{n}_\Omega = 0 \quad \text{on } \partial\Omega \times (0, t_F) \quad \forall c \in \mathcal{C}, \quad (3.5.4d)$$

$$\Phi_H \cdot \mathbf{n}_\Omega = 0 \quad \text{on } \partial\Omega \times (0, t_F). \quad (3.5.4e)$$

Thus, the component fluxes Φ_c and the energy flux Φ_H have continuous normal trace in a proper weak sense, the governing equations (2.2.2) and (3.2.1) are satisfied with a weak divergence, and the boundary conditions (2.2.6) and (3.2.5) hold in the normal trace sense. This in particular motivates the flux reconstructions (2.4.14d) and (3.4.3d).

3.5.2 Error measure

Consider the approximate solution as specified in Sections 2.4.2 and 3.4.1–3.4.2, defined on the whole space–time slab $\Omega \times (0, t_F)$ (we omit here the indices n, k, i for simplicity). The error measure from Section 2.3.3 in Chapter 2 for the isothermal multiphase compositional model consists here of the quantities $\mathcal{N}_c, c \in \mathcal{C}$, and $\mathcal{N}_p, p \in \mathcal{P}$, depending on $\mathbf{P}_{h\tau}, T_{h\tau}, \mathbf{S}_{h\tau}, (\mathbf{C}_{p,h\tau})_{p \in \mathcal{P}}$, defined as, respectively by,

$$\mathcal{N}_c := \sup_{\varphi \in X, \|\varphi\|_X=1} \int_0^{t_F} \{(\partial_t l_c - \partial_t l_{c,h\tau}, \varphi)(t) - (\Phi_c - \Phi_{c,h\tau}, \nabla \varphi)(t)\} dt, \quad (3.5.5)$$

with the exact component fluxes Φ_c defined by (2.2.3) and $\Phi_{c,h\tau}$ given by

$$\Phi_{c,h\tau} := \sum_{p \in \mathcal{P}_c} \Phi_{p,c,h\tau}, \quad \Phi_{p,c,h\tau} := \nu_p(P_{p,h\tau}, T_{h\tau}, \mathbf{S}_{h\tau}, \mathbf{C}_{p,h\tau}) C_{p,c,h\tau} \mathbf{v}_p(P_{p,h\tau}, T_{h\tau}, \mathbf{C}_{p,h\tau}), \quad (3.5.6)$$

and

$$\mathcal{N}_p := \inf_{\delta_p \in X} \left\{ \sum_{c \in \mathcal{C}_p} \int_0^{t_F} \|\Psi_{p,c}(P_{p,h\tau})(t) - \Psi_{p,c}(\delta_p)(t)\|^2 dt \right\}^{\frac{1}{2}}, \quad (3.5.7)$$

where, for a space–time function $\varphi \in L^2((0, t_F); H^1(\mathcal{M}))$ (piecewise regular in space with respect to the partitions \mathcal{M}^n), we have let

$$\Psi_{p,c}(\varphi) := \nu_p(P_{p,h\tau}, T_{h\tau}, \mathbf{S}_{h\tau}, \mathbf{C}_{p,h\tau}) C_{p,c,h\tau} \mathbb{K} \nabla \varphi. \quad (3.5.8)$$

As we consider a nonisothermal flow, we need to add some other contributions to define an error measure taking into account the energy equation. We define

$$\begin{aligned} \mathcal{N}_H &= \mathcal{N}_H(\mathbf{P}_{h\tau}, T_{h\tau}, \mathbf{S}_{h\tau}, (\mathbf{C}_{p,h\tau})_{p \in \mathcal{P}}) \\ &:= \sup_{\varphi \in X, \|\varphi\|_X=1} \int_0^{t_F} \{(\partial_t e_H - \partial_t e_{H,h\tau}, \varphi)(t) - (\Phi_H - \Phi_{H,h\tau}, \nabla \varphi)(t)\} dt, \end{aligned} \quad (3.5.9)$$

with Φ_H defined by (3.2.3) and $\Phi_{H,h\tau}$ given by

$$\Phi_{H,h\tau} := \mathbf{J}_{h\tau}(T_{h\tau}) + \sum_{p \in \mathcal{P}} \Phi_{p,H,h\tau}, \quad (3.5.10)$$

where

$$\Phi_{p,H,h\tau} := \nu_p(P_{p,h\tau}, T_{h\tau}, \mathbf{S}_{h\tau}, \mathbf{C}_{p,h\tau}) H_p(P_{p,h\tau}, T_{h\tau}, \mathbf{C}_{p,h\tau}) \mathbf{v}_p(P_{p,h\tau}, T_{h\tau}, \mathbf{C}_{p,h\tau}), \quad (3.5.11)$$

and for a space-time function $\varphi \in L^2((0, t_F); H^1(\mathcal{M}))$, we have let

$$\mathbf{J}_{h\tau}(\varphi) := -\lambda \nabla \varphi. \quad (3.5.12)$$

Note here that the definition (3.5.9) corresponds to the dual norm of the residual for the weak formulation (3.5.3h) related to the energy equation. We supplement this term by defining a nonconformity measure for the temperature,

$$\mathcal{N}_T = \mathcal{N}_T(\mathbf{P}_{h\tau}, T_{h\tau}, \mathbf{S}_{h\tau}, (\mathbf{C}_{p,h\tau})_{p \in \mathcal{P}}) := \inf_{\theta \in X} \left\{ \int_0^{t_F} \|\mathbf{J}_{h\tau}(T_{h\tau})(t) - \mathbf{J}_{h\tau}(\theta)(t)\|^2 dt \right\}^{\frac{1}{2}}. \quad (3.5.13)$$

Collecting all the previous contributions, we define the error measure for the multiphase thermal compositional model as

$$\mathcal{N}_e = \mathcal{N}_e(\mathbf{P}_{h\tau}, T_{h\tau}, \mathbf{S}_{h\tau}, (\mathbf{C}_{p,h\tau})_{p \in \mathcal{P}}) := \left\{ \sum_{c \in \mathcal{C}} \mathcal{N}_c^2 + \mathcal{N}_H^2 \right\}^{\frac{1}{2}} + \left\{ \sum_{p \in \mathcal{P}} \mathcal{N}_p^2 + \mathcal{N}_T^2 \right\}^{\frac{1}{2}}. \quad (3.5.14)$$

A localized version of this error measure can be obtained as follows: For each approximation as defined in Sections 2.4.2.1 and 3.4.1–3.4.2, we let

$$\mathcal{N}_e^{n,k,i} := \left\{ \sum_{c \in \mathcal{C}} \mathcal{N}_c^{n,k,i^2} + \mathcal{N}_H^{n,k,i^2} \right\}^{\frac{1}{2}} + \left\{ \sum_{p \in \mathcal{P}} \mathcal{N}_p^{n,k,i^2} + \mathcal{N}_T^{n,k,i^2} \right\}^{\frac{1}{2}}, \quad (3.5.15)$$

with $\mathcal{N}_c^{n,k,i}$, $c \in \mathcal{C}$, $\mathcal{N}_p^{n,k,i}$, $p \in \mathcal{P}$, $\mathcal{N}_H^{n,k,i}$, and $\mathcal{N}_T^{n,k,i}$ localized versions of respectively (3.5.5), (3.5.7), (3.5.9), and (3.5.13), where the time integration is performed on I_n instead of $(0, t_F)$.

The error measure for the exact solution satisfying Assumption 3.5.1 is zero. Conversely, shall the approximate solution satisfy exactly the initial condition and the algebraic constraints and relations and have the error measure zero, then it satisfies Assumption 3.5.1.

3.5.3 An a posteriori error estimate distinguishing the space, time, linearization, and algebraic errors

In this section we propose an a posteriori estimate for the time-localized error measure (3.5.15) that we subsequently adapt to distinguish the different components of the error.

3.5.3.1 A basic time-localized a posteriori error estimate

For $1 \leq n \leq N$, we define the piecewise constant space functions $q_{c,h}^n$, $c \in \mathcal{C}$, and $Q_{H,h}^n$, such that $q_{c,h}^n|_M = \int_{I_n} \int_M q_c / (|M|\tau_n)$, $c \in \mathcal{C}$, and $Q_{H,h}^n|_M = \int_{I_n} \int_M Q_H / (|M|\tau_n)$, respectively. For further use we also define the piecewise constant space–time functions $q_{c,h\tau}$, $Q_{H,h\tau}$, such that $q_{c,h\tau}|_{I_n} = q_{c,h}^n$, $Q_{H,h\tau}|_{I_n} = Q_{H,h}^n$, respectively, for all $1 \leq n \leq N$.

Let $1 \leq n \leq N$, a Newton linearization iteration $k \geq 1$, and an algebraic solver iteration $i \geq 1$ be fixed. It follows from (2.4.8), (3.3.11), the definitions (2.4.14d) and (3.4.3d) of the flux reconstructions $\Theta_{c,h}^{n,k,i}$, $c \in \mathcal{C}$, and $\Theta_{H,h}^{n,k,i}$, and Green's theorem that there holds,

$$\left(q_{c,h}^n - \frac{l_{c,M}(\mathcal{X}_{\mathcal{M}}^{n,k-1}) + \mathcal{L}_{c,M}^{n,k,i} - l_{c,M}^{n-1}}{\tau^n} - \nabla \cdot \Theta_{c,h}^{n,k,i}, 1 \right)_M = 0 \quad \forall M \in \mathcal{M}^n, \quad (3.5.16a)$$

$$\left(Q_{H,h}^n - \frac{e_{H,M}(\mathcal{X}_{\mathcal{M}}^{n,k-1}) + \mathfrak{E}_{c,M}^{n,k,i} - e_{H,M}^{n-1}}{\tau^n} - \nabla \cdot \Theta_{H,h}^{n,k,i}, 1 \right)_M = 0 \quad \forall M \in \mathcal{M}^n. \quad (3.5.16b)$$

Let $C_M := \min\{C_{P,M}, \varepsilon^{-\frac{1}{2}}\}h_M$. Then as in the previous chapter we define the following estimators:

$$\eta_{R,M,c}^{n,k,i} := C_M \left\| q_{c,h}^n - (\tau^n)^{-1} (l_{c,M}(\mathcal{X}_{\mathcal{M}}^{n,k-1}) + \mathcal{L}_{c,M}^{n,k,i} - l_{c,M}^{n-1}) - \nabla \cdot \Theta_{c,h}^{n,k,i} \right\|_M, \quad \forall c \in \mathcal{C}, \quad (3.5.17a)$$

$$\eta_{R,M,H}^{n,k,i} := C_M \left\| Q_{c,h}^n - (\tau^n)^{-1} (e_{H,M}(\mathcal{X}_{\mathcal{M}}^{n,k-1}) + \mathfrak{E}_{c,M}^{n,k,i} - e_{H,M}^{n-1}) - \nabla \cdot \Theta_{H,h}^{n,k,i} \right\|_M, \quad (3.5.17b)$$

$$\eta_{F,M,c}^{n,k,i}(t) := \left\| \Theta_{c,h}^{n,k,i} - \Phi_{c,h\tau}^{n,k,i}(t) \right\|_M \quad \forall t \in I_n, \forall c \in \mathcal{C}, \quad (3.5.17c)$$

$$\eta_{F,M,H}^{n,k,i}(t) := \left\| \Theta_{H,h}^{n,k,i} - \Phi_{H,h\tau}^{n,k,i}(t) \right\|_M, \quad \forall t \in I_n, \quad (3.5.17d)$$

$$\eta_{NC,M,p,c}^{n,k,i}(t) := \left\| \Psi_{p,c}(P_{p,h\tau}^{n,k,i})(t) - \Psi_{p,c}(\mathfrak{P}_{p,h\tau}^{n,k,i})(t) \right\|_M \quad \forall t \in I_n, \forall c \in \mathcal{C}, \forall p \in \mathcal{P}_c, \quad (3.5.17e)$$

$$\eta_{NC,M,T}^{n,k,i}(t) := \left\| \mathbf{J}_{h\tau}^{n,k,i}(T_{h\tau}^{n,k,i})(t) - \mathbf{J}_{h\tau}^{n,k,i}(\mathfrak{T}_{h\tau}^{n,k,i})(t) \right\|_M, \quad \forall t \in I_n, \quad (3.5.17f)$$

$$\eta_{NA,M,c}^{n,k,i} := \varepsilon^{-\frac{1}{2}} h_M (\tau^n)^{-1} \left\| l_{c,M}(\mathcal{X}_{\mathcal{M}}^{n,k,i}) - l_{c,M}(\mathcal{X}_{\mathcal{M}}^{n,k-1}) - \mathcal{L}_{c,M}^{n,k,i} \right\|_M, \quad \forall c \in \mathcal{C}, \quad (3.5.17g)$$

$$\eta_{NA,M,H}^{n,k,i} := \varepsilon^{-\frac{1}{2}} h_M (\tau^n)^{-1} \left\| e_{H,M}(\mathcal{X}_{\mathcal{M}}^{n,k,i}) - e_{H,M}(\mathcal{X}_{\mathcal{M}}^{n,k-1}) - \mathfrak{E}_{c,M}^{n,k,i} \right\|_M, \quad (3.5.17h)$$

where the functions $\Psi_{p,c}$, $p \in \mathcal{P}$, $c \in \mathcal{C}_p$, are defined by (3.5.8), and $\Phi_{c,h\tau}^{n,k,i}$ and $\Phi_{H,h\tau}^{n,k,i}$ respectively as in (3.5.6) and (3.5.10).

The proof of the following result is a straightforward generalization of that of Corollary 2.4.4 in the previous chapter / reference [25, Theorem 3.3] and is omitted for the sake of brevity:

Corollary 3.5.3 (Time-localized a posteriori error estimate). *Consider a time step $1 \leq n \leq N$, a Newton linearization iteration $k \geq 1$, and an algebraic solver iteration $i \geq 1$. Under Assumption 3.5.1 there holds, with the estimators given by (3.5.17),*

$$\mathcal{N}_c^{n,k,i} \leq \left\{ \int_{I_n} \sum_{M \in \mathcal{M}^n} (\eta_{R,M,c}^{n,k,i} + \eta_{F,M,c}^{n,k,i}(t) + \eta_{NA,M,c}^{n,k,i})^2 dt \right\}^{\frac{1}{2}} \quad c \in \mathcal{C}, \quad (3.5.18a)$$

$$\mathcal{N}_p^{n,k,i} \leq \left\{ \sum_{c \in \mathcal{C}_p} \int_{I_n} \sum_{M \in \mathcal{M}^n} (\eta_{NC,M,p,c}^{n,k,i}(t))^2 dt \right\}^{\frac{1}{2}} \quad p \in \mathcal{P}, \quad (3.5.18b)$$

$$\mathcal{N}_H^{n,k,i} \leq \left\{ \int_{I_n} \sum_{M \in \mathcal{M}^n} (\eta_{R,M,H}^{n,k,i} + \eta_{F,M,H}^{n,k,i}(t) + \eta_{NA,M,H}^{n,k,i})^2 dt \right\}^{\frac{1}{2}}, \quad (3.5.18c)$$

$$\mathcal{N}_T^{n,k,i} \leq \left\{ \int_{I_n} \sum_{M \in \mathcal{M}^n} (\eta_{NC,M,T}^{n,k,i}(t))^2 dt \right\}^{\frac{1}{2}}. \quad (3.5.18d)$$

3.5.3.2 Distinguishing the different error components

For all $1 \leq n \leq N$, $k \geq 1$, $i \geq 1$, and $M \in \mathcal{M}^n$, we define the *spatial estimators* evaluating the error related to the spatial mesh choice,

$$\eta_{sp,M,c}^{n,k,i}(t) := \eta_{R,M,c}^{n,k,i} + \left\| \Theta_{dis,c,h}^{n,k,i} - \Phi_{c,h\tau}^{n,k,i}(t^n) \right\|_M + \left\{ \sum_{p \in \mathcal{P}_c} (\eta_{NC,M,p,c}^{n,k,i}(t))^2 \right\}^{\frac{1}{2}} \quad t \in I_n, \quad (3.5.19a)$$

$$\eta_{sp,M,H}^{n,k,i}(t) := \eta_{R,M,H}^{n,k,i} + \left\| \Theta_{dis,H,h}^{n,k,i} - \Phi_{H,h\tau}^{n,k,i}(t^n) \right\|_M + \eta_{NC,M,T}^{n,k,i}(t) \quad t \in I_n, \quad (3.5.19b)$$

the *temporal estimators* evaluating the error related to the size of the time step,

$$\eta_{tm,M,c}^{n,k,i}(t) := \left\| \Phi_{c,h\tau}^{n,k,i}(t^n) - \Phi_{c,h\tau}^{n,k,i}(t) \right\|_M \quad t \in I_n, \quad (3.5.19c)$$

$$\eta_{tm,M,H}^{n,k,i}(t) := \left\| \Phi_{H,h\tau}^{n,k,i}(t^n) - \Phi_{H,h\tau}^{n,k,i}(t) \right\|_M \quad t \in I_n, \quad (3.5.19d)$$

the *linearization estimators* measuring the error in the linearization of the nonlinear system (2.2.20), (3.3.2),

$$\eta_{lin,M,c}^{n,k,i} := \left\| \Theta_{lin,c,h}^{n,k,i} \right\|_M + \eta_{NA,M,c}^{n,k,i} \quad (3.5.19e)$$

$$\eta_{lin,M,H}^{n,k,i} := \left\| \Theta_{lin,H,h}^{n,k,i} \right\|_M + \eta_{NA,M,H}^{n,k,i} \quad (3.5.19f)$$

and the *algebraic estimators* that quantify the error in the algebraic iterative resolution of the linear system (2.4.2), (3.3.9),

$$\eta_{\text{alg},M,c}^{n,k,i} := \left\| \Theta_{\text{alg},c,h}^{n,k,i} \right\|_M, \quad (3.5.19g)$$

$$\eta_{\text{alg},M,H}^{n,k,i} := \left\| \Theta_{\text{alg},H,h}^{n,k,i} \right\|_M. \quad (3.5.19h)$$

Global versions of these estimators are given by

$$\eta_{\text{sp},c}^{n,k,i} := \left\{ 4 \int_{I_n} \sum_{M \in \mathcal{M}^n} (\eta_{\text{sp},M,c}^{n,k,i}(t))^2 dt \right\}^{\frac{1}{2}}, \quad (3.5.20a)$$

$$\eta_{\text{tm},c}^{n,k,i} := \left\{ 2 \int_{I_n} \sum_{M \in \mathcal{M}^n} (\eta_{\text{tm},M,c}^{n,k,i}(t))^2 dt \right\}^{\frac{1}{2}}, \quad (3.5.20b)$$

$$\eta_{\text{lin},c}^{n,k,i} := \left\{ 2\tau^n \sum_{M \in \mathcal{M}^n} (\eta_{\text{lin},M,c}^{n,k,i})^2 \right\}^{\frac{1}{2}}, \quad (3.5.20c)$$

$$\eta_{\text{alg},c}^{n,k,i} := \left\{ 2\tau^n \sum_{M \in \mathcal{M}^n} (\eta_{\text{alg},M,c}^{n,k,i})^2 \right\}^{\frac{1}{2}} \quad (3.5.20d)$$

and

$$\eta_{\text{sp},H}^{n,k,i} := \left\{ 4 \int_{I_n} \sum_{M \in \mathcal{M}^n} (\eta_{\text{sp},M,H}^{n,k,i}(t))^2 dt \right\}^{\frac{1}{2}}, \quad (3.5.21a)$$

$$\eta_{\text{tm},H}^{n,k,i} := \left\{ 2 \int_{I_n} \sum_{M \in \mathcal{M}^n} (\eta_{\text{tm},M,H}^{n,k,i}(t))^2 dt \right\}^{\frac{1}{2}}, \quad (3.5.21b)$$

$$\eta_{\text{lin},H}^{n,k,i} := \left\{ 2\tau^n \sum_{M \in \mathcal{M}^n} (\eta_{\text{lin},M,H}^{n,k,i})^2 \right\}^{\frac{1}{2}}, \quad (3.5.21c)$$

$$\eta_{\text{alg},H}^{n,k,i} := \left\{ 2\tau^n \sum_{M \in \mathcal{M}^n} (\eta_{\text{alg},M,H}^{n,k,i})^2 \right\}^{\frac{1}{2}}. \quad (3.5.21d)$$

Using the triangle and Cauchy–Schwarz inequalities and Corollary 3.5.3, we can estimate the time-localized norm $\mathcal{N}_e^{n,k,i}$ of (3.5.15) for the complete multiphase compositional thermal model of the present chapter as follows:

Corollary 3.5.4 (Distinguishing the space, time, linearization, and algebraic errors). *Under the assumptions of Corollary 3.5.3, there holds, with the estimators given by (3.5.20)–(3.5.21),*

$$\begin{aligned} \mathcal{N}_e^{n,k,i} \leq & \left\{ \sum_{c \in \mathcal{C}} (\eta_{\text{sp},c}^{n,k,i} + \eta_{\text{tm},c}^{n,k,i} + \eta_{\text{lin},c}^{n,k,i} + \eta_{\text{alg},c}^{n,k,i})^2 \right. \\ & \left. + (\eta_{\text{sp},H}^{n,k,i} + \eta_{\text{tm},H}^{n,k,i} + \eta_{\text{lin},H}^{n,k,i} + \eta_{\text{alg},H}^{n,k,i})^2 \right\}^{\frac{1}{2}}. \end{aligned} \quad (3.5.22)$$

3.5.4 Balancing and stopping criteria

Criteria can be proposed in the same spirit as for the isothermal case considered in Section 2.4.6 of the previous chapter / reference [25] for stopping the iterative algebraic solver and the iterative linearization solver when the corresponding error components do not affect significantly the overall error.

Let two user-given parameters $\Gamma_{\text{lin}}, \Gamma_{\text{alg}} \in (0, 1)$ be given. Following [9, 7, 15, 39, 29, 31], we propose to stop the iterative algebraic solver whenever

$$\eta_{\text{alg},c}^{n,k,i} \leq \Gamma_{\text{alg}} \left(\eta_{\text{sp},c}^{n,k,i} + \eta_{\text{tm},c}^{n,k,i} + \eta_{\text{lin},c}^{n,k,i} \right), \quad c \in \mathcal{C}, \quad (3.5.23a)$$

$$\eta_{\text{alg},H}^{n,k,i} \leq \Gamma_{\text{alg}} \left(\eta_{\text{sp},H}^{n,k,i} + \eta_{\text{tm},H}^{n,k,i} + \eta_{\text{lin},H}^{n,k,i} \right). \quad (3.5.23b)$$

Similarly, the iterative linearization solver is stopped whenever

$$\eta_{\text{lin},c}^{n,k,i} \leq \Gamma_{\text{lin}} \left(\eta_{\text{sp},c}^{n,k,i} + \eta_{\text{tm},c}^{n,k,i} \right), \quad c \in \mathcal{C}, \quad (3.5.23c)$$

$$\eta_{\text{lin},H}^{n,k,i} \leq \Gamma_{\text{lin}} \left(\eta_{\text{sp},H}^{n,k,i} + \eta_{\text{tm},H}^{n,k,i} \right). \quad (3.5.23d)$$

Adaptive spatial-temporal mesh refinement can also be proposed in the spirit of [52, 30, 27] and of the adaptive algorithm of Section 2.4.6 of the previous chapter. Let $\Gamma_{\text{tm}} > \gamma_{\text{tm}} > 0$ be again two user-given parameters, typically close to 1. We propose to balance the space-time error by selecting the time step τ^n and adjusting the spatial meshes \mathcal{M}^n so that

$$\gamma_{\text{tm}} \eta_{\text{sp},c}^{n,k,i} \leq \eta_{\text{tm},c}^{n,k,i} \leq \Gamma_{\text{tm}} \eta_{\text{sp},c}^{n,k,i}, \quad c \in \mathcal{C}, \quad (3.5.23e)$$

$$\gamma_{\text{tm}} \eta_{\text{sp},H}^{n,k,i} \leq \eta_{\text{tm},H}^{n,k,i} \leq \Gamma_{\text{tm}} \eta_{\text{sp},H}^{n,k,i}. \quad (3.5.23f)$$

Remark 3.5.5. Let $1 \leq n \leq N$, $k \geq 1$, $i \geq 1$. The stopping and balancing criteria (3.5.23a)–(3.5.23f) imply

$$\eta_{\text{sp},c}^{n,k,i} + \eta_{\text{tm},c}^{n,k,i} + \eta_{\text{lin},c}^{n,k,i} + \eta_{\text{alg},c}^{n,k,i} \leq C \eta_{\text{sp},c}^{n,k,i}, \quad c \in \mathcal{C}, \quad (3.5.24)$$

$$\eta_{\text{sp},H}^{n,k,i} + \eta_{\text{tm},H}^{n,k,i} + \eta_{\text{lin},H}^{n,k,i} + \eta_{\text{alg},H}^{n,k,i} \leq C \eta_{\text{sp},H}^{n,k,i}, \quad (3.5.25)$$

with C a generic constant only dependent on Γ_{alg} , Γ_{lin} , and Γ_{tm} .

3.A Application to the thermal dead oil model

We consider here the application of the above analysis to a specific example involving three phases in a nonisothermal flow condition: the *oil phase*, the *water phase* and the *steam phase*, represented by lowercase letters w, o, s as indices, respectively, and two components: water and oil, with the uppercase letters W, O as indices. This configuration corresponds to a model called the *dead oil* model which will be also discussed in the next chapter from an industrial view-point and illustrated by detailed numerical results.

3.A.1 Dead oil model

The system of governing equations of the thermal dead oil model consists of the *mass conservation* equation of the water component

$$\partial_t(\phi(\zeta_w S_w + \zeta_s S_s)) + \nabla \cdot (\nu_w \mathbf{v}_w + \nu_s \mathbf{v}_s) = q_w, \quad (3.A.1a)$$

of the oil component

$$\partial_t(\phi \zeta_o S_o) + \nabla \cdot (\nu_o \mathbf{v}_o) = q_o, \quad (3.A.1b)$$

and of the *energy conservation* equation

$$\partial_t e_H + \nabla \cdot (\mathbf{u} - \lambda \nabla T) = Q_H, \quad (3.A.1c)$$

$$(3.A.1d)$$

with

$$e_H := \phi e + (1 - \phi) \zeta_r e_r; \quad e := \sum_{p \in \{w, o, s\}} S_p \zeta_p e_p, \quad \mathbf{u} := \sum_{p \in \{w, o, s\}} \zeta_p H_p \mathbf{v}_p.$$

The system is complemented by the *volume conservation* equation

$$S_w + S_o + S_s = 1, \quad (3.A.1e)$$

by the *conservation of the quantity of matter* equalities

$$C_{w,W} = C_{o,O} = C_{s,W} = 1, \quad (3.A.1f)$$

and by the *thermodynamic liquid–steam equilibrium* relation

$$S_s S_w (T - T_{\text{sat}}(P)) = 0, \quad (3.A.1g)$$

with T_{sat} the temperature of saturation at which the steam is in equilibrium with its liquid (water) phase. *No-flow boundary* conditions are prescribed for the component fluxes,

$$\begin{aligned} (\nu_w \mathbf{v}_w + \nu_s \mathbf{v}_s) \cdot \mathbf{n}_\Omega &= 0, & \text{on } \partial\Omega \times (0, t_F), \\ (\nu_o \mathbf{v}_o) \cdot \mathbf{n}_\Omega &= 0, & \text{on } \partial\Omega \times (0, t_F), \end{aligned}$$

and also a condition of no-flow for the total energy flux,

$$(-\lambda \nabla T + \mathbf{u}) \cdot \mathbf{n}_\Omega = 0, \quad \text{on } \partial\Omega \times (0, t_F).$$

Finally the initial conditions are given by

$$\begin{aligned} e_H(\cdot, 0) &= e_H^0, \\ \phi(\zeta_w S_w + \zeta_s S_s) &= l_W^0, \\ \phi \zeta_o S_o &= l_O^0. \end{aligned}$$

Remark 3.A.1 (Liquid-Steam equilibrium). *With the equation (3.A.1g) we have three possibilities:*

- *If the temperature is below the temperature of saturation $(T - T_{\text{sat}}(P)) < 0$, then we obtain the water, i.e. $(S_w \geq 0)$, and the steam saturation is zero;*
- *When the temperature equals the temperature of saturation $T = T_{\text{sat}}(P)$, then we have equilibrium between the steam and water phases with typically $S_w > 0, S_s > 0$;*
- *If the temperature exceeds the temperature of saturation $(T - T_{\text{sat}}(P)) > 0$, then there is evaporation and we obtain the steam, i.e. $(S_s \geq 0)$, and the water saturation is zero.*

3.A.2 A posteriori error estimate for the thermal dead oil model

In this section we give the precise form of the a posteriori error estimate for the thermal dead oil model.

3.A.2.1 Local-in-time residual error norm

Let $1 \leq n \leq N$, a Newton linearization iteration $k \geq 1$, and an algebraic solver iteration $i \geq 1$ be fixed. Using the definition of the local-in-time norm of the thermal multiphase compositional model given in Section 3.5.2, equation (3.5.15), the local-in-time residual error norm for the thermal dead oil reads

$$\mathcal{N}_e^{n,k,i} := \left\{ \mathcal{N}_W^{n,k,i^2} + \mathcal{N}_O^{n,k,i^2} + \mathcal{N}_H^{n,k,i^2} \right\}^{\frac{1}{2}} + \left\{ \sum_{p \in \{\text{w,o,s}\}} \mathcal{N}_p^{n,k,i^2} + \mathcal{N}_T^{n,k,i^2} \right\}^{\frac{1}{2}}, \quad (3.A.2)$$

with two residual error norms: one for the water component conservation equation,

$$\mathcal{N}_W^{n,k,i} := \sup_{\varphi \in X, \|\varphi\|_X=1} \int_{t^{n-1}}^{t^n} \left\{ \left([\partial_t(\phi(\zeta_w S_w + \zeta_s S_s)) - \partial_t^n(\phi(\widehat{\zeta}_w S_{w,h\tau}^{n,k,i} + \widehat{\zeta}_s S_{s,h\tau}^{n,k,i}))], \varphi \right)(t) - \left([(\nu_w \mathbf{v}_w + \nu_s \mathbf{v}_s) - (\widehat{\nu}_w \mathbf{v}_{w,h\tau}^{n,k,i} + \widehat{\nu}_s \mathbf{v}_{s,h\tau}^{n,k,i})], \nabla \varphi \right)(t) \right\} dt,$$

and the other for the oil component conservation equation,

$$\mathcal{N}_O^{n,k,i} := \sup_{\varphi \in X, \|\varphi\|_X=1} \int_{t^{n-1}}^{t^n} \left\{ \left([\partial_t(\zeta_o S_o) - \partial_t^n(\widehat{\zeta}_o S_{o,h\tau}^{n,k,i})], \varphi \right)(t) - \left([\nu_o \mathbf{v}_o - \widehat{\nu}_o \mathbf{v}_{o,h\tau}^{n,k,i}], \nabla \varphi \right)(t) \right\} dt,$$

with

$$\mathbf{v}_{p,h\tau}^{n,k,i} := \mathbf{v}_p(P_{p,h\tau}^{n,k,i}, T_{h\tau}^{n,k,i}), \quad \forall p \in \{\text{w, o, s}\}, \quad (3.A.3)$$

and

$$\widehat{\zeta}_p := \zeta_p(P_{p,h\tau}^{n,k,i}, T_{h\tau}^{n,k,i}), \quad \forall p \in \{\text{w, o, s}\}; \quad \widehat{\nu}_p := \nu_p(P_{p,h\tau}^{n,k,i}, T_{h\tau}^{n,k,i}, S_{p,h\tau}^{n,k,i}), \quad \forall p \in \{\text{w, o, s}\}.$$

The residual error norm for the energy conservation equation is

$$\mathcal{N}_H^{n,k,i} := \sup_{\varphi \in X, \|\varphi\|_X=1} \int_{t^{n-1}}^{t^n} \left\{ \left([\partial_t e_H - \partial_t^n e_{H,h\tau}^{n,k,i}], \varphi \right) - \left([(\mathbf{u} - \lambda \nabla T) - (\mathbf{u}_{h\tau}^{n,k,i} - \lambda \nabla T_{h\tau}^{n,k,i})], \nabla \varphi \right) \right\} dt,$$

with

$$\mathbf{u}_{h\tau}^{n,k,i} := \mathbf{u}(P_{h\tau}^{n,k,i}, T_{h\tau}^{n,k,i}) = \sum_{p \in \{w, o, s\}} \widehat{\zeta}_p \widehat{H}_p \mathbf{v}_{p,h\tau}^{n,k,i}; \quad \widehat{H}_p := H_p(P_{p,h\tau}^{n,k,i}, T_{h\tau}^{n,k,i}), \quad (3.A.4)$$

and

$$e_{H,h\tau}^{n,k,i} := \phi e_{\alpha,h\tau}^{n,k,i} + (1 - \phi) \zeta_r e_r, \quad e_{\alpha,h\tau}^{n,k,i} := \sum_{p \in \{w, o, s\}} S_{p,h\tau}^{n,k,i} \widehat{\zeta}_p e_p(P_{p,h\tau}^{n,k,i}, T_{h\tau}^{n,k,i}).$$

The nonconformity error norm for the pressures simplifies to

$$\mathcal{N}_p^{n,k,i} := \inf_{\delta_p \in X} \left\{ \int_{t^{n-1}}^{t^n} \left\| \widehat{\nu}_p \mathbb{K} (\nabla P_{p,h\tau}^{n,k,i}(t) - \nabla \delta_p(t)) \right\|^2 dt \right\}^{\frac{1}{2}}, \quad p \in \{w, o, s\},$$

and finally the nonconformity error norm for the temperature becomes

$$\mathcal{N}_T^{n,k,i} := \inf_{\theta \in X} \left\{ \int_{t^{n-1}}^{t^n} \left\| \lambda (\nabla T_{h\tau}^{n,k,i}(t) - \nabla \theta(t)) \right\|^2 dt \right\}^{\frac{1}{2}}.$$

3.A.2.2 Space-time local error indicators and a posteriori estimate for the thermal dead oil model

Let $1 \leq n \leq N$, a Newton linearization iteration $k \geq 1$, and an algebraic solver iteration $i \geq 1$ be fixed. Following Section 3.5.3, we consider the *residual estimators*

$$\eta_{R,M,W}^{n,k,i}, \eta_{R,M,O}^{n,k,i}, \eta_{R,M,H}^{n,k,i}, \quad (3.A.5a)$$

as defined in (3.5.17a)–(3.5.17b), the *nonlinear accumulation estimators*:

$$\eta_{NA,M,W}^{n,k,i}, \eta_{NA,M,O}^{n,k,i}, \eta_{NA,M,H}^{n,k,i}, \quad (3.A.5b)$$

as defined in (3.5.17g)–(3.5.17h), the *flux estimators* following (3.5.17c)–(3.5.17d):

$$\eta_{F,M,W}^{n,k,i}(t) := \left\| \Theta_{W,h}^{n,k,i} - (\widehat{\nu}_w \mathbf{v}_{w,h\tau}^{n,k,i} + \widehat{\nu}_s \mathbf{v}_{s,h\tau}^{n,k,i})(t) \right\|_M, \quad \forall t \in I_n, \quad (3.A.5c)$$

$$\eta_{F,M,O}^{n,k,i}(t) := \left\| \Theta_{O,h}^{n,k,i} - (\widehat{\nu}_o \mathbf{v}_{o,h\tau}^{n,k,i})(t) \right\|_M, \quad \forall t \in I_n, \quad (3.A.5d)$$

$$\eta_{F,M,H}^{n,k,i}(t) := \left\| \Theta_{H,h}^{n,k,i} - (\mathbf{u}_{h\tau}^{n,k,i} - \lambda \nabla T_{h\tau}^{n,k,i})(t) \right\|_M, \quad \forall t \in I_n, \quad (3.A.5e)$$

and the *nonconformity estimators* following (3.5.17e)–(3.5.17f):

$$\eta_{\text{NC},M,p,W}^{n,k,i}(t) := \left\| \widehat{\nu}_p C_{p,W,h\tau}^{n,k,i} \mathbb{K} \nabla \left(P_{p,h\tau}^{n,k,i}(t) - \nabla \mathfrak{P}_{p,h\tau}^{n,k,i}(t) \right) \right\|_M, \quad \forall t \in I_n, \forall p \in \{w, s\}, \quad (3.A.5f)$$

$$\eta_{\text{NC},M,o,O}^{n,k,i}(t) := \left\| \widehat{\nu}_o C_{o,O,h\tau}^{n,k,i} \mathbb{K} \left(\nabla P_{o,h\tau}^{n,k,i}(t) - \nabla \mathfrak{P}_{o,h\tau}^{n,k,i}(t) \right) \right\|_M, \quad \forall t \in I_n, \quad (3.A.5g)$$

$$\eta_{\text{NC},M,T}^{n,k,i}(t) := \left\| \lambda \nabla T_{h\tau}^{n,k,i}(t) - \lambda \nabla \mathfrak{T}_{h\tau}^{n,k,i}(t) \right\|_M, \quad \forall t \in I_n, \quad (3.A.5h)$$

where, for all $p \in \{w, o, s\}$; $P_{p,h\tau}^{n,k,i}$, $\mathfrak{P}_{p,h\tau}^{n,k,i}$, $T_{h\tau}^{n,k,i}$, and $\mathfrak{T}_{h\tau}^{n,k,i}$, are specified in Sections 2.4.2.1, 2.4.3, 3.4.1 and 3.4.3. The reconstructed fluxes $\Theta_{c,h}^{n,k,i}$, $c \in \{W, O\}$, and $\Theta_{H,h}^{n,k,i}$ are given following Sections 2.4.4 and 3.4.4. With these estimators, we can bound the local-in-time residual error norm defined in (3.A.2) for the thermal dead oil model following Corollary 3.5.3:

Corollary 3.A.2 (Local-in-time a posteriori error estimate). *Consider a time step $1 \leq n \leq N$, a Newton linearization iteration $k \geq 1$, and an algebraic solver iteration $i \geq 1$. Consider the residual error norm defined by (3.A.2) and the approximate solutions and reconstructions described in Sections 2.4.2–2.4.4 and 3.4. With the estimators given by (3.A.5), there holds*

$$\mathcal{N}_W^{n,k,i} \leq \left\{ \int_{I_n} \sum_{M \in \mathcal{M}^n} \left(\eta_{R,M,W}^{n,k,i} + \eta_{F,M,W}^{n,k,i}(t) + \eta_{NA,M,W}^{n,k,i}(t) \right)^2 dt \right\}^{\frac{1}{2}}, \quad (3.A.6a)$$

$$\mathcal{N}_O^{n,k,i} \leq \left\{ \int_{I_n} \sum_{M \in \mathcal{M}^n} \left(\eta_{R,M,O}^{n,k,i} + \eta_{F,M,O}^{n,k,i}(t) + \eta_{NA,M,O}^{n,k,i}(t) \right)^2 dt \right\}^{\frac{1}{2}}, \quad (3.A.6b)$$

$$\mathcal{N}_H^{n,k,i} \leq \left\{ \int_{I_n} \sum_{M \in \mathcal{M}^n} \left(\eta_{R,M,H}^{n,k,i} + \eta_{F,M,H}^{n,k,i}(t) + \eta_{NA,M,H}^{n,k,i}(t) \right)^2 dt \right\}^{\frac{1}{2}}, \quad (3.A.6c)$$

$$\mathcal{N}_T^{n,k,i} \leq \left\{ \int_{I_n} \sum_{M \in \mathcal{M}^n} \left(\eta_{\text{NC},M,T}^{n,k,i}(t) \right)^2 dt \right\}^{\frac{1}{2}}, \quad (3.A.6d)$$

and, for all $p \in \{w, o, s\}$,

$$\mathcal{N}_p^{n,k,i} \leq \left\{ \int_{I_n} \sum_{M \in \mathcal{M}^n} \left(\eta_{\text{NC},M,p,c_p}^{n,k,i}(t) \right)^2 dt \right\}^{\frac{1}{2}}, \quad (3.A.6e)$$

with $c_p = W$ for $p \in \{w, s\}$ and $c_p = O$ for $p = o$.

Now we can distinguish the different error components.

3.A.2.3 Distinguishing the different error components

Let the reconstructed fluxes $\Theta_{\text{dis},c,h}^{n,k,i}$, $\Theta_{\text{lin},c,h}^{n,k,i}$, $\Theta_{\text{alg},c,h}^{n,k,i}$, $c \in \{W, O\}$, and $\Theta_{\text{dis},H,h}^{n,k,i}$, $\Theta_{\text{lin},H,h}^{n,k,i}$, and $\Theta_{\text{alg},H,h}^{n,k,i}$ be defined as in Sections 2.4.4 and 3.4.4, respectively. Based on the estimate

given by (3.A.6) we define, for all $M \in \mathcal{M}^n$, the *water component spatial estimators*

$$\begin{aligned} \eta_{\text{sp},M,W}^{n,k,i}(t) &:= \eta_{\text{R},M,W}^{n,k,i} + \left\| \Theta_{\text{dis},W,h}^{n,k,i} - (\widehat{\nu}_w \mathbf{v}_{w,h}^{n,k,i} + \widehat{\nu}_s \mathbf{v}_{s,h}^{n,k,i}) \right\|_M \\ &\quad + \left\{ (\eta_{\text{NC},M,w,W}^{n,k,i}(t))^2 + (\eta_{\text{NC},M,s,W}^{n,k,i}(t))^2 \right\}^{\frac{1}{2}} \quad t \in I_n, \end{aligned} \quad (3.A.7a)$$

the *oil component spatial estimators*

$$\eta_{\text{sp},M,O}^{n,k,i}(t) := \eta_{\text{R},M,O}^{n,k,i} + \left\| \Theta_{\text{dis},O,h}^{n,k,i} - \widehat{\nu}_o \mathbf{v}_{o,h}^{n,k,i} \right\|_M + \eta_{\text{NC},M,o,O}^{n,k,i}(t) \quad t \in I_n, \quad (3.A.7b)$$

the *energy spatial estimators*

$$\eta_{\text{sp},M,H}^{n,k,i}(t) := \eta_{\text{R},M,H}^{n,k,i} + \left\| \Theta_{\text{dis},H,h}^{n,k,i} - (\mathbf{u}_h^{n,k,i} - \lambda \nabla T_h^{n,k,i}) \right\|_M + (\eta_{\text{NC},M,T}^{n,k,i}(t)) \quad t \in I_n, \quad (3.A.7c)$$

the *water component temporal estimators*

$$\eta_{\text{tm},M,W}^{n,k,i}(t) := \left\| (\widehat{\nu}_w \mathbf{v}_{w,h\tau}^{n,k,i} + \widehat{\nu}_s \mathbf{v}_{s,h\tau}^{n,k,i})(t) - (\widehat{\nu}_w \mathbf{v}_{w,h}^{n,k,i} + \widehat{\nu}_s \mathbf{v}_{s,h}^{n,k,i}) \right\|_M \quad t \in I_n, \quad (3.A.7d)$$

the *oil component temporal estimators*

$$\eta_{\text{tm},M,O}^{n,k,i}(t) := \left\| (\widehat{\nu}_o \mathbf{v}_{o,h\tau}^{n,k,i})(t) - (\widehat{\nu}_o \mathbf{v}_{o,h}^{n,k,i}) \right\|_M \quad t \in I_n, \quad (3.A.7e)$$

the *energy temporal estimators*

$$\eta_{\text{tm},M,H}^{n,k,i}(t) := \left\| (\mathbf{u}_{h\tau}^{n,k,i} - \lambda \nabla T_{h\tau}^{n,k,i})(t) - (\mathbf{u}_h^{n,k,i} - \lambda \nabla T_h^{n,k,i}) \right\|_M \quad t \in I_n, \quad (3.A.7f)$$

the *linearization estimators*

$$\eta_{\text{lin},M,c}^{n,k,i} := \left\| \Theta_{\text{lin},c,h}^{n,k,i} \right\|_M + \eta_{\text{NA},M,c}^{n,k,i} \quad c \in \{W, O\}, \quad (3.A.7g)$$

$$\eta_{\text{lin},M,H}^{n,k,i} := \left\| \Theta_{\text{lin},H,h}^{n,k,i} \right\|_M + \eta_{\text{NA},M,H}^{n,k,i}, \quad (3.A.7h)$$

and the *algebraic estimators*

$$\eta_{\text{alg},M,c}^{n,k,i} := \left\| \Theta_{\text{alg},c,h}^{n,k,i} \right\|_M \quad c \in \{W, O\}, \quad (3.A.7i)$$

$$\eta_{\text{alg},M,H}^{n,k,i} := \left\| \Theta_{\text{alg},H,h}^{n,k,i} \right\|_M. \quad (3.A.7j)$$

The global versions of these estimators are given by: For $c \in \{W, O\}$

$$\eta_{\text{sp},c}^{n,k,i} := \left\{ 4 \int_{I_n} \sum_{M \in \mathcal{M}^n} (\eta_{\text{sp},M,c}^{n,k,i}(t))^2 dt \right\}^{\frac{1}{2}}, \quad (3.A.8a)$$

$$\eta_{\text{tm},c}^{n,k,i} := \left\{ 2 \int_{I_n} \sum_{M \in \mathcal{M}^n} (\eta_{\text{tm},M,c}^{n,k,i}(t))^2 dt \right\}^{\frac{1}{2}}, \quad (3.A.8b)$$

$$\eta_{\text{lin},c}^{n,k,i} := \left\{ 2\tau^n \sum_{M \in \mathcal{M}^n} (\eta_{\text{lin},M,c}^{n,k,i})^2 \right\}^{\frac{1}{2}}, \quad (3.A.8c)$$

$$\eta_{\text{alg},c}^{n,k,i} := \left\{ 2\tau^n \sum_{M \in \mathcal{M}^n} (\eta_{\text{alg},M,c}^{n,k,i})^2 \right\}^{\frac{1}{2}} \quad (3.A.8d)$$

and

$$\eta_{\text{sp},H}^{n,k,i} := \left\{ 4 \int_{I_n} \sum_{M \in \mathcal{M}^n} (\eta_{\text{sp},M,H}^{n,k,i}(t))^2 dt \right\}^{\frac{1}{2}}, \quad (3.A.8e)$$

$$\eta_{\text{tm},H}^{n,k,i} := \left\{ 2 \int_{I_n} \sum_{M \in \mathcal{M}^n} (\eta_{\text{tm},M,H}^{n,k,i}(t))^2 dt \right\}^{\frac{1}{2}}, \quad (3.A.8f)$$

$$\eta_{\text{lin},H}^{n,k,i} := \left\{ 2\tau^n \sum_{M \in \mathcal{M}^n} (\eta_{\text{lin},M,H}^{n,k,i})^2 \right\}^{\frac{1}{2}}, \quad (3.A.8g)$$

$$\eta_{\text{alg},H}^{n,k,i} := \left\{ 2\tau^n \sum_{M \in \mathcal{M}^n} (\eta_{\text{alg},M,H}^{n,k,i})^2 \right\}^{\frac{1}{2}}. \quad (3.A.8h)$$

The following is the version of Corollary 3.5.4 in the dead oil setting:

Corollary 3.A.3 (An a posteriori error bound for the residual error norm distinguishing the space, time, linearization, and algebraic errors). *Let the assumptions of Corollary 3.A.2 be satisfied. Let the estimators be given by (3.A.8). Then*

$$\begin{aligned} \mathcal{N}_e^{n,k,i} \leq & \left\{ \sum_{c \in \{\text{W}, \text{O}\}} (\eta_{\text{sp},c}^{n,k,i} + \eta_{\text{tm},c}^{n,k,i} + \eta_{\text{lin},c}^{n,k,i} + \eta_{\text{alg},c}^{n,k,i})^2 \right. \\ & \left. + (\eta_{\text{sp},H}^{n,k,i} + \eta_{\text{tm},H}^{n,k,i} + \eta_{\text{lin},H}^{n,k,i} + \eta_{\text{alg},H}^{n,k,i})^2 \right\}^{\frac{1}{2}}. \end{aligned} \quad (3.A.9)$$

In the next chapter, we develop a simplified formula for computing the different estimators which can be easily applied in practice.

Bibliography

- [1] I. Aavatsmark, T. Barkve, O. Bøe, and T. Mannseth. Discretization on non-orthogonal, curvilinear grids for multi-phase flow. In *Proc. of the 4th European Conf. on the Mathematics of Oil Recovery*, volume D, Røros, Norway, 1994.
- [2] Y. Achdou, C. Bernardi, and F. Coquel. A priori and a posteriori analysis of finite volume discretizations of Darcy's equations. *Numer. Math.*, 96(1):17–42, 2003.
- [3] G. Acs and E. Farkas. General purpose compositional model. *Society of Petroleum Engineers*, 25(4):543–553, 1985.
- [4] L. Agélas, D. A. Di Pietro, and J. Droniou. The G method for heterogeneous anisotropic diffusion on general meshes. *M2AN Math. Model. Numer. Anal.*, 44(4):597–625, 2010.
- [5] L. Agélas, D. A. Di Pietro, and R. Masson. A symmetric and coercive finite volume scheme for multiphase porous media flow problems with applications in the oil industry. In *Finite volumes for complex applications V*, pages 35–51. ISTE, London, 2008.
- [6] M. Ainsworth. Robust a posteriori error estimation for nonconforming finite element approximation. *SIAM J. Numer. Anal.*, 42(6):2320–2341, 2005.
- [7] M. Arioli, D. Loghin, and A. J. Wathen. Stopping criteria for iterations in finite element methods. *Numer. Math.*, 99(3):381–410, 2005.
- [8] K. Aziz and A. Settari. *Petroleum Reservoir Simulation*. Applied Science Publisher, Ltd, London, 1979.
- [9] R. Becker, C. Johnson, and R. Rannacher. Adaptive error control for multigrid finite element methods. *Computing*, 55(4):271–288, 1995.
- [10] J. B. Bell and J. Trangenstein. Mathematical structure of compositional reservoir simulation. *SIAM J. Sci. Stat. Comput.*, vol. 10, pp. 817–845, 1989.
- [11] J. B. Bell and J. Trangenstein. Mathematical structure of the black-oil model for petroleum reservoir simulation. *SIAM J. Appl. Math.*, vol.49, pp. 749–783, 1989.

-
- [12] I. Ben Gharbia and J. Jaffré. Gas phase appearance and disappearance as a problem with complementarity constraints. HAL Preprint 00641621, submitted for publication, 2011.
- [13] F. Brezzi and M. Fortin. *Mixed and hybrid finite element methods*, volume 15 of *Springer Series in Computational Mathematics*. Springer-Verlag, New York, 1991.
- [14] C. Cancès, I. S. Pop, and M. Vohralík. An a posteriori error estimate for vertex-centered finite volume discretizations of immiscible incompressible two-phase flow. *Math. Comp.*, 2013. DOI 10.1090/S0025-5718-2013-02723-8.
- [15] A. L. Chaillou and M. Suri. Computable error estimators for the approximation of nonlinear problems by linearized models. *Comput. Methods Appl. Mech. Engrg.*, 196(1-3):210–224, 2006.
- [16] Z. Chen and R. Ewing. From single-phase to compositional flow: Applicability of mixed finite elements. *Transport in Porous Media*, 27:225–242, 1997.
- [17] Z. Chen, G. Huan, and Y. Ma. *Computational methods for multiphase flows in porous media*. Computational Science & Engineering. Society for Industrial and Applied Mathematics (SIAM), Philadelphia, PA, 2006.
- [18] Z. Chen, G. Qin, and R. E. Ewing. Analysis of a compositional model for fluid flow in porous media. *SIAM J. Appl. Math.*, 60(3):747–777, 2000.
- [19] Z. Chen and X. Yu. Implementation of mixed methods as finite difference methods and applications to nonisothermal multiphase flow in porous media. *Math. Comp.*, 24:281–294, 2006.
- [20] J. Christensen, G. Darche, B. Dechelette, H. Ma, and P. Sammon. Applications of dynamic gridding to thermal simulations. *Society of Petroleum Engineers*, 16-18 March 2004.
- [21] K. H. Coats. An equation of state compositional model. *Society of Petroleum Engineers*, 20(5):363–376, 1980.
- [22] K. H. Coats. Implicit compositional simulation of single porosity and dual-porosity reservoirs. *Society of Petroleum Engineers*, pages 6–8, February 1989.
- [23] M. Delshad, S. Thomas, and M. Wheeler. Parallel numerical reservoir simulations of non-isothermal compositional flow and chemistry. *Society of Petroleum Engineers*, 16(2):727–742, 2011.
- [24] P. Destuynder and B. Métivet. Explicit error bounds for a nonconforming finite element method. *SIAM J. Numer. Anal.*, 35(5):2099–2115, 1998.
- [25] D. A. Di Pietro, E. Flauraud, M. Vohralík, and S. Yousef. A posteriori error estimates, stopping criteria, and adaptivity for multiphase compositional Darcy flows in porous media. HAL Preprint 00839487, submitted for publication, June 2013.

-
- [26] D. A. Di Pietro and S. Lemaire. An extension of the Crouzeix–Raviart space to general meshes with application to quasi-incompressible linear elasticity and Stokes flow. *Math. Comp.*, 2013.
- [27] V. Dolejší, A. Ern, and M. Vohralík. A framework for robust a posteriori error control in unsteady nonlinear advection-diffusion problems. *SIAM J. Numer. Anal.*, 51(2):773–793, 2013.
- [28] J. Douglas, Jr., R. E. Ewing, and M. F. Wheeler. The approximation of the pressure by a mixed method in the simulation of miscible displacement. *RAIRO Modél. Math. Anal. Numér.*, 17(1):17–33, 1983.
- [29] L. El Alaoui, A. Ern, and M. Vohralík. Guaranteed and robust a posteriori error estimates and balancing discretization and linearization errors for monotone nonlinear problems. *Comput. Methods Appl. Mech. Engrg.*, 200(37-40):2782–2795, 2011.
- [30] A. Ern and M. Vohralík. A posteriori error estimation based on potential and flux reconstruction for the heat equation. *SIAM J. Numer. Anal.*, 48(1):19–223, 2010.
- [31] A. Ern and M. Vohralík. Adaptive inexact Newton methods with a posteriori stopping criteria for nonlinear diffusion PDEs. *SIAM J. Sci. Comput.*, 2013. DOI 10.1137/120896918.
- [32] R. E. Ewing, B. A. Boyett, D. K. Babu, and R. F. Heinemann. Efficient use of locally refined grids for multiphase reservoir simulation. *Society of Petroleum Engineers*, 1989.
- [33] R. Eymard, T. Gallouët, and R. Herbin. Finite volume approximation of elliptic problems and convergence of an approximate gradient. *Appl. Numer. Math.*, 37(1-2):31–53, 2001.
- [34] R. Eymard, C. Guichard, R. Herbin, and R. Masson. Vertex-centred discretization of multiphase compositional Darcy flows on general meshes. *Comput. Geosci.*, 16(4):987–1005, 2012.
- [35] R. Eymard, R. Herbin, and A. Michel. Mathematical study of a petroleum-engineering scheme. *M2AN Math. Model. Numer. Anal.*, 37(6):937–972, 2003.
- [36] Z. E. Heinemann. Using local grid refinement in a multiple-application reservoir simulator. *Society of Petroleum Engineers*, 1983.
- [37] C. Huang, Y. Yang, and M. Deo. A new thermal-compositional reservoir simulator with a novel “equation line-up” method. *Society of Petroleum Engineers*, 11-14 November 2007.
- [38] R. Huber and R. Helmig. Node-centered finite volume discretizations for the numerical simulation of multiphase flow in heterogeneous porous media. *Comput. Geosci.*, 4(2):141–164, 2000.
- [39] P. Jiránek, Z. Strakoš, and M. Vohralík. A posteriori error estimates including algebraic error and stopping criteria for iterative solvers. *SIAM J. Sci. Comput.*, 32(3):1567–1590, 2010.

-
- [40] S. Lacroix, Y. Vassilevski, J. Wheeler, and M. Wheeler. Iterative solution methods for modeling multiphase flow in porous media fully implicitly. *SIAM J. Sci. Comput.*, 25(3):905–926, 2003.
- [41] A. Lauser, C. Hager, R. Helmig, and B. I. Wohlmuth. A new approach for phase transitions in miscible multi-phase flow in porous media. *Advances in Water Resources*, 34(8):957–966, 2011.
- [42] M. R. Laydi and M. Ghilani. A general finite volume scheme for an elliptic-hyperbolic system using a variational approach. *Zeitschrift für angewandte Mathematik und Physik ZAMP*, 49(4):630–643, 1998.
- [43] K. Liu, G. Subramanian, D. Dratler, J. Lebel, and J. Yerian. A general unstructured grid, EOS-based, fully implicit thermal simulator for complex reservoir processes. *Society of Petroleum Engineers*, 26-28 February 2007.
- [44] J. Nilsson, M. Gerritsen, and R. Younis. An adaptive, high-resolution simulation for steam-injection processes. *Society of Petroleum Engineers*, 2005.
- [45] M. J. O’Sullivan, K. Pruess, and M. J. Lippmann. State of the art of geothermal reservoir simulation. *Geothermics*, 30(4):395 – 429, 2001.
- [46] U. Pasarai and N. Arihara. A simulator for predicting thermal recovery behavior based on streamline method. *Society of Petroleum Engineers*, 5-6 December 2005.
- [47] G. S. H. Pau, A. S. Almgren, J. B. Bell, and M. J. Lijewski. A parallel second-order adaptive mesh algorithm for incompressible flow in porous media. *Philos. Trans. R. Soc. Lond. Ser. A Math. Phys. Eng. Sci.*, 367(1907):4633–4654, 2009.
- [48] G. S. H. Pau, J. B. Bell, A. S. Almgren, K. M. Fagnan, and M. J. Lijewski. An adaptive mesh refinement algorithm for compressible two-phase flow in porous media. *Comput. Geosci.*, 16(3):577–592, 2012.
- [49] P. H. Sammon. Dynamic grid refinement and amalgamation for compositional simulation. *Society of Petroleum Engineers*, 2003.
- [50] J. A. Trangenstein. Multi-scale iterative techniques and adaptive mesh refinement for flow in porous media. *Advances in Water Resources*, 25(8-12):1175 – 1213, 2002.
- [51] O. Van, E. A. Daniel, J. B. Bell, F. Monmont, and N. Nikiforakis. The mathematical structure of multiphase thermal models of flow in porous media. *Proc. R. Soc. Lond. Ser. A Math. Phys. Eng. Sci.*, 465(2102):523–549, 2009.
- [52] R. Verfürth. A posteriori error estimates for finite element discretizations of the heat equation. *Calcolo*, 40(3):195–212, 2003.
- [53] M. Vohralík. Residual flux-based a posteriori error estimates for finite volume and related locally conservative methods. *Numer. Math.*, 111(1):121–158, 2008.
- [54] M. Vohralík and M. F. Wheeler. A posteriori error estimates, stopping criteria, and adaptivity for two-phase flows. *Comput. Geosci.*, 2013. DOI 10.1007/s10596-013-9356-0.

- [55] L. C. Young and R. E. Stephenson. A generalized compositional approach for reservoir simulation. *Society of Petroleum Engineers*, 23(5):727–742, 1983.

Chapter 4

Steam-assisted gravity drainage: a posteriori estimates with simplified evaluation and application of adaptive mesh refinement

This chapter consists of a paper in preparation for an industrial journal.

Contents

4.1	Introduction	152
4.2	SAGD characterization and modeling	153
4.2.1	Common characteristics	153
4.2.2	Types of SAGD	154
4.2.3	SAGD modeling	154
4.2.4	Mathematical model of the thermal dead oil system	155
4.3	Evaluation of the estimators using a practical simplified formula	155
4.3.1	A general simplification formula	156
4.3.2	Evaluation of the estimators	157
4.4	SAGD test case	163
4.4.1	Model description	163
4.4.2	Initialization and production scheme	164
4.4.3	Model simulation	165
4.4.4	Approximate solution and a posteriori estimate	166
4.4.5	Adaptive mesh refinement	166
	Bibliography	168

Abstract

In this chapter we consider the Steam-Assisted Gravity Drainage (SAGD) process, a thermal oil-recovery technique of steam injection designed to increase the oil mobility. We apply the a posteriori analysis of the isothermal model of Chapter 2 and of nonisothermal condition of Chapter 3. Moreover, in order to implement these a posteriori estimators in industrial codes we simplify their computation. Then we propose an adaptive mesh refinement algorithm combined with a balancing criterion on the choice of the time step. Numerical results for a real-life reservoir engineering example for the dead oil model in three dimension is discussed. Using the adaptive refinement strategy, we obtain a significant gain in terms of the number of mesh cells compared to a fine mesh resolution, and this without affecting the accuracy of the predicted oil production.

Key words: a posteriori error analysis, adaptive mesh refinement, steam-assisted gravity drainage, dead oil model, quadrature formula, simplified evaluation, finite volume method.

4.1 Introduction

The steam-assisted gravity drainage, see the description in the Introduction, is a technique for producing heavy oil that otherwise is not easily recovered due to its high viscosity and low mobility cf. Butler [1]. The process typically includes two horizontal wells, an injection one above a production one, see Figure 4.1, left. The upper well injects steam which forms a steam chamber, see Figure 4.1, right, in which the oil is heated thereby reducing its viscosity. This raises the oil mobility and then gravity forces the oil downward (cf. Butler [2] or Farouq [4]). The production well at the bottom of the steam chamber then receives the oil and leads it to the surface.

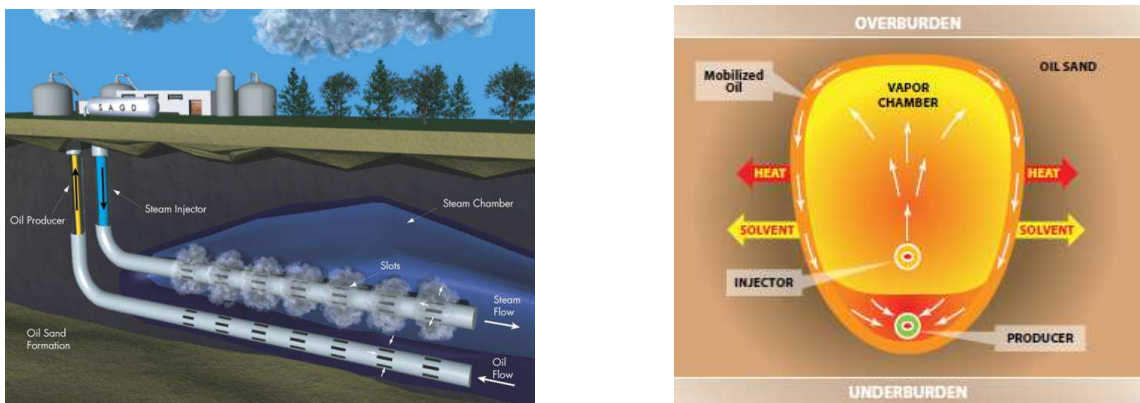


Figure 4.1: SAGD process: wells (left) and steam chamber (right).

Some previous works proposed adaptive mesh refinement (AMR) techniques for SAGD processes. In Lacroix et al. [6], an AMR method is developed based on the displacement of a thermal front by proposing a dynamic subgridding technique; this approach leads to

significant gains in computation times. A similar application of dynamic gridding to thermal simulations is considered in Christensen et al. [3]. Large gradients of specific quantities such as temperatures, fluid saturations, and compositions are used to locate the position of the front and trigger a corresponding refinement of the grid. In Wang et al. [10] a detailed analysis of the implementation of the AMR technique to one-dimensional three-phase flows in heterogeneous porous media, including phase change, is presented. The authors consider discontinuous saturations across interfaces between different rock types, and propose a specific refining procedure and refinement criterion to deal with this discontinuity.

Recently, Mamaghani et al. [7] have designed a new refinement criterion that focuses more on the oil saturation discontinuities for better locating the front position; the criterion is based on local a posteriori error estimators for finite volume schemes for hyperbolic equations, see Kröner and Ohlberger [5]. As the estimators are not constant-free, some threshold values need to be specified. These only depend on the initial data of the problem, but computing them requires some preliminary runs on the fine grid.

In this chapter we propose an efficient adaptive method for the resolution of the SAGD problem, based on the a posteriori error analysis of the previous chapter. In particular, as the estimators are fully computable no threshold values need to be set. First, we present a simple way to compute the different estimators for the thermal dead oil model described in Section 3.A.2 of Chapter 3. Then, we propose a space–time adaptive mesh refinement algorithm based on these estimators. We consider the application of the theory to an implicit cell-centered finite volume scheme with phase-upwind and two-point discretization of diffusive fluxes. Numerical results on an example of real-life thermal oil-recovery in a reservoir simulation illustrate the performance of the refinement strategy and in particular show that a significant gain in terms of the number of necessary mesh cells can be achieved.

4.2 SAGD characterization and modeling

We present in this section some characteristics of the SAGD process and quote some of types of SAGD [8] currently used in practice. We will also describe the most popular reservoir models for this process.

4.2.1 Common characteristics

The SAGD process has many characteristics based on the steam chamber and on the different wells. The most important ones are:

- In the steam chamber, the pressure does not vary.
- The steam injection rate does not have an important impact on the oil production rate.
- The oil motion is driven only by gravitational drainage.
- The vertical production is technically useless because the flows are relatively slow.

4.2.2 Types of SAGD

There are many types of SAGD in terms of the number and location of wells, the types of wells (vertical and horizontal), the method of drilling and steam injection, and other parameters, see [8]. Some common types of SAGD are:

- Shaft and Tunnel Access (SATAAC);
- Access and Drilling from Surface (SAC-SAGD);
- Multi-drain SAGD;
- Single Well SAGD (SW-SAGD);
- Vertical/Horizontal wells combination;
- Fast-SAGD;
- Enhanced Steam Assisted Gravity Drainage (ESAGD).

4.2.3 SAGD modeling

We now briefly describe the most popular reservoir models for the SAGD process: The *black oil* model and the *dead oil* model. The two models represent a three-phase flow (oil, gas, water). The gas could be a steam of water or hydrocarbon such as methane or ethane. In the development of these models we consider a nonisothermal flow, so the equation of the conservation of energy will always be present.

4.2.3.1 Black oil model

In this model we have three phases constituted by water, oil, and gas. The oil phase contains two types of components: nonvolatile oil and volatile oil which we call here oil component and gas component respectively. This is due to the fact that in this model the hydrocarbon components are divided into light and heavy components. The light component can dissolve into the liquid oil phase or volatilize in the gas phase according to the pressure and temperature. The water phase contains only the water component.

4.2.3.2 Dead oil model

The dead oil is an oil that has lost all its light components (gas components). Therefore it differs from the black oil model in that the oil phase in the dead oil model contains only the heavy component (nonvolatile oil component). For the water phase, it contains only the water component as in the black oil model. Finally, the gas phase is in fact a steam phase and contains only the water component.

Remark 4.2.1. In SAGD processes, the reservoirs are not very deep. Thus the absolute permeability and porosity are high, and consequently the capillary pressures are relatively small, which allows us to neglect them.

4.2.4 Mathematical model of the thermal dead oil system

The system of governing equations of the thermal dead oil model is given by (3.A.1) in Section 3.A.1 of Chapter 3. In practice, in the dead oil model the capillary pressures are neglected because of their relatively low values, see Remark 4.2.1. Thus we only consider one pressure P for all phases: $P_w = P_o = P_s = P$, whereas we keep three different phase saturations: S_w, S_o, S_s . The temperature T is an unknown of the problem, since we consider the nonisothermal condition. Thus we define the vector of unknowns by setting

$$\mathcal{X} := \begin{pmatrix} P \\ T \\ (S_p)_{p \in \{w, o, s\}} \end{pmatrix}. \quad (4.2.1)$$

The discretization and the resolution of the thermal dead oil model (3.A.1) is given in the previous chapters as the dead oil model is a special case of the general thermal multiphase compositional model. We can thus directly apply the a posteriori analysis described in details in Section 3.A.2 of Chapter 3.

In order to implement the different estimators in a reservoir simulation code, we propose here to simplify them. Our simplification is based on the following observations:

- Our estimators are expressed in terms of norms of various discrete quantities; therefore we only need to compute these norms and not necessarily the quantities themselves.
- All these norms are integrals; therefore they can be computed/approximated on each adequate quadrature formulas by mesh element.
- We thus only need to know the values of the various quantities at the quadrature points.
- The implementation of RTN spaces and the physical construction of the flux reconstructions can be consequently avoided.

Let us now describe our simplification process in all details.

4.3 Evaluation of the estimators using a practical simplified formula

The a posteriori estimates of Section 3.A.2 use the reconstruction of the different fluxes $\Theta_{\text{dis},c,h}^{n,k,i}$, $\Theta_{\text{lin},c,h}^{n,k,i}$, $\Theta_{\text{alg},c,h}^{n,k,i}$, $c \in \{W, O\}$, and $\Theta_{\text{dis},H,h}^{n,k,i}$, $\Theta_{\text{lin},H,h}^{n,k,i}$, and $\Theta_{\text{alg},H,h}^{n,k,i}$ in the space $\mathbf{RTN}(\mathcal{M}^n)$ (see Sections 2.4.4 and 3.4.4). Furthermore, the pressure and temperature reconstructions $P_{p,h\tau}^{n,k,i}$, $p \in \{w, o, s\}$, and $T_{h\tau}^{n,k,i}$ also involve $\mathbf{RTN}(\mathcal{M}^n)$ spaces (see Sections 2.4.2.1 and 3.4.1) in a way that for all $M \in \mathcal{M}^n$,

$$-\left(\mathbb{K}\nabla P_{p,h\tau}^{n,k,i}\right)|_M \in \mathbf{RTN}(\mathcal{M}^n), \quad p \in \{w, o, s\} \quad \text{and} \quad -\left(\lambda\nabla T_{h\tau}^{n,k,i}\right)_M \in \mathbf{RTN}(\mathcal{M}^n).$$

Hence, a priori, implementing these estimators requires operations with \mathbf{RTN} spaces as seen in the previous chapter. Unfortunately, so far \mathbf{RTN} spaces are not implemented in industrial

codes. Therefore we look for a simplification of these estimators that avoids the use of **RTN** spaces.

4.3.1 A general simplification formula

Let a mesh cell M be given and let $\mathbf{\Delta}_h \in \mathbf{RTN}(M)$. Then $\mathbf{\Delta}_h$ can be expressed by

$$\mathbf{\Delta}_h = \sum_{\sigma \in \mathcal{E}_M} c_\sigma \mathbf{\Lambda}_\sigma, \quad (4.3.1)$$

where c_σ are the degrees of freedom on the face σ , i.e., the face fluxes $(\mathbf{\Delta}_h \cdot \mathbf{n}_M, 1)_\sigma$, and $\mathbf{\Lambda}_\sigma$ are the lowest-order Raviart–Thomas–Nédélec basis functions, given by (for parallelepiped meshes such as the ones used in the tests cases of Section 4.4 below)

$$\mathbf{\Lambda}_\sigma = \frac{1}{|M|} \mathbf{E}_{\sigma, \sigma'} \cdot (\mathbf{x} - \mathbf{x}_{\sigma'}),$$

where $\mathbf{x}_{\sigma'} = (x_{\sigma'}, y_{\sigma'}, z_{\sigma'})$ is the barycenter of the face σ' opposite to the face σ , and

$$\mathbf{E}_{\sigma, \sigma'} := \begin{pmatrix} e_{\sigma, \sigma'}^x := \bar{1}_{x_\sigma, x_{\sigma'}} & 0 & 0 \\ 0 & e_{\sigma, \sigma'}^y := \bar{1}_{y_\sigma, y_{\sigma'}} & 0 \\ 0 & 0 & e_{\sigma, \sigma'}^z := \bar{1}_{z_\sigma, z_{\sigma'}} \end{pmatrix}, \quad \bar{1}_{w, w'} = \begin{cases} 1 & \text{if } w \neq w', \\ 0 & \text{otherwise.} \end{cases} \quad (4.3.2)$$

Consider now the following quadrature formula exact for polynomials of total degree three, on a cubic domain $K = (-1, 1)^3$:

$$\int_{-1}^1 \int_{-1}^1 \int_{-1}^1 g(x, y, z) dx dy dz \approx |K| \sum_{i=1}^2 \sum_{j=1}^2 \sum_{l=1}^2 w_i w_j w_l g(\alpha_i, \beta_j, \gamma_l).$$

Here $w_1 = w_2 = \frac{1}{2}$, $\alpha_1 = \beta_1 = \gamma_1 = \frac{-1}{\sqrt{3}}$, and $\alpha_2 = \beta_2 = \gamma_2 = \frac{1}{\sqrt{3}}$. We can also rewrite this formula with vector symbols by

$$\int_K g(\mathbf{x}) d\mathbf{x} \approx |K| \sum_{k=1}^8 W_k g(\mathbf{\Pi}^k), \quad (4.3.3)$$

with $W_k = \frac{1}{8}$, $k \in \{1, 2, \dots, 8\}$, and $\mathbf{\Pi}^k = (\Pi_x^k, \Pi_y^k, \Pi_z^k)$ as given in Table 4.1.

k		1	2	3	4	5	6	7	8
$\mathbf{\Pi}^k$	Π_x^k	$\frac{1}{\sqrt{3}}$	$\frac{1}{\sqrt{3}}$	$\frac{1}{\sqrt{3}}$	$\frac{1}{\sqrt{3}}$	$\frac{-1}{\sqrt{3}}$	$\frac{-1}{\sqrt{3}}$	$\frac{-1}{\sqrt{3}}$	$\frac{-1}{\sqrt{3}}$
	Π_y^k	$\frac{1}{\sqrt{3}}$	$\frac{1}{\sqrt{3}}$	$\frac{-1}{\sqrt{3}}$	$\frac{-1}{\sqrt{3}}$	$\frac{-1}{\sqrt{3}}$	$\frac{1}{\sqrt{3}}$	$\frac{1}{\sqrt{3}}$	$\frac{-1}{\sqrt{3}}$
	Π_z^k	$\frac{1}{\sqrt{3}}$	$\frac{-1}{\sqrt{3}}$	$\frac{-1}{\sqrt{3}}$	$\frac{1}{\sqrt{3}}$	$\frac{1}{\sqrt{3}}$	$\frac{1}{\sqrt{3}}$	$\frac{-1}{\sqrt{3}}$	$\frac{-1}{\sqrt{3}}$

Table 4.1: Integration points

To apply the formula (4.3.3) to the integration of a function over a cell $M := (x_1, x_2) \times (y_1, y_2) \times (z_1, z_2)$ of our parallelepiped mesh, we consider the transformation $\mathbf{f}^k = (f_x^k, f_y^k, f_z^k)$ such that,

$$f_x^k = \frac{x_2 - x_1}{2} \Pi_x^k + \frac{x_2 + x_1}{2}, \quad (4.3.4a)$$

$$f_y^k = \frac{y_2 - y_1}{2} \Pi_y^k + \frac{y_2 + y_1}{2}, \quad (4.3.4b)$$

$$f_z^k = \frac{z_2 - z_1}{2} \Pi_z^k + \frac{z_2 + z_1}{2}. \quad (4.3.4c)$$

Now we can evaluate the $[L^2(M)]^3$ norm of the function $\Delta_h \in \mathbf{RTN}(M)$ given by (4.3.1), using the quadrature formula (4.3.3) and the transformations in (4.3.4), as follows

$$\begin{aligned} \|\Delta_h\|_{L^2(M)}^2 &= \frac{|M|}{8} \sum_{k=1}^8 \left[\sum_{\sigma \in \mathcal{E}_M} c_\sigma \frac{1}{|M|} \mathbf{E}_{\sigma, \sigma'} \cdot (\mathbf{f}^k - \mathbf{x}_{\sigma'}) \right]^2, \\ &= \frac{1}{8|M|} \sum_{k=1}^8 \left\{ \left[\sum_{\sigma \in \mathcal{E}_M} c_\sigma (f_x^k - x_{\sigma'}) e_{\sigma, \sigma'}^x \right]^2 + \left[\sum_{\sigma \in \mathcal{E}_M} c_\sigma (f_y^k - y_{\sigma'}) e_{\sigma, \sigma'}^y \right]^2 \right. \\ &\quad \left. + \left[\sum_{\sigma \in \mathcal{E}_M} c_\sigma (f_z^k - z_{\sigma'}) e_{\sigma, \sigma'}^z \right]^2 \right\}. \end{aligned} \quad (4.3.5)$$

As a conclusion, to compute an $[L^2]^3$ norm of reconstructed flux functions in the space $\mathbf{RTN}(\mathcal{M}^n)$, we just need to obtain the degrees of freedom c_σ , represented by the face normal fluxes. These can be obtained directly without any flux reconstruction. In what follows we use these simplifications to evaluate the estimators for the thermal dead oil model.

4.3.2 Evaluation of the estimators

We begin with the spatial estimators. Recall the reconstructions of the conservative fluxes $\Theta_{W,h}^{n,k,i}$, $\Theta_{O,h}^{n,k,i}$, and $\Theta_{H,h}^{n,k,i}$ given by (2.4.14d) and (3.4.3d). For $\Theta_{c,h}^{n,k,i}$, $c \in \{W, O\}$, one has

$$\left(\Theta_{c,h}^{n,k,i} \right) |M = \left(\Theta_{\text{dis},c,h}^{n,k,i} + \Theta_{\text{lin},c,h}^{n,k,i} + \Theta_{\text{alg},c,h}^{n,k,i} \right) |M.$$

Owing to the reconstruction of $\Theta_{\text{dis},c,h}^{n,k,i}$ in (2.4.14a), $\Theta_{\text{lin},c,h}^{n,k,i}$ in (2.4.14b), and $\Theta_{\text{alg},c,h}^{n,k,i}$ (2.4.14c), we satisfy (3.5.16a), cf. section 3.5.3.1, up to a neglected maladjustment from the practical construction of $\Theta_{\text{alg},c,h}^{n,k,i}$ (Corollary 4.3.4 and Remark 2.4.3). Then, the residual estimators $\eta_{R,M,W}^{n,k,i}$, and $\eta_{R,M,O}^{n,k,i}$ given by (3.5.17a) will be neglected. Note that, however, if we construct the algebraic flux $\Theta_{\text{alg},c,h}^{n,k,i}$ following 2.4.14c then the residual estimators $\eta_{R,M,W}^{n,k,i}$, and $\eta_{R,M,O}^{n,k,i}$ are zero. A similar result is obtained for the other residual estimator $\eta_{R,M,H}^{n,k,i}$ given by (3.5.17b). Therefore, it takes very small values and will be neglected in what follows.

Consider now the contribution $\left\| \Theta_{\text{dis},O,h}^{n,k,i} - (\widehat{\nu}_o \mathbf{v}_{o,h}^{n,k,i}) \right\|_{L^2(M)}$ which represents the second term of the oil component spatial estimator (3.A.7b). Following (3.A.3), the velocity $\mathbf{v}_{o,h}^{n,k,i}$ is given by, for $p = o$

$$\mathbf{v}_{p,h}^{n,k,i} = -\mathbb{K}(\nabla P_{p,h}^{n,k,i} - \rho_p(P_{p,h}^{n,k,i}, T_h^{n,k,i})\mathbf{g}). \quad (4.3.6)$$

Then by the post-processing of the oil pressure $P_{o,h}^{n,k,i}$ given by (2.4.11) and by the definition (2.4.14a) of the reconstructed flux $\Theta_{\text{dis},O,h}^{n,k,i}$, we conclude that

$$\begin{aligned} \left(\widehat{\nu}_o \mathbf{v}_{o,h}^{n,k,i} \right) |_M &= \left(-\widehat{\nu}_o \mathbb{K}(\nabla P_{o,h}^{n,k,i} - \rho_o(P_{o,h}^{n,k,i}, T_h^{n,k,i})\mathbf{g}) \right) |_M \\ &= \left(\widehat{\nu}_o \mathbf{\Gamma}_{o,h}^{n,k,i} \right) |_M \\ &\approx \left(\Theta_{\text{dis},O,h}^{n,k,i} \right) |_M, \end{aligned}$$

so that

$$\left\| \Theta_{\text{dis},O,h}^{n,k,i} - (\widehat{\nu}_o \mathbf{v}_{o,h}^{n,k,i}) \right\|_{L^2(M)} \approx 0, \quad (4.3.7)$$

and we neglect this term in the simplified evaluation.

Similarly, considering the postprocessings of the water and steam pressures $P_{p,h\tau}^{n,k,i}$, $p \in \{w, s\}$, given by (2.4.11), the velocity formula (4.3.6), and the reconstructed flux $\Theta_{\text{dis},W,h}^{n,k,i}$ given by (2.4.14a), we obtain

$$\left(\Theta_{\text{dis},W,h}^{n,k,i} \right) |_M \approx \left(\widehat{\nu}_w \mathbf{v}_{w,h}^{n,k,i} + \widehat{\nu}_s \mathbf{v}_{s,h}^{n,k,i} \right) |_M \Rightarrow \left\| \Theta_{\text{dis},W,h}^{n,k,i} - (\widehat{\nu}_w \mathbf{v}_{w,h}^{n,k,i} + \widehat{\nu}_s \mathbf{v}_{s,h}^{n,k,i}) \right\|_{L^2(M)} \approx 0. \quad (4.3.8)$$

Finally, the postprocessing of the phase pressures given by (2.4.11), the formula (3.A.4), the temperature postprocessing (3.4.2), and the reconstructed flux $\Theta_{\text{dis},H,h}^{n,k,i}$ given by (3.4.3a) give

$$\left\| \Theta_{\text{dis},H,h}^{n,k,i} - (\mathbf{u}_h^{n,k,i} - \lambda \nabla T_h^{n,k,i}) \right\|_{L^2(M)} \approx 0. \quad (4.3.9)$$

As a conclusion, we can remark that the first two terms of each of the estimators $\eta_{\text{sp},M,W}^{n,k,i}$, $\eta_{\text{sp},M,O}^{n,k,i}$, and $\eta_{\text{sp},M,H}^{n,k,i}$, given by (3.A.7a)–(3.A.7c), can be neglected. Then, the evaluation of the spatial estimators will concern just the estimators of nonconformity.

As all non conformity estimators are evaluated in the same way, we will only discuss one of them, for example $\eta_{\text{NC},M,T}^{n,k,i}$. This estimator involves the difference of two terms: $(\lambda \nabla T_{h\tau}^{n,k,i})|_M$ and $(\lambda \nabla \mathfrak{T}_{h\tau}^{n,k,i})|_M$. In order to apply formula (4.3.5), these two terms must be expressed in the $\mathbf{RTN}(\mathcal{M}^n)$ space. This is the case of the first contribution $(\lambda \nabla T_{h\tau}^{n,k,i})|_M$ (by construction, see (3.4.2)), but not the case of the second contribution $(\lambda \nabla \mathfrak{T}_{h\tau}^{n,k,i})|_M$. Therefore, we lift this contribution $(\lambda \nabla \mathfrak{T}_{h\tau}^{n,k,i})|_M$ into the $\mathbf{RTN}(\mathcal{M}^n)$ space by preserving the corresponding normal fluxes over the faces: Let $\{\varphi_i^M\}_{i \in \{1,2,\dots,8\}}$ be the piecewise linear nodal basis functions of \mathbf{Q}_1 on the three-dimensional element M . Then for all $M \in \mathcal{M}^n$ the continuous temperature $\mathfrak{T}_{h\tau}^{n,k,i}$ can be expressed as

$$\mathfrak{T}_{h\tau}^{n,k,i} |_M(\mathbf{x}) = \sum_{V_i \in \mathcal{V}_M^n} T_{h\tau}^{n,k,i}(V_i) \varphi_i^M(\mathbf{x}).$$

To alleviate the industrial implementation, we then approximate the value of the temperature in the nodes by

$$T_{h\tau}^{n,k,i}(V) = \frac{1}{N_{\mathcal{M}_V^n}} \sum_{M \in \mathcal{M}_V^n} T_M^{n,k,i} =: T_V^{n,k,i}, \quad (4.3.10)$$

where $N_{\mathcal{M}_V^n}$ stands for the cardinality of the set \mathcal{M}_V^n , of the cells from \mathcal{M}^n sharing the node V ; it is equal to 8 for interior vertices in the three-dimensional case. But the values of $T_{h\tau}^{n,k,i}$ are preferable since they are more precise. The normal fluxes of $(\lambda \nabla \mathfrak{T}_{h\tau}^{n,k,i})|_M$ over the faces of M can then be expressed explicitly by: for all $\sigma \in \mathcal{E}_M^{i,n}$,

$$(\lambda \nabla \mathfrak{T}_{h\tau}^{n,k,i} \cdot \mathbf{n}_\Omega, 1)_\sigma = \sum_{V_i \in \mathcal{V}_M^n} T_{V_i}^{n,k,i} (\lambda \nabla \varphi_i^M \cdot \mathbf{n}_\Omega, 1)_\sigma. \quad (4.3.11)$$

Then using formula (4.3.5) with relation (3.4.2) and formula (4.3.11) we evaluate the nonconformity estimators $\eta_{\text{NC},M,T}^{n,k,i}$, given by (3.A.5h), as

$$\left(\eta_{\text{NC},M,T}^{n,k,i} \right)^2 \approx \frac{1}{8|M|} \sum_{k=1}^8 \left[\sum_{\sigma \in \mathcal{E}_M} \left(G_{M,\sigma}(\mathcal{X}_M^{n,k,i}) - \sum_{V_i \in \mathcal{V}_M^n} T_{V_i}^{n,k,i} (\lambda \nabla \varphi_i^M \cdot \mathbf{n}_\Omega, 1)_\sigma \right) \mathbf{E}_{\sigma,\sigma'} \cdot (\mathbf{f}^k - \mathbf{x}_{\sigma'}) \right]^2. \quad (4.3.12)$$

A similar technique is used to compute the other nonconformity estimators: Define for all $V \in \mathcal{V}^n$ the approximate value of the phase pressures at the node V ,

$$P_{p,V}^{n,k,i} := \frac{1}{N_{\mathcal{M}_V^n}} \sum_{M \in \mathcal{M}_V^n} P_{p,M}^{n,k,i}, \quad \forall p \in \{\text{w}, \text{o}, \text{s}\}. \quad (4.3.13)$$

Then for all $p \in \{\text{w}, \text{o}, \text{s}\}$,

$$\left(\eta_{\text{NC},M,p}^{n,k,i} \right)^2 \approx \frac{\nu_p^\uparrow}{8|M|} \sum_{k=1}^8 \left[\sum_{\sigma \in \mathcal{E}_M} \left(\mathcal{F}_{p,M,\sigma}(\mathcal{X}_M^{n,k,i}) - \sum_{V_i \in \mathcal{V}_M^n} P_{p,V_i}^{n,k,i} (\mathbf{K}_M^\sigma \nabla \varphi_i^M \cdot \mathbf{n}_\Omega, 1)_\sigma \right) \mathbf{E}_{\sigma,\sigma'} \cdot (\mathbf{f}^k - \mathbf{x}_{\sigma'}) \right]^2, \quad (4.3.14)$$

where

$$\mathcal{F}_{p,M,\sigma}(\mathcal{X}_M^{n,k,i}) := |\sigma| \frac{\alpha_M \alpha_L}{\alpha_M + \alpha_L} \left[P_{p,M}^{n,k,i} - P_{p,L}^{n,k,i} \right], \quad \alpha_K := \frac{\mathbf{K}_K^\sigma}{d_{K\sigma}} \quad \forall K \in \{M, L\}.$$

This leads to a simple evaluation of the local *spatial estimators* $\eta_{\text{sp},M,\text{W}}^{n,k,i}$, $\eta_{\text{sp},M,\text{O}}^{n,k,i}$, $\eta_{\text{sp},M,\text{H}}^{n,k,i}$ for all $M \in \mathcal{M}^n$. Note that a more precise formula could be obtained by replacing the piecewise linear nodal basis functions of \mathbf{Q}_1 by the piecewise quadratic basis functions of \mathbf{Q}_2 .

Summarizing the above developments, we have:

Corollary 4.3.1 (Simple formula to evaluate the local spatial estimators). *Following (4.3.12)–(4.3.14), we can approximate the spatial estimators (3.A.7a)–(3.A.7c) as*

$$\eta_{\text{sp},M,H}^{n,k,i} \approx \left\{ \frac{1}{8|M|} \sum_{k=1}^8 \left[\sum_{\sigma \in \mathcal{E}_M} \left(G_{M,\sigma}(\mathcal{X}_M^{n,k,i}) - \sum_{V_i \in \mathcal{V}_M^n} T_{V_i}^{n,k,i} (\lambda \nabla \varphi_i^M \cdot \mathbf{n}_\Omega, 1)_\sigma \right) \mathbf{E}_{\sigma,\sigma'} \cdot (\mathbf{f}^k - \mathbf{x}_{\sigma'}) \right]^2 \right\}^{\frac{1}{2}}, \quad (4.3.15)$$

$$\eta_{\text{sp},M,O}^{n,k,i} \approx \left\{ \frac{\nu_o^\uparrow}{8|M|} \sum_{k=1}^8 \left[\sum_{\sigma \in \mathcal{E}_M} \left(\mathcal{F}_{o,M,\sigma}(\mathcal{X}_M^{n,k,i}) - \sum_{V_i \in \mathcal{V}_M^n} P_{o,V_i}^{n,k,i} (K_M^\sigma \nabla \varphi_i^M \cdot \mathbf{n}_\Omega, 1)_\sigma \right) \mathbf{E}_{\sigma,\sigma'} \cdot (\mathbf{f}^k - \mathbf{x}_{\sigma'}) \right]^2 \right\}^{\frac{1}{2}}, \quad (4.3.16)$$

$$\eta_{\text{sp},M,W}^{n,k,i} \approx \left\{ \sum_{p \in \{w,s\}} \frac{\nu_p^\uparrow}{8|M|} \sum_{k=1}^8 \left[\sum_{\sigma \in \mathcal{E}_M} \left(\mathcal{F}_{p,M,\sigma}(\mathcal{X}_M^{n,k,i}) - \sum_{V_i \in \mathcal{V}_M^n} P_{p,V_i}^{n,k,i} (K_M^\sigma \nabla \varphi_i^M \cdot \mathbf{n}_\Omega, 1)_\sigma \right) \mathbf{E}_{\sigma,\sigma'} \cdot (\mathbf{f}^k - \mathbf{x}_{\sigma'}) \right]^2 \right\}^{\frac{1}{2}}, \quad (4.3.17)$$

with $T_V^{n,k,i}$, $P_{p,V}^{n,k,i}$ given by (4.3.10), (4.3.13), respectively, and \mathbf{f}^k , $\mathbf{E}_{\sigma,\sigma'}$ given by (4.3.4), (4.3.2), respectively.

Finally to evaluate the global spatial estimators (3.A.8a), (3.A.8e) we approximate the time integral by a one-dimensional integration formula.

Now for the *temporal estimators*, recall that for all $M \in \mathcal{M}^n$, the reconstructions of the phase pressures $P_{p,h\tau}^{n,k,i}|_M$, $p \in \{w, o, s\}$, are such that $\mathbb{K} \nabla P_{p,h\tau}^{n,k,i}|_M$ are in the $\mathbf{RTN}(\mathcal{M}^n)$ space. Also the reconstruction of the temperatures $T_{h\tau}^{n,k,i}|_M$ are such that $\lambda \nabla T_{h\tau}^{n,k,i}|_M$ are in the $\mathbf{RTN}(\mathcal{M}^n)$ space. Thus, the evaluation of the local temporal estimators can be again done using formula (4.3.5). More precisely, using the relations (4.3.7)–(4.3.9) in the global temporal

estimators 3.A.7d–3.A.7f, we approximate the integrals in time by

$$\eta_{\text{tm,W}}^{n,k,i} \approx \left\{ \frac{2\tau^n}{3} \sum_{M \in \mathcal{M}^n} \left\| \Theta_{\text{dis,W,h}}^{n,k,i} - \Theta_{\text{dis,W,h}}^{n-1} \right\|_{L^2(M)}^2 \right\}^{\frac{1}{2}}, \quad (4.3.18)$$

$$\eta_{\text{tm,O}}^{n,k,i} \approx \left\{ \frac{2\tau^n}{3} \sum_{M \in \mathcal{M}^n} \left\| \Theta_{\text{dis,O,h}}^{n,k,i} - \Theta_{\text{dis,O,h}}^{n-1} \right\|_{L^2(M)}^2 \right\}^{\frac{1}{2}}, \quad (4.3.19)$$

$$\eta_{\text{tm,H}}^{n,k,i} \approx \left\{ \frac{2\tau^n}{3} \sum_{M \in \mathcal{M}^n} \left\| \Theta_{\text{dis,H,h}}^{n,k,i} - \Theta_{\text{dis,H,h}}^{n-1} \right\|_{L^2(M)}^2 \right\}^{\frac{1}{2}}. \quad (4.3.20)$$

Then we can evaluate the global temporal estimators as proposed in the following corollary:

Corollary 4.3.2 (Simple formula to evaluate the temporal estimators). *By applying formula (4.3.5) to equation (4.3.18) and using the reconstructions formulations (2.4.14a)–(3.4.3a), we can approximate the temporal estimators as*

$$\begin{aligned} \eta_{\text{tm,W}}^{n,k,i} \approx & \left\{ \frac{\tau^n}{12} \sum_{M \in \mathcal{M}^n} \frac{1}{|M|} \sum_{k=1}^8 \left[\sum_{\sigma \in \mathcal{E}_M} \left(\nu_w^\uparrow [F_{w,M,\sigma}(\mathcal{X}_M^{n,k,i}) - F_{w,M,\sigma}(\mathcal{X}_M^{n-1})] \right. \right. \right. \\ & \left. \left. \left. + \nu_s^\uparrow [F_{s,M,\sigma}(\mathcal{X}_M^{n,k,i}) - F_{s,M,\sigma}(\mathcal{X}_M^{n-1})] \right) \mathbf{E}_{\sigma,\sigma'} \cdot (\mathbf{f}^k - \mathbf{x}_{\sigma'}) \right]^2 \right\}^{\frac{1}{2}}, \end{aligned} \quad (4.3.21a)$$

$$\eta_{\text{tm,O}}^{n,k,i} \approx \left\{ \frac{\tau^n}{12} \sum_{M \in \mathcal{M}^n} \frac{1}{|M|} \sum_{k=1}^8 \left[\sum_{\sigma \in \mathcal{E}_M} \left(\nu_o^\uparrow [F_{o,M,\sigma}(\mathcal{X}_M^{n,k,i}) - F_{o,M,\sigma}(\mathcal{X}_M^{n-1})] \right) \mathbf{E}_{\sigma,\sigma'} \cdot (\mathbf{f}^k - \mathbf{x}_{\sigma'}) \right]^2 \right\}^{\frac{1}{2}}, \quad (4.3.21b)$$

$$\begin{aligned} \eta_{\text{tm,H}}^{n,k,i} \approx & \left\{ \frac{\tau^n}{12} \sum_{M \in \mathcal{M}^n} \frac{1}{|M|} \sum_{k=1}^8 \left[\sum_{\sigma \in \mathcal{E}_M} \left(\sum_{p \in \{w,o,s\}} \nu_p^\uparrow H_p^\uparrow [F_{p,M,\sigma}(\mathcal{X}_M^{n,k,i}) - F_{p,M,\sigma}(\mathcal{X}_M^{n-1})] \right. \right. \right. \\ & \left. \left. \left. + [G_{M,\sigma}(\mathcal{X}_M^{n,k,i}) - G_{M,\sigma}(\mathcal{X}_M^{n-1})] \right) \mathbf{E}_{\sigma,\sigma'} \cdot (\mathbf{f}^k - \mathbf{x}_{\sigma'}) \right]^2 \right\}^{\frac{1}{2}}, \end{aligned} \quad (4.3.21c)$$

with $\mathbf{f}^k, \mathbf{E}_{\sigma,\sigma'}$ given by (4.3.4), (4.3.2), respectively.

For the *linearization estimators*, the error in the linearization of the accumulation terms in (3.A.7g) and (3.A.7h) is numerically very small and will be neglected. Then for the other local linearization estimators in (3.A.7g) and (3.A.7h), we remark that the fluxes which compose the estimators are the reconstructed fluxes in the $\mathbf{RTN}(\mathcal{M}^n)$ space: $\Theta_{\text{lin,c,h}}^{n,k,i}, c \in \{W, O\}$, given by (2.4.14b) and $\Theta_{\text{lin,H,h}}^{n,k,i}$ given by (3.4.3b). Thus evaluating of these local estimators is straightforward using formula (4.3.5):

Corollary 4.3.3 (Simple formula to evaluate the linearization estimators). *By applying formula (4.3.5) in equations (3.A.7g) and (3.A.7h) and using the reconstructions formulations (2.4.14b) and (3.4.3b), we can approximate the global linearization estimators as*

$$\eta_{\text{lin,W}}^{n,k,i} \approx \left\{ \frac{\tau^n}{4} \sum_{M \in \mathcal{M}^n} \frac{1}{|M|} \sum_{k=1}^8 \left[\sum_{\sigma \in \mathcal{E}_M} \left(\nu_w^\uparrow [F_{w,M,\sigma}^{n,k,i} - F_{w,M,\sigma}(\mathcal{X}_M^{n,k,i})] + \nu_s^\uparrow [F_{s,M,\sigma}^{n,k,i} - F_{s,M,\sigma}(\mathcal{X}_M^{n,k,i})] \right) \mathbf{E}_{\sigma,\sigma'} \cdot (\mathbf{f}^k - \mathbf{x}_{\sigma'}) \right]^2 \right\}^{\frac{1}{2}}, \quad (4.3.22a)$$

$$\eta_{\text{lin,O}}^{n,k,i} \approx \left\{ \frac{\tau^n}{4} \sum_{M \in \mathcal{M}^n} \frac{1}{|M|} \sum_{k=1}^8 \left[\sum_{\sigma \in \mathcal{E}_M} \left(\nu_o^\uparrow [F_{o,M,\sigma}^{n,k,i} - F_{o,M,\sigma}(\mathcal{X}_M^{n,k,i})] \right) \mathbf{E}_{\sigma,\sigma'} \cdot (\mathbf{f}^k - \mathbf{x}_{\sigma'}) \right]^2 \right\}^{\frac{1}{2}}, \quad (4.3.22b)$$

$$\eta_{\text{lin,H}}^{n,k,i} \approx \left\{ \frac{\tau^n}{4} \sum_{M \in \mathcal{M}^n} \frac{1}{|M|} \sum_{k=1}^8 \left[\sum_{\sigma \in \mathcal{E}_M} \left(\sum_{p \in \{w,o,s\}} \nu_p^\uparrow H_p^\uparrow [F_{p,M,\sigma}^{n,k,i} - F_{p,M,\sigma}(\mathcal{X}_M^{n,k,i})] + [G_{M,\sigma}^{n,k,i} - G_{M,\sigma}(\mathcal{X}_M^{n,k,i})] \right) \mathbf{E}_{\sigma,\sigma'} \cdot (\mathbf{f}^k - \mathbf{x}_{\sigma'}) \right]^2 \right\}^{\frac{1}{2}}, \quad (4.3.22c)$$

with $\mathbf{f}^k, \mathbf{E}_{\sigma,\sigma'}$ given by (4.3.4), (4.3.2), respectively.

Finally, for the *algebraic estimators* (3.A.7i) and (3.A.7j), the evaluation of the local $[L^2]^3$ norms is also straightforward using formula (4.3.5), as by construction all contributions involved in these norms are in the $\mathbf{RTN}(\mathcal{M}^n)$ space by construction: $\Theta_{\text{alg},c,h}^{n,k,i}, c \in \{W, O\}$, given by (2.4.14c) and $\Theta_{\text{alg},H,h}^{n,k,i}$ given by (3.4.3c). Following Remark 2.4.3, we arrive at the following approximation formula:

Corollary 4.3.4 (Computing practically the algebraic error). *Following Remark 2.4.3 in Chapter 2 to compute approximately the algebraic error, we perform j additional iterations of the algebraic solver from the stage (2.4.8), (3.3.11), with j a user-defined fixed number. Then, the global algebraic error estimators can be evaluated using formula (4.3.5) as follow:*

$$\eta_{\text{alg,W}}^{n,k,i} \approx \left\{ \frac{\tau^n}{4} \sum_{M \in \mathcal{M}^n} \frac{1}{|M|} \sum_{k=1}^8 \left[\sum_{\sigma \in \mathcal{E}_M} \left(\nu_w^\uparrow [F_{w,M,\sigma}^{n,k,i+j} - F_{w,M,\sigma}^{n,k,i}] + \nu_s^\uparrow [F_{s,M,\sigma}^{n,k,i+j} - F_{s,M,\sigma}^{n,k,i}] \right) \mathbf{E}_{\sigma,\sigma'} \cdot (\mathbf{f}^k - \mathbf{x}_{\sigma'}) \right]^2 \right\}^{\frac{1}{2}}, \quad (4.3.23a)$$

$$\eta_{\text{alg,O}}^{n,k,i} \approx \left\{ \frac{\tau^n}{4} \sum_{M \in \mathcal{M}^n} \frac{1}{|M|} \sum_{k=1}^8 \left[\sum_{\sigma \in \mathcal{E}_M} \left(\nu_o^\uparrow [F_{o,M,\sigma}^{n,k,i+j} - F_{o,M,\sigma}^{n,k,i}] \right) \mathbf{E}_{\sigma,\sigma'} \cdot (\mathbf{f}^k - \mathbf{x}_{\sigma'}) \right]^2 \right\}^{\frac{1}{2}}, \quad (4.3.23b)$$

$$\eta_{\text{alg},H}^{n,k,i} \approx \left\{ \frac{\tau^n}{4} \sum_{M \in \mathcal{M}^n} \frac{1}{|M|} \sum_{k=1}^8 \left[\sum_{\sigma \in \mathcal{E}_M} \left(\sum_{p \in \{\text{w,o,s}\}} \nu_p^\uparrow H_p^\uparrow [F_{p,M,\sigma}^{n,k,i+j} - F_{p,M,\sigma}^{n,k,i}] + [G_{M,\sigma}^{n,k,i+j} - G_{M,\sigma}^{n,k,i}] \right) \mathbf{E}_{\sigma,\sigma'} \cdot (\mathbf{f}^k - \mathbf{x}_{\sigma'}) \right]^2 \right\}^{\frac{1}{2}}, \quad (4.3.23\text{c})$$

with \mathbf{f}^k , $\mathbf{E}_{\sigma,\sigma'}$ given by (4.3.4), (4.3.2), respectively.

As a conclusion, the evaluation of the different estimators for the thermal dead oil model (3.A.1) can be carried out while avoiding the physical reconstructions of fluxes in the $\mathbf{RTN}(\mathcal{M}^n)$ space. The key is the use of a quadrature formula for computing the $[L^2(M)]^3$, $M \in \mathcal{M}^n$, norms by (4.3.5), knowing the normal fluxes over all faces of any cell $M \in \mathcal{M}^n$. Using this technique greatly simplifies the implementation of the estimators (in particular into industrial codes) and yields an important computational saving compared to the previous technique where we need to build the \mathbf{RTN} flux reconstructions.

4.4 SAGD test case

In this section we present numerical simulations of the SAGD dead oil model.

4.4.1 Model description

The reservoir considered in this test case is a 3-dimensional parallelepiped (100m \times 1400m \times 55m) discretized by a nonuniform Cartesian grid, see Figure 4.2, right. We consider a homogeneous anisotropic reservoir with 35% porosity, $1.94 \cdot 10^{-12}$ m² horizontal permeability, and $0.97 \cdot 10^{-12}$ m² vertical permeability. Two horizontal wells, injection and production well (in the Y direction) perforate the reservoir, see Figure 4.2 left.

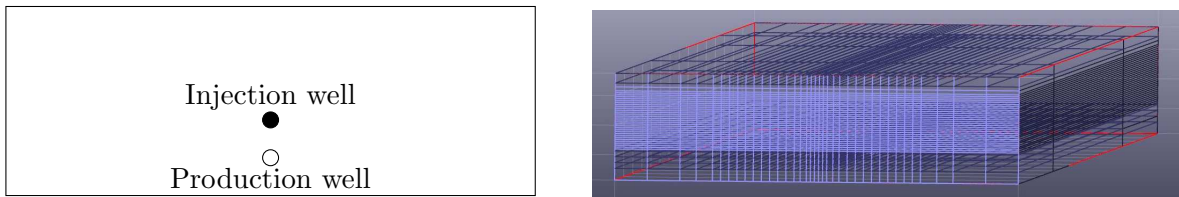


Figure 4.2: Reservoir mesh

The fluid is a heavy, viscous oil. Its viscosity range is tabulated as a function of temperature, from $1.68 \cdot 10^3$ Pa·s (at 23.89°C) to $0.741 \cdot 10^{-3}$ Pa·s (at 455.44°C). The initial water saturation is equal to 0.15 so that the initial oil saturation is equal to 0.85.

The mass density of the oil for this test case is given by the following formula

$$\rho_o(P, T) = \rho_{o,O}(P, T) = \rho_o^{\text{ref}} [1 + c_O(P - P^{\text{ref}}) + d_O(T - T^{\text{ref}})],$$

with a constant compressibility of the oil component $c_O = 72.5 \cdot 10^{-11} \text{Pa}^{-1}$, a constant thermal expansion of the oil component $d_O = 8.5 \cdot 10^{-4} \text{K}^{-1}$, and a constant reference mass density $\rho_o^{\text{ref}} = 1014.035 \text{ kg} \cdot \text{m}^{-3}$. The water mass density is given by

$$\rho_w(T) = \alpha_1 + \alpha_2 T + \alpha_3 T^2,$$

with $\alpha_1 = 7.81 \cdot 10^2$, $\alpha_2 = 1.63 \cdot 10^0$, and $\alpha_3 = -3.06 \cdot 10^{-3}$. Water viscosity is given as for standard water following [9], ($1.002 \cdot 10^{-3} \text{Pa} \cdot \text{s}$ at 20°C).

The capillary pressure is set to zero and the relative permeability is shown in Figure 4.3. The thermal conductivity $\lambda(t)$ of the rock is constant equal to $2.38 \text{W}/(\text{m} \cdot ^\circ\text{C})$. We mention that the thermal properties of the rock are those of the so-called saturated rock. The compressibility of the rock is constant equal to $43.5 \cdot 10^{-10} \text{Pa}^{-1}$ and the loss in heat at the foot-wall is not simulated.

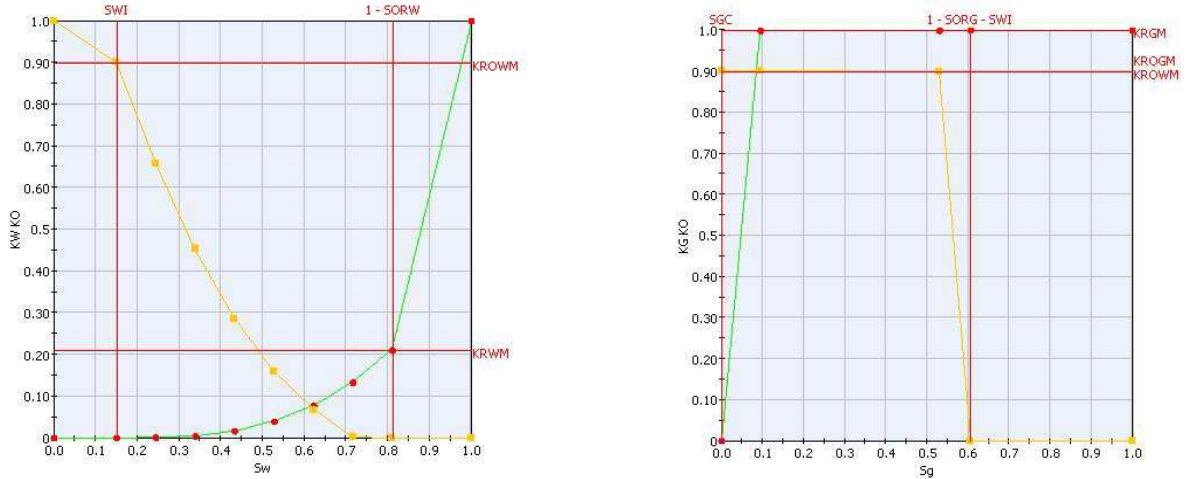


Figure 4.3: Relative permeability.

4.4.2 Initialization and production scheme

The SAGD process is simulated for $t_F = 10$ years. The reservoir is initially assumed at hydrostatic equilibrium with a constant temperature equaling 11°C . The initial pressure is $7.27 \cdot 10^5 \text{Pa}$ at -400m . To start the production of the reservoir, we begin with a heating phase of the surrounding region of production and injection wells in a period of 90 days. Then, the production well is put into production for one day with a high rate of liquid flow without injection to bring down the pressure in the injection zone. Finally a period of injection/production (until 10 years) is held during the simulation. In the model, the injection and production rates are controlled by the pressure ($24.81 \cdot 10^5 \text{Pa}$ for the producer and $25.36 \cdot 10^5 \text{Pa}$ for the injector).

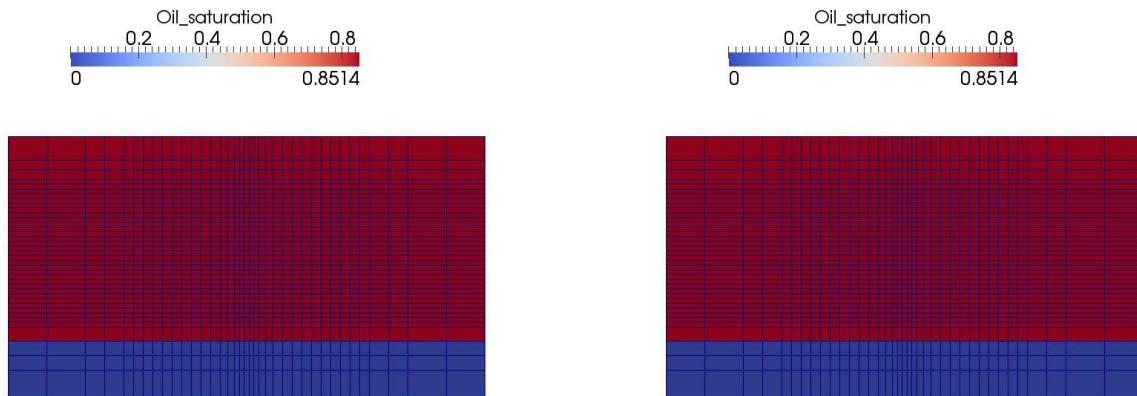


Figure 4.4: Initial saturation of water (left) and oil (right).

4.4.3 Model simulation

In the simulation of the thermal dead oil model we can distinguish four different steps:

- **Heating:** The wells heating period (90 days) is necessary to promote the injection, see Figure 4.5. Without heating, steam injection is not possible.

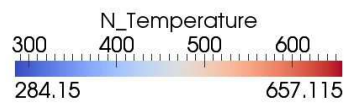


Figure 4.5: Temperature of reservoir at 90 days.

- **Forming the steam chamber:** A steam chamber is formed at the opening of the injection well. In a first phase the steam chamber grows and takes an ovoid shape until the steam has reached the top of the reservoir, see Figure 4.6.
- **Expanding the steam chamber:** The steam chamber expands along the top of the reservoir to the side boundaries of the domain, see Figure 4.7.
- **Drainage:** Steam invades the lower part of the reservoir; the production mechanism is further a displacement mechanism of oil forced by steam more than a mechanism for gravity drainage, see Figure 4.8.

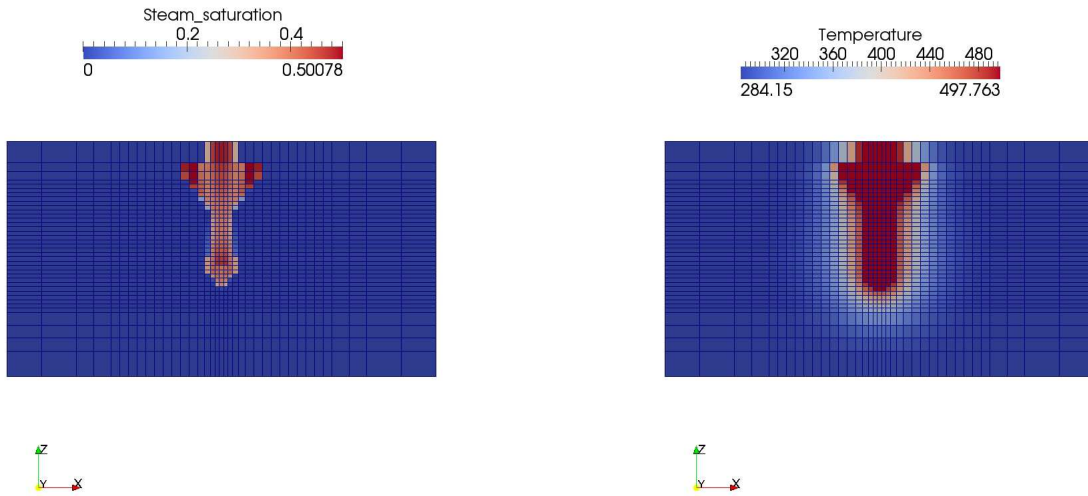


Figure 4.6: Forming the steam chamber: steam saturation (left) and temperature of the reservoir (right) at 600 days.

4.4.4 Approximate solution and a posteriori estimate

We show here the behaviour of the approximate solution and of the corresponding a posteriori error estimate during the simulation on a fine fixed grid.

Figure 4.9 shows the evolution of the oil saturation and the corresponding spatial estimator of the oil component $\eta_{\text{sp},M,O}^n$ (4.3.16) at different time steps. We see an error detected by the estimator around the wells; importantly, this estimator detects the error that follows the movement of the oil front in the reservoir. This result demonstrates that we have a good indicator of the corresponding error and suggests its use in an algorithm of mesh adaptivity.

The results of the evolution of temperature and the temperature spatial estimator $\eta_{\text{sp},M,H}^n$ (4.3.15) are summarized in Figure 4.10. Remark that the prediction error points out an important error in the zone that follows the diffusion of the temperature during the simulation, which shall help us refine wisely the mesh in order to equilibrate the distribution of the error over the domain and then reduce the size of the system for resolution.

4.4.5 Adaptive mesh refinement

In this section we numerically assess an adaptive mesh refinement (AMR) strategy based on the space error indicators derived in Section 3.5.3.2 with the simplification of Section 4.3.2, by comparing the results with a reference solution obtained on a fine grid. As the flow of the fluid (see Figure 4.9), as well as the temperature diffusion (see Figure 4.10) are both symmetric in the domain, we present the results in what follows on the half of the domain

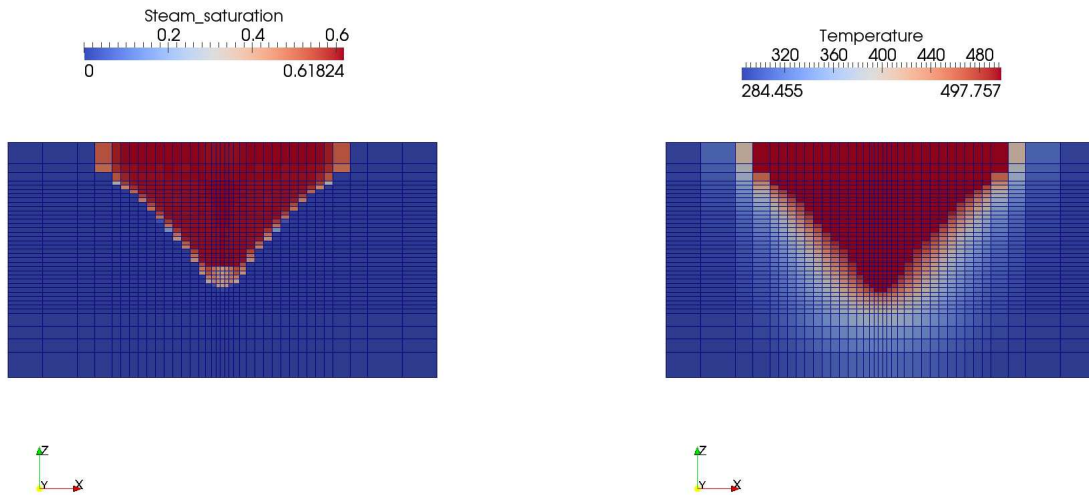


Figure 4.7: Expansion of the steam chamber: steam saturation (left) and temperature of the reservoir (right) at 2000 days.

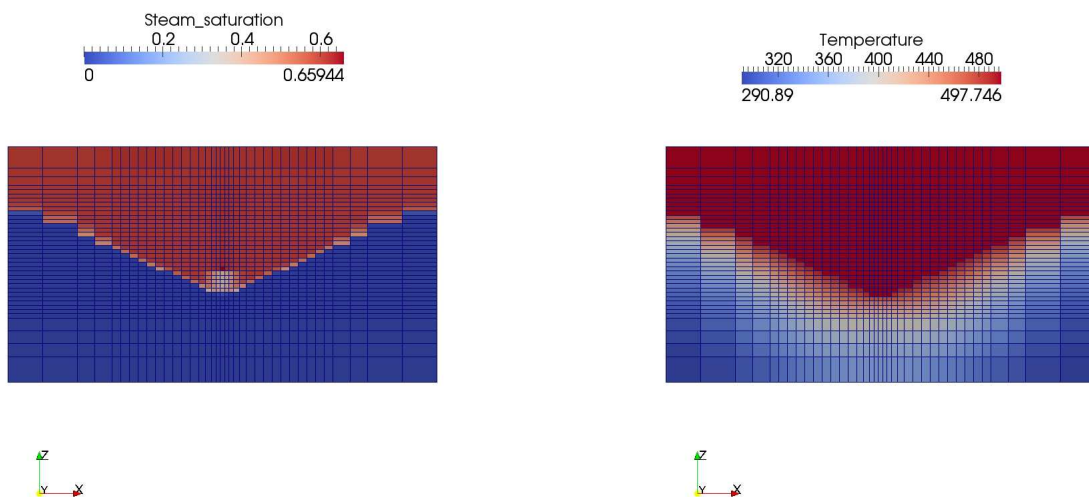


Figure 4.8: steam saturation (left) and temperature of the reservoir (right) at 4000 days.

only. To refine the mesh adaptively we use the space criterion based on the spatial estimator of the oil component $\eta_{\text{sp},M,\text{O}}^n$ (4.3.16). The algorithm that describes the adaptive strategy can be sketched as follows:

Algorithm 4.4.1 (Adaptive algorithm).

Fix the fractions of cells to refine, ζ_{ref} , and to derefine, ζ_{deref}

while $t^n \leq t_{\text{F}}$ **do** {Time loop}

Solve the system (2.2.20), (3.3.2).

Compute $\eta_{\text{tm},M,\text{o}}^n, \eta_{\text{sp},M,\text{o}}^n$.

Refine the cells $M \in \mathcal{M}^n$ such that $\eta_{\text{sp},M,\text{o}}^n \geq \zeta_{\text{ref}} \max_{L \in \mathcal{M}^n} \{\eta_{\text{sp},L,\text{o}}^n\}$.

Derefine the cells $M \in \mathcal{M}^n$ such that $\eta_{\text{sp},M,\text{o}}^n \leq \zeta_{\text{deref}} \max_{L \in \mathcal{M}^n} \{\eta_{\text{sp},L,\text{o}}^n\}$.

Adapt the time step if necessary.

end while

Figure 4.11 shows the evolution of the approximate oil saturation at different simulation times. We remark that the refinement follows the saturation front as time evolves, and then the derefinement process is effected in the zones abandoned by the front of oil saturation.

Similar results can be appreciated in Figure 4.12 where we present the evolution of the temperature at several chosen time steps. A refinement that follows the diffusion of temperature can be observed, as well as a derefinement in the non-exposed zones.

The efficiency of the adaptive algorithm based on the spatial a posteriori estimator can be appreciated in Figure 4.13. Figure 4.13b in particular illustrates the cumulated rate of oil production during the simulation; we compare here the result on the fine grid and the result with adaptive mesh refinement. We observe that applying the refinement strategy does not affect the accuracy of the predicted oil production, which is industrially the most important quantity.

The cumulative number of cells during the simulation is finally shown in Figure 4.14a. We remark an important reduction in the number of cells using the adaptive refinement strategy compared with the resolution on the fine grid. On average, the number of cells is reduced by 75%, see Figure 4.14b, which is a very important gain.

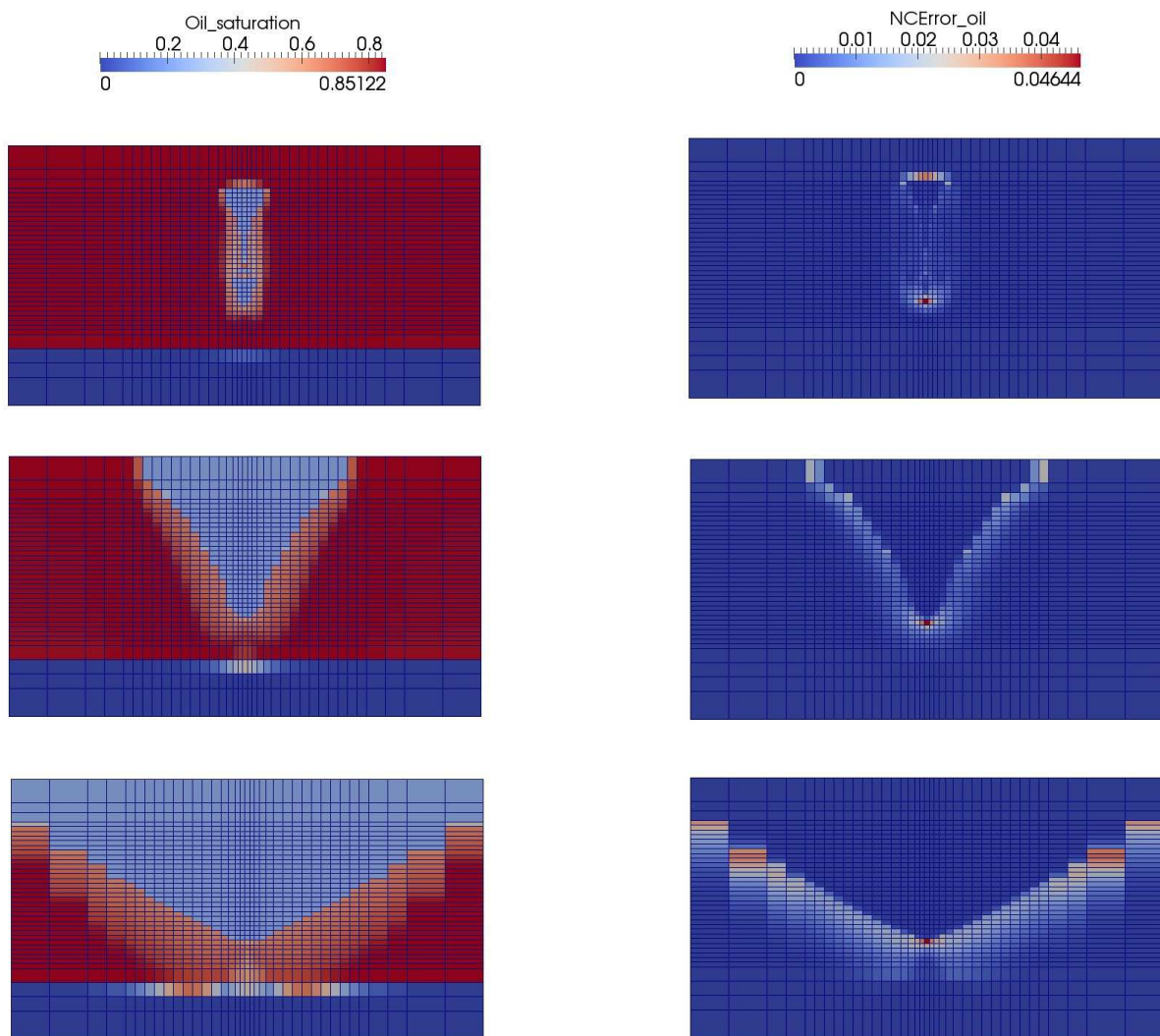


Figure 4.9: Approximate oil saturation (left) and spatial estimator of the oil component (right) at 400, 1100, and 2800 days.

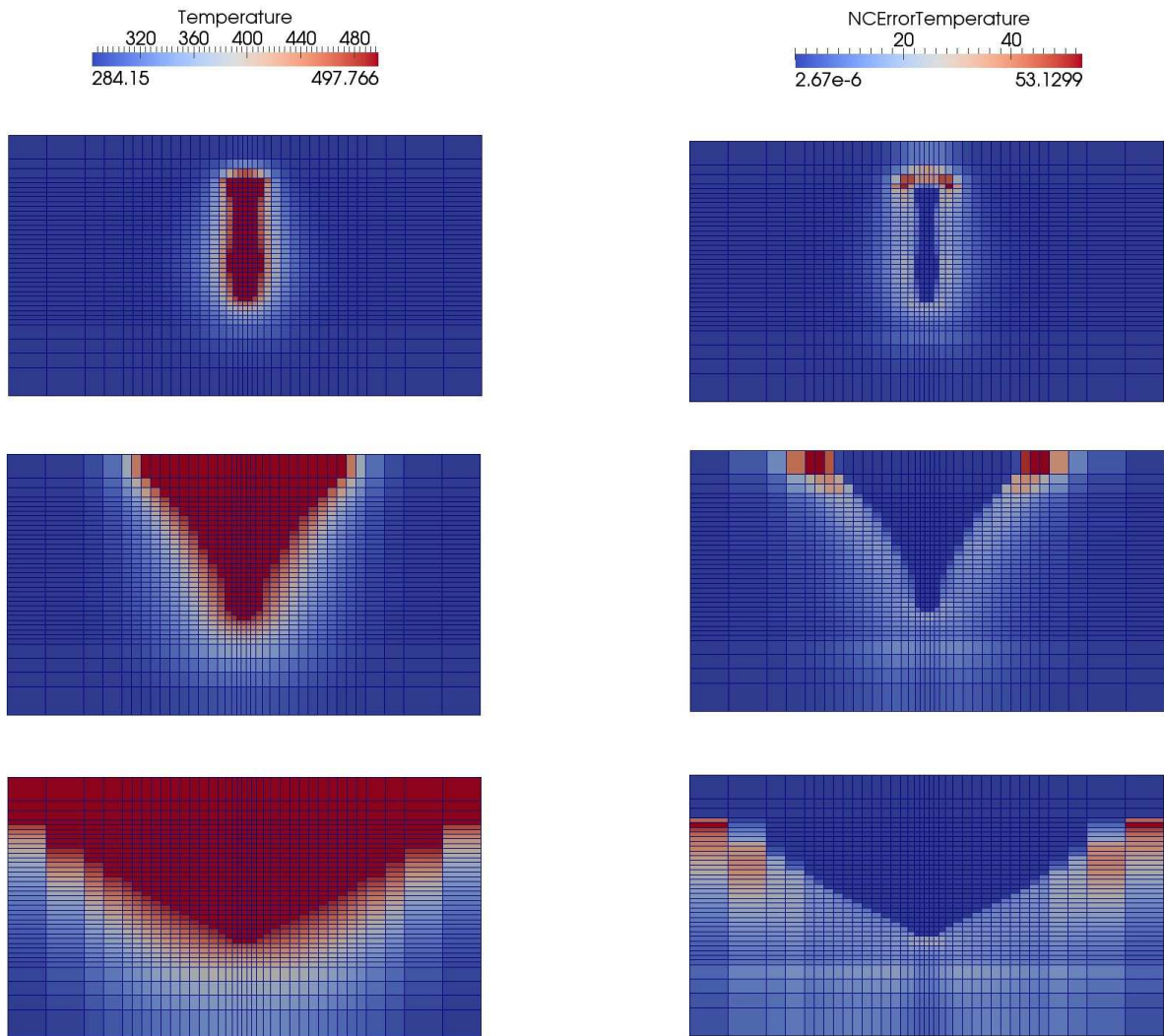


Figure 4.10: Approximate temperature (left) and temperature spatial estimator (right) at 400, 1100, and 2800 days.

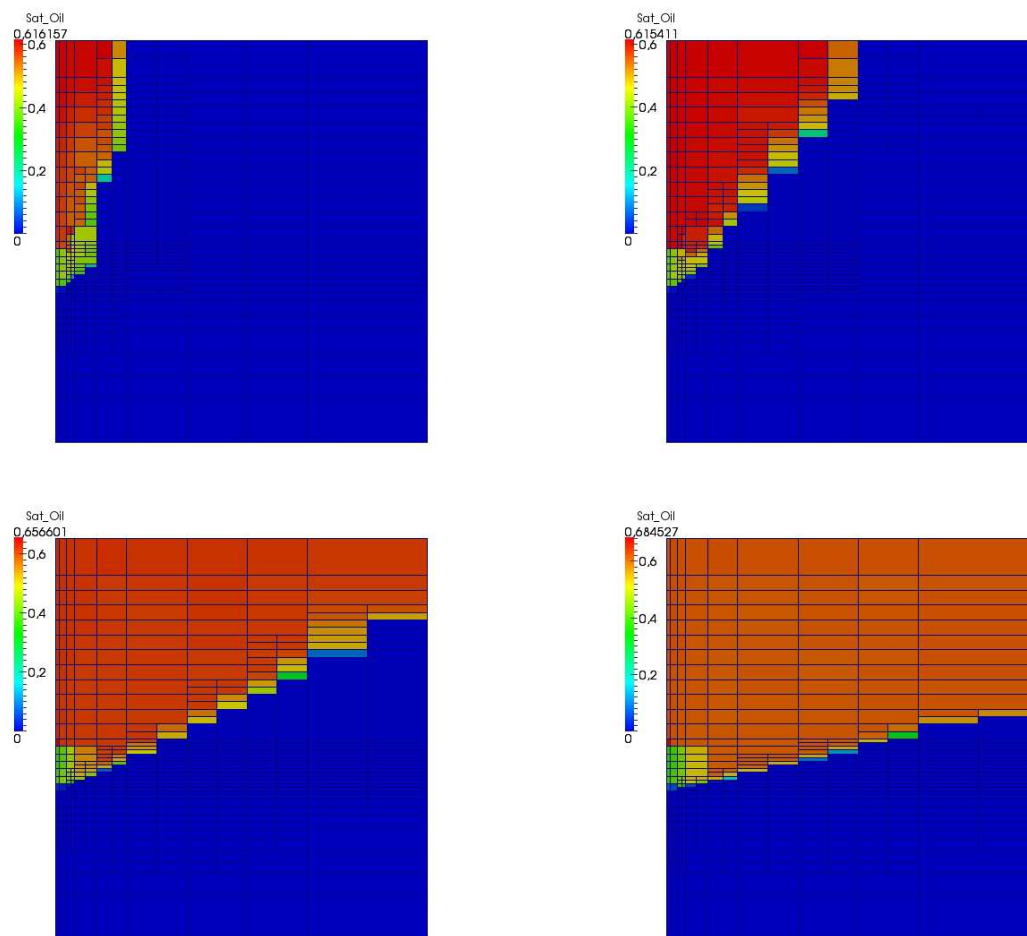


Figure 4.11: Approximate oil saturation at 2, 4, 8, and 10 years (adaptively refined mesh)

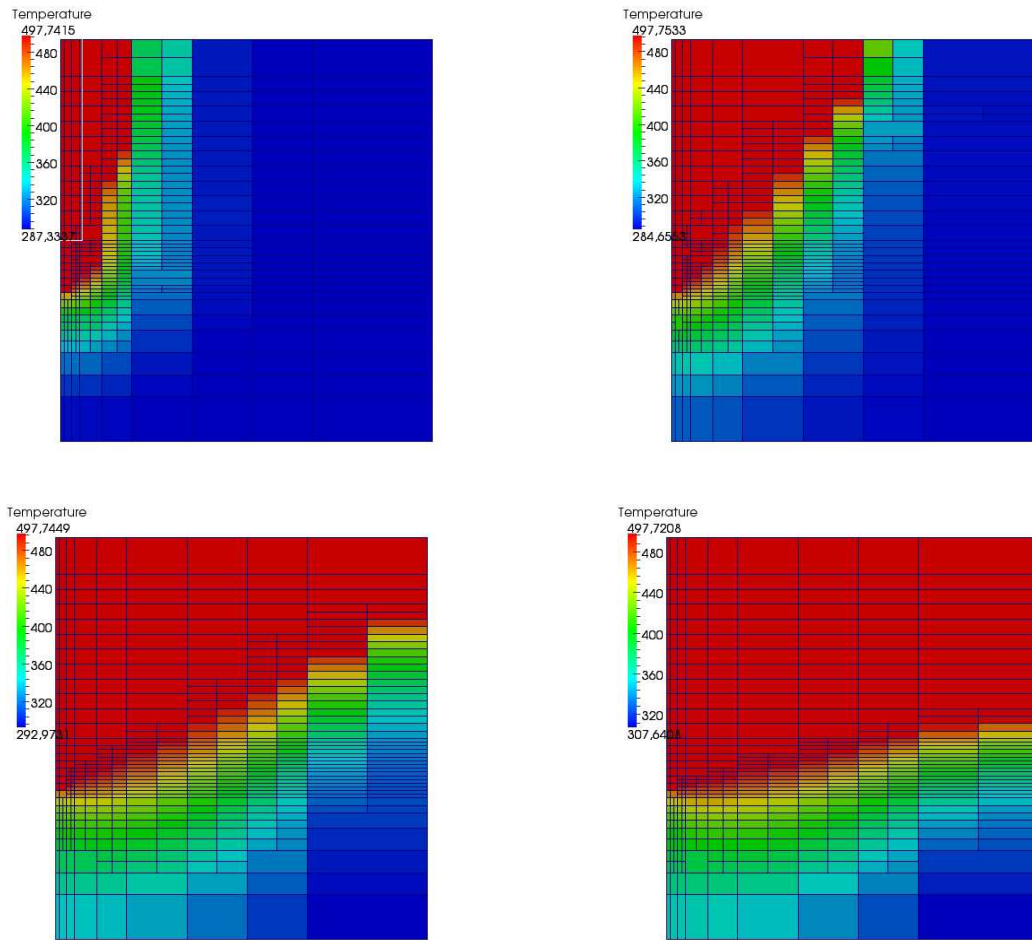
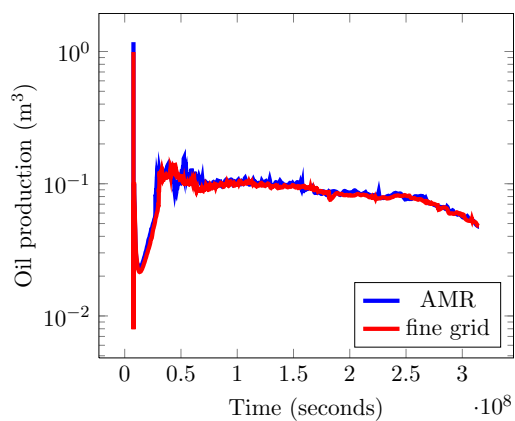
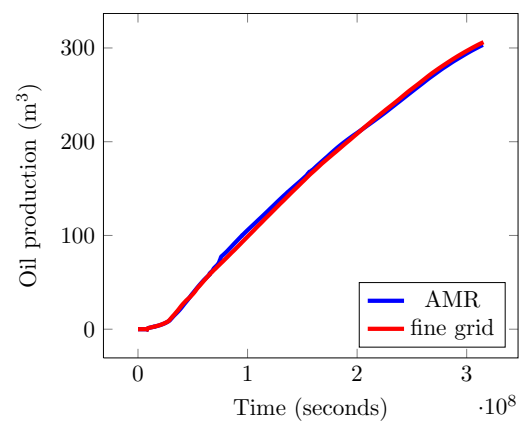


Figure 4.12: Approximate temperature at 2, 4, 8, and 10 years (adaptively refined mesh)

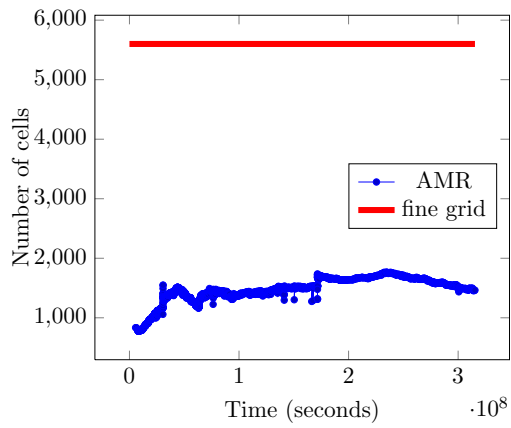


(a) Rate of oil production as a function of time

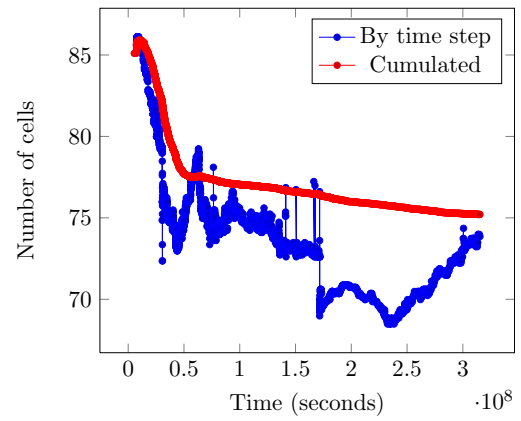


(b) Cumulated rate of oil production as a function of time

Figure 4.13: Fine grid vs. adaptive mesh refinement for the rate of oil production.



(a) Number of cells as a function of time



(b) Reduction of the total Number of cells

Figure 4.14: Fine grid vs. adaptive mesh refinement.

Bibliography

- [1] R. Butler. *Thermal recovery of oil and bitumen*. Prentice Hall, Englewoods Cliffs, New Jersey, 1991.
- [2] R. Butler. Steam-Assisted Gravity Drainage: Concept, development, performance and future. *JCPT*, 33(2):44–50, 1994.
- [3] J. Christensen, G. Darche, B. Dchelette, H. Ma, and P. Sammon. Applications of dynamic gridding to thermal simulations. *SPE*, 2004.
- [4] A. Farouq. *SAGD steam assisted gravity drainage*. University of Alberta, Edmonton, Canada, 1997.
- [5] D. Kröner and M. Ohlberger. A posteriori error estimates for upwind finite volume schemes for nonlinear conservation laws in multidimensions. *Math. Comp.*, 69(229):25–39, 2000.
- [6] S. Lacroix, P. Lemonnier, G. Renard, and C. Taieb. Enhanced numerical simulations of oil processes through dynamic sub-gridding. Technical report, Canadian International Petroleum Conference, 2003.
- [7] M. Mamaghani, G. Enchéry, and C. Chainais-Hillairet. Development of a refinement criterion for adaptive mesh refinement in steam-assisted gravity drainage simulation. *Comput Geosci*, 15:17–34, 2011.
- [8] E. Rodríguez and J. Orjuela. Feasibility to apply the steam assisted gravity drainage (SAGD) technique in the country’s heavy crude-oil fields. *CT&F*, 2(5):7–22, 2004.
- [9] E. Schmidt. *Properties of water and steam in S.I units*. Springer, Pennsylvania State University, 1981.
- [10] X. Wang, M. Quintard, and G. Darche. Adaptive mesh refinement for one dimensional three-phase flow with phase change in porous media. *Numer. Heat Transf*, 50:231–268, 2006.

List of Figures

1	Classification of hydrocarbon recovery methods.	6
2	Gas injection.	6
3	SAGD and Steam Drive process.	7
4	VAPEX and THAI process.	7
1.1	An example of a function β and a regularization β_ϵ	23
1.2	Simplicial mesh \mathcal{T}^n and the associated vertex-centered dual mesh \mathcal{D}^n and the fine simplicial mesh \mathcal{K}_D of $D \in \mathcal{D}^n$	37
1.3	Evolution of the spatial, temporal, regularization, and linearization error estimators as a function of Newton iterations for a fixed mesh, time step, and regularization parameter	42
1.4	Error estimator as a function of the cumulated Newton iterations at each time step	43
1.5	Evolution of the spatial, temporal, and regularization error estimators as a function of ϵ^{-1} for a fixed mesh and time step	44
1.6	Effect of the time step adaptation strategy on the global error estimator.	45
1.7	Actual and estimated error distribution for adaptive Algorithm.	46
1.8	Exact and approximate enthalpy corresponding to the adaptive Algorithm	47
1.9	Comparison between adaptive and uniform refinement. Dual norm, energy-like norm. Error and estimators, effectivity indices	47
2.1	Configuration for the numerical test cases	86
2.2	Evolution of the spatial, temporal, linearization, and algebraic error estimators for a fixed mesh at a fixed time, as a function of Newton iterations and GMRes iterations on the first Newton iteration	89
2.3	Cumulated rate of oil production for the test case of Section 2.5.2	89
2.4	Liquid saturation, classical vs. adaptive resolution for the test case of Section 2.5.2	90

2.5	Reference pressure, classical vs. adaptive resolution for the test case of Section 2.5.2	91
2.6	Spatial error distribution for the test case of Section 2.5.2	92
2.7	Newton iterations at each time step and cumulated number of Newton iterations as a function of time for the test case of Section 2.5.2	92
2.8	GMRes iterations for each time and Newton iteration step and cumulated number of GMRes iterations as a function of time for the test case of Section 2.5.2	93
2.9	Configuration for the numerical test case of Section 2.5.3.1	93
2.10	Cumulated rate of oil production for the test case of Section 2.5.3.1	94
2.11	Liquid saturation, classical and adaptive resolutions for the test case of Section 2.5.3.1	95
2.12	Reference pressure, classical and adaptive resolution for the test case of Section 2.5.3.1	96
2.13	Spatial error distribution for the test case of Section 2.5.3.1	97
2.14	Newton iterations at each time step and cumulated number of Newton iterations as a function of time for the test case of Section 2.5.3.1	98
2.15	GMRes iterations at each time and Newton step and cumulated number of GMRes iterations as a function of time for the test case of Section 2.5.3.1	98
2.16	Configuration for the numerical test case of Section 2.5.3.2	99
2.17	Cumulated rate of oil production for the test case of Section 2.5.3.2	99
2.18	Liquid saturation, classical and adaptive resolutions for the test case of Section 2.5.3.2	100
2.19	Reference Pressure, classical and adaptive resolution for the test case of Section 2.5.3.2	101
2.20	Spatial error distribution for the test case of Section 2.5.3.2	102
2.21	Newton iterations at each time step and cumulated number of Newton iterations as a function of time for the test case of Section 2.5.3.2	103
2.22	GMRes iterations at each time and Newton step and cumulated number of GMRes iterations as a function of time for the test case of Section 2.5.3.2	103
2.23	Configuration for the numerical test case of Section 2.5.4.1	104
2.24	Cumulated rate of oil production for the test case of Section 2.5.4.1	105
2.25	Liquid saturation, classical and adaptive resolutions for the test case of Section 2.5.4.1	106
2.26	Reference pressure (a), classical and adaptive resolution for the test case of Section 2.5.4.1	107
2.27	Reference pressure (b), classical and adaptive resolution for the test case of Section 2.5.4.1	107
2.28	Spatial error distribution for the test case of Section 2.5.4.1	108

2.29	Newton iterations at each time step and cumulated number of Newton iterations as a function of time for the test case of Section 2.5.4.1	109
2.30	GMRes iterations at each time and Newton step and cumulated number of GMRes iterations as a function of time for the test case of Section 2.5.4.1	109
2.31	Configuration for the numerical test cases of Section 2.5.4.2	110
2.32	Cumulated rate of oil production for the test case of Section 2.5.4.2	110
2.33	Liquid saturation, classical and adaptive resolutions for the test case of Section 2.5.4.2	111
2.34	Reference pressure, classical and adaptive resolution for the test case of Section 2.5.4.2	112
2.35	Spatial error distribution for the test case of Section 2.5.4.2	113
2.36	Newton iterations at each time step and cumulated number of Newton iterations as a function of time for the test case of Section 2.5.4.2	113
2.37	GMRes iterations at each time and Newton step and cumulated number of GMRes iterations as a function of time for the test case of Section 2.5.4.2	114
4.1	SAGD process	152
4.2	Reservoir mesh	163
4.3	Relative permeability	164
4.4	Initial oil and water saturations	165
4.5	Heating: Temperature of the reservoir at 90 days.	165
4.6	Forming the steam chamber	166
4.7	Expansion of the steam chamber	167
4.8	Drainage by steam	167
4.9	Spatial estimator of the oil phase	169
4.10	Spatial estimator of the temperature	170
4.11	Approximate oil saturation, AMR	171
4.12	Approximate temperature, AMR	172
4.13	Rate of oil production. SAGD	172
4.14	Number of cells	173

List of Tables

1.1	Comparison of the experimental orders of convergence (e.o.c.) in the uniform and fully adaptive cases. The total number of space–time unknowns is denoted by N_{st} . The actual error $\ \mathcal{R}(u_{h\tau})\ _{X'}$ and the estimated error η are defined by (1.3.2) and (1.3.8) respectively.	48
3.1	Dependence of the model’s parameters	125
4.1	Integration points	156